Functional NMDA receptors in red blood cells and heart

Dissertation

zur

Erlangung der naturwissenschaftlichen Doktorwürde

(Dr. sc. nat.)

vorgelegt der

Mathematisch-naturwissenschaftlichen Fakultät

der

Universität Zürich

von

Asya Victorovna Makhro

aus

Russland

Promotionskomitee
Prof. Dr. Max Gassmann (Vorsitz)
PD Dr. Anna Yu. Bogdanova (Leitung der Dissertation)
Prof. Dr. Michael Hengartner
Prof. Dr. med. Stephan Rohr

Zürich, 2014

Table of contents

1. Abbreviations

AMPA – α-amino-3-hydroxy-5-methyl-4-isoxazolepropionic acid

ARC – adult rat cardiomyocytes

ATD – amino-terminal domain

CTD – carboxyl-terminal domain

D-APV – (2R)-amino-5-phosphonovaleric acid

EPC – erythroid precursor cells

Glu – L-glutamate

Gly – L-glycine

GSH – γ-L-Glutamyl-L-cysteinylglycine, glutathione reduced

GSSG – glutathione oxidized

iGluR – ionotropic glutamate receptor

LBD – ligand binding domain

NMDA – N-Methyl-D-aspartate

NO – nitric oxide

NOX – NADPH oxidase

NR – NMDA receptor subunit (NR1, NR2A etc.)

NRC – neonatal rat cardiomyocytes

NTD – N-terminal domain (of the protein)

PFK – phosphofructokinase

PLC – phospholipase C

PKC – protein kinase C

RBC – red blood cells

SCD – sickle cell disease

2. Summary

N-methyl D-aspartate (NMDA) receptor is a nonselective cation channel formed four out of seven known subunits capable of binding glutamate or glycine. These amino acids are the agonists of the NMDA receptors in the brain where this receptor is involved in neurotransmission and intracellular signaling. Recently NMDA receptor expression and function were shown in several non-neuronal tissues. NMDA receptors were found in human bone marrow in osteoclasts, osteoblasts and hematopoietic precursor lineages. Expression of several of the NMDA receptor subunits was reported in mammalian myocardial tissue, however, the NMDA receptor function in the heart was never investigated.

The aim of the present study was to characterize NMDA receptor expression and its physiological and pathophysiological roles in the heart, and in red blood cells (RBC) as well as in erythroid precursor cells (EPCs). We were the first to report the presence of NMDA receptors in RBCs of rats and humans and in human and rat EPCs. Subunit composition of the erythroid receptors varied depending on the differentiation stage in human EPCs and differed substantially from that in the brain with NR2D and NR3B were the dominating over the neuronal NR1 and NR2B common in neurons. Erythroid receptors could be activated by the NMDA and glutamate. Stimulation of the NMDA receptors in humans EPCs as well as in human and rat RBCs resulted in massive transient Ca^{2+} uptake. Plasma-born glutamate and glycine were sufficient to maintain basal receptor activity which was controlled by the plasma agonists levels and, most likely, other humoral factors. We have demonstrated that abnormally high numbers of receptor copies in RBCs of sickle cell disease patients translate into excessive permeability of RBC membranes for Ca^{2+}. As calcium is a master regulator of various processes in RBCs, its uptake upon stimulation of the erythroid NMDA receptors resulted in the alterations of cytoskeletal structure and cell volume, modulation of oxidative state, intracellular pH, and RBC half-life in the circulation. In the EPCs NMDA receptors are required for survival of precursor cells, particular at the earlier differentiation stages.

Our motivation to investigate the expression and function of the NMDA receptors in the heart was based on the fact that elevation of the plasma levels of the

agonist of these receptors, homocysteine, was reported to be associated with several heart diseases including heart failure. We have characterized expression of the NMDA receptor subunits in different parts of rat myocardium and elaborated on the relation between the subunit composition of cardiac NMDA receptors and their pharmacology using “brainless rat heart model” (isolated blood-perfused heart) and sarcolemmal membrane preparations. Similar to that in RBCs, subunit composition of cardiac NMDA receptors differed substantially from that in the brain and showed remarkable chamber-dependent heterogeneity with NR3A and NR2D dominating. Expression of the NR2B subunit was age-dependent and most likely associated with hypertrophic remodeling. Expression of the subunits NR2A and 2C was restricted to atria. We found that NMDA receptor agonists and antagonists regulated autonomous heart rate and rhythmicity. Myocardial repolarization and depolarization rate were prolonged by the NMDA receptor antagonists. Our data indicate that cardiac NMDA receptors are an attractive target for pharmacological interventions to treat arrhythmias and other cardiovascular disorders.

3. Zusammenfassung

Die N-methyl D-aspartate (NMDA) Rezeptoren sind nicht-selektive Kationenkanäle, die sich aus 4 von 7 möglichen Untereinheiten zusammensetzen und Bindungsstellen für Glutamat und Glycin besitzen. Beide Aminosäuren fungieren als NMDA Rezeptoragonisten im Gehirn, wo der Rezeptor Neurotransmission und intrazelluläre Signalwege reguliert. Interessanterweise wurde Expression und Funktionalität der NMDA Rezeptoren auch in verschiedenen nicht-neuronalen Geweben, unter anderem in Osteoklasten, Osteoblaten und hämatopoetischen Vorläuferzellen des menschlichen Knochenmarks, nachgewiesen. Auch im Myokardgewebe von Säugetieren wurden verschiedene NMDA Rezeptoruntereinheiten entdeckt, wobei deren Funktion allerdings noch nicht bekannt ist.

Das Ziel dieser Studie war es die NMDA Rezeptorexpression und die physiologische und pathophysiologische Rolle im Herzen, in roten Blutkörperchen (RBK) und in erythroiden Vorläuferzellen (EVZ) zu charakterisieren. In dieser Studie zeigen wir erstmalig, dass NMDA Rezeptoren in EVZ und RBK bei Ratten sowie Menschen exprimiert werden können. Die Rezeptorzusammensetzung aus den verschiedenen Untereinheiten variiert dabei in Abhängigkeit des Reifungs- und Differenzierungsgrades der EVZ und unterscheidet sich generell von der Zusammensetzung im Gehirn. Während Neurone primär NR1 und NR2B Untereinheiten exprimieren, fanden wir in EVZ hauptsächlich NR2D und NR3B Untereinheiten. Diese Rezeptoren liessen sich durch NMDA und Glutamat aktivieren und die daraus resultierende Stimulation führte zu einer massiven, transienten Ca^{2+} Aufnahme in human EVZ sowie humanen und Ratten RBK. Die Konzentrationen von Glutamat und Glycin im Plasma reichen aus, um eine basale NMDA Rezeptoraktivität zu erzeugen und aufrecht zu erhalten. Zusätzlich zu den im Plasma enthaltenen Agonisten Glutamat und Glycin wird diese Rezeptoraktivität jedoch sehr wahrscheinlich durch weitere humorale Faktoren kontrolliert. Interessanterweise exprimieren rote Blutzellen von Sichelzellanämie Patienten eine ausserordentlich hohe Anzahl von NMDA Rezeptoren, was zu einer zu einer stark erhöhten Aufnahme von Ca^{2+} führt. Kalzium ist ein Schlüsselregulator verschiedenster Prozessen in

EVZ und RBK. NMDA Rezeptoren sind dabei besonders in frühen Differenzierungsstadien essentiell für das Überleben der EVZ. Aktivierung vom NMDA Rezeptoren in RBK führt weiterhin zu Veränderungen des Zytoskeletts und des Zellvolumens, zu einer Modulation des oxidativen Status und des intrazellulären pH, sowie zu einer Anpassung der Lebensdauer zirkulierender RBK.

Erhöhte Plasmakonzentrationen von NMDA Rezeptorantagonisten (wie z.B. Homocystein) sind mit verschiedenen Herzkrankheiten, inklusive Herzversagen, assoziiert. Daher war die genaue Charakterisierung von Expression und Funktion der NMDA Rezeptoren im Herz ein wesentlicher Bestandteil dieser Studie. Wir haben die Expression der NMDA Rezeptor Untereinheiten in verschiedenen Bereichen des Rattenmyokards analysiert und konnten einen Zusammenhang zwischen der Zusammensetzung der Herz NMDA Rezeptoren und deren Pharmakologie herausgearbeitet. Dabei haben wir ein ex vivo Model (isoliertes blut-perfundiertes Rattenherz) sowie Sarkolemma Membranpräparationen verwendet, mit dem wir den NMDA Metabolismus im Herz unabhängig von dem im Gehirn analysieren konnten. Wie bei RBK unterschied sich die Zusammensetzung der NMDA Rezeptoren im Herz (hauptsächlich NR3A und NR2D Untereinheiten) von denen im Gehirn und zeigte ausserdem eine ausserordentliche Heterogenität zwischen beiden Herzammern. Die Expression der NR2B Untereinheiten war altersabhängig und ist sehr wahrscheinlich mit einer hypertrophen Remodellierung assoziiert. Die Expression der Untereinheiten NR2A und 2C beschränkte sich hauptsächlich auf die Vorhöfe. Wir fanden heraus, dass NMDA Rezeptor Agonisten und Antagonisten die Herzrate und den Herzrhythmus autonom regulieren. Dabei zeigte sich, dass die myokardiale Repolarisierungs- und Depolarisierungsrate durch NMDA Rezeptorantagonisten verlängert wurde. Unsere Daten verdeutlichen, dass Herz NMDA Rezeptoren sehr geeignete Ziele für pharmakologische Interventionen sind, um Arrhythmien und andere kardiovaskuläre Krankheiten zu behandeln.

4. Introduction

Chapter 1

NMDA receptor properties and pharmacology

Ionotropic glutamate receptors (iGluR)

iGluR belongs to group of ligand-gated ion channels (GABA receptors, ATP-gated channels, nicotinic acetylcholine receptors etc). These channels are capable of coupling the ligand binding to the opening of an electrical pore. Thus, they convert chemical signals into appropriate electrical responses. Ionotropic glutamate receptors are integral membrane proteins composed of four large subunits that form a central ion channel pore. iGluRs subunits have a module-based structure and contain four discrete domains: the extracellular amino-terminal regulatory domain (R or ATD), the extracellular ligand-binding domain (LBD or S1/S2), four transmembrane helices (M1, M2, M3, M4), and an intracellular carboxyl-terminal domain (CTD) (Fig 1).

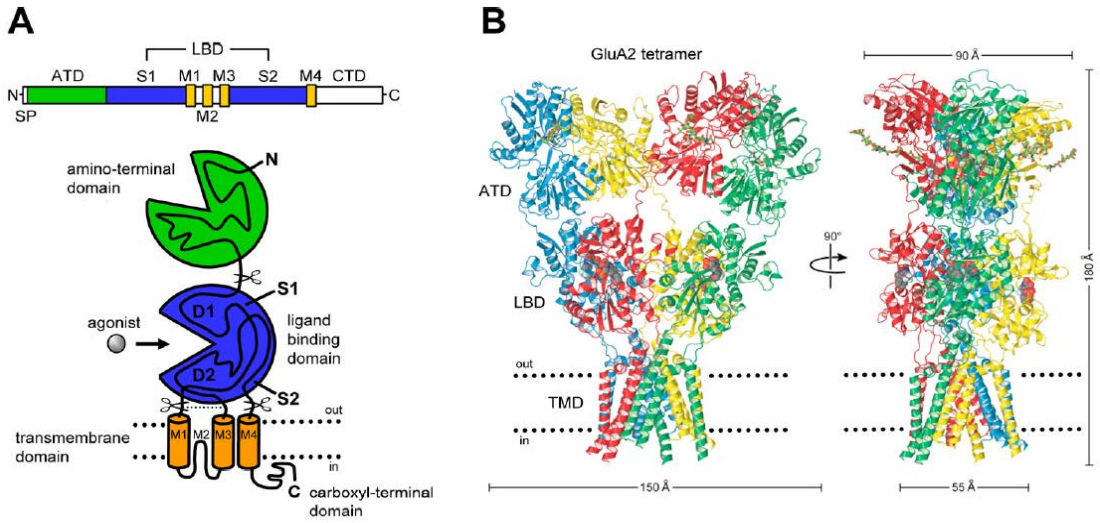

Figure 1.1. Domain organization and structure of iGluR. **A**. A linear representation of the subunit polypeptide chain and schematic illustration of the subunit topology. **B**. Crystal structure of the tetrameric iGluR (here the AMPA receptor) [1].

The mammalian iGluR superfamily consists of α-amino-3-hydroxy-5-methyl-4-isoxazolepropionic acid receptor (AMPAR), kainate, N-methyl D-aspartate 10otentia (NMDAR) and delta receptor families. Most of these receptors require

glutamate (Glu) binding to their ligand-binding domain for the receptor activation, with three exceptions: NMDARs formed by the NR1 and NR3A or B subunits due to the structural properties of their LBS are activated by glycine (Gly) or D-serine, and delta receptor subunit 2 can only bind D-serine [2]. Ligand binding induces subsequent conformational changes first in LBD and then in position of trance-membrane helices which are directly coupled to LBD (see Fig 1 A upper panel). The channel pore opens and allows cations to pass through the pore down their chemical gradients.

Unlike phylogenetically related K^+-channels (see Chapter 2), iGluR have larger channel pore (0.17 nm in diameter for K^+-channel in frog nerve vs 0.55-0.78 nm for different types of iGluR [3]). Thus, interactions between the ions and the pore walls are weaker and pore selectivity is reduced [4]. The iGluR channel pore is permeable for alkali metal ions (Li^+, Na^+, K^+, Rb^+, Cs^+). Moreover, large size of the channel pore allows Ca^{2+} permeabilization (mostly in NMDA and LBD-mutated delta receptors [2]) and Mg^{2+} binding to the channel pore (as well as binding or permeability for other divalent cations like Zn^{2+}, Ba^{2+}, Fe^{2+} [5, 6] and probably Cd^{2+}, Hg^{2+} and Ni^{2+} [7].

Activity of iGluR can be efficiently modified by various regulatory molecules, interacting with ATD, LBD and channel pore. Cytoplasmic C-terminal domain has multiple sites of phosphorylation, S-nitrosylation and palmitoylation [1].

The diversity and complexity of iGluR in mammalian CNS produces broad spectrum of receptor types mediating and regulating synaptic transmission. In the present study we focused on the NMDA receptor family proteins.

NMDA receptor: general properties

The NMDA receptor was named after the specific agonist N-methyl D-aspartate [8] which was used to differentiate between this class of receptor and other classes of ionotropic glutamate receptors. Most of the studied subtypes of neuronal NMDA receptors from rodents (containing NR1/NR2 subunits) have four important properties unique for this family of iGluR:

1) Binding of both agonist L-glutamate and co-agonist L-glycine is required for the complete activation of the receptor [9];

2) Voltage-dependent channel blockade by Mg^{2+} [10] (Fig 2) as well as by other channel-binding divalent cations. Mg^{2+} blocks from both extracellular and intracellular sides, therefore, the NMDA receptor works as a bidirectional rectifier. It passes ions in a voltage range around 0 mV and progressively reduces the current as membrane potential is increased or decreased [11].
3) High permeability for Ca^{2+} [12].
4) Slow activation and deactivation kinetics[13].

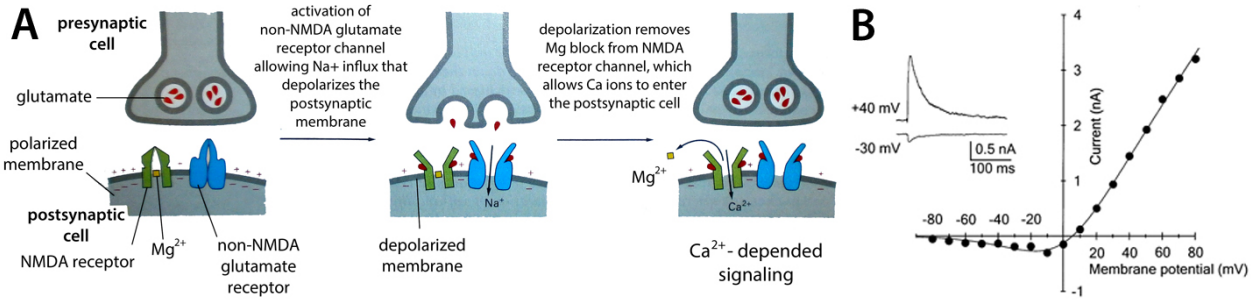

Figure 1.2. Openings of the NMDA receptor channel requires both, receptor activation by agonists and membrane depolarization. **A.** A scheme of the NMDA receptor activation in the synaptic cleft. Glutamate released from presynaptic neuron binds to the NMDA and non-NMDA iGlu receptors permeable for Na^+ and K^+ ions. Following the depolarization of postsynaptic membrane Mg^{2+} ion is released from the NMDA receptor channel pore. That makes NMDA receptor ion channel permeable for the extracellular Ca^{2+} and monovalent cations ([14], p 655). **B.** Voltage-dependent Mg^{2+} block of activated NMDA receptor channels during synaptic transmission [15].

In mammalian brain NMDARs are not critical for the basal synaptic transmission. Though NMDARs have high affinity for glutamate, ion fluxes are blocked by internal Mg^{2+} bound within the opened channel pore at the negative membrane potentials (Fig 2). As a result, the NMDAR channel activation requires both glutamate binding and membrane depolarization. Since NMDARs have much slower activation kinetics than AMPA receptors (AMPAR $\tau_{deactivation}$ < 1 ms, NMDAR activation time ~5 ms [1]), only a strong membrane depolarization (or a sequence of depolarization events) lasting for more than 5 ms will result in NMDAR-related ion fluxes. Thus, NMDARs in the brain act as a molecular coincidence detectors (glutamate release and long-lasting strong depolarization)

and thereby regulate functional plasticity of individual synapses by Ca^{2+}-dependent signaling cascades [16]. The ability of NMDAR to discriminate frequency of synaptic impulses (single depolarization event or low frequency events versus multiple high frequency events) is used by neuronal networks for memory formation [17].

NMDA receptor: molecular organization

The NMDA receptor is a homo- or heteromeric complex composed of four subunits. Each subunit may belong to one of three types (in mammals): NR1, NR2 (subtypes A-D) and NR3 (subtypes A and B) [18]. Properties of NMDA receptor are defined by the domain structure of the receptor subunits. As with all iGlu receptors, each subunit is composed of an extracellular amino terminal, four hydrophobic channel forming domains and intracellular carboxyl terminal. The extracellular part of the receptor contains amino terminal domain (ATD) that binds allosteric modulators like Zn^{2+} (NR2A) or polyamines (NR2B) (Fig 2A). The amino acid binding domain is formed by S1 segment located between ATD and first transmembrane domain (M1) and S2 segment located on extracellular loop between M3 and M4. The S1 and S2 segments form bilobed structure with the cavity for glutamate (NR2 subunits) of glycine (NR1 and NR3 subunits) binding.

Different expression systems used for detailed investigation of the NMDA receptor properties have introduced substantial variability in the obtained data. For example, when HEK293 cells was used as a model expression system for the NR1 and NR2A subunits, channel pore opening was achieved only if *both* Gly and Glu were present for binding NR1 and NR2A subunits respectively (Figure 3B), [19]. Similar NR1/NR2A-containing receptors expressed in *Xenopus* oocyte produced high amplitude but slow deactivation current when stimulated with glycine alone. Experiments with Glu-site antagonist APV showed that Gly was probably binding to Glu site and therefore causing receptor activation [20]. Receptors built exclusively by NR1 and NR3 subunits unlike “classical” NR1/NR2 containing receptors have an intermediate opening state when only one type of subunits interacts with agonist (NR3 on Fig 2C).

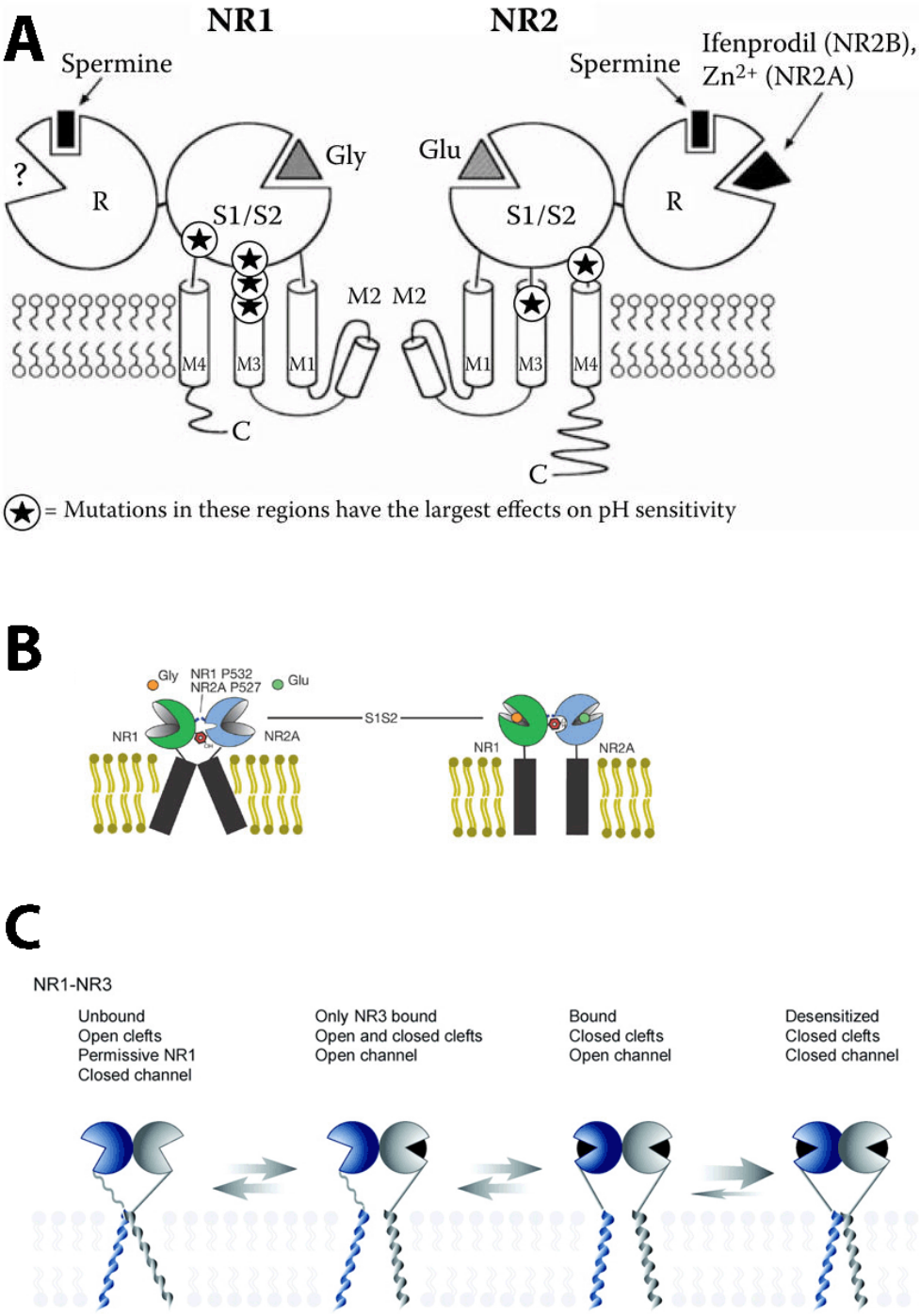

Figure 1.3. A. Domain organization of the NMDA receptor NR1 and NR2 subunits. Glycine and glutamate bind to the shell-like structure formed by S1/S2 compartments of ligand binding domains (LBD). External ATD I domain binds various allosteric modulators. pH-sensitive residues were identified in M3 and M4 regions of both NR1 and NR2 subunits [21]. **B.** Proposed mechanism of agonist-dependent channel opening in NR1/NR2 heterotetramer [19]. **C.** Model for the intermediate activation state of NR1/NR3 receptors [22].

The M2 and M3 transmembrane regions are participating in channel pore formation. Point mutations in the M2 region of NR1 subunit may significantly alter the channel selectivity for mono and bivalent cations [23]. A single residue within the M3 segment of the NR2 subunit define the single-channel conductance, selectivity for cations, in particular to Ca^{2+} ions, and affinity to Mg^{2+}. Mutation of a Ser-632 to Leu in this segment of the NR2A subunit makes the NR2A/NR1-receptor acquire the properties of the channel formed by the NR2D and NR1 subunits [24].

Receptors, containing NR3 subunits are resistant to Mg^{2+} block under physiological conditions. NR1/NR2/NR3 heteromeres cannot be blocked by 1 mM of Mg^{2+} at negative membrane potentials [25]. Site-directed mutagenesis of the NR1 and NR2 subunits within the channel pore region revealed that Mg^{2+} ion is coordinated four Asn residues, one from each NR1 and NR2 subunits. In rodents NR3 subunits have Gly residue instead of Asn in these positions. Voltage-dependent Mg^{2+} block could be recovered in NR1/NR3 receptors by replacement of Gly or nearby amino acid residues with Asn in NR3 subunit [26]. Thus, incorporation of NR3 subunit dramatically changes NMDA receptor channel properties. In human NR3B subunit same position is occupied by arginine residue [27]. Properties of human NR3B-containing receptors were not studied so far.

At present "the existence" of functional NR3/NR2 channels remains a matter of discussion. Smothers *et al* have recorded the Glu-Gly-depended currents in HEK293 cells expressing NR3 and NR2 cDNA [28]. Earlier on it was claimed that, when expressed in HEK293 cell line, NR3/NR2 oligomers can assemble in the endoplasmic reticulum, but their trafficking to the plasma membrane is not possible in the absence of NR1 subunit [29]. The reason of this controversy could be related to the various culturing conditions and cell type. For example, functional NR1/NR3 receptors were successfully expressed in *Xenopus* oocytes [30], [22]. In HEK293 cell line only one group obtained electrophysiological recordings from native and mutant NR1-NR3 receptors [28], whereas the other group failed to express functionally active NR1-NR3 receptors in that cell line [31]. So far it is not clear if NR3 subunit may replace NR1 for the receptor assembly and trafficking. Under the current paradigm NR1 subunit is necessary for the

NMDA receptor translocation to the cytoplasmic membrane and function. Based on this assumption, many researchers concentrate on the NR1 abundance when looking for NMDA receptor in non-neuronal tissues. That approach can be fruitless.

NMDA receptor: channel properties

Depending on the subunit composition the properties of the NMDARs are very diverse. Based on the knowledge obtained using various expression systems the following structural-functional interactions are revealed linking the receptor subunit composition, the channel cation selectivity, amplitude of currents, inactivation time, and sensitivity to Mg^{2+} block and synthetic antagonists.

NR1-NR2 receptors are 4-8-fold more permeable for Ca^{2+} than for alkali cations. Receptors containing NR3 subunits have about 2-4-fold higher permeability for alkali ions compared to that for Ca^{2+} (see Table 1). The cation selectivity is believed to be determined by a single amino acid residue at the tip of the reentrant pore loop in the region called QRN (framed in Fig 4). In iGluR the residue in the apex of M2 region is either Gln (Q) in AMPA receptors, or Arg I in kainite, and Asn (N) in NMDA receptors. Notably, this position in NR3 is occupied by Gly (Figure 4) leaving more space for the cations to pass through the pore and opting for poor selectivity of the channel filter to cations [26], [32].

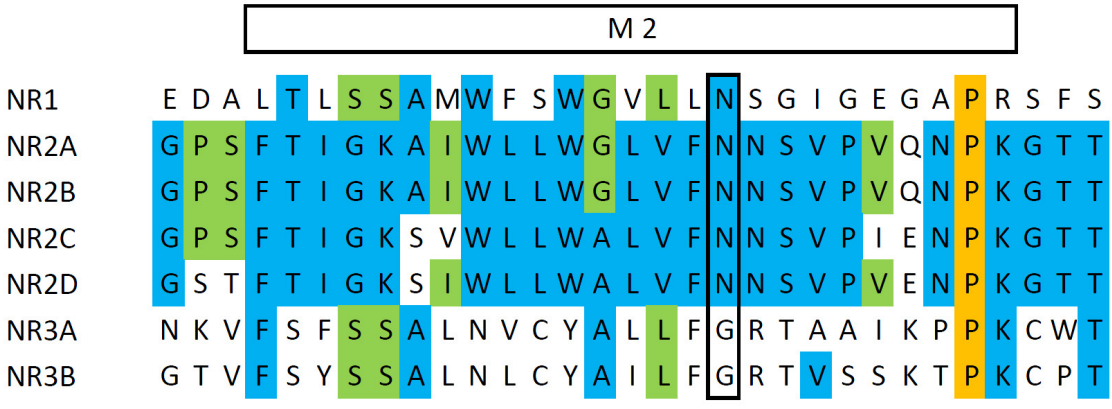

Figure 1.4. Amino acid sequence alignment of M2 region in human NMDA receptor subunits. Fully conserved residues are orange, conserved residues are blue, and less conserved residues are shown in green. QRN residue marked in the

black frame. The NR3A and B amino acid sequences in this region are highly different from both NR1 and NR2 subunits. Modified from [33].

In contrast to Ca^{2+}-permeable NR1-NR2 receptors with pronounced Mg^{2+} block, NR1-NR3 receptors are resistant to Mg^{2+} inhibition, but can be blocked by other divalent cations such as Ca^{2+} and Ba^{2+} at negative membrane potentials [5], [34]. Notably, NR1-NR3A receptor expressed in *Xenopus* oocytes was blocked by extracellular Ca^{2+} ions at negative membrane potentials within the physiological range (1.8 mM of $CaCl_2$ is present in the blood plasma).

For **Mg^{2+} block** to occur **NR2** subunit should be present in the NMDAR in which Asn (N) is conserved in the QRN domain [35]. Whereas NR2 is replaced by NR3, blocking by Mg^{2+} does not occur at negative membrane potentials as it lacks N in the QRN region (Fig 4). Moreover, even the slight differences in M2 sequence between NR2A/B and NR2C/D subunit types are sufficient to produce high variety in sensitivity of the receptors to Mg^{2+} block (see Table 1 and Fig 4).

The QRN region in **NR1** subunit is responsible for **Ca^{2+} selectivity**, the replacement of Asn (N) to Gln (Q) or Arg I substantially decreases channel permeability for Ca^{2+}.

The following structural/functional interactions may be postulated for the NMDA receptors:

1) NR1 + NR2 ➔ high Ca^{2+} permeability, Mg^{2+} block
2) NR1 + NR3 ➔ low Ca^{2+} permeability, no Mg^{2+} block, but potential-dependent Ca^{2+} block, altered I/V curve
3) NR1 + NR2 + NR3 ➔ reduced Ca^{2+} permeability, reduced Mg^{2+} block
4) NR2 + NR3 ➔ (predicted) low Ca^{2+} permeability, normal Mg^{2+} block, very slow deactivation kinetics, altered I/V curve.

Deactivation time of the receptor (τ) is controlled by the type of NR2 subunit and by the splice variant of NR1 subunit (Table 1). NMDA receptors demonstrate great variability in the time of current decay depending on the subunit composition. Slow decay kinetics of the ion currents is produced in presence of NR2D subunit due to the slow dissociation of glutamate from this receptor subtype. A point mutation in glutamate binding site of the NR2D subunit

produced up to a 60-fold faster deactivation of the ion current [36]. Thereby, properties of the LBD (or ligands with the different affinity to the receptor) may influence the kinetics of ion currents. Exon 5 splicing in NR1 combined with NR2 results in prolongation of the deactivation time (see NR1a, NR1e splice variants in Table 1). The presence of exon 5 is associated with much shorter channel opening time interval (NR1b, NR1g) [37]. Two other NR1 exons, 21 and 22, can also undergo alternative splicing, however, they are present in carboxyl-terminal domain and have much smaller influence on channel properties (for example, both NR1a and NR1b consist of 21 and 22 exons but both NR1e and NR1g do not, see Table 1).

In neuronal cells NMDA receptors exist within the multi-protein complex consisting of several dozens of proteins involved in signal transduction [38]. Many of them are calcium-sensitive kinases and phosphatases that can be directly activated by Ca^{2+} within the micro-domain around NMDA receptor ion channel. But, despite the local increase in Ca^{2+} concentration, NMDA receptors may affect cellular concentration of Ca^{2+} due to high single channel conductance (around 40-50 pS) [39]. This value exceeds conductance of L-type calcium channels by ~20-fold [40]). Even a single opening of the NR1/NR2 containing NMDA receptor channel is sufficient to raise Ca^{2+} concentration within 1 μm^3 volume (for example, in a spine head of dendrite) by 1 μM [39]. The exact amount of Ca^{2+} passing through the NMDAR channel can be efficiently adjusted by altering the subunit composition of the receptor, duration and frequency of agonist exposure [41], by various allosteric modulators, lipid-protein and protein-protein interactions, and secondary modifications of the receptor. Due to the low Ca^{2+} permeability and other specific properties, physiological role of the NR3-containing receptors probably differs from that of the receptor formed by the NR1 and NR2 subunits, see Chapter 3 for examples.

NMDA receptors: ligand binding domain

Agonist-induced control over the channel gating is similar in all types of iGluRs. Crystallorgaphic studies indicate that ligand binding to the cleft formed by S1/S2 domain is followed by cross-dimerization of both hydrophibic and

nonhydrophobic regions of the S1 domains of the neighboring pairs of NMDAR subunits (Fig 3B). Mechanical movement of S1/S2 domain during the ligand binding leads to the rotation of M3 helices away from the central axis of the pore and opening of the channel gate.

The S1/S2 domain is forming clamshell-like structure with amino acid (agonist) binding pocket interacting with α-carboxyl and α-amino groups. In Glu-binding NR2 subunits ligand-interacting residues in S2 region are fully conserved within all four types (A-D). However, in S1 region the NR2 sequences are much more diverse. Glycine-binding NR1 and NR3 subunits together with non-functional delta receptors (GluD) have the lowest sequence similarities among all iGluRs (Fig 5). These differences suggest that Glu-binding ability was preserved during evolution of iGluR, while glycine/D-serine binding ability emerged later in time, and probably independently, for the NR1 and NR3 subunits. Pronounced differences in the LBD sequences of the NR1 and NR3 subunits S1/S2 domain are associated with a broad range of their ligand-binding properties. While the receptor formed by the NR1 subunits has fairly high affinity to glutamate (EC50 0.81 μM, see Table 1), heteromer containing NR1 and NR3 subunits has very low affinity to Glu with a Kd = 9.6 mM, which is well above the physiological range (peak Glu concentration in the synaptic cleft in around 1 mM [42]). Affinity of these heterotetramers to Gly is fairly high (Kd = 40 nM) and Kd for D-serine is within the micromolar range [43]. However, despite the similar affinity to the LBD of NR1 and NR3 subunits, D-Ser is activating only 25% of the current amplitude evoked by Gly in NR1/NR3 receptors [28].

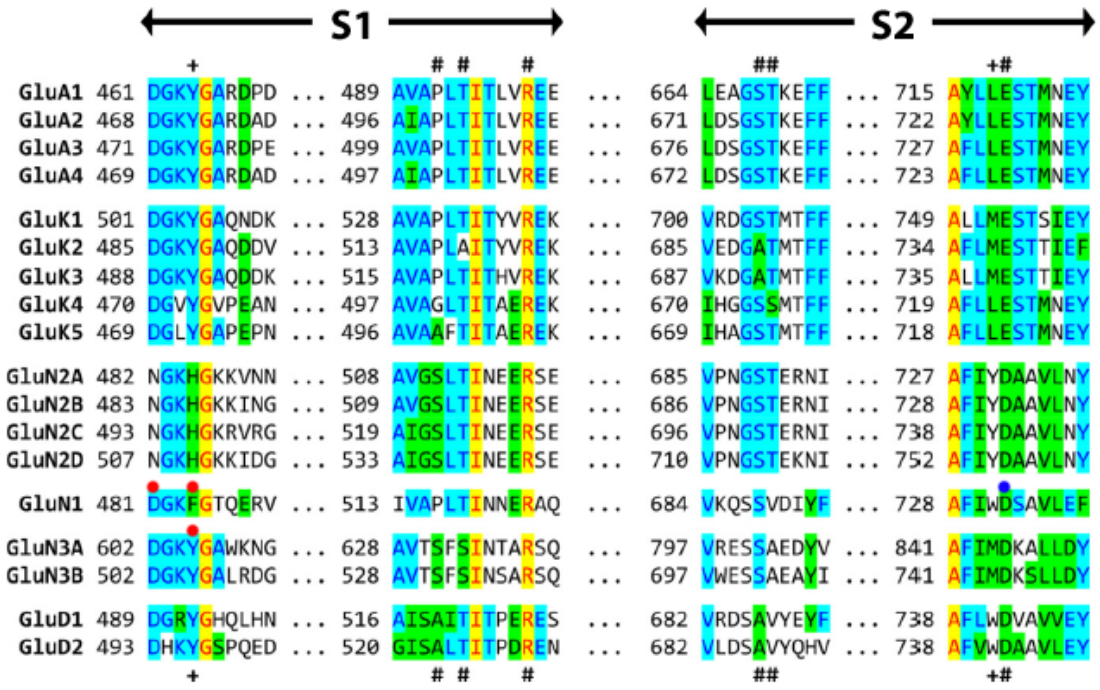

Figure 1.5. Agonist-binding residues of human glutamate receptor subunits. Fully conserved residues are shown in yellow, conserved residues are shown in blue, and similar residues highlighted in green. # denotes residues capable of forming hydrogen bonds or electrostatic interactions with the agonist; + denotes residues capable of forming van der Waals contacts with the agonist. Red dots indicate residues replacement of which leads to dysfunctional binding site for Gly. Blue dot indicates residue replacement of which was not affecting Gly sensitivity. Modified from [1].

To evaluate role of NR3 subunits within the NMDA receptor point-mutagenesis studies were performed [22]. Binding of both Gly and Glu is required to activate the "classical" NMDA receptor consisting of two NR1 and two NR2 subunits [19], Fig 3B. When Phe residue in position 484 of NR1 subunit (see Fig 5, red dot) was replaced by Ala, agonist binding to these subunits was completely abolished. The receptor formed by the mutated NR1(F484A) and NR2 was not producing detectible current in response to activation with 200 μM NMDA and 1 mM Gly. In contrast, NR1(F484A)/NR3 receptors were able to produce even higher Gly-activated currents than non-mutated NR1/NR3 receptors. To explain these findings Furukawa *et al* have proposed the existence of a subconductance state in the NR3-containing receptors (Fig 3C). The subconductance state was described for AMPA (GluA) and kainite (GluK) receptors [44], however, was never observed for NR1/NR2 receptors. Amino acid sequence of S1 region of NR3

subunits resembles of GluA and GluK rather than NR2 subunits (see Fig 5). Smothers and Woodward showed that glycine-activated currents of NR1/NR3 receptors displayed characteristics similar to those shown by AMPA receptor [28]. These currents with a fast onset showed rapid desensitization to the steady-state levels. But, unlike AMPA receptors, these currents were not activated by glutamate, and desensitization was unaffected by AMPA receptor allosteric modulator cyclothiazide [28]. The NR1/NR3(Y605A) receptor with dysfunctional Gly-binding site in NR3 subunit was unable to conduct any currents. Thus, the NR3 subunit seems necessary for effective engagement of NR1 in NR1/NR3 receptor activation [22] and displays unusual properties of the receptor activation.

Enantiomers of Gly and Glu are capable to activate NMDA receptors with different efficiency. The most potent agonist binding to NR1 subunit is D-serine. D-Ser has about the same affinity to NR1-NR2(A-D) receptors as Gly (0.16-1.3 μM). D-serine is currently suggested to be the dominant NMDAR co-agonist in the brain [45]. At the same time L-serine is 100 times less potent in induction the NMDA receptor activation than D-serine. Furthermore, NR1 subunit is also capable to distinguish between D- and L- isoforms of other amino acids. For example, affinity of the receptor to L-alanine is 10- to 100-fold lower than that to D-alanine [1].

Similarly to NR1, NR2(A-D) subunits are also capable to distinguish between the L and D isoforms of their main agonists Glu (IC_{50} for radiolabeled L-[^{3}H]glutamate replacement is 0.31 μM for L-Glu and 23 μM for D-Glu) and NMDA (14.5 μM for L-isoform, NMLA, and 3.68 μM for D-isoform) [46]. At the same time, for the other structurally similar amino acids, such as aspartate, NMDA receptors did not develop such strong selectivity for D over the L-isoforms. Thus, two main NMDA receptor agonists are D-amino acids. Similar to that highly conserved delta receptors are also capable of binding D-amino acid serine. Based on these observations a hypothesis has been proposed that D-amino acids were used earlier on in evolution for the signal transduction in attempt to distinguish them from metabolically active L-amino acids before glutamatergic synapse had appeared (see Chapter 2).

NMDA receptors: physiological allosteric modulators

Extracellular proton concentration is an important regulator of the NMDA receptor function within the living tissue. Amino acids in control of the receptor pH-sensitivity are highlighted as stars in Fig 3A. NMDA receptor channel opening probability for all known receptor types is maximal with alkali pH above 9, and all types of NMDA receptors are inhibited when pH is below 4 [47]. Human brain extracellular pH varies between 6.8 and 7.5 [48]. Within this interval different NMDA receptor subunits possess various pH sensitivity. About half of the receptors composed of NR1/NR2 (A or B or D) are inhibited at pH 7 [49]. NR1/NR2C receptors are resistant to "low" pH values and only 15% of them are inhibited at pH 7 [47]. In NR1 homotetramers pH sensitivity is highly dependent from the presence of exon 5 (Table 1) [50]. NR1/NR3 receptors are very sensitive to proton-induced inhibition with either of NR1 splice variants [30].

Zn^{2+} is one more major regulator of NMDA receptor activity under physiological conditions is Zn^{2+} ion. Zn^{2+} accumulates in synaptic vesicles of specific neurons and can be released into the synaptic upon stimulation [51]. In NR1/NR2A receptors low Zn^{2+} concentrations (nanomolar range, see Table 1) are reducing channel opening probability independently of the membrane potential [52]. The apparent concentration of free Zn^{2+} ions in the brain is between 1 and 10 nM, that is sufficient for partial receptor inactivation [53]. At higher Zn^{2+} concentrations (10-100 μM) and negative membrane potentials Zn^{2+} produced voltage-dependent fast channel block. Notably, Zn^{2+}-dependent block was shown to form more than an order of magnitude faster than Mg^{2+} block. Furthermore, at depolarized potentials Zn^{2+} had higher affinity to the NMDA receptor channel than Mg^{2+} (K_d 0.9 mM vs 8.8 mM) [52]. The amount of Zn^{2+} released into the synaptic cleft upon stimulation was estimated to be between 10 – 30 μM [53]. Thus, we can conclude that both voltage-dependent and voltage-independent mechanisms of NR1/NR2 receptor inhibition may occur in the brain. Surprisingly, Gly-induced currents through the NR1/NR3 receptor were potentiated by 50 μM of Zn^{2+} at negative membrane potentials due to the relief of voltage-dependent Ca^{2+} block [5]. Thus, while Glu-activated NR1/NR2 receptors

are inhibited by Zn^{2+} during the Zn^{2+}-sensitive synaptic transmission, Gly-activated NR1/NR3 receptors are potentiated.

NMDA receptor: channel pore antagonists

Many synthetic NMDA receptor antagonists were designed to study the receptor properties *in vitro.* Some of them are used *in vivo* for various purposes (anesthesia, treatment of neurological disorders, recreational drug abuse). In the present study three of NMDA receptor pore-targeting antagonists were investigated: the anesthetic drug ketamine, anti-Alzheimer drug memantine and MK-801 (the most popular channel pore targeting blocker of the NMDA receptor). Although it is believed that all of them are targeting the "PCP-binding site" within the channel pore, they are actually interacting with different amino acid residues. In ***rodent*** NMDA receptor MK-801 interacts with M1, M2 and M3 transmembrane domains, while memantine binds mostly to M2 domain and shows 100-fold lower affinity to the receptor than MK-801 [23]. The NR2 subunit composition does not influence the receptor affinity to MK-801, but does impact its affinity to ketamine and memantine (Table 1). Under physiological conditions Mg^{2+} ions act as an endogenous NMDAR channel blocker displacing the antagonists from their binding sites and reducing thereby their inhibitory power [54, 55]). NR1/NR2A and NR1/NR2B receptors have high affinity to Mg^{2+} (Table 1) and in such receptors memantine and ketamine inhibition is ineffective. In contrast NR1/NR2C and NR1/NR2D receptors with low Mg^{2+} affinity shows pronounced inhibition by memantine and ketamine [54]. For that reason memantine and ketamine mostly affect NR1/NR2C and NR1/NR2D receptors in the rodent brain.

The presence of the NR3 subunits in heterotretrameric NR1-NR2-NR3 receptors does not affect the receptor sensitivity to ketamine (as well as its sensitivity to Mg^{2+} block) when compared to the corresponding NR1-NR2 receptor [33]. NR1/NR3 receptors are highly resistant to the inhibition by MK-801, memantine and ketamine making these receptors difficult to study (Table 1).

Table 1.1. Pharmacological properties of NMDA receptors as a function of their subunit composition. Where possible, EC_{50} and IC_{50} values were taken from a single study for all variety of the heteromeric receptors. Those values may be highly dependent from the experimental setup and the NR1 subunit splice variant. Note the highly specific properties of the NR1/NR3 receptors compared to those of the NR1 homomers and the receptors formed by the NR1 and NR2 subunits.

	NR1	NR2A	NR2B	NR2C	NR2D	NR3A/B+NR1
Glycine EC_{50}	0.18 μM (homomer) [56]	2.1 μM [57]	0.3 μM [57]	0.2 μM [57]	0.1 μM [57]	0.04 μM, 1-6 μM [18] 20-50 μM [28]
Glutamate EC_{50}	0.81 μM (homomer) [56]	1.7 μM [57]	0.8 μM [57]	0.7 μM [57]	0.4 μM [57]	Nd [43], Kd = 9.6 mM [58]
τ_w (deactivation time)	**NR1a 745 ms NR1b 194 ms NR1e 563 ms NR1g 167 ms [37]	50 ms [59]	300 ms [59]	280 ms [59]	1.7 s [59]	Seconds [60]
Mg^{2+} block	High affinity [30]	High affinity [61], 34 μM (-80 mV), 0.7 mM (-40 mV) [62]	High affinity [61]	Lower affinity [61]	Lower affinity [61], -80 mV: 91 μM, -40 mV: 1.6 mM [62]	Resistant? [34], [25]
$P_{Ca^{2+}}/P_{Cs^+}$*	?	8 [24]	7 [24]	5 [24]	4 [24]	0.8 or 0.6 for NR1/NR2/NR3 [25] [29], NR1/NR3 0.4 [26] <0.25, voltage-depended Ca^{2+} block [5]
pH, IC_{50}	6.6 (+ exon 5) 7.4 (- exon 5) (homomer) [50]	7 [47], 6.9 [49], 7.2 [57]	6.8 [47], 7.5 [49], 7.3 [57]	6.4 [47], 6.2 [57]	7.5 [49], 7.3 [57]	Approx. 7.4 [30]
Zn^{2+}, IC_{50}	**+ exon 5**: <1 μM potentiation, >1 μM	10 nM [49]	1 μM [49]	30 μM [64]	10 μM [49]	Potent activator [5]

	inhibition; **- exon 5**: inhibition only (homomer) [63]					
MK-801, IC_{50}	18 nM (homomer) [65]	13 nM [66]	13 nM [66]	11 nM [66]	38 nM [67]	NR1/NR3 10 μM no effect [28]
Ketamine, IC_{50}	?	16100 nM [67]	1550 nM [67]	1110 nM [67]	1500 nM [67]	NR1/NR3 5% inhibition by 100 μM [28]
Memantine, IC_{50}	?	4360 nM [67]	1200 nM [67]	601 n M [	820 nM [67]	NR1/NR3 10 μM no effect [28]
Ifenprodil, IC_{50}	0.28 μM (homomer) [68]	146 μM [68]	0.34 μM [68]	Low [69]	Low [69]	NR1/NR3 10 μM no effect [28]

* Na^+ and Cs^+ are considered to be equally permeable

** In combination with NR2B

Chapter 2

NMDA receptors: origin and evolution

Origin of iGluRs

iGluRs were first discovered and studied [70] in vertebrates, mainly in mammals. Since then iGluRs were mostly studied in the context of excitatory neurotransmission processes in the central nervous system of vertebrates. However, in 1998 the first four and by 2003 16 other homologue of mammalian iGluRs genes were discovered in organism lacking nervous system, in the plant *Arabidopsis thaliana* [71]. This finding suggested that iGluRs-like receptors (GLR) were expressed in the ancestor organisms existing prior to divergence of plants and animals, sometime before 1.6 billion years ago [72].

iGluRs share physiological properties of ligand-gated ion channels with the acetylcholine and GABA receptors and transmembrane topology of a channel-forming domain in voltage-gated potassium channels [73]. It was proposed that iGluRs appeared as a product of chimeric genes assembled by an exon shuffling between the genes coding for the K^+ channel-like protein and the amino acid binding protein [74], [75], (Fig 1).

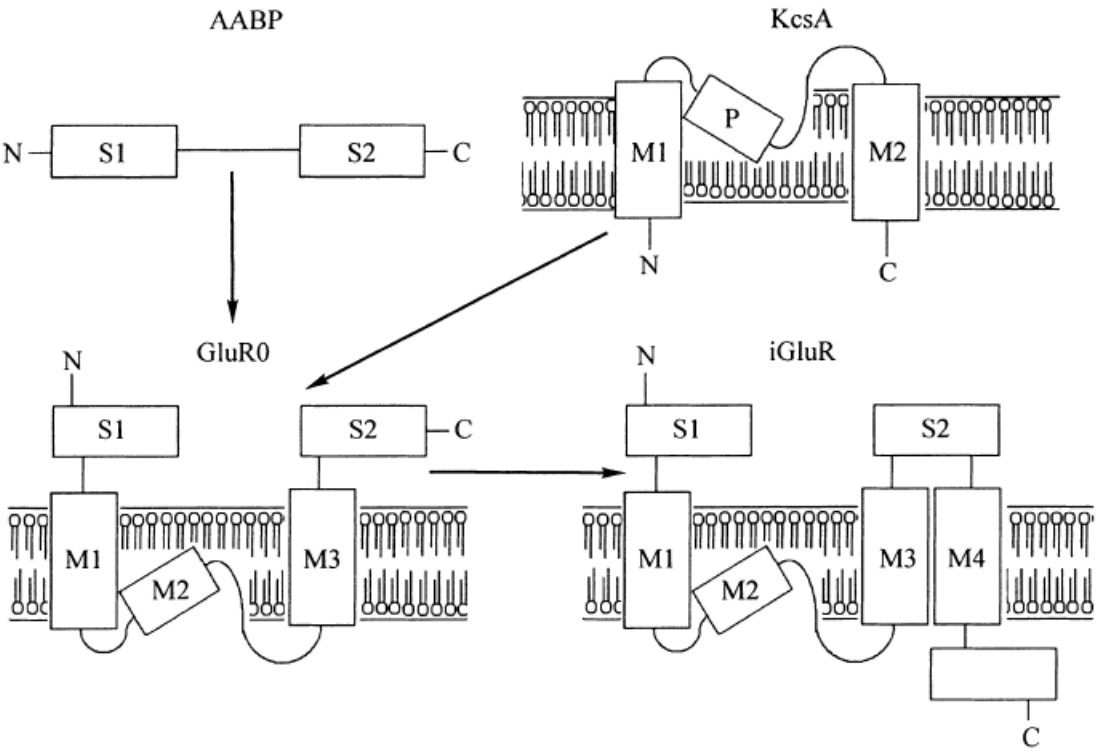

Figure 2.1. Possible origin of iGluRs. Insertion of the channel-forming domain (KcsA) between the amino acid-binding protein (AABP) domains (S1 – **M1 – P – M2** – S2) leads to the formation of a potassium-specific channel (GluR0) in bacteria. M4 transmembrane segment appears in eukaryotic receptors (iGluR) [75].

Such shuffling of mobile domains played a major role in the evolution at the time of metazoan radiation [76]. That hypothesis was supported by discovery of GluR0 receptor in prokaryotic organisms [77]. This receptor is highly homologous to eukaryotic iGluRs ligand-binding domain and at the same time the selective filter of the channel has sequence which is typical for K^+ channels. Activation of GluR0 receptors induces potassium-mediated outward current hyperpolarizing the membrane thus stabilizing the negative resting potential (in E. coli resting membrane potential is between -220 and -140 mV depending on the growth stage [78]). The iGluR channels of eukaryotic organisms lack cation selectivity and the channel opening leads to membrane depolarization [75]. Based on these findings it was suggested that such changes were developed during the rise of multicellularity for the purpose of the cell-to-cell signaling.

However, genealogical analysis showed that the animal iGluRs along with plant GLR are representing distinct ion channel class [77] (Fig 2). They claim that

similarity of the iGluR structure to other cation channels may be due to the convergent evolution.

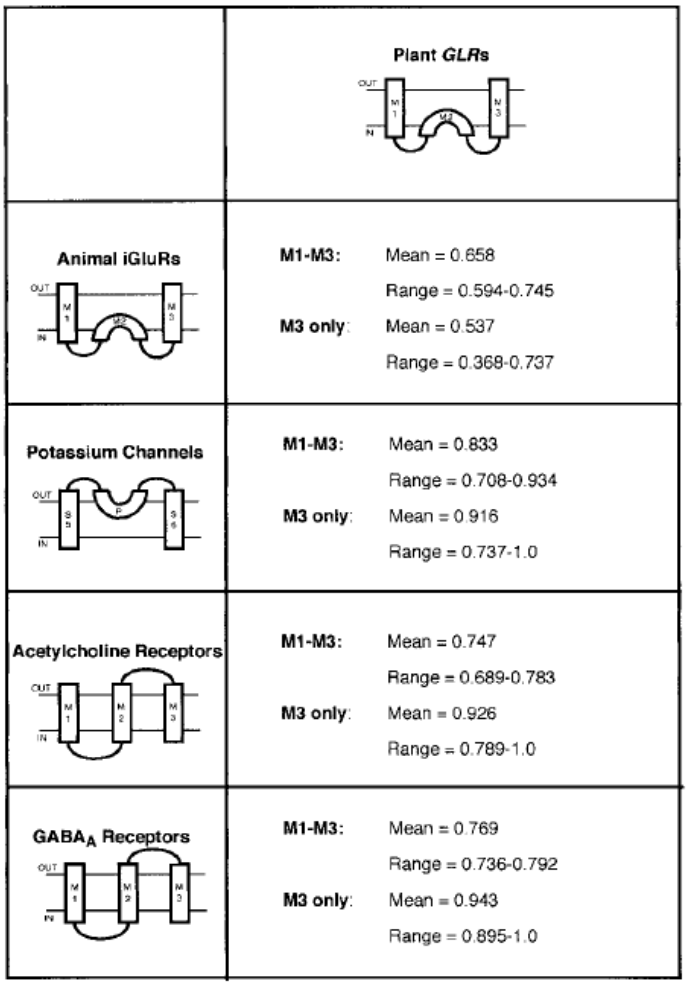

Figure 2.2. Absolute distances between plant GLRs and four classes of ion channels in transmembrane regions [73]. The smaller the distance values, the more related the sequences.

It was proposed that iGluRs arose via series of point mutations from ancestral receptor most closely related to plant GLRs [79]. At present 20 different GLR subunits were found to be encoded in the *Arabidopsis* genome (from that amount of subunits 8855 unique tetramers may be produced). Electrophysiological and pharmacological properties of one of them (GLR3.4) were studied in transfected animal cells. GLR3.4-based receptors showed several-fold higher preferences to Asn, Ser and Gly over the Glu and high selectivity for Ca^{2+} over Na^{+} ($5*10^4$) under physiological conditions [80]. Sequences of GLR subunits are highly homologous to the animal NMDA receptor subunits. 19 of them are activated by Gly and only

one subunit may efficiently bind Glu [81]. In *Arabidopsis* seedlings (very young plants) GLR regulates hypocotyl ("stem") elongation via Gly-activated Ca^{2+}-dependent signaling. In young *Arabidopsis* plants GLR subunits were expressed in all tissues, but highest variety of subunits was found in roots [82]. In plants GLN receptors play an essential role in maintenance of carbon to nitrogen balance [83], regulation of abscisic acid (plant signaling molecule which regulates germination, transpiration, fruit ripening and other processes) biosynthesis, and in signaling and control of the root growth [84].

During evolution of animal cells four types of iGlu receptors appeared: delta receptors, NMDA, AMPA and kainite receptors. Higher degree of conservation was found between the plant GLRs and animal delta iGluRs in all functional domains (ligand binding domains, transmembrane M1-M3 domains and intermediate protein sequences) [73]. Thus, delta receptors are closest relatives of the ancestor animal iGluR and plant GLR. Similarly to plant GLRs delta receptors are non-responsive to Glu, but they bind glycine and D-serine [85].At some point of delta receptor evolution it lost its ligand-activating property. Therefore, delta receptor channel was studied only in chimeric proteins where ligand binding domain from delta receptors was replaced by the same domain from AMPA or kainite receptors [86]. Remarkably, in contrast to AMPA and kainite iGluRs, chimeric delta receptors were permeable for Ca^{2+} with a ratio 0.86 to monovalent cations (Ca^{2+}: X^{+}). In mammalian brain delta receptors lack the channel activity, however they may participate in signal transduction via metabotropic signaling [87]. Therefore, we may assume that the first ionotropic "glutamate" receptors of eukaryotic cells living more than a billion years ago were most likely Ca^{2+}-permeable and activated by small molecules with Gly-like structure more resembling modern delta and NR1 receptors then glutamate binding AMPA and kainite receptors.

Apparently, rising complexity of the ionotropic glutamate receptors was associated with the raise of multicellularity. In genomes of unicellular organisms *Paramecium* and *Tetrahymena* no NMDA receptor homologous genes were detected [88, 89]. However, in both organisms glycine-binding proteins similar to the NR1 amino acid binding domain were found.

iGluRs in Hydra vulgaris

Perhaps the most ancient iGluRs were reported to be present in hydras. Hydra belongs to the Cnidaria phylum, the most primitive eumetazoans. Cnidaria appeared around 580 million years ago and existed as non-mobile epibentic (sitting on the see bed) organisms (Fig 3A). They were closely associated with microbial mats where dissolved nutrients were abundant [90]. For such animals chemoreception was driving their feeding behavior. Chemoreception in *Hydra* (Fig 3B) is mediated by iGluRs responding to the stimulation with reduced glutathione (GSH). GSH stimulates tentacle movements and mouth opening and oxidized glutathione (GSSG) inhibits that response. Glutamate itself, as well as other agonists of iGluRs (NMDA, D-Ser, quisqualate, kainate) affect feeding behavior and specific antagonists of NMDA receptor (D-APV, Glu site antagonist, DCKA and I2CA, Gly site antagonists, MK-801, channel pore blocker) prevent those effects [91, 92, 93, 94].

[^{3}H]glutamate competed with GSH and GSSG for the binding sites on isolated cellular membranes of *Hydr*a [91]. Moreover, GSH, as well as Glu and Gly, increased binding of [^{3}H]MK-801 to *Hydra* membranes [94]. Those observations indicated that GSH may binds to the ligand binding site of NMDA receptors and therefore increases channel opening probability and, as a result, facilitates MK-801 binding. Furthermore, agonists of other iGluRs, AMPA and kainate, were decreasing specific binding of [^{3}H]glutamate and had functional effects on nematocyst discharge and tentacle pulses (Fig 3C and E) [91, 92, 95]. Of note, physiological response in *Hydra* was observed only when both specific agonists NMDA and D-serine were present [94] (Fig 3D). Later only one type of NMDA receptor subunit was identified in *Hydra* genome. This subunit is highly homologous to Gly (or D-serine) specific NR1 subunit types [96] (Fig 4). Thus, it is possible that an ancient *Hydra* NMDA receptor subunit shares similarities with both NR1 and NR2 subunit types.

In mammalian neurons function of the NMDA receptor is usually coupled with AMPA or kainate receptor. Activated by glutamate Na^+/K^+ permeable AMPA or kainate receptors initiate membrane depolarization releasing thereby voltage-dependent Mg^{2+}-block from the NMDA receptor channel (see Chapter 1). Similar AMPA/kainate – NMDA receptor coupling was shown for *Hydra*. NMDA or

kainate alone had on effect on Hydra's feeding behavior, while together they produced same response as glutamate (Fig 3E,F).

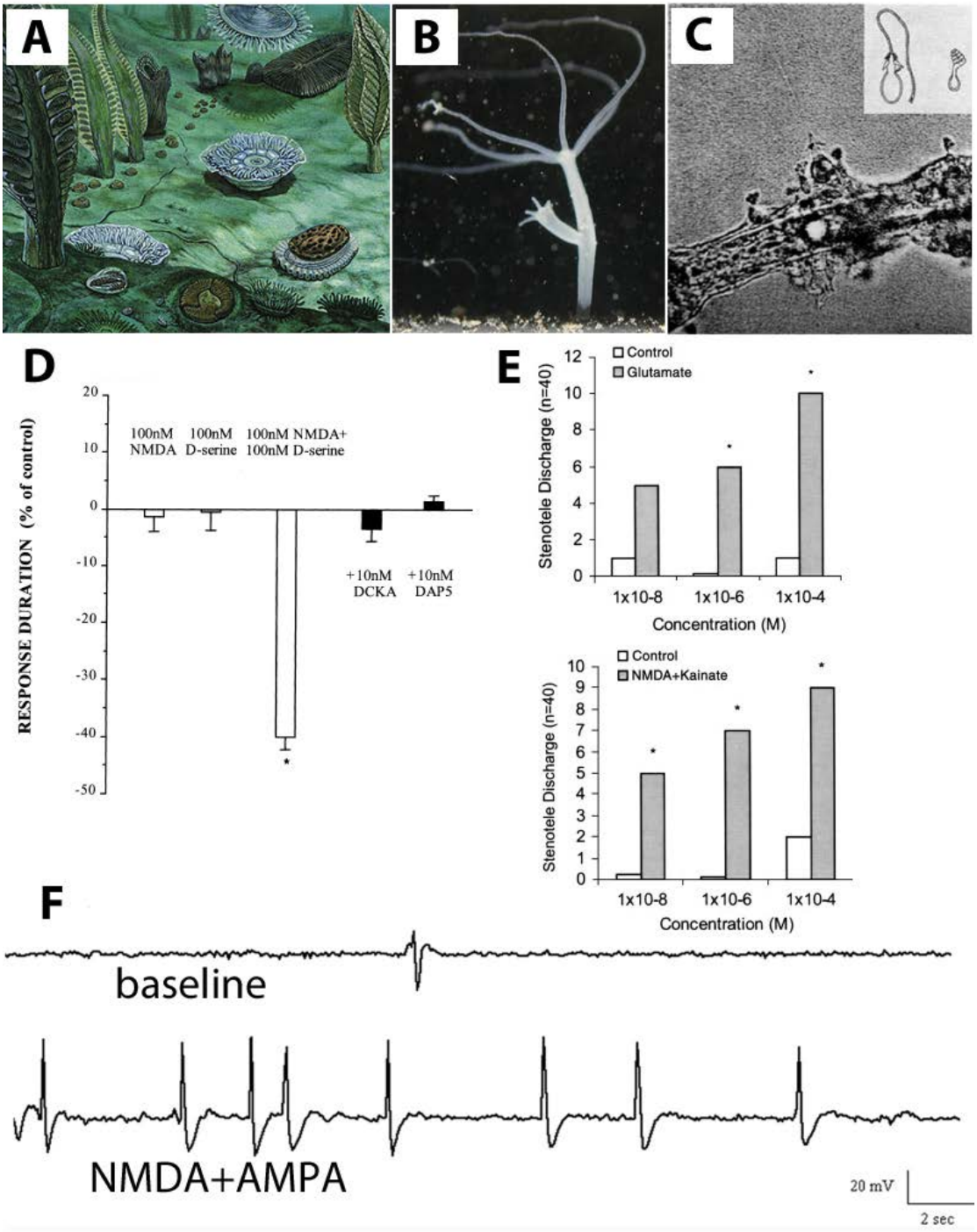

Figure 2.3. Ionotropic glutamate receptors in Cnidaria. **A.** Ediacara biota (635-541 million years ago). Members of the Ediacara biota belong to the first cnidarians and evolutionary precursors of annelids, arthropods and echinoderms [90]. **B.** *Hydra vulgaris*, a modern cnidarian. **C.** Nematocyst discharge

in isolated tentacle of *Hydra vulgaris*. **D**. In a presence of glutathione (10 μM) *Hydra* opens its "mouth" for about 22 min. When both specific agonists of NMDA receptor NMDA and D-serine are present, about 40% reduction in the longitude of GSH-response was observed. Neither NMDA nor D-serine alone had any effect on the GSH-induced response. Specific Gly/D-Ser binding site targeting antagonist DCKA or Glu/NMDA binding site targeting antagonist D-APV both had no effect as well [94]. **E**. Discharge of nematocysts can be activated by glutamate or by a combination of NMDA and kainate [92]. **F.** Recordings from the electrode attached to the tentacle of *Hydra* from a single experiment. "Baseline" is a recording from the control period; "NMDA+AMPA" is a recording corresponding to the treatment period (0.1 μM of each drug) [91].

Functional studies of iGluRs were mainly conducted on *Hydra*. The genomic analysis was made on another cnidarian, sea anemone (*Nematostella vectensis*). Several types of AMPA-like and NMDA-like receptors' subunits, and only one kainate-like receptor subunit sequences were described in *Nematostella* genome [97]. The AMPA receptor orhtologues show higher similarity with their bilaterian counterparts than NMDA receptor. Among NMDA receptor orthologues one NR1-like and four NR2-like genes were identified, which were similar to higher animals where diverse properties of NMDA receptor complex are supported by different types of NR2 subunits. *Nematostella* belongs to the class Anthozoa, phylogenetically basal class of Cnidarians. *Hydra* represents class Hydrozoa, which is further from the ancestor of Cnidarians and bilateral animals (e.g. us). It is possible that *Hydra*'s ancestors lost some of the NMDA receptor genes and thus they were not detected in *Hydra*'s genome [96]. In conclusion, NMDA receptor-based sensing was already used by the most primitive true multicellular organisms.

NMDA receptor in animal evolution

Based on the comparative genomic analysis of the modern animals belonging to different phyla, the conclusion was made that, along with gene duplication, gene loss has been a major factor in genome evolution since divergence from the common ancestor [98]. Gene loss of NMDA receptor subunits probably occurred in roundworm *Caenorhabditis elegance* and fruit fly *Drosophila melanogaster*. These two species are standing much higher in evolutional hierarchy than Cnidarians,

however, both of them have only one type of NR2 subunit and their NR1 subunit gene produces only one type of NR1 protein [99]. Moreover, in *C. elegance* NMDA receptors are expressed only in a few neuronal cells, and their functional role is highly reduced in this animal [100].

Cnydarians are the closest relatives to the ancestor of modern multicellular organisms. The genome analysis of Nematostella and Acropora showed that ancestor organism had higher genetic complexity than modern worms and insects. However, most of the genes (coding cell signaling pathways, membrane receptors and channels, signaling peptides) were preserved in the chordate lineage [101].

All of the three types NMDA receptor gene were identified in our primitive relatives Hemichordata – acorn worm (*Saccoglossus kowalevslii*, [96], Fig 4.). A simplified Chordata *Ciona intestinalis* lost many of its genes during the evolution [102], and only NR1 and one NR2A-like subunits were detected in their genome [103], [96].

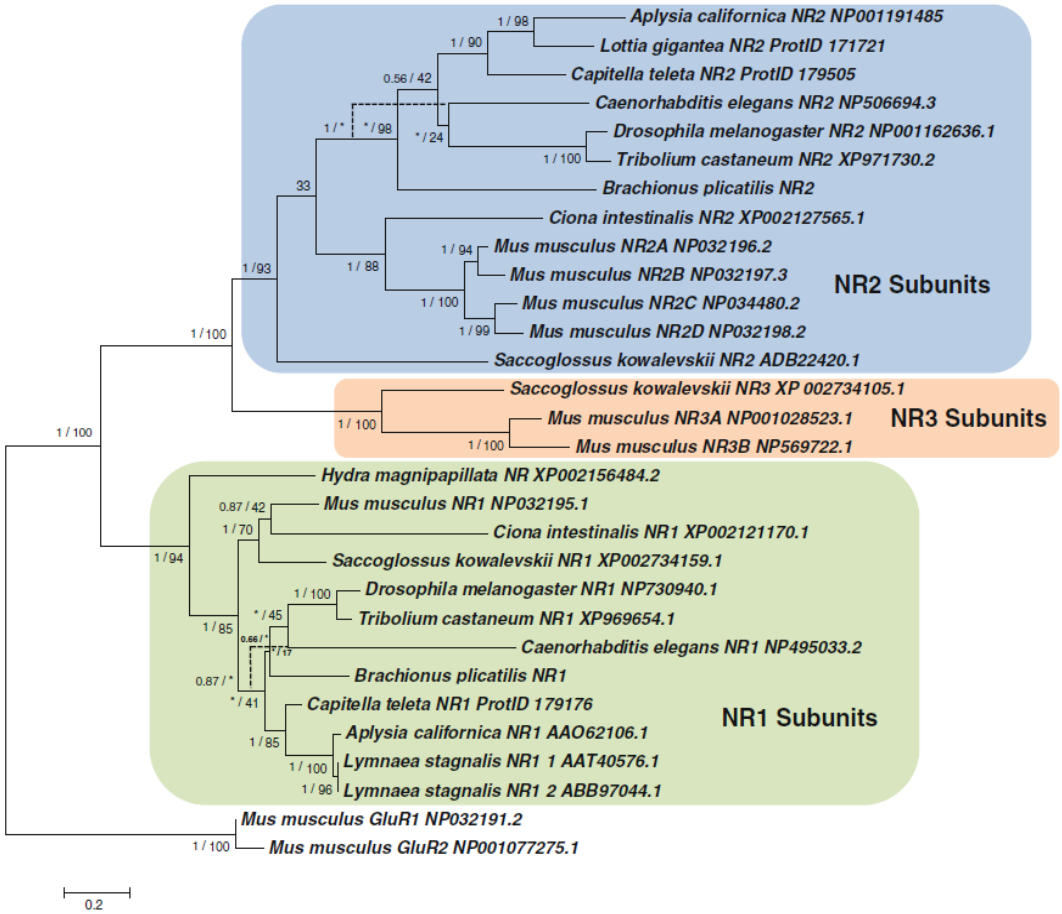

Figure 2.4. The phylogenetic tree of NMDA receptor subunits in animal kingdom (GluR1 and GluR2 – AMPA receptor subunits) [96]. There are three types of NMDA receptor subunits in Chordata (mouse, *Mus musculus*) and in Hemichordata acorn worm (*Saccoglossus kowalevskii*). A simplified Chordata (*Ciona intestinalis*) lost their NR3 subunit type. Animals from the non-chordata lineage (worms, insects and mollusks) have only one type of NR2 subunit and no NR3 subunits. In Hydra only NR1 subunit was identified, however, in more primitive Cnidarians from the class Anthozoa four types of NR2 subunits and one NR1 were detected [97].

Thus, it is uncertain to state which NMDA receptor subunits were present in our early Chordate ancestors. Modern primitive Chordates do not necessarily resemble ancient forms; moreover, they took the same long evolutionary pass as we did, adapting to the specific environmental conditions and loosing many of their genes along with anatomical and physiological characteristics. In our closest non-Chordate relatives Echinoderms NMDA receptors were not studied, however, accidentally NMDA receptor antagonist memantine was found to be toxic for the developing sea urchin embryo [104].

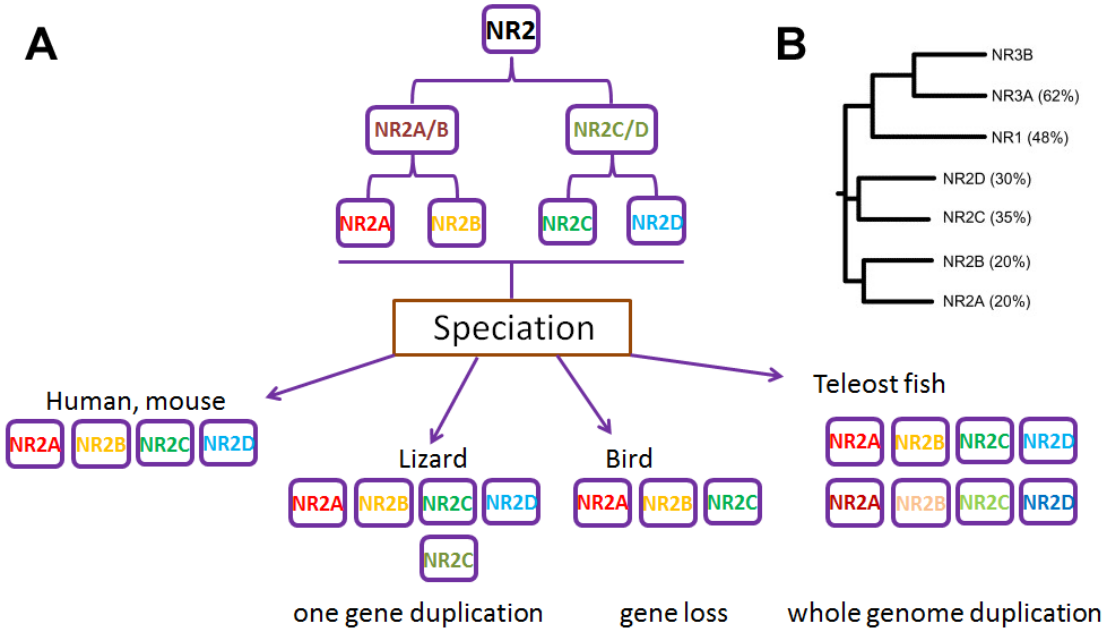

Figure 2.5. A. Divergence of the vertebrate GRIN2 genes [105] **B**. Phylogenetic analysis of NMDA receptor subunits in mouse illustrating phylogenetic relations between NR3A and NR3B subunits and other NMDA receptor subunits [31]. NR3 subunits were found in Hemichordatae, teleost fishes, amphibians, reptiles, birds and mammals.

In genome of bony fishes all types of NMDA receptor subunits similar to those in mammals are already present (Fig 5A). Moreover, in teleost fishes the whole-genome duplication event led to the doubling of all NMDA receptor subunits (for example, NR2D-1 and NR2D-2) [105]. The genome duplication occurred in early Triassic period was beneficial for adaptation to diverse ecological niches [106]. At present teleosts is the largest group of fishes populating salty and sweet waters. Curiously, none of NR2B paralogues appear to be expressed in zebrafish nervous system, but it is present in some other tissue types since expression of NR2B subunit was shown in whole fish homogenate at certain developmental stages [107]. These data suggest that in fishes NMDA receptor expression is not restricted to the neuronal system and its function is not limited to participation in the synaptic transmission.

In genome of lizard only NR2C subunit was duplicated, both genes share high similarity (>99%) and are located in tandem in chromosomal segment, which is a sign of single-gene duplication (Fig 5A). In birds NR2D genes are dysfunctional [105]. Similarly, NR3B subunit is now degenerating in human lineage; about 10% of European population lacks the NR3B subunit [108]. In non-human primates accelerated evolution of NR2A subunit increased the spatial orientation abilities [109]. In humans variations in NR2A and NR2B genes were associated with episodic memory (contextual declarative memory) performance [110].

At present no studies are available on the evolution ofNR3 subunits. However, it is known that mammalian NR3 shares higher homology with mammalian NR1 than with the NR1 subunits of nematode or fly NR1 [111]. Therefore, NR3 has most likely emerged somewhere in the lineage of chordate before the divergence of vertebrates (Fig5B).

NMDA receptors of first multicellular organisms were activated by molecules coming from the environment. Later in evolution NMDA receptors were used for the cell-to-cell communication within the organisms. Thus, production and release of ligands for the NMDA receptors should be precisely controlled in the vicinity of the NMDA receptor complex.. The first NMDA receptor ligand probably was NMDA itself (Table 1). Neuronal tissues of Echinodermata and primitive Chordatae contain high amounts of NMDA, moreover, the highest NMDA concentration was found in the fish brain. Terrestrial animals produce

much less NMDA in the brain but their Glu concentration is rather high compared to that in lancelet's brain. Since metabolism of D-amino acids is slow, there is a possibility that NMDA is used for the tonic activation of neurons rather than for synaptic transmission.

Lancelets produce NMDA from D-aspartate in reaction catalyzed by D-aspartate methyl transferase, similar to rats, but in much higher amounts [112]. The possible reason for "glutamate switch" in terrestrial animals is higher speed of glutamate turnover. Use of Glu allows to decrease the time of neuronal adaptation to new conditions and therefore may have a positive impact on learning abilities.

Table 2.1. Concentration of NMDA and glutamate in neuronal tissues of animals placed in evolutionary order.

Animal, tissue	**NMDA, nmol/g tissue**	**Glu, nmol/g tissue**
Rat, brain	2.97 ± 0.34 [113]	6.0 ± 0.18 [114]
Sheep, brain	2.23 ± 0.49 [113]	?
Chicken, brain	2.22 ± 0.22 [113]	?
Frog, brain	2.24 ± 0.38 [113]	?
Fish, brain	30.55 ± 4.02 [113]	?
Lancelet, cephalic vesicle	10.52 ± 1.41 [112]	2.3 ± 0.4 [112]
Ciona, cerebral ganglion	25.5 ± 4.5 [115]	?
Starfish, radial nerve	17.8 ± 14.3 [116]	?

Together with D-aspartate, D-serine is a second major D-amino acid synthesized in substantial quantities in mammals [117]. Since D-serine has no known function in normal metabolism of animals, it was suggested to participate in the NMDA receptor activation. D-serine binds to glycine site of NR1 and together with NMDA or glutamate and activates the receptor. Unlike glycine, D-serine is a specific NMDA receptor ligand, it shows no cross reactivity with glycine receptors. Similarly to NMDA, D-serine transport systems possess low affinity to their substrate. Therefore, D-serine is retained in the extracellular spaces of the brain for a very long time and its concentration at the synapse is influenced mainly by synthesis and diffusion. However, in the evolutionary new regions

(forebrain) of mammalian brain concentration of D-serine is maintained much higher than in the spinal cord, brainstem, cerebellum and medulla [111] due to the low activity of D-amino acid oxidase in NMDA receptor-rich regions. Higher activity of D-amino acid oxidase discovered in some forms of schizophrenia causes NMDA receptor hypofunction. Moreover, D-serine supplementation was successfully used as a therapeutic approach for that disorder [111]. The combination of two types of NMDA receptor specific agonists within the mammalian brain provides advanced regulation of neurotransmission. Slowly metabolizing D-serine and probably NMDA supports the basal receptor activity and Gly together with Glu are needed for the short-term activation episodes.

Conclusion

NMDA receptors appeared as early in animal kingdom as the first multicellular organisms. NMDA receptor in cnidarians exists beyond the highly specialized neuronal cells and is used for food sensing, hunting and feeding. That indicates a possibility that the NMDA receptors may have functions outside of neuronal system, in different cell types and organs. Studies using primitive laboratory animals such as *C. elegance* and *Drosophila* could be misleading for understanding of NMDA receptor evolution, since they most likely lost some of the NMDA receptor genes during the evolution.

In much more complex organisms like vertebrates NMDA receptor subunit diversity and complexity was increasing along the evolution timeline. Already in bony fishes all types of NMDA receptor subunits are present. Moreover, in fish expression of NMDA receptor was detected outside of the brain. In recent years evidence was accumulating in support of the idea that NMDA receptor expression and function in mammals is not limited by neuronal system as well. NMDA receptors were found and characterized in kidney [118], bone [119] and white blood cells [120]. Moreover, indirect evidences indicate that NMDA receptor has multiple organ-specific physiological functions.

Chapter 3 Implications for NMDA receptors in mammalian heart and red blood cells

Over the billions years of animal evolution NMDA receptors were selected and optimized as efficient ionotropic receptors. In mammalian genome seven types of NMDA receptor subunits coded by individual genes are present. Functions of human and rodent NMDA receptors were most extensively studied predominantly in neurons and in cellular model systems where NMDA receptors were artificially introduced. It was shown that NMDA receptors are involved in control of intracellular calcium levels and calcium-driven processes such as Ca^{2+}-dependent control over kinases and phosphatases, free radical and NO production by NO synthases and NADPH oxidases, regulation of calcium-dependent proteases and gene expression machinery [121, 122, 123, 124].

Unfortunately, too little information is currently available on the expression, composition and function of NMDA receptor in vast majority of tissues with one exception. We know a lot about the NMDA receptors in the brain. This chapter is an overview of the recent developments in our understanding on the role these receptors play in red blood cells and in the heart, on which my PhD project was formed. Before addressing this poorly explored area some selected information is given on the NMDA receptor in our "reference organ", the brain.

Brain

In the brain NMDA receptors are used for modulation of synaptic transmission pathways involved in the formation of memory and in learning. These receptors are abundant in postsynaptic membrane, but also in adjacent astroglial cells contributing to the synapse formation (see Fig 1). Postsynaptic receptors sense transient increase of glutamate levels in the synaptic cleft as it is released from the presynaptic terminal occurring along with the postsynaptic membrane depolarization. Astroglial cells contribute to the synaptic glutamate turnover and to the tonic activation of neurons by D-serine [125]. In rat hippocampus astrocytes mediate glutamate reuptake, they sense the ambient glutamate levels by their

own NMDA receptors which may be formed by all the seven different NMDAR subunits they were found to express [126,127].

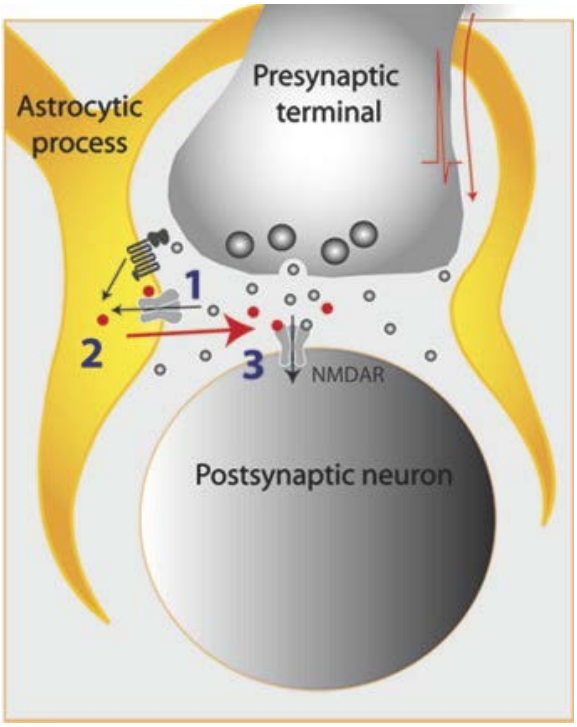

Figure 3.1. NMDA receptors in the synaptic transmission. Activation of the presynaptic neuron results in glutamate release from the intracellular vesicles into the synaptic cleft (gray circles). Glutamate may activate NMDA and other glutamate receptors on both postsynaptic neuron and astrocyte. Astrocytes respond to the glutamate activation by releasing other NMDA receptor agonist D-serine (red circles). D-serine facilitates activation of the postsynaptic NMDA receptors [125]).

Thus, two types of brain cells, neurons and astrocytes, are expressing functional NMDA receptors. In the interstitial fluid of the brain glutamate concentration is controlled by glial cells within the 0.5 – 2 μM range [128]. However, in the synaptic cleft local glutamate concentration may reach 1 mM during synaptic transmission. That glutamate concentration is sufficient for the NMDA receptor activation in neurons and astrocytes.

What may activate NMDA receptors in non-neuronal tissues? Glutamate is an abundant amino acid in mammalian tissues. In the blood plasma glutamate concentration in humans, rats and horses varies from 10 to at least 200 μM (Bogdanova, Makhro unpublished data). NMDA receptor co-agonist glycine also present in the blood plasma of those species in concentration above 300 μM, which should be saturating for the Gly binding site (see Table 1 in Chapter 1).

Initial membrane depolarization is a second condition required for NMDA receptor activation as Mg^{2+} block renders the receptor non-functional under resting potential conditions. In the brain cells this initial depolarization is mediated by activation of the other class of ionotropic glutamate receptors located in the postsynaptic membrane, AMPA receptors. Other cell types, such as heart and muscle cells regularly undergo membrane depolarization-repolarization cycles. Membranes of some cells, like erythrocytes, are already depolarized to potential close to the -10 mV. One cannot exclude the presence of AMPA or kainite receptors assisting in depolarization similar to that in synaptic membranes (as it appears to be in *Hydra*, see Chapter 2). And finally, presence of the NR3 type subunits reduces receptor sensitivity to the potential-dependent Mg^{2+} block (Chapter 1, Table 1.1). Thus, NMDA receptors from non-neuronal tissues do not require membrane depolarization event for their activation if they have NR3 subunit.

NMDA receptors appeared long time before the formation of neuronal system. Therefore, it is highly improbable that in the modern organism their expression is restricted to the brain. In recent years functional NMDA receptors were described in various non-neuronal tissues, for example, in bone [125], kidney cells [118], smooth muscle [129], megakaryocytes [130] and leucocytes [120] as well as in the myocardium [131] and red blood cells (our group). The summary of glutamate receptors expression in the mammalian peripheral tissues is presented in the Table 3.1.

Table 3.1. Expression of glutamate handeling proteins (receptors and transporters) in peripheral tissues. A – AMPA, K – kainate, N – NMDA receptors, mGluR – metabotropic glutamate receptors, GluT – glutamate transporter, VGLUT – vesicular glutamate transporter [132].

Tissue/cell	iGluR	mGluR	GluT	VGLUT
Osteoblast	+ (A,K,N)	+ (I, II)	+ (1)	+ (1)
Osteoclast	+ (N)	ND	ND	ND
Osteocyte	ND	ND	+ (1)	ND
Testis	+ (A,K,N)	+ (I, II)	+ (1,2,5)	ND
Pancreas	+ (A,K,N)	+ (I, II, III)	+ (2)	+ (1,2)
Adrenal gland	+ (A,K,N)	?	+ (1)	ND
Pituitary gland	+ (A,K,N)	ND	ND	ND
Pineal gland	+ (A,K,N)	+ (I, II)	+ (1,2)	+ (2)
Hepatocyte	ND	+ (I)	ND	ND
Lingual epithelium	+ (K,N)	+ (III)	ND	ND
Thymus	ND	+ (I, II)	ND	ND
T lymphocyte	?	ND	ND	ND
Platelet	?	ND	ND	ND
Megakaryocyte	+ (N)	ND	ND	ND
Heart	+ (A,K,N)	+ (I, II)	+ (1,3)	ND
Lung	+ (N)	ND	ND	ND
Keratinocyte	+ (A,N)	ND	+ (2,3)	ND
Melanocyte	ND	+ (I)	ND	ND

In the present study we have characterized the expression, composition and function of the NMDA receptors in the electrically active tissue with a resting potential of ∼-60 mV, the myocardium, and in non-excitable type of cells with a transmembrane potential of -10 mV, red blood cells.

Heart

NMDA receptor expression in heart

Several groups have been reporting the presence of the GRIN (**G**lutamate **R**eceptor **I**onotropic **N**MDA) gene transcripts of certain subunits and the corresponding proteins (NR1, NR2B) in the myocardium of a rat, mouse, Californian sea lion and humans. However, the reported findings have been

somewhat controversial. Using immunoblotting Leung *et al* [131] reported expression of the NR1 subunit protein in all heart regions including aorta and pulmonary artery. This subunit was detected in whole heart homogenates obtained from 4 days old, 12 days old and adult rats. At the same time, these authors could not detect any of the NR2 subunits in rat myocardium. Seeber and colleagues [133] showed transient expression of NR2B subunit (but not of NR1 or any other subunits) in developing heart from embryonic day 18 (average time of pregnancy in rats is 21-22 days) to postnatal day 21 using immunoblotting and immunihostochemistry. Interestingly, the NR2B-specific staining was localized in the cytosol within the perinuclear space. Later on the same group isolated NR2B protein by immunopecipitation and identified it by mass spectrometry [134]. Surprisingly, NR2B protein co-immunoprecipitaded with ryanodine receptor 2 but not with the other NMDA receptor subunits. Using antibodies against different parts of NR2B peptide, they found that C-terminal (cytoplasmic) domain of cardiac NR2B subunit underwent tissue-specific post-translational modifications. Transcripts of the Grin2B were reported in rat heart homogenates by Hu *et al* [135].

Several groups detected NMDA receptors in heart tissue of other mammalian species. NR1 subunit was cloned from heart tissue of sea lions [136]. Based on immunohistochemical imaging Gill and co-workers claimed that NR1 protein expression was associated with heart conductive system. Same group detected NR1 in the heart conductive system in primates, human and monkey (*Macaca fascicularis*) [137], [138]. The group of Tyagi monitored the NR1 subunit expression in mouse heart using immunoblotting and immunohistochemistry [139], [140]. Similar to Seeber and colleagues, Tyagi and co-workers could not confirm membrane localization of the NR1 subunit in isolated cardiomyocytes. Lack of any positive (e.g. brain extracts and sections) or negative controls in both staining an Western blotting leaves some doubts in the antibody specificity. This group has been intensively investigating the role of cardiac NMDA receptors in homocysteine cardiotoxicity. Based on these studies we may conclude that (i) no systematic investigation of the expression of all known NMDA receptor subunits NR1, NR2A-D, NR3A-B in the myocardium at the transcript and protein levels has been performed; (ii) for some reasons immunostaining of the cardiac NMDA receptor

subunits is technically demanding and caution has to be taken, and positive and negative controls used when detecting the NR proteins, which may undergo cardiac-specific secondary modifications; (iii) no attempts to detect NR3 subunits were done; (iv) mostly NR1 subunit was studied, so NR3/NR2 receptor types could be missed.

NMDA receptor activity in cardiac cells

For the functional studies two cellular models were used, neonatal rat cardiomyocytes (NRC) obtained from 1-4 days old rats and growing in culture from 1 to 5 days and freshly isolated adult ventricular cardiomyocytes from rat (ARC). Whole cells recordings were performed by Seeber *et al* in NRCs derived from Wistar rats after 4 days of culturing revealed the inability of NMDA (up to 1 mM) or Glu (up to 3 mM) in the presence of 50 μM Gly to induce electric currents [133]. Frequencies of calcium oscillations were monitored by Winter and Backer as a readout of responses of NRCs from Sprague-Dawley rats cultured for 1-3 days old to NMDA or Glu (100 μM each), as well as to kainate and AMPA. Each of the agonists mediated an increase in Ca^{2+} oscillation frequencies which were attributed to the presence of "novel glutamate receptor composed of both non-NMDA and NMDA subunits on cultured rat myocardial cells". Increase in oscillations' frequency caused by the agonists could be antagonized by MK-801, glutamate site-specific competitive antagonist AP7 and the AMPA/kainate receptor antagonist DNQX. Basal intracellular calcium levels remained unchanged [141]. In contrast to that Gao *et al* reported an increase in the cytoplasmic calcium in the 1-3 days old NRC culture caused by the treatment with NMDA (100 μM). Raise in cytoplasmic calcium level caused by NMDA administration was followed by reactive oxygen species production and apoptosis. MK-801 and antioxidants protected NRC from NMDA-induced calcium overload and the following induction of ROS [142]. Based on our own observations this controversy most probably is related to the gradual remodeling of NRCs in culture and the associated progressive modification of gene and protein expression. Exposure to the unphysiologically high oxygen levels (20% in the culture incubator vs 2% in newborn heart and 6-7% in adult heart [143], [144]), 2-D culturing, lack of cell-cell interactions with other cell types forming the heart

tissue, absence of tissue-specific cytokines and mechanical stress result in gross molecular and morphological changes in the course of transformation of the NRCs towards the embryonic phenotype initiated already after 1 day of incubation. Therefore, the outcome of the study may differ remarkably if no standardized protocol is used and the cellular responses are not compared for the cultures of identical age.

These instabilities of experimental model may be avoided by using freshly isolated adult cardiomyocytes. This model has been used twice for testing of the effects of NMDA receptor antagonist MK 801 on the action potential duration and cation currents. In both studies the availability of the NMDA receptor agonists (Glu and Gly) was not controlled. Prolongation of the action potential duration during early and late phase of repolarization and maximal upstroke velocity observed in response to MK 801 treatment was attributed to the non-specific binding of MK 801 to sodium channels in inactivated state and to potassium channels in resting state [145]. Treatment of adult guinea pig cardiomyocytes with the pore-targeting NMDA receptor antagonist ketamine resulted in a ~20% reduction in transsarcolemmal calcium entry observed by single cell voltage clamp [146].

NMDA receptors in isolated heart models

In the other set of studies rat and guinea pig heart preparations were exposed to the NMDA receptor antagonists. When added to the organ bath solutions, MK 801 in rat and ketamine in guinea pig spontaneously beating right atria dose-dependently reduced contraction rate. Preparations of artificially paced left atria and papillary muscles showed dose-dependent decrease in contraction force in response to MK 801 or ketamine [145], [147]. Thus, in myocardial tissue NMDA receptor antagonists were producing negative inotropic and chronotropic effects.

Similar results were obtained when NMDA receptor antagonists were present in solutions used for coronary perfusion of isolated hearts. In guinea pig heart ketamine dose-dependently reduced spontaneous heart rate starting from 100 μM concentrations and decreased left ventricular pressure at concentrations as low as 50 μM. These effects could not be attributed to the alterations in coronary

flow which was insensitive to ketamine even at the concentration of 1 mM [148]. In rabbit heart model spontaneous heart rate was decreased by ketamine. Ketamine also dose-dependently (50 – 200 μM) reduced longitudinal and transverse conduction velocity measured at ventricular surface without the changes in anisotropy [149].

These observations suggest that cardiac NMDA receptor most likely participates in the spontaneous depolarization of the pacemaker cells and in conduction of the depolarization in the ventricular tissue. However, both MK-801 and ketamine have more than one target to interact with (see table in supplement data for the paper 1). Thus, more detailed studies of cardiac NMDA receptor properties and function are required.

Systemic administration of NMDA receptor antagonists

5. ECG

Several cardiac-related effects of NMDA receptor antagonists were observed during clinical trials in human subjects [150]. Both glutamate binding site antagonist (CGS19755) and channel blocker (aptinagel) induced ST segment abnormalities in healthy human volunteers. ST segment of the ECG recording represents depolarized state of the ventricles and ST elevation is often associated with myocardial infarction, pericarditis, Brugada syndrome and other disorders; however, changes in the ST segment amplitude could be related to several conditions and are not *per se* an indicative of any myocardia disorder. NR2B specific (polyamine binding site) antagonist eliprodil at high doses induced prolongation of QTc interval in similar toxicity studies on human subjects. Prolongation of the QTc interval occurs when the action potential of a significant proportion of ventricular cardiomyocytes is prolonged due to the suppression of one or more repolarizing currents, or an augmentation of inward currents or both ([151]: Chapter 18).

Ketamine was historically used for anesthesia in human patients and is currently acquired in special cases for treatment of depression and post-surgical and neurological pain in combination with other drugs, but has severe side effects and its repetitive use causes addiction. It is a common anesthetic in veterinary medicine and in animal experimentation. Ketamine overdose in healthy young

individual results in transient ST elevation (Brugada-like ECG pattern) [152]. Similar effects were observed in mouse model of ketamine abuse, where ST elevation appeared in 30% of mice [153]. Used as anesthetic agent, ketamine induced P wave prolongation (prolonged atrial depolarization) in addition to the QT prolongation in mice [154].

Thus, glutamate antagonists targeting amino acid-, polyamine- and channel pore binding sites NMDA receptor affect ECG intervals, mostly ST segment amplitude and QT interval longitude.

6. Rhythmicity

Autonomous heart rhythm is generated by the pacemaker cells located in the sinus node. However, *in vivo* sinus node is innervated and the heart rhythm is regulated by sympathetic and parasympathetic fibers which also possess NMDA receptors. Therefore, application of NMDA receptor antagonists triggers complex effects driven by neuronal system and by the sinus node itself.

In conscious subjects different NMDA receptor antagonists applied systemically either increased or did not affected the heart rate (Table 3.2).

Table 3.2. Treatment of the consciousness humans and rats with NMDA receptor antagonists.

Compound	Species	Effect on HR	Link
Ketamine 0,5 mg/kg	Human	↑	[155]
Memantine 0.16 mg/kg	Human	Not changed	[155]
MK-801 0.025-0.25mg/kg	Rat	↑*	[156]
Ifenprodil 5 mg/kg	Rat	Not changed	[157]

_* Authors concluded that HR increase could be related to the increased mobility of animals. Drugged rats were showing stereotypical behavior (running in circles), head shaking and nodding.

Heart rate measured in anesthetized unconscious rats threated with NMDA receptor antagonists was decreasing similarly to that in isolated not-paced heart models [158], [159]. Bradykardic effects of the antagonists were also observed in anesthetized rabbits [159]. Thus, in the absence of vagal control NMDA receptor antagonists mediate bradycardia.

NMDA receptor antagonists applied to different pro-arrhythmogenic models reduced the frequency of arrhythmic events including tachycardia and ventricular fibrillations. Animals treated with these compounds recovered their mean blood pressure and normal heart rate faster than untreated controls and had higher survival rate (Table 3).

Table 3.3. Antiarrhythmic action of NMDA receptor antagonists in experimental animal models.

Compound	Species	Model	Arrhythmia	Other effects	Link
Ketamine 100 mg/kg Diazepam 10 mg/kg	Rat	Ischemia (6 min) – reperfusion	↓	High survival rate	[160]
MK-801 0,5 mg/kg	Dog	Cocaine 2 mg/kg, electrical stimulation	↓		[161]
MK-801 0,3 mg/kg Ketamine 10 mg/kg Memantine 1,5 mg/kg	Rat	Ischemia (5 min) – reperfusion	↓	High survival rate	[162]

Most of the NMDA receptor antagonists have sedative or narcotic effects in animals changing their behavior and, secondary to that, the heart rate. However, this is not always the case as, in contrast to sedative drug lorazepam, MK-801 (0,16 mg/kg) increased heart rate variability in Rhesus monkeys [163]. At the same time heart rate and arterial pressure were not affected. Interestingly, similar dose of MK-801 (~0,2 mg/kg) which was well-tolerated by monkeys appeared to be lethal for humans [164].

7. Pressure

Like heart rate, arterial pressure-related effects of NMDA receptor antagonists were dependent on experimental conditions. In unconscious rats and rabbits systemic administration of NMDA receptor antagonists significantly reduced mean arterial pressure along with the heart rate [165], [159]. Ifenprodil in low concentrations didn't affect blood pressure in resting rats and prevented exercise-induced increase in systolic and diastolic pressure [157]. In awake humans ketamine (0,5 mg/kg) increased systolic (~115 to ~130 mmHg) and diastolic (~60 to ~70 mmHg) pressure [155]. Similarly, MK-801 dose-dependently increased mean arterial pressure in conscious rats [156].

Central effects of NMDA receptors in heart regulation

NMDA receptors participate in central regulation of heart contractility. Microinjections of NMDA or Glu into *nucleus tractus solitarius* reduced heart rate and arterial pressure in rats. MK-801 and AP-5 blocked these effects, but could produce the opposite effect on the heart function when applied at higher doses [166], [167]. Moreover, NMDA receptor subunits (NR1, NR2A, NR2B) were found in vagal preganglionic neurons projecting to the heart (*dorsal vagal nucleus* and *nucleus ambiguus*) [168]. Intracerebroventricular injections of MK-801 had no effect on the heart rate or arterial pressure, but modified chronotropic responses to other drugs [169]. Thus, effects observed after systemic administration of NMDA receptor antagonists to conscious subjects (tachycardia, increase of the arterial pressure) may be at least in part attributed to the central regulation.

Mechanosensitivity

An important property of NMDA receptor is sensitivity to mechanical pressure [170]. That feature was reported almost 20 years ago. However, since the mechanical deformation is highly atypical for glutamatergic neurons, possible physiological role of mechanosensing by the NMDA receptors was not investigated in detail. Patch-clump recordings showed that administration of pressure of 60 mbar (45 mmHg) resulted in facilitation of the stimulatory effect of 10 μM NMDA and 10 μM Gly on neuronal NMDA receptors by 2.5-fold, and

application of 85 mbar (63.75 mmHg) amplified the receptor activity by 5.6-fold. In humans left ventricular pressure varies from 3-12 mmHg in diastole to 100-140 mmHg in systole. Mechano-stimulation within this pressure range is sufficient to alter the activity of NMDA receptors contributing to the mechano-electrical feedback mediated by the mechano-sensitive cation channels described in cardiomyocytes and fibroblasts in the heart [171]. Over the past decades tight relationships was demonstrated between the mechano-sensitivity and cardiac disorders (arrhythmias, hypertrophy and ischemic heart disease) [172]. It is therefore tempting to speculate that cardiac NMDA receptors could also be involved in pathophysiology related to pressure overload.

A variety of mechanosensitive channels appear to acquire this property early in evolution [173]. Evolutionary mechano-sensitivity was used for osmotic regulation in single cells, gravitropism in plants, and probably in primitive sessile animals. At present mechano-electrical coupling is a key mechanism regulating cardiac output known as Frank-Starling law. Considering that, there is no wonder that NMDA receptors have retained mechanosensitive properties, which are not required within the brain. However, in non-neuronal tissues, such as the bone mechanosentitivity of these receptors turns to be very essential. In here NMDA receptors are involved in calcium reabsorption in osteoclasts and their activity and expression of the receptor subunits is reported to be tightly linked to the mechanical load in the limbs [174].

Blood

Several lineages of cells derived from hematopoietic stem cells were known to express functional NMDA receptors (Fig 3.2). The subunit composition of those receptors was not fully characterized so far, however, at least NR1 subunit protein or transcript was detected. Prior to our study, NMDA receptors were found in lymphocytes, macrophages, neutrophils and megakaryocytes (see below).

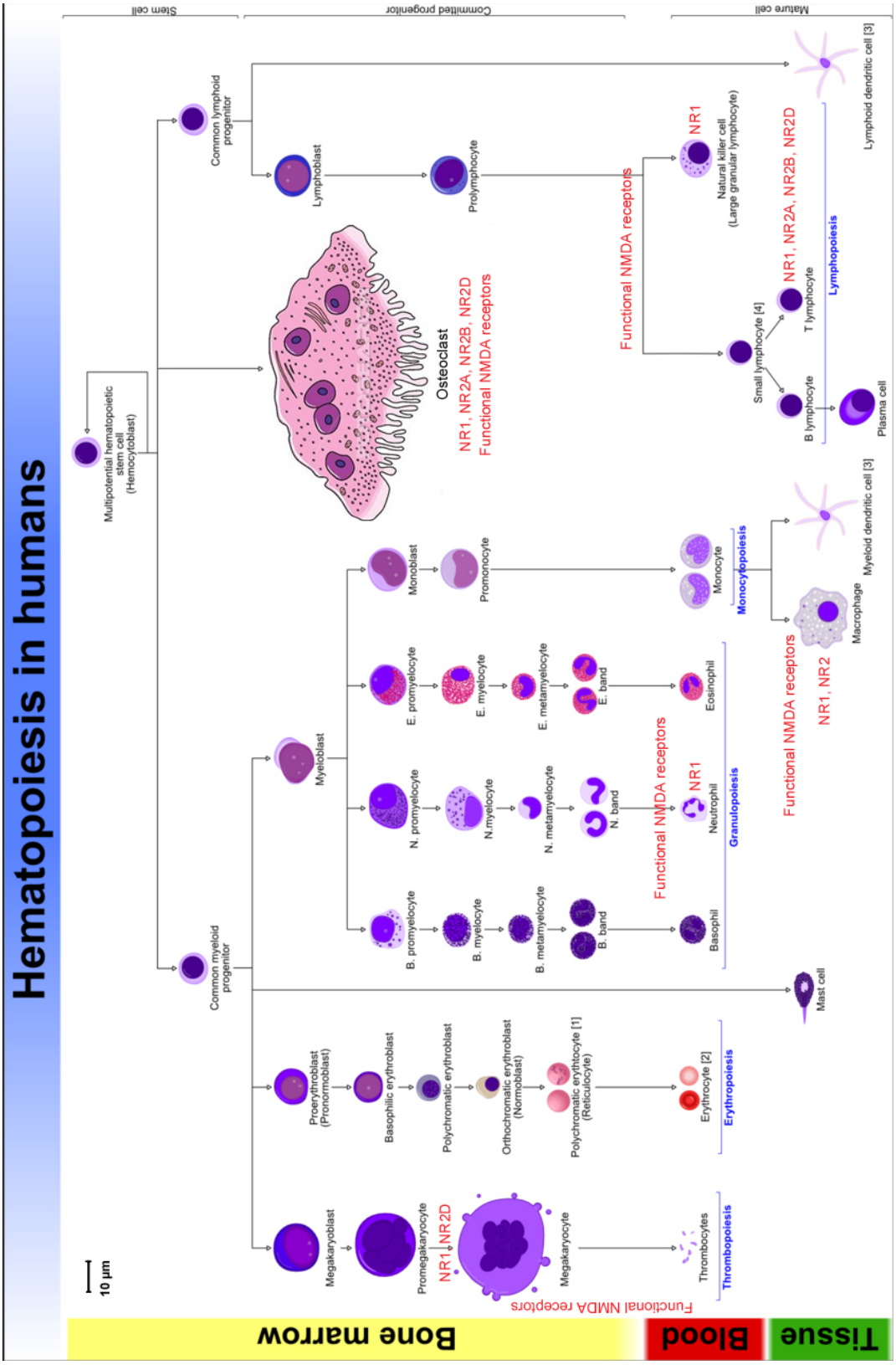

Figure 2. Hematopoietic lineages in humans (modified scheme from WikiMedia). NMDA receptors were detected in both lymphoid and myeloid lineages, mostly in the cells on the terminal stages of erythropoiesis: in lymphocytes [175, 176], neutrophils [177], macrophages [178] and megakaryocytes [179]. Osteoclasts are also derived from the multipotential hematopoietic stem cells [180]. NMDA receptors

were detected in osteoclasts' precursors and influenced their development [181]. In mature osteoclasts NMDA receptors regulate bone resorption processes [182].

NMDA receptors in lymphoid lineage and in lymphocytes

Lymphocytes use NMDA receptor as a tool for the feed-back regulation of the inflammation. Lymphocyte activation induces expression of NMDA receptors. In turn, NMDA receptor-expressing lymphocytes decrease production of the interferon gamma. Thus, NMDA receptors participates in suppression of inflammatory response [175].

NMDA receptors are also involved in autoimmune response by regulating the production of induced regulatory T-cells. In mice treatment with memantine (but not with antagonists of other glutamate receptors) promoted formation of regulatory T-lymphocytes and delayed the development of arthritis [183]. NMDA antagonists (MK-801 and ketamine) could also suppress T-helper lymphocytes differentiation and cytokines production [184]. For T-lymphocytes expression of NR1, NR2A, NR2B and NR2D but not NR2C and NR3 was shown [185, 186]. NR1 and NR2B expression was also observed in immortalized Jurkat T cells (derived from human T cells). The receptors controlled cell growth and adhesion to fibronectin [187].

NMDA receptors in myeloid lineage

8. **Megakaryocytes and platelets**

Myeloid progenitor cells are the early precursors within the myeloid cell lineage. This lineage gives rise to thrombocytes, granulocytes, macrophages and RBCs. (Fig 2). Megakaryocytes are large nucleated cells responsible for the production of thrombocytes (platelets). The presence of NR1 and N2D subunit transcripts in rat bone marrow, human megakaryocytes, and MEG-01 clonal megakaryoblastic cells was shown using PCR analysis and northern blotting [179]. Immunoblots revealed that molecular mass of the NR1 subunit in megakaryocytes is lower than that of brain-derived subunit (~100 kDa vs ~116 kDa respectively) which probably reflects the de-glycosylation. NMDA receptor activity was essential for differentiation of megakaryoblastic cells [179]. Furthermore, NMDA receptor

function was detected in platelets and its activation resulted in suppression of coagulation [188].

Enucleated platelets apparently inherited NMDA receptors from their precursors megakaryocytes. However, properties of platelet derived-NMDA receptors differ from neuronal NMDA receptors [189]. Although Kd for [^{3}H]glutamate and [^{3}H]glycine binding was similar to neuronal NMDA receptors, presence of agonists was not required for [^{3}H]MK-801 binding to platelet membranes. NMDA or glutamate alone were not affecting platelet aggregation. However, presence of agonists influenced Ca^{2+}-mediated effects of arachidonic acid and cAMP-dependent pathway [189]. That study raises the question: How glutamate may affect NMDA receptor-dependent Ca^{2+} influx if it doesn't increase channel opening probability according to [^{3}H]MK-801 binding studies? The possible answer is that functional experiments were conducted in the platelet rich blood plasma where some other NMDA receptor agonists may be present keeping the receptor in active state. Further studies of the same group in the platelet-enriched human blood plasma revealed that NMDA is a potent inhibitor of platelet aggregation and thromboxane B2 synthesis [188]. The physiological function of NMDA receptor in platelets remains unclear. It is known that platelets express vesicular glutamate transporters and release glutamate during the aggregation [190]. That is quite confusing, because glutamate inhibits platelet aggregation. Another possibility is that glutamate release by platelets is affecting other cells participating in clot formation. For example injury requires both clot formation and activation of macrophages and neutrophils to confront invading microbes.

(ii) NMDA receptors in granulocytes and macrophages

Neuronal NMDA receptors are known to mediate ROS-depended signaling [191]. Upon discovery of these receptors in macrophages [178] similar function of the NMDARs was suggested in these cells [192]. Indeed, in rat macrophages Ca^{2+} influx triggered by NMDA receptor agonists was associated with induction of free radical generation and upregulated cyclooxygenase 2 (COX-2) expression. These effects were abolished by pre-treatment with the NMDA receptor antagonist MK-801 and silencing of GRIN1 expression using mRNA interferences [192]. In neuronal

cells free radical and H_2O_2 generating systems responding to an increase in Ca^{2+} include NADPH oxidases (NOXes) [193], dual oxidases (DUOXes), uncoupled endothelial and neuronal NO synthases (eNOS and iNOS) and mitochondrial components [194]. Leucocytes and neutrophils generate substantial amount of reactive oxygen and nitrogen species by controlled activation of NOXes, iNOS, cytochrome 450 and 53 otentia oxidoreductase whereas mitochondrial production of free radicals is low [195]. In each cell type calcium uptake by the NMDA receptors therefore triggers superoxide anion production (with the following increase in $ONOO^-$, H_2O_2 and $HO^{\bullet-}$) [177] which is presumably mediated by NOXes. NOX activity is also required for megacariocyte differentiation [196]. Calcium binding domain in the NOX protein appeared very early in evolution and already present in unicellular organisms like amoeba [197]. Thus, NMDA receptor was probably used for the regulation of ROS production for feeding and protection of primitive unicellular organisms before neuronal system was developed [198].

The studies of NMDA receptors in the non-neuronal tissues including blood are in their initial phase and the reported findings are incomplete and raise more questions than answers. In the synapse NMDA receptors are sensing membrane depolarization and glutamate release. In the blood plasma two main NMDA receptor agonists glutamate and glycine are constantly present. Glutamate release machinery was recently shown to be present in bone marrow cells (Table 3.1). What are the mechanisms in control of NMDA receptor activity in blood cells? These cells do not undergo depolarization-repolarization cycles and remain more or less permanently "depolarized" and thus most likely unable to preserve Mg^{2+} block. Permanent cycling between the basal activation and deactivation states may be expected. Blood cells experience significant changes in redox state which was shown to influence NMDA receptor activity in neurons [199], [200]. Apart of possessing regulatory thiols these receptors in *Hydra* are sensing glutathione release into the extracellular space. What are the ligands for the NMDA receptors in blood cells? It could be Gly and Glu fluctuations, pro-inflammatory cytokines, GSH or some other unknown ligands.

(iii) NMDA receptors in red blood cells: pharmacological and pathophysiological implications

NMDA receptors studied in neurons and in artificial expression systems are known to function as sensors. They sense the presence of various agonists (amino acids, polyamines, Zn^{2+} ions), membrane potential, pH, redox state and mechanical stress. In response to various stimuli NMDA receptor provides Ca^{2+} entrance into the pre-membrane intracellular space resulting in activation of signaling cascades. In neurons, leucocytes and macrophages Ca^{2+} signaling is also involved in generation of reactive oxygen species. In erythrocytes intracellular free cytoplasmic calcium concentration is usually maintained between 20 – 60 nM being 50 000 times lower than that in blood plasma [201]. This tremendous gradient is used to regulate the most important biochemical processes in human red blood cell including glycolysis and pentose phosphate pathway, protein cleavage, cell volume and pH. Many of red blood cell disorders, including the most widespread RBC disease like sickle cell anemia, are associated with abnormal cytoplasmic levels of Ca^{2+}. The presence of NMDA receptors in RBCs has never been looked before and its role in Ca^{2+} homeostasis never studied.

a) Calcium transport pathways in erythroid precursor cells and in circulating red blood cells

Ca^{2+}-dependent signaling plays an important role in erythroid precursor cells (EPC) maturation and differentiation [202], [203]. In the absence of extracellular Ca^{2+} erythropoiesis is inhibited [204]. In EPC Ca^{2+} influx is mediated by TRPC channels and regulated by Epo [205]. However, in mature RBC more channels were identified suggesting that other transport pathways for Ca^{2+} are present in precursor cells as well (see below). At the latest stages of maturation these cells are getting rid of multiple receptors, most of the glycolytic machinery, ion transporters, and organelles including mitochondria. By the end of maturation cell size is dramatically reduced and energy is provided exclusively by anaerobic processes [206]. Reduction in metabolic activity occurs along with a decrease in passive and active ion transport rates including those for Ca^{2+} ions. The remaining ion channels in membranes of circulating RBCs are dormant most of the time under normal physiological conditions [207]. Due to the low abundance of

ion channels permeable for Ca^{2+} very limited number of studies were focused on the molecular identification of these channels in mature RBCs. However, growing awareness of special importance of calcium overload in progression of various forms of hereditary anemia resulted in substantial progress in characterization of the Ca^{2+} uptake pathways in the recent past. In human RBC those include:

1) ***P-type Ca^{2+} channel ($Ca_v2.1$)*** [208], [209] (slow, kinase-mediated process in response to platelet-generated lysophosphatidic acid). Similarly to NMDA receptors, this channel can be activated by mechanical stress (osmotic shock) [210]. There is a possibility that mechano-sensitivity and some other properties of this channel actually belong to the NMDA receptor.
2) ***Transient receptor potential cation channel (TRPC) 6*** expression at the mRNA level was observed in human erythroid precursor cells and TRPC6 protein was detected by antibodies in mature erythrocytes [211]. Cation channels from this family are Ca^{2+}-permeable and have polymodal activation properties, e.g. they can be activated by various ligands (endogenous lipids, purine nucleotides, inorganic ions) and by mechanical stress [212]. However, for the TRPC6 no physiological extracellular ligands were discovered so far and their mechanosensitivity is also questionable [213]. There is a possibility that TRPC6 proteins in circulating erythrocytes are remains from the early stages of erythropoiesis when they were participating in Epo-related signaling [214] and have no function in mature red blood cells.
3) ***The ligand-activated voltage-dependent non-selective cation channel (VDNSCC***) in mature erythrocytes was well described electrophysiologically. However, the protein identity of this channel remains unknown. Some properties of VDNSCC including hysteresis [215] also can be attributed to $Ca_v2.1$ channels. Some of the VDNSCC properties listed below are similar to the NMDA receptors studied in neuronal cells or in artificial expression systems. Nevertheless, all known channel properties neither fit to the description of NMDA receptor nor to $Ca_v2.1$ channel. It is possible that the researchers recorded both channels simultaneously.

Table 3.4. Comparison between NMDA receptors and ligand-activated voltage-dependent non-selective cation channel from RBC.

Similarities between NMDA receptor and VDNSCC	
Voltage-dependence	Both channels are blocked at negative membrane potentials. NMDAR channel is blocked by divalent cations (Mg^{2+} or others depending on subunit composition), however, even in absence of Me^{2+} voltage-depended block is present [216]. For VDNSCC mechanism is unknown, for divalent cations very short (about 10 ms) channel opening events at negative membrane potentials between −80 and −100 mV were observed [217].
Hysteresis	Open state probability depends on the history of changes of membrane potential for both channels [217], [216].
Ion permeability	Both channels are permeable for Na^+, K^+, Rb^+, Cs^+, NH_4^+, Ba^{2+}; VDNSCC is permeable for Ca^{2+} and Mg^{2+}, NMDA receptor permeability for this cations depends from the subunit composition (see Chapter 1).
Ligand-depended activation	VDNSCC can be further activated by nicotine and carbachol, however, channel properties are highly different from nAch receptors [218].
La^{3+}	Inhibition [219]
Differences between NMDA receptor and VDNSCC	
Channel conductance	49 pS for NMDA receptors [220], 21 pS for VDNSCC [221]
Opening probability	VDNSCC opening probability is shifted to the positive membrane potential [217] (above +20 mV), therefore, that channel is closed at the basal potentials of -10 mV reported in RBC under physiological conditions.

4) ***Piezo1*** (mechano-sensitive channel) is involved in volume regulation in zebra fish erythrocytes [222]. Mutations in Piezo1 are associated with pathology of dehydrated hereditary stomatocytosis [223], [224] although their function was never studied in human erythrocytes.
5) ***Voltage-dependent anion channels*** in the super-channel mode (S. Egée, ERCS meeting 2013, personal communication).
6) ***P sickle*** (sickling-induced permeability pathway in RBCs of sickle cell disease (SCD) patients) is a current present only in erythrocytes of patients suffering from sickle cell disorder. This current is further activated by deoxygenation and sickling process. Sickling process is increasing the Ca^{2+} permeability of the erythrocyte membrane six times over the normal physiological range ([225]: p 392). The molecular identity of P sickle channel (or channels) remains obscure and most likely is a superposition of several conductance pathways. Possible NMDA receptor contribution into the P sickle pathway is summarized below:

Table 3.5. Similarities between NMDA receptor and P sickle.

Ion permeability	Both are permeable for: Li^+, Na^+, K^+, Rb^+, Cs^+, Ca^{2+}, tetraethylammonium [226], [227]
Gd^{3+}	Inhibits P sickle (IC50 2 μM) [228], partially inhibits NMDA-induced Zn^{2+} currents (10 μM) [229]
Zn^{2+}	At 100 μM concentration Zn^{2+} inhibits P sickle current [228], same concentration induces fast channel block of NMDA receptor channel [52].
Voltage-dependence	P sickle (K^+) is increased upon membrane depolarization [230]
pH sensitivity	Activation of the deoxygenation-induced pathway was promoted by alkaline pH (7.5). Optimum for cation movements was observed around pH 6.9. However, the highest degree of sickling was achieved at alkaline pH independently from flux intensity [230]. NMDA receptor pH dependence is related to the subunit composition (see Chapter 1), in general acidic pH (below 7,0) inhibit

	the receptor, while at alkaline pH (more than 7.5) most of the receptors are active. pH changes upon the deoxygenation could be the direct mechanism of P sickle activation. Measured by nuclear magnetic resonance pH in intact healthy erythrocytes was changed from 7.15 in completely oxygenated cells (pO_2 = 121 mmHg) to 7.29 in deoxygenated cells (pO_2 = 1 mmHg) [231].

7) ***Carrier-mediated passive Ca^{2+} influx*** [232].
8) ***Ca^{2+}-pump*** leak [232] (highly questionable under physiological conditions).

Besides sickle cell disease elevated Ca^{2+} (and ouabain-independent Na^{+}) uptake was observed in erythrocytes of patients with thalassemia, PFK deficiency [233], congenital spherocytosis [234] and several other forms of hereditary anemia. In RBCs of patients with β-thalassemia increased Ca^{2+} uptake rates were suggested to be caused by the higher abundance Ca^{2+} transporters per cell [235].

There are three possible mechanisms underlying the high cation permeability of RBCs of patients with certain forms of hemoglobinopathy (SCD, thalassemia). **(I)** Abnormal forms of hemoglobin have altered proton dissociation constants and, since human hemoglobin is a main intracellular buffer in RBC [236], cellular pH is also altered. . This hypothesis is supported by studies of sickle cell hemoglobin solubility and pH, where was calculated that sickle cell erythrocytes in oxygenated state have intracellular pH 7.4, while healthy erythrocytes have pH 7.15 (increasing during deoxygenation) [237]. This involuntary intracellular "alkalinisation" inevitably affects structure and function of multiple proteins, including metabolic enzymes, signaling proteins, ion transporters, cytoskeletal elements and others resulting in uncoupling of multiple processes and reduction in cellular stability and life span. **(II)** Structural abnormalities in erythrocyte cytoskeleton due to the facilitated binding of mutated hemoglobin molecules to cytoskeletal proteins. Extensive adherence of HbS to the band 3 protein and the cytoskeleton demonstrated earlier [238], [239] reduces deformability of erythrocytes facilitating their premature clearance and hemolysis. **(III)** Third explanation is

related to potential disruption of the maturation processes of erythroid precursor cells by mutated hemoglobin and abnormal clearance of ion transporters and other transmembrane proteins including receptors.

b) Physiological and pathophysiological role of Ca^{2+} in red blood cells

In erythrocytes Ca^{2+} regulates several groups of enzymes which are important for cell function and survival including metabolic pathways, regulation of cell volume and deformability (Figure 3.3). Glycolysis assessed as lactate production was reported to be dose-dependently stimulated by Ca^{2+} in cells in which intracellular Ca^{2+} was clamped using Ca^{2+}-ionophore A23187 [240]. In particular, Ca^{2+} stimulated oligomerization and activation of the rate-limiting glycolytic enzyme phosphofructokinase (PFK) [241]. Ca^{2+}- dependent activation of tyrosine-kinases lead to the increase Band 3 protein phosphorylation. Phosphorylated Band 3 release membrane-bound (inactive) PFK into the cytoplasm. Thus, Ca^{2+}-dependent phosphorylation increases cytoplasmic pool of oligomerized PFK molecules and intensifies glycolysis [242], [243]. Glycolysis provides fuel for Ca^{2+}- and Na^{+}/K^{+}-pumps, therefore, in pathologies such hereditary phosphofructokinase deficiency Ca^{2+} is accumulating inside erythrocytes presumably due to the ATP depletion, although facilitated Ca^{2+} leak in PFK erythrocytes was also observed [233]). Increase in the activity of Ca^{2+}-sensitive K^{+}-channels (Gardos channels) results in excessive K^{+} loss and RBC dehydration [233]. In healthy erythrocytes Gardos channels are believed to be inactive most of the time, since Ca^{2+} concentration needed for their activation is far above physiological levels [207], [244]. However, stretch-activated Ca^{2+} influx, induced by the mechano-sensitive Ca^{2+} channels may provide transient increase of Ca^{2+} concentration in pre-membrane space, and trigger Gardos channel activation in healthy red blood cells [245].

While glycolysis is stimulated by Ca^{2+} uptake, glucose transport can be dose-dependently inhibited by ionophore-mediated Ca^{2+} [246]. Ca^{2+}/calmodulin-depended activation of deaminase leads to decrease of cellular AMP content [247], [248]. AMP is a positive modulator of GLUT1 transporter in erythrocytes [249]. Therefore, Ca^{2+} accumulation decreases basal level of GLUT1

activity. However, the apparent half maximal concentration of Ca^{2+}-depended inhibition of glucose transport is 250 μM, which is way out of physiologically relevant Ca^{2+} concentration range (20-60 nM of free Ca^{2+} and up to 10 μM of protein-bound Ca^{2+} in unstimulated intact RBC). Though local Ca^{2+} concentrations in pre-membrane space close to the Ca^{2+} influx pathways and GLUT1 could be much higher, physiological relevance of Ca^{2+}-depended glucose uptake inhibition needs to be confirmed.

Besides affecting cellular volume and metabolism, stimulation of Ca^{2+} uptake provokes echinocitic transformation in human RBCs [250]. Those shape changes are independent of the presence of monovalent cations, transemembrane osmotic gradient and ghost volume. Ca^{2+}-inducible formation of spiculi was prevented only by the removal of water-soluble membrane-bound proteins by repetitive washing procedures. Band 4.1R protein was reported to be the main Ca^{2+}/calmodulin target within the cytoskeleton. Calcium-calmodulin complexes bind to the band 4.1R protein causing the changes in its conformation and decrease in affinity to the interacting partners within the cytoskeletal network such as p55, glycophorin C, spectrin and actin [251]. These changes require Ca^{2+} levels as high as 0.1 μM (within calmodulin affinity to Ca^{2+}). Therefore Ca^{2+}-induced acute cytoskeletal modifications are physiologically relevant and may occur in pre-membrane space of circulating erythrocytes in which Ca^{2+} uptake is stimulated.

Activation of PKCα by Ca^{2+} induces translocation of the kinase to the erythrocyte membrane [252]. Phosphorylation of the protein kinase C (PKC) targets (band 4.1 and band 4.9 proteins) translates into an increase in erythrocyte deformability [253], [254]. However, half-maximal activation of PKCα occurs in the presence of ~35 μM of free Ca^{2+} [255]. Thus, that type of Ca^{2+}-mediated response is unlikely to be directly implemented in healthy human RBCs. One possible scenario for induction of Ca^{2+}-depended PKC activation in erythrocytes may involve phospholipase C (PLC). EC50 for 1.2-diacylglycerol production was reported to occur in the presence of 0.1 μM of Ca^{2+} in hemoglobin-free ghosts [256]. Maximal activity of the enzyme is reached in the presence of 1 μM of free Ca^{2+}ions. Activation of PLC translates into the stimulation of PKC and the changes

in RBC rheology within the physiological range of intracellular Ca^{2+} concentrations through the following scheme:

Ca^{2+} entrance → active PLC → DAG → active PKC → 4.1-P and 4.9-P → RBC deformability↑

Artificially activated by phorbol 12-myristate 13-acetate, PKC in erythrocytes phosphorylates and stimulates Ca^{2+}-pump and decreases intracellular Ca^{2+} content [257]. Similarly, activation of PKC down-regulates activity of Ca^{2+}-depended K^{+}-channels (Gardos channels) [258]. Both these processes (mediated by PLC) may function as a feedback mechanism triggered in response to Ca^{2+} uptake.

Activity of the erythrocytic Ca^{2+}-pump can be also modulated by direct interactions with Ca^{2+}/calmodulin. Maximal activity (10-fold increase) of the Ca^{2+} pump (V_{max}) may be reached in the presence of 10 μM of free Ca^{2+}, while 1 μM Ca^{2+} triggered about 4-fold increase [259]. Alternatively, up-regulation of the Ca^{2+}-pump activity by excessive Ca^{2+} concentrations can be achieved by the regulatory cleavage of the cytosolic domain of the pump by calpain I. In cleaved enzyme (124 kDa instead of intact 136 kDa protein) both the initial rates of calcium ion uptake and ATP hydrolysis were increased to near maximal levels [260]. Calpain activation is calcium-induced and occurs as free Ca^{2+} levels reach ~ 0. 5 μM [261]. Thus, transient increase in Ca^{2+} uptake in RBCs is associated with adaptive stimulation of Ca^{2+} pump due to the 61otential61i cleavage of the Ca^{2+}-pump by calpain [262]. However, prolonged calpain activation by Ca^{2+} result in degradation of Ca pump protein (along with Band 3 protein cleavage) [262].

In RBCs loaded with Ca^{2+} the limiting factor of the Ca^{2+}-pump transport rate is ATP availability. The pump is fuelled preferentially by a pre-membrane ATP pool [248], [251], [263]. Under conditions of permanent Ca^{2+}-leak, activation of the Ca^{2+}-pump results in rapid ATP depletion. Since ATP is used to produce glucose-6-phosphate, a substrate for pentose phosphate shunt, ATP depletion results in decreased NADPH production. Therefore, Ca^{2+} overload suppresses glutathione regeneration in erythrocytes due to the reduction of intracellular ATP concentration [264]. Glutathione is an important intracellular antioxidant that protects the cell against free radical damage. Erythrocytes depleted in reduced glutathione are subjected to oxidative damage. However, similarly to regulation of intracellular Ca^{2+} content, at some point, transient Ca^{2+} influx may help to

prevent oxidative damage due to the activation of eNOS [265] (only then NOS substrates NADPH and arginine are also present). This enzyme is present in erythrocytes [266] and produces NO, which is a scavenger of superoxide anions. Endothelial NO synthase is activated by Ca^{2+}-calmodulin and hence may sense even subtle changes in the intracellular Ca^{2+} levels [267]. Oxidative state of erythrocytes is an important hallmark for senescence. Band 3 protein clusters forming as a result of oxidative damage serve as binding sites for naturally occurring anti-band 3 antibodies. So marked RBCs are recognized by the macrophages and targeted for clearance from the blood flow [268], [269].

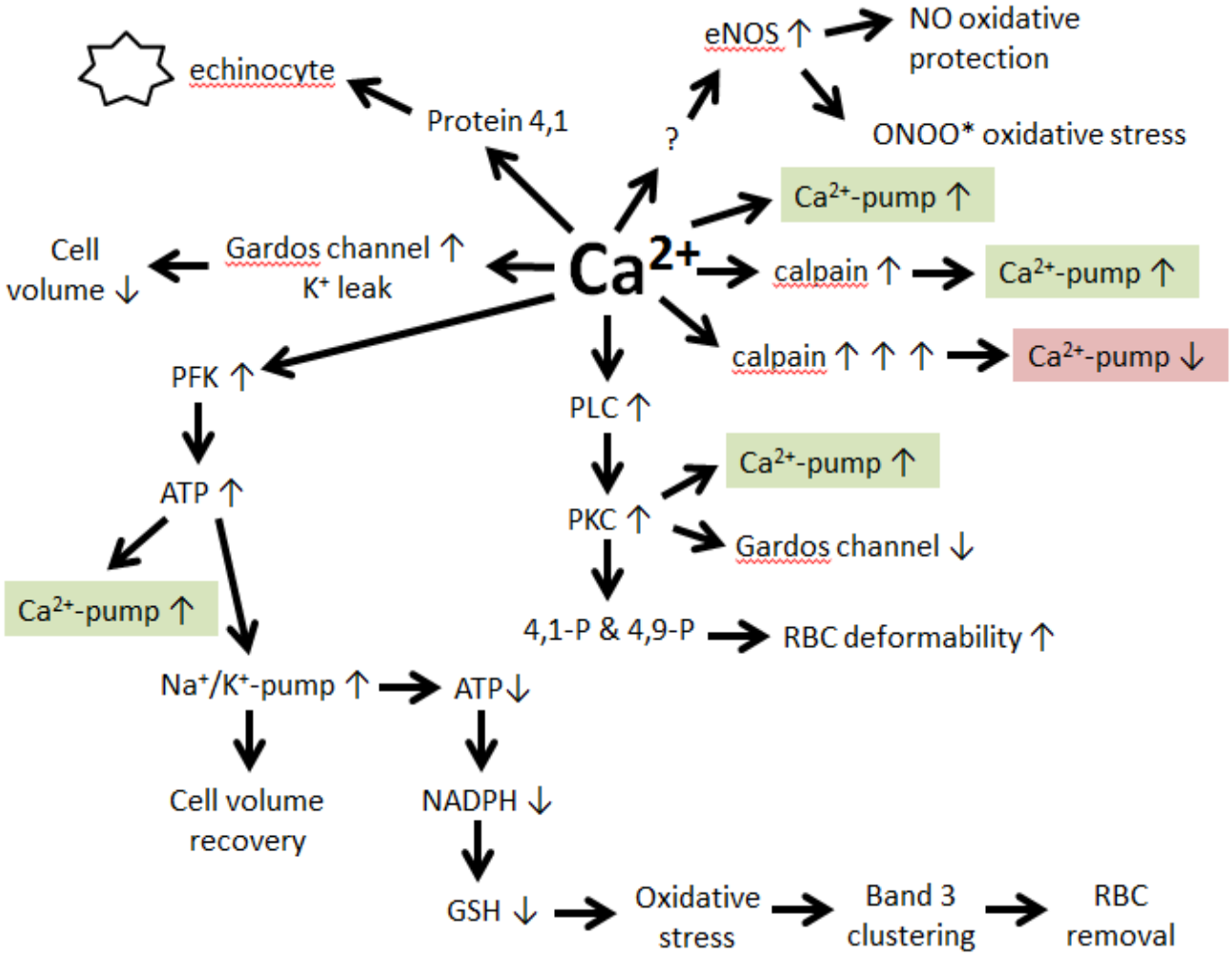

Figure 3.3. Several Ca^{2+}-mediated mechanisms in human RBC featured above. Green rectangles designate Ca^{2+}-ATPase activation induced by Ca^{2+} entrance directly and through the calpain, PKC and PFK-dependent pathways. Red rectangle shows Ca^{2+}-ATPase deactivation as a result of excessive calpain activation caused by prolonged Ca^{2+} stimulation. Ca^{2+} entrance directly activates Gardos channels resulting in cellular dehydration. Simultaneously Ca^{2+} deactivate Gargos channel via PKC-dependent pathway and facilitates ion gradient recovery via stimulation of glycolysis (ATP as a fuel for Ca^{2+}- and

Na^+/K^+-ATPases is produced) as a feedback mechanism. In healthy erythrocytes Ca^{2+} entrance activates reversible volume changes, NO production, increases cell deformability and activates Ca^{2+}-ATPase (transiently or permanently). Excessive Ca^{2+} leak/accumulation in pathological conditions (Table 3.6) result in Ca-pump degradation, decrease of deformability (as a result of dehydration and echinocytosis), oxidative stress, facilitated aging and RBC clearance from the circulation.

Table 3.6. Pathological conditions associated with chronic elevation of intraerythrocytic Ca^{2+}.

$[Ca^{2+}]_i$	Target	Known related pathologies	Possible related pathologies
> 150 nM [244]	Gardos channel (activation)	Sickle cell anaemia; Familial phosphofructokinase deficiency [233]; Hb O(ARAB) mutation [270]	Drug-induced acute hemolytic anemia [271]; Murine spherocytosis (4.1R-/-), compensatory [272]; Murine spherocytosis, mild, 4.2(-/-) [273]; Dehydrated hereditary stomatocytosis [274]
> 500 nM [275]	Calmodulin	Sickle cell anaemia, adenosine monophosphate deaminase hyperactivation leading to PS exposure and faster cellular clearance [276]; Familial phosphofructokinase deficiency, similar mechanism [248]; Sickle cell anaemia, lack of binding to PMCA [277]	Spectrin filaments formation abnormalities [278]; Hereditary elliptocytosis (4.1R inefficiency) [279]; 4.1 deficiency-related Na^+/H^+ exchanger hyperactivation [280]
> 200 nM [277]	PKCα	Sickle cell anaemia, ROS generation via NADPH	Cell volume abnormalities (KCl contrasporter inhibitory

		activation [281]; phosphorylation of adductin, cytoskeletal abnormalities in SCD [282]	phosphorylation) [283]; Deformability abnormalities [253]; Altered volume and cytoskeletal abnormalities due to elevated Band 3 phosphorylation [284]; Band 3 related alterations in activities of metabolic enzymes [285]
> 200 nM [286]	μ-Calpain	β-thalassaemia, α-spectrin digestion [287]; Acute hemolytic crisis in favism, spectrin, band 3 and band 4,1 digestion [288]	Sperocytosis related to cleaved spectrin, band 3 and band 4.1 proteins.

5. Experimental part

Standing hypothesis and rationale

The idea of the present work came from the epidemiological data indicating possible relationships between plasma concentration of homocysteine and the probability of cardiovascular disorders [289]. Homocysteine and its metabolite homocysteic acid are known to be NMDA receptor agonists [290]. Thus, cardiovascular effects of homocysteine at least in part could be attributed to cardiac NMDA receptor activation. Retrospective analysis of studies focusing on the cardiac effects of anesthetics showed that some of the effects caused by NMDA receptor antagonists originate directly from myocardium (see Chapter 3). Moreover, cardiomyocytes similarly to neurons were shown to undergo regular depolarization-repolarization cycles suggesting that voltage-dependent activation of NMDA receptors may occur in these cells. Based on this information we proposed that NMDA receptors could be present and function in mammalian myocardium.

Pilot studies were performed on the isolated blood-perfused rat heart model. We applied several types of NMDA receptor agonists and antagonists adding them to the blood used for coronary perfusion. Blood perfusion through the myocardium was provided by peristaltic pump. As in human heart-lung machine settings, contact of RBCs with the elements of our perfusion system (synthetic materials, peristaltic pump) resulted in RBC damage and visible hemolysis detected in the blood plasma after the experiment. We noticed that in our experimental settings NMDA receptor agonists triggered hemolysis and NMDA receptor antagonists had an opposite effect protecting erythrocytes (see Fig 1). These observations suggested that active NMDA receptors could be present in erythrocytes.

Application of NMDA receptor agonists produced tachy-arrhythmic response whereas antagonists produced bradycardia and regular heart rhythm. In sinus arrhythmia NMDA receptor antagonists normalized heart rhythmicity.

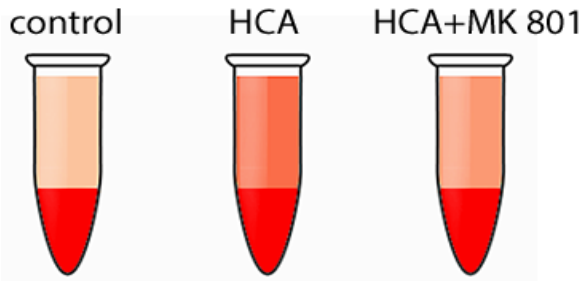

Figure 1. Separated blood plasma on top of sedimented erythrocytes colored by released hemoglobin. NMDA receptor agonists (here homocysteic acid, HCA) intensified hemolysis caused by mechanical damage in peristaltic pump. Pre-treatment with NMDA receptor antagonists (here MK 801) reduced hemolysis.

Based on this pilot study and the following facts discussed in detail in the previous chapters the standing hypothesis was formulated as a basis for the PhD thesis work:

- **NMDA receptors are not intrinsic feature of the brain**

  This follows from the fact that NMDA-like receptors evolved before the appearance of nervous system and is supported by the current studies in which NMDA receptor presence was reported in multiple tissue types. Due to the impressive plasticity and numerous "building blocks" properties of these receptors and their physiological role may display marked tissue-specific variation depending on the tasks they fulfill.

- **These receptors are most likely present in the erythroid lineage and mature red cells**

  Although no attempts were undertaken to search for the NMDA receptors in red blood cells and erythroid precursor cells, several hematopoietic stem cell lineages were shown to express functional NMDA receptors. Furthermore, homocysteine was showing distinct cytotoxicity when applied to red blood cells.

- **NMDA receptors are most likely expressed in the myocardium and are involved in control of heart function**

Multiple evidences including those of our pilot study reveal cardiotoxicity of the NMDA receptor agonists. NMDA receptor antagonists used as anesthetics in the clinic were reported to have cardiac-specific side effects.

Based on these assumptions the following goals of the study were formulated:

Goals

Our first goal was to prove the existence of NMDA receptor in myocardial tissue and erythrocytes. We intended to characterize subunit composition of NMDA receptors in cardiac and erythroid precursor cells and to characterize their pharmacological properties. The second goal was to investigate the physiological role of erythroid and cardiac NMDA receptors. We planned to explore the effects of NMDA receptor agonists and antagonists on autonomic heart rhythm regulation, depolarization and repolarization of the myocardial tissue.

The impact of NMDA receptors into the maintenance of intracellular Ca^{2+} concentration had to be investigated in normal (blood donors: healthy humans and rats) and pathophysiological (blood donors: sickle cell disease patients) conditions. Our goal was to reveal the role of NMDA receptor-mediated Ca^{2+} influx for red blood cell function in health and disease.

Experimental models

1. Isolated autonomously beating rat heart perfused with autologous blood or saline.
2. Rat erythrocytes and bone marrow cells.
3. Human erythrocytes and erythroid precursor cells obtained from the blood of healthy donors.
4. Human erythrocytes and erythroid precursor cells obtained from the blood of sickle cell disease patients.

Section 1: per-reviewed original articles

Paper 1

Functional NMDA receptors in rat erythrocytes

Asya Makhro, Jue Wang, Johannes Vogel, Alexander A. Boldyrev, Max Gassmann, Lars Kaestner and Anna Bogdanova.

Am J Physiol Cell Physiol 298:1315-1325, 2010. First published Mar 24, 2010

Contribution:

Makhro A. participated in study design and discussion. In the result section quantification of the number of [^{3}H]MK-801 binding sites per cell and results showed on Figures 1, 2, 6, 7 were performed by Makhro A.

Functional NMDA receptors in rat erythrocytes

Asya Makhro, Jue Wang, Johannes Vogel, Alexander A. Boldyrev, Max Gassmann, Lars Kaestner and Anna Bogdanova

Am J Physiol Cell Physiol 298:1315-1325, 2010. First published Mar 24, 2010;
doi:10.1152/ajpcell.00407.2009

Am J Physiol Cell Physiol 298: C1315–C1325, 2010.
First published March 31, 2010; doi:10.1152/ajpcell.00407.2009.

Functional NMDA receptors in rat erythrocytes

Asya Makhro,[1] Jue Wang,[2] Johannes Vogel,[1] Alexander A. Boldyrev,[3] Max Gassmann,[1] Lars Kaestner,[2] and Anna Bogdanova[1]

[1]*Institute of Veterinary Physiology and the Zurich Center for Integrative Human Physiology (ZIHP), University of Zurich, Zurich, Switzerland;* [2]*Institute for Molecular Cell Biology, Medical Faculty, Saarland University, Homburg/Saar, Germany; and* [3]*International Biotechnology Centre, Department of Biochemistry, Moscow State University, Moscow, Russia*

Submitted 8 September 2009; accepted in final form 17 March 2010

Makhro A, Wang J, Vogel J, Boldyrev AA, Gassmann M, Kaestner L, Bogdanova A. Functional NMDA receptors in rat erythrocytes. *Am J Physiol Cell Physiol* 298: C1315–C1325, 2010. First published March 31, 2010; doi:10.1152/ajpcell.00407.2009.—*N*-methyl-D-aspartate (NMDA) receptors are ligand-gated nonselective cation channels mediating fast neuronal transmission and long-term potentiation in the central nervous system. These channels have a 10-fold higher permeability for Ca^{2+} compared with Na^+ or K^+ and binding of the agonists (glutamate, homocysteine, homocysteic acid, NMDA) triggers Ca^{2+} uptake. The present study demonstrates the presence of NMDA receptors in rat erythrocytes. The receptors are most abundant in both erythroid precursor cells and immature red blood cells, reticulocytes. Treatment of erythrocytes with NMDA receptor agonists leads to a rapid increase in intracellular Ca^{2+} resulting in a transient shrinkage via Gardos channel activation. Additionally, the exposure of erythrocytes to NMDA receptor agonists causes activation of the nitric oxide (NO) synthase facilitating either NO production in L-arginine-containing medium or superoxide anion ($O_2^{\cdot -}$) generation in the absence of L-arginine. Conversely, treatment with an NMDA receptor antagonist MK-80, or the removal of Ca^{2+} from the incubation medium causes suppression of Ca^{2+} accumulation and prevents attendant changes in cell volume and $NO/O_2^{\cdot -}$ production. These results suggest that the NMDA receptor activity in circulating erythrocytes is regulated by the plasma concentrations of homocysteine and homocysteic acid. Moreover, receptor hyperactivation may contribute to an increased incidence of thrombosis during hyperhomocysteinemia.

red blood cells; homocysteic acid; calcium

NMDA RECEPTORS (NRs) are ligand-gated nonselective cation channels that mediate fast neuronal transmission and long-term potentiation in the central nervous system (CNS) (4). Glutamate is a primary regulator of activity of the NRs in the brain. This specific class of glutamate receptors plays an essential role in regard to memory, cognition, sensation, and motor control. Itako contributes to the glutamate excitotoxicity that is involved with numerous neurological disorders including stroke, schizophrenia, Alzheimer's disease, and Parkinson's disease (39). Recently, NR expression has been reported to exist also outside the CNS in a number of peripheral tissues such as the lungs, heart, kidney, liver, spleen, bone, vascular endothelium, and lymphoid cells (7, 11, 18, 19, 29, 32). The physiological role of NRs in nonneuronal tissues remains largely unclear.

The nature of NR agonist(s) in control of receptor function in nonneuronal tissues is a matter of debate. Glutamate concentration in the synaptic cleft of the brain reaches millimole levels, whereas the circulating plasma concentrations of glutamate in healthy human subjects ranges from 14 to 70 μM (13, 47). These concentrations are below the 100 μM threshold recognized as the IC50 for the receptor activation in neurons (26). Glutamate, thus, is most likely not a major contributor to the regulation of the NRs in blood cells in healthy humans. In addition to glutamate, homocysteine (HC), and homocysteic acid (HCA) have also been shown to function as NR agonists in mammals. Total plasma HC concentration in healthy subjects is ~7–10 μM, which can increase to 22.3 ± 12.6 μM in response to normal aging (42). Pathological increases of HC have also been observed as a result of either a hereditary predisposition affecting methionine metabolism or conditions of folate or vitamin B12 deficiency (16). For instance, in hyperhomocysteinemic patients HC has been observed to reach as high as 476 μM (43). Both HC and HCA possess a high affinity to bind to NRs such that even a modest increase in plasma concentrations may result in activation of the receptors (6).

As previously mentioned, NRs are nonselective ligand-gated cation channels; however, the selectivity of the NR channels for Ca^{2+} exceeds that for Na^+ 10-fold and thus ligand-mediated activation of the receptors typically results in an induction of transient inward Ca^{2+} current. Consequently, both activation and inactivation of NRs, irrespective of host tissue, are linked to the local changes in intracellular Ca^{2+} levels. Such changes in intracellular Ca^{2+} have been reported to assist in facilitating the proliferation of the vascular smooth muscle cells and aortic endothelia cells in response to HC- or HCA-mediated NR activation (11, 46). Megakaryoblasts initiate differentiation and reduction in pro-platelet formation in response to NMDA exposure, whereas proliferation rate and survival remain unaltered (25).

Lymphocytes and thrombocytes are among the blood cells expressing NRs (7, 17). To the best of our knowledge no studies have been performed to assess the presence of functional NRs in erythrocytes, although interaction of noncompetitive and competitive NR antagonists [^{3}H]MK-801 and [^{3}H]CGS-19755, respectively, with red blood cells (RBCs) has previously been reported (36). Furthermore, dehydration of erythrocytes was reported in patents with hyperhomocysteinemia (34). In this study, with the use of rat erythrocytes, we have demonstrated the presence of functional NRs in RBCs and investigated their distribution pattern in addition to their role in regulation of cell volume, osmotic resistance, endothelial nitric oxide synthase (eNOS, NOS3) activity, and cellular redox state.

MATERIALS AND METHODS

Cell isolation and handling. For all experiments we used RBCs from adult male Wistar rats (200–300 g). The animals were purchased

Address for reprint requests and other correspondence: A. Bogdanova, Institute of Veterinary Physiology, Univ. of Zurich, Winterthurerstrasse 260, CH-8057 Zurich, Switzerland (e-mail: annab@access.uzh.ch).

from Elevage Janvier (Le-Genest-Saint-Ile, France) and kept on commercial rodent chow in the sterile laboratory animal facilities at the Institute of Veterinary Physiology. Animal handling and experimentation were reviewed, approved, and carried out in accordance with the Swiss animal protection laws and institutional guidelines. Blood samples were withdrawn from the caudal vena cava into heparinized syringes, and erythrocytes were isolated via centrifugation at 1,000 *g* for 5 min. The buffy coat and plasma were discarded while the remaining RBCs were washed three times with an incubation medium of the following composition (in mM): 145 NaCl, 5 KCl, 1 $CaCl_2$, 0.15 $MgCl_2$, 15 glucose, and 10 Tris·HCl, pH 7.4. Packed cells were then resuspended in the incubation medium supplemented with 0.1% BSA to a hematocrit of 40%.

UT-7/Epo cells were cultured in α-MEM supplemented with 20% fetal calf serum and 3 U/ml human recombinant erythropoietin (EPREX, Janssen-Cilag, Neuss, Germany). Bone marrow cells were harvested from the femur bone. Cells were suspended, filtered through a 200-nm mesh, concentrated by centrifugation at 2,000 *g* for 5 min, and used for either [^{3}H]MK-801 binding experiments or immunoblotting.

Cerebellar tissue was isolated from rat pups at postnatal *day 10* ($n = 5$) and used for immunoblotting. Cerebellar granule cells were isolated from rat pups at postnatal *day 10* as described elsewhere (40) and used for [^{3}H]MK-801 binding experiments.

Erythrocyte cytoskeleton-free membrane preparation. Packed RBCs (about 500 μl) were hemolyzed in 2 ml of ice-cold lysis buffer containing (in mM) 10 Tris·HCl (pH 7.4), 1 EDTA, 0.1 PMSF, 10 $Na_4P_2O_7$, 10 NaF, plus 10 μg/ml pepstatin A, 10 μg/ml leupeptin, and 5 μg/ml aprotinin. Membranes were pelleted at 47 000 *g* for 20 min at 4°C. To enrich the membrane fraction for the NR protein, the obtained ghosts were deprived of most of the cytoskeletal proteins as described elsewhere (23). Protein concentration in the obtained smooth membrane samples was determined by using BCA Protein Assay (Pierce; Rockford, Ill) with BSA as standard.

Radiolabeling with MK-801. A radioactive labeling assay was used to detect the number of putative NRs in erythrocytes, UT-7/Epo cells, and cerebellar granule cells. The respective cells were washed in PBS and incubated with 5 nM [^{3}H]MK-801 (20 Ci/mmol American Radiolabeled Chemicals) per 10^6 cells. The unspecific binding was assessed by treatment of cells with the radiolabeled antagonist in the presence of 100 μM of unlabeled *dl*-5-methyl-10,11-dihydro-5H-dibenzo[a,b]-cyclohepten-5,10-imine (MK-801) for 1 h. The amount of bound [^{3}H]MK-801 was assessed with a Packard 1600 TR liquid scintillation counter, and the number of receptors were calculated thereafter using the following equation:

$$N_{NR} = \frac{A_{cells}}{A_{sp}(MK-801) \cdot N_A \cdot N_{cells}}, \quad (1)$$

where N_{NR} is a number of NRs, A_{cells} is activity of the MK-801 bound to the cells in [Bq], A_{sp} is a specific activity of the [^{3}H]MK-801 in [Bq/mmol], N_A is the Avogadro number (6.022×10^{23} mol^{-1}), and N_{cells} are the number of cells in the sample.

Western blot analysis. For Western blot analysis cells were washed two times in PBS (2,000 *g*, 5 min) and lysed in Laemmli buffer. Membrane proteins were first separated on the 7.5% SDS-PAGE (500 μg protein/lane) and then transferred to Protan BA83 nitrocellulose membranes. Even protein transfer was controlled by Ponceau red staining. Membranes were then blocked for 1 h at room temperature followed by an overnight incubation at 4°C with primary antibodies against the NR1 subunit of NRs (dilution 1:1,000; 1–564 fragment, Novus Biologicals) dissolved in TBS containing 5% milk. The membranes were then washed three times in TBST and incubated for 1 h at room temperature with suitable horseradish peroxidase-conjugated secondary antibodies (1:1,000 dilution; antimouse, Jackson ImmunoResearch Laboratories, West Grove, PA). The enhanced chemiluminescent detection Western blotting system (Fujifilm LAS-3000 System, FUJIFILM Life Science) was used for detection and quantification of protein. Actin served as a loading control.

Immunohistochemistry and flow cytometry. To assess the NR levels in the membranes of reticulocytes and mature erythrocytes, staining for both the NR1 and NR2 subunits of the NR and for the transferrin receptor (TrR) as a marker of reticulocytes was performed. For fluorescent imaging the cells were suspended in the incubation medium at hematocrit of 0.4% and incubated for 60 min on ice with a cocktail of the following primary antibodies: mouse monoclonal anti-NMDA NR1 Pan antibody (1:100 dilution, Novus Biologicals), rabbit polyclonal anti-NMDA NR2 antibody (1:100 dilution; Affinity BioReagents), and rat monoclonal anti-transferrin receptor antibodies (1:100 dilution; Abcam). Thereafter, the cells were washed from the primary antibodies (centrifugation for 5 min at 500 *g* at 10°C) and incubated for an additional 60 min on ice with the corresponding secondary antibodies: anti-rabbit Cy3-conjugated, and anti-mouse Cy5-conjugated, and anti-rat Cy2-conjugated, all in dilution 1:50. After one wash of the secondary antibodies was completed, the specific staining was assessed microscopically (Zeiss Axiovert 200M). Flow cytometry was used to assess the distribution of the NR in RBC population. Erythrocytes in suspension were treated with the mouse monoclonal anti-NR1 antibody (dilution 1:50; Novus Biologicals) for 60 min on ice and thereafter with the secondary anti-mouse Cy-5 conjugated antibody (1:50 dilution) and fluo-4 (final concentration 10 μM) for further 30 min at room temperature. Cells treated with only secondary antibodies were used as a negative control.

Unidirectional K^+(^{86}Rb) influx measurements. Unidirectional influx rates for K^+ were assessed by using ^{86}Rb as a tracer. Unidirectional residual (ouabain-resistant Cl^--independent) K^+ influx was detected in erythrocytes incubated at hematocrit of 5–8% in the chloride-free medium containing (mM) 145 $NaCH_3SO_4$, 5 KCH_3SO_4, 0.15 $MgSO_4$, 1 Ca-gluconate (when not Ca^{2+} free), 10 glucose, 10 sucrose, and 10 HEPES-Tris, pH 7.4 at room temperature. Incubation medium was always supplemented with 1 mM ouabain to block active K^+ influx and with 100 μM L-arginine. Various amounts of NMDA, HCA or glutamate, 1 μM clotrimazole, or 50 μmol MK-801 were added to some of the samples. Cells were preincubated for 15 min to achieve full inhibition of the Na-K-ATPase and allow agonists and inhibitor of the NRs and the blocker of Gardos channels, clotrimazole, to bind to their targets. Influx was then initiated and measured by addition of ^{86}Rb. Aliquots of the RBC suspension (400 μl) were collected 10, 20, 30, 45, and 60 min after the onset of incubation with the tracer and washed from the extracellular ^{86}Rb with ice-cold washing medium containing 100 mM $Mg(NO_3)_2$ and 10 mM imidazol buffered with HNO_3 to the pH 7.4 when on ice. After washing was completed, the cell pellet was lysed in 5% trichloracetic acid (TCA), and the amount of ^{86}Rb accumulated in erythrocytes was assessed in deproteinized supernatant and normalized to the amount of the radioactive tracer in the incubation medium. Unidirectional K^+ influx was then calculated from the slope of the linear part of the radioactive tracer uptake plot.

Intracellular calcium content monitoring. Live cell imaging was performed to monitor intracellular Ca^{2+} kinetics in individual cells treated with NMDA. Cells were loaded with fluo-4 AM (Molecular Probes) at a concentration of 5 μM for 1 h at 37°C. Then cells were washed in Tyrode solution containing (mM) 135 NaCl, 5.4 KCl, 10 glucose, 1 $MgCl_2$, 1.5 $CaCl_2$, and 10 HEPES. The pH was adjusted to 7.35 by using NaOH. Cells were plated on poly-L-lysin (Sigma)-coated coverslips in Tyrode solution, and then the cell sedimentation and dye de-esterification were allowed to occur. Fluorescence was finally measured on an inverted microscope (TE2000, Nikon) equipped with a ×100 Plan Apo 1.4 objective. Attached to the microscope was a video imaging setup (TILL Photonics) consisting of a monochromator (Polychrome IV), a camera (Imago), and the control hard- and software (TILL-vision). Cells were observed at an excitation of 480 nm and images were collected every 5 s. A 505-nm long-pass dichroic mirror separated the emission light from the

excitation light, and a 535/40 bandpass filter was used to further improve the image quality. A local perfusion system was utilized to quickly exchange solutions in the field of view and to apply the agonist NMDA at a concentration of 100 μM. Images were processed in ImageJ (Wayne Rasband, National Institute of Mental Health) and traces handled by Igor Pro software (WaveMetrics).

Osmotic resistance and hemolysis. The effect of agonists and antagonists of the NR on osmotic resistance was assessed acutely by preincubated cells with 1 mM of NMDA or HCA for 1 min at room temperature in the incubation medium. Thereafter, 3 μl of packed cells were added to the cuvette equipped with a magnetic stirrer containing 2 ml of 0.9% NaCl solution (final cell number ~10^7 cells/2 ml). A bolus of distilled water was added to reduce the osmolarity from 300 to 130 mosM. Optical density was monitored at 630 nm every 0.25 s after the initiation of hypoosmotic stress to assess hemolysis. A detailed description of this method may be found elsewhere (48).

Cellular fragility was determined by monitoring shear stress-induced hemolysis. The cells were suspended in either Ca^{2+}-containing or nominally Ca^{2+}-free medium at hematocrit of 40% and incubated for 1 h at 37°C in an Eppendorff Thermomixer (900 rpm shaking speed) in the presence and absence of 100 μM NMDA and/or 100 μM MK-801. Hemolysis was assessed at the end of the incubation as the amount of hemoglobin released into the medium. After centrifugation (5,000 *g* for 10 min at 4°C), supernatant was collected and hemoglobin concentration was determined spectrophotometrically using Drabkin reagent.

Morphological changes of RBCs exposed to the NR agonist. Erythrocytes were suspended in the incubation medium at a ratio 1:200, allowed to settle on the imaging chamber bottom, and pretreated with 10 μM clotrimazole or 5 mM Na_3VO_4 for 15 min at room temperature. Thereafter, HCA at a final concentration of 1 mM was added just before the measurement, and time course of the morphological alterations was followed.

Reduced and oxidized glutathione measurement. Cellular reduced (GSH) and oxidized (GSSG) glutathione content was determined by using Ellmann's reagent as described elsewhere (44). After incubation in the presence or absence of 100 μM NMDA, 100 μM HCA and/or 50 μM MK-801 in L-arginine-free or L-arginine-containing medium for 60 min, 100-μl aliquots of erythrocytes suspension (40% hematocrit) were mixed with 900 μl of 5% TCA, and the obtained lysates were centrifuged for 10 min at 16,000 *g* to pellet denatured proteins. Formation of the colored complex of GSH with the Ellmanns reagent was assessed spectrophotometrically at 412 nm.

Nitrite and nitrate assessment. Erythrocytes in suspension (40% hematocrit) or whole blood were incubated with 100 μM of NMDA, or HCA, or 50 μM MK-801 for 60 min at 25°C in presence or in absence of 200 μM L-arginine or N^G-nitro-L-arginine methyl ester (L-NAME). After the incubation nitrite levels were assessed in the incubation medium or plasma by using a chemiluminescence detection technique. After incubation the erythrocytes were pelleted by centrifugation (16,000 *g*) and the supernatant (medium or plasma) was collected. Nitrate was reduced to nitrite using Cd coated with Cu and (NO_2^- + NO_3^-) assessed by a chemiluminiscence detector CLD 88 (Eco Medics AG, Switzerland) as described elsewhere (33).

Statistical analysis. All data are mean values of at least 5 independent experiments and are presented as means ± SE when not stated specially. The comparison between the experimental groups was performed by using a normality test followed by the two-tailed Student's *t*-test for paired or unpaired samples (GraphPad Instat.V3.05). The level of statistical significance was set at $P < 0.05$, $P < 0.01$, or $p < 0.001$. Fitting of the data obtained for the dose dependence of the HCA and glutamate effects on the residual K^+ influx was performed by using SigmaPlot 8.0 nonlinear regression module (100 iteration steps). The equation chosen for fitting was $y = y_0 + ax/(b+x)$, assuming pseudo-single binding site kinetics for the agonist-receptor interaction.

RESULTS

Presence of NMDA receptor in mature RBCs and bone marrow. The presence of NRs in rat erythrocytes and in erythroid precursor cells has been addressed by using several independent techniques including: immunoblotting, immunohistochemistry, flow cytometry, and radiolabled antagonist binding assay. Double staining of the bone marrow-derived precursor cells with the antibodies against CD36, a marker of erythroid lineage, and against the NR1 subunit of the NRs revealed the presence of cells expressing both CD36 and the NR (Fig. 1*A*). These observations were confirmed via immunoblotting (Fig. 1*B*). NRs were expressed in rat bone marrow and UT-7/Epo human erythroleukemic cell line and could also be detected in the erythrocyte membrane fraction. The size of NR1 subunit (~120 kDa) in erythroid cells was similar to that in rat cerebellum (Fig. 1*B*). The number of receptor copies per cell was assessed from the binding of the radiolabeled NR antagonist [^{3}H]MK-801 covalently interacting with the receptor unit (a tetramer composed of two NR1 and two NR2 subunits) at a 1:1 stoichiometry. Binding studies revealed the presence of 3.5×10^5 copies/cell in UT-7/Epo cells and 8×10^6 copies/cell in dispersed cerebellar granule cells, whereas 8 ± 1.4 binding sites are retained in circulating erythrocytes when equal binding of the antagonist to all cells in the population was assumed. This assumption proved to be false when the distribution of NR (NR1 and NR2 subunits) was assessed in the RBC population with immunocytochemistry and flow cytometry. As depicted in Fig. 1*C*, very few cells contained a high number of NR1 and NR2 subunits. Most of these receptor-possessing cells showed positive staining for the reticulocytes marker TrR. Some cells retained high number of NRs, whereas TrRs was already lost. Figure 2 depicts the scatter plots for RBCs stained with only secondary Cy5-conjugated anti-mouse antibody used as a negative control (Fig. 2*A*), and the cells were loaded with fluo-4 (*Y*-axis) and exposed to the monoclonal mouse anti-NR1 antibodies (*X*-axis) followed by the above-mentioned secondary antibodies (Fig. 2*B*). As can be seen from the Fig. 2*B* a low number (2.37 ± 0.32%, $N = 5$) of cells appearing in the G1 quadrant are characterized by high numbers of the NR copies and high intracellular Ca^{2+} levels. The amount of these receptor-enriched cells could be underestimated as they were found to be more susceptible to hemolysis under conditions of shear stress and could have been lost during centrifugation and the passage through the cytometer (see below). It varied from 0.5 and 4% in different animals. Many more cells in the population residing in G2 quadrant at the scatter plot contained significantly less copies of the receptor and low intracellular Ca^{2+} levels (Fig. 2*B*).

Function of the NRs. NRs are nonselective cation channels that are more sensitive to transport Ca^{2+} into neuronal cells upon activation. High intracellular Ca^{2+} levels in RBCs containing the highest number of NR copies, as indicated in Fig. 2*B*, suggests that the NRs in erythrocyte membrane are functional and mediate basal Ca^{2+} influx into the cells even in the absence of the agonists in the incubation medium. Treatment of the cells with NMDA dramatically facilitated Ca^{2+} accumulation in some but not all cells. Kinetics of the NMDA-induced Ca^{2+} entry into single rat erythrocytes was assessed with live imaging. In agreement with flow cytometry data (Fig. 2*B*), live imaging revealed presence of two subpopulation of RBCs: *1*) "responders," in which the addition of 100 μM NMDA

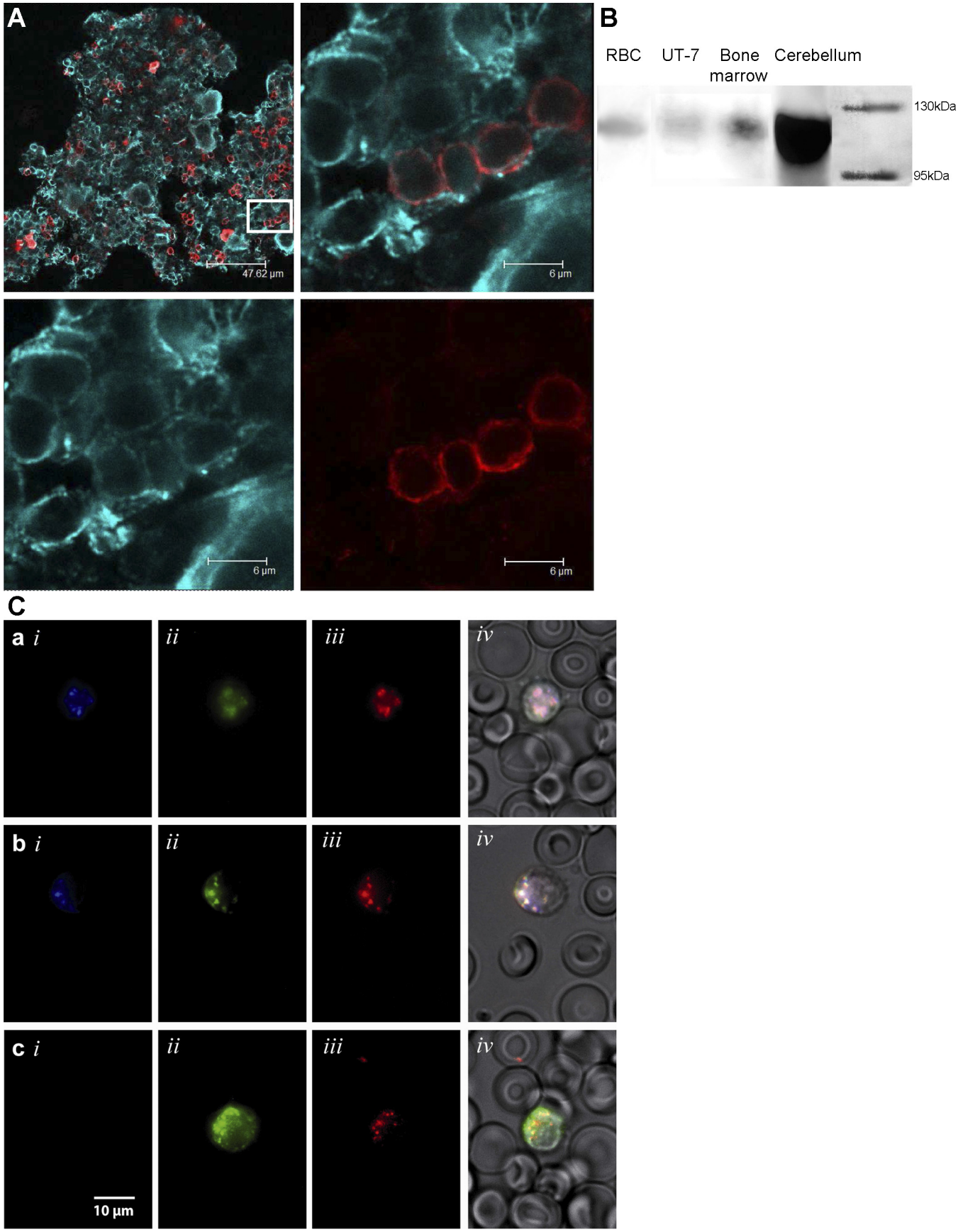

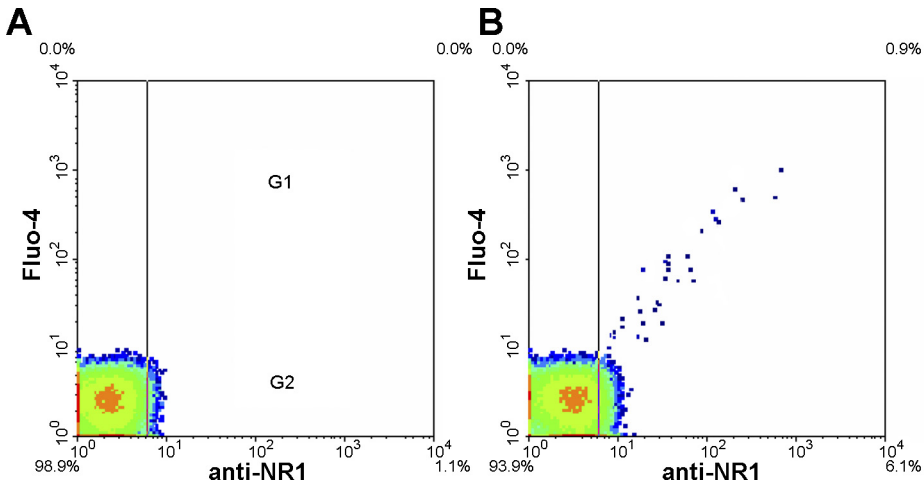

Fig. 2. Correlation between the abundance of the NRs and the intracellular Ca^{2+} levels. *A*: negative control scatter dot plot showing red blood cell (RBC) population chosen according the size (forward scatter) and granularity (side scatter) after incubation with secondary Cy5-conjugated anti-mouse antibodies only. Gating conditions were chosen so that all the cells were located in the lower left quadrant when emission in green fluorescent channel (λ_{em} 488 nm) is shown in *Y*-axes and far red fluorescence intensity (λ_{em} 650 nm) plotted at *X*-axes. *B*: scatter dot plot of the RBCs loaded with fluo-4 and incubated with the anti-NR1 mouse monoclonal primary antibody followed by Cy5-conjugated anti-mouse secondary antibody. Two subpopulations seen in the dot plot represent subpopulation with the high intracellular Ca^{2+} and high number of NR1 copies shifting to the G1 quadrant and the subpopulation with low intracellular Ca^{2+} and low numbers of the NR1 copies in the G2 quadrant. Each plot represents readouts from 10,000 cells. Similar results were obtained in five independent experiments with RBCs obtained from different animals of various age and gender.

triggered a rapid Ca^{2+} accumulation; and *2*) NMDA-insensitive "nonresponders" (Fig. 3). The subpopulation of "responders" consituted 92 of 627 erythrocytes (14.7%). However, of the 92 responding cells only 60 could be used for the final analysis (Fig. 3*B*) since the other 32 lysed during the 15 min of observation. In the control group (524 cells recorded), the Ca^{2+} levels remained stable and low (Fig. 3*B*). Minor but statistically significant increase in the intracellular Ca^{2+} content was thus observed in the whole erythrocyte population treated with NMDA, although the separation of cells into "responders" and "nonresponders" subpopulations revealed that changes in Ca^{2+} were much more pronounced and restricted to the limited number of cells.

Treatment of the cells with HCA, glutamate, or NMDA caused a dose-dependent increase in a unidirectional, residual (ouabain-resistant, chloride-independent) K^+ influx, which was measured by using ^{86}Rb as a tracer for K^+ transport (Fig. 4). Doses of the agonists required to cause the half-activation of the K^+ influx (IC50) was estimated by fitting the respective curves and were found to be 21.1 ± 0.78 μM for HCA and 88.2 ± 0.1 μM glutamate (Fig. 4*A*). Although the exact estimation of the IC50 value for NMDA could not have possibly been determined, maximal specific activation was already observed at 50 and 10 μM without an effect (Fig. 4*B*). This suggests an IC50 value of about 30 μM. Higher supraphysiological concentrations (500–1,000 μM) of the synthetic NR agonist further resulted in a nonspecific increase in the residual K^+ influx. The NMDA sensitivity of the K^+ influx was lost in the presence of MK-801, an antagonist of NRs (Fig. 5*A*). NMDA-mediated upregulation in K^+ influx was clearly secondary to the Ca^{2+} uptake as it was suppressed in Ca^{2+}-free medium (Fig. 5*B*). This finding along with sensitivity of NMDA-induced fluxes to clotrimazole, a Gardos channel blocker, suggests that entry of Ca^{2+} into the cells through the NR facilitates the opening of the Gardos channel.

Cell volume control, osmotic resistance, and morphological alterations. Activation of Gardos channels is known to have a profound effect on cell volume. The Ca^{2+} uptake kinetics (Fig. 3) suggests that NMDA-induced cellular shrinkage occurs within the first several minutes of treatment. The corresponding alterations in cellular morphology were observed in response to HCA treatment in some cells within the first 80 s of exposure to the NR agonist; however, this effect was not ubiquitous among all cells (Fig. 6*A*). The respective alterations in morphology were completely reversed within 180 s of cellular exposure to HCA alone but not during the simultaneous treatment of HCA and the Ca^{2+} pump inhibitor Na_3VO_4. Vanadate treatment did, however, increase the number of responding cells suggesting that the low Ca^{2+} levels in erythrocytes with few NRs (Fig. 2*B*) was maintained due to the efficiency of the Ca^{2+} pump. Activation of the Gardos channels was involved in the temporary morphological changes as treatment of the cells with clotrimazole almost entirely suppressed the HCA-induced cupping and echniocytosis (Fig. 6*A*).

Fig. 1. Presence of the *N*-methyl-D-aspartate (NMDA) receptors (NR) in the membranes of erythroid precuror cells and circulating erythrocytes. *A*: confocal image of the bone marrow tissue stained using the antibodies against CD36 (red channel) and NR1 (cyan channel). The magnified area is framed and the single channels and the overlay of the magnified area are shown. The staining was repeated four times. *B*: presence of the NR1 subunit at the protein level in rat erythrocyte cytoskeleton-free smooth membranes, UT-7/Epo cell line, rat bone marrow cells, and rat cerebellum. The experiment was repeated four times. *C*: abundance of NR in erythrocytes. Staining with the antibodies against transferrin receptor (TrR) (blue channel, *i*), NR1 (green channel, *ii*), and NR2 (red channel, *iii*), was performed in nonfixed cells. Shown are the single channel recording and an overlay of all three fluorescent channels with the bright field image. Cells in *a* and *b* subset of images contain both subunits of the NR and a TrR, whereas the cell in *c* subset contains NR1 and NR2 subunits but lacks TrR. Staining was repeated four times and at least 10 fields were analyzed in a single experiment.

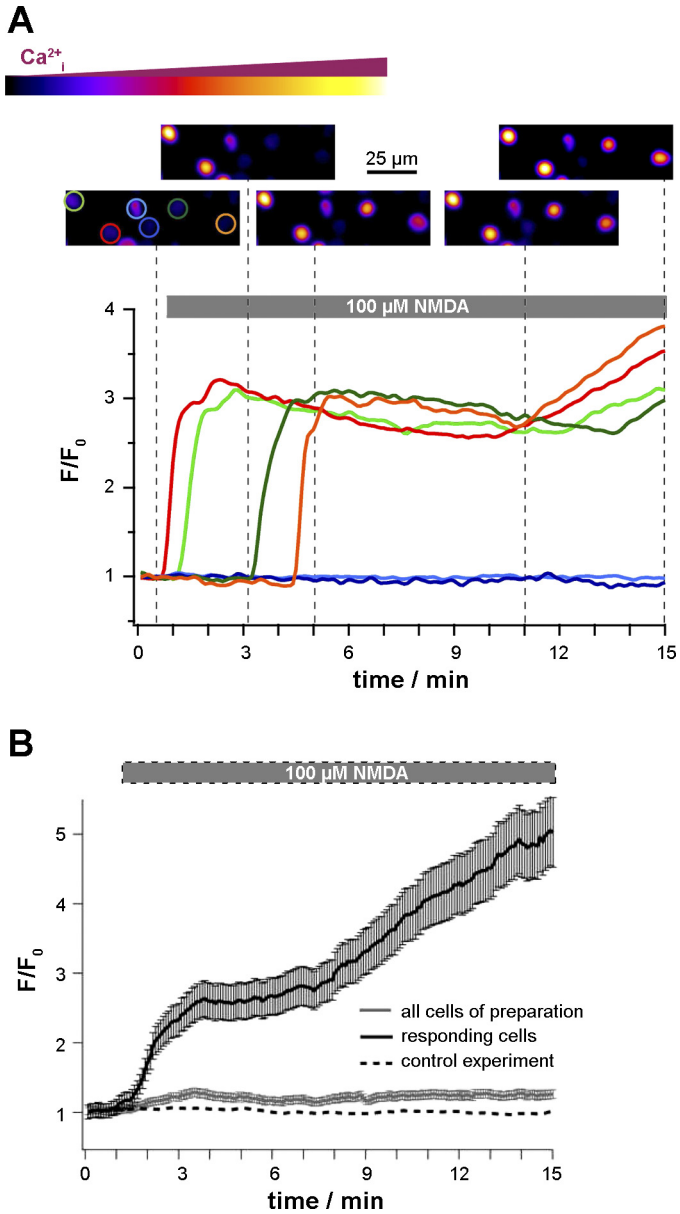

Fig. 3. Kinetics of Ca^{2+} uptake by the NMDA-treated erythrocytes. *A*: original recordings of the changes in the intracellular Ca^{2+} levels in single cells visualized by monitoring fluorescence from the fluo-4 Ca^{2+} sensor in response to 100 μM NMDA treatment. Time of incubation with NMDA is shown with a grey bar. Images of single cells are shown and those that were chosen for analysis are marked as regions of interest with colored circles. The changes in the fluorescent intensity (*F*) normalized to the initial one (*Fo*) over time is plotted below in the corresponding colors. The color coding scale for the relative changes in the intracellular Ca^{2+} levels is shown above. *B*: statistical analysis of cell populations exposed to 100 μM NMDA (grey and black plots) and control cells (dotted plot). The grey plot represents mean values ± SE of 627 randomly chosen cells from three independent preparations of different animals exposed to NMDA for 15 min, whereas the black plot shows means ± SE for the responding subpopulation of 60 cells (for details see text). The variety of the onset time of individual cells leads to a slower increase compared with single erythrocytes as shown in *A*.

An acute osmotic resistance test also indicated that both HCA and NMDA result in RBC shrinkage thus making the cells more resistant to osmotic hemolysis (Fig. 6*B*). Hemolysis rate was assessed via the observation of hemoglobin liberation into the medium during the first 60 s of cells exposure to hypoosmotic shock.

Cellular shrinkage is known to trigger a regulatory volume increase response (RVI) mediated by the volume-sensitive Na/H exchanger or Na-K-2Cl cotransporter in rat erythrocytes (37). We have also observed the late RVI response in rat erythrocytes treated with NMDA or HCA. Swelling of cells treated with NR agonists for 1 h was monitored and water content was seen to increase from 65.8 ± 1.0% in control to 66.7 ± 0.6% in cells exposed to 100 μM HCA and 67.2 ± 1.7% after treatment with 100 μM NMDA at 37°C. The fact that long-term treatment with the NR agonists made the cells more susceptible to the shear stress-induced hemolysis (Fig. 6*C*) could also be explained as a result of secondary swelling. This agonist-induced hemolysis could be completely abolished by treating erythrocytes with MK-801 and significantly reduced through the use of a nominally Ca^{2+}-free medium.

NO synthase activation and glutathione oxidation. Function of the eNOS present in the red cell membrane of rodents and humans (27, 33) is Ca^{2+} dependent (45). Treatment of the whole blood with MK-801 resulted in a dose-dependent inhibition of NO_2^- + NO_3^- accumulation in plasma, whereas exposure to NMDA facilitated de novo NO production (Fig 7A). These observations were confirmed using erythrocytes suspension

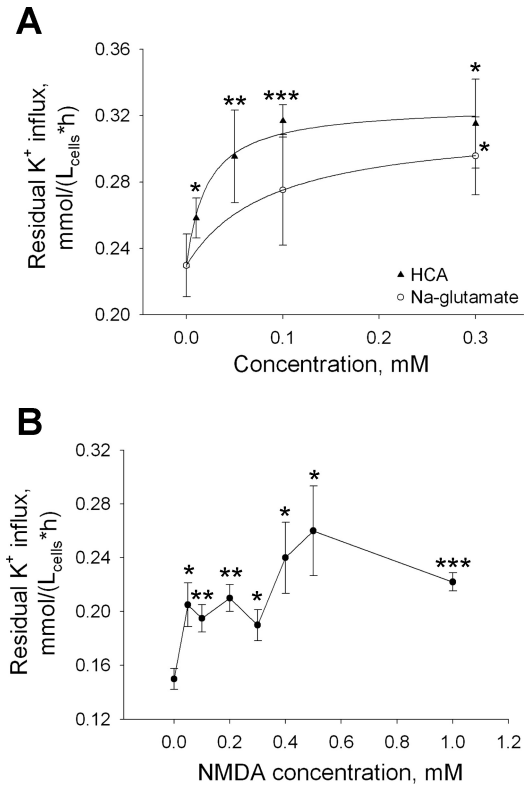

Fig. 4. Effect of NR agonists on the residual (ouabain-insensitive, chloride-independent) K^+ influx in rat erythrocytes. *A*: dose dependence of the effect of the physiological agonists, glutamate, and homocysteic acid (HCA) on the residual K^+ influx. Data are means of five independent experiments ± SE. The curve was obtained by fitting using the equation $y = y_0 + ax/(b+x)$. The constants obtained for the HCA plot were $y_0 = 0.229$, $a = 0.0972$, $b = 0.0211$ and the corresponding coefficient for the glutamate curve were $y_0 = 0.229$, $a = 0.0854$, $b = 0.0882$. *B*: dose-response curve for the effect of the synthetic agonist NMDA on the residual K^+ influx. Data are means of 6–10 experiments ± SE. $^*P < 0.05$, $^{**}P < 0.01$, and $^{***}P < 0.001$ in paired Student's t-test compared with the nontreated control.

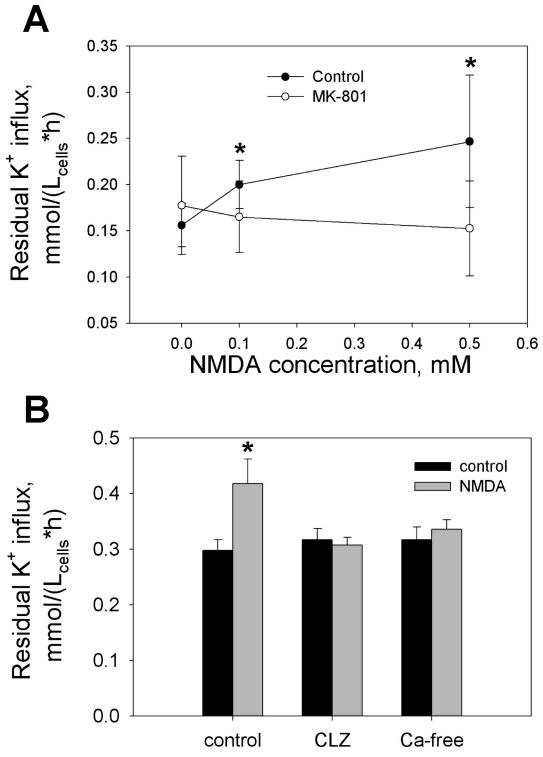

Fig. 5. Pharmacological inhibition of the NMDA-induced activation of the residual K^+ influx. *A*: inhibition of the NMDA-sensitive component of the K^+ influx by antagonist of the NR MK-801 (50 μM). Data are means of six independent experiments ± SE. *B*: lack of the NMDA-induced stimulation of the residual K^+ influx in cell pretreated with the Gardos channel blocker clotrimazole (1 μM) as well as in Ca^{2+}-free incubation medium. Data are means of five independent experiments ± SE. $^*P < 0.05$ in paired Student's *t*-test compared with the nontreated control.

(Fig. 7*B*). Conversely, exposure of erythrocytes to the NR agonists NMDA or HCA for 1 h resulted in an increased (NO_2^- + NO_3^-) generation in erythrocytes suspension (Fig. 7*B*). Agonist-induced activation of NO production was initiated through the activation of the NR, which can be antagonized by MK-801. HCA-induced generation of NO required the presence of extracellular L-arginine and was blocked by L-NAME, which suggests that it was mediated by the eNOS (Fig. 7*B*).

Oxidative burst in cells suspended in L-arginine-free medium was concomitant to the activation of the RBC-eNOS by either NMDA or HCA as observed by the increase in the intracellular GSSG levels (Fig. 7*C*). In the L-arginine-supplemented medium, treatment of the cells with HCA (Fig. 7*C*) or NMDA (data not shown) had negligible effects on the intracellular GSSG levels. HCA-induced oxidation was also inhibited by the NR antagonist MK-801 or by L-NAME (Fig. 7*C*). In the absence of NR agonists L-NAME or L-arginine supplementation to the incubation medium did not cause any changes in the intracellular GSSG content (data not shown).

DISCUSSION

In this study we present data that demonstrates the presence of functional NMDA receptors in mammalian RBCs. The combination of both subunits (NR1 and NR2) are required to form a functional channel in neurons (28), and we provide evidence of both subunits in membrane of the erythrocyte (Fig. 1, *B* and *C*). Pharmacological characteristics of these receptors resemble those reported for NRs in neurons. Agonists and antagonist both interact with these receptors at concentrations reported for neurons (14, 26, 30). We have established evidence suggesting that the number and the activation state of NRs in circulating erythrocytes (the latter dependent on HC and/or HCA levels in plasma) are critical in control of the intracellular Ca^{2+} levels (Figs. 2 and 3).

The physiological role of the NR receptor may only be fully understood once we know the abundance of the receptor present in erythrocytes as well as the mechanisms regulating the function of the receptor as well as the nature of agonists and antagonists. Whereas some speculations may be made on the nature of agonists, mechanisms in control over the NRs abundance in red cell membrane remains unknown. Plasma glutamate concentration in healthy subjects (14 to 47 μM; 3, 13, 47) are significantly lower than that measured in the synaptic cleft where it reaches several millimoles (14). Our data indicate that glutamate binding to the NRs in rat brain and erythrocytes share similar IC50 of 96 ± 2 μM (26) and 88.2 ± 0.01 μM (Fig. 4*A*), respectively. Plasma HC and HCA concentrations reported in healthy subjects range between 8 and 15 μM (24). These values may rise substantially (up to 400 μM) as a result of folate or vitamin B12 deficiency, pregnancy, aging, or as a result of a hereditary methionine metabolism-related disorder (41). Values reported for the NR's IC50 in the brain for HC and HCA are 14 ± 4 μM (51) and 14 μM (51), respectively, whereas it is 21.1 ± 0.78 μM for erythrocytes (Fig. 4*A*). These data suggest that in healthy subjects these two agonists predominantly control NR activity in circulating RBCs, whereas glutamate will only be of importance in pathological cases such as stroke when plasma glutamate concentration may rise up to 200 μM (10). Magnesium is one of the physiologically relevant inhibitors of NRs in the brain. In the present study we only tested responses of NRs present in erythrocytes to pharmacological inhibitors that are more selective and well-characterized. In erythrocytes MK-801 irreversibly inhibits the receptor-mediated ion transport and downstream processes at micromolar concentrations used in electrophysiological studies on brain slices (e.g., 49).

The NRs were not homogeneously distributed in the erythrocyte population and were most prevelant in reticulocytes (Fig. 1*C*). Although the number of receptor copies per reticulocytes were high compared with mature and senescent red cells, they were 3500-fold lower than that in UT-7(Epo) cell line suggesting that receptor levels are dramatically reduced during the late stages of differentiation of the erythroid precursors. Moreover, reduction in numbers has also been shown for other receptor types, some of which (e.g., TrR) are used as a marker of reticulocyte count. Although not all cells lacking TrR were also deprived of NR (Fig. 1*C*) suggesting that the NR is not present solely in reticulocytes and thus cannot be used as marker for them. Existence of erythrocytes with particularly either high or low levels of NRs may also be observed by using flow cytomery (Fig. 2). We have recently reported a similar distribution pattern for the erythropoietin receptors in mouse erythrocytes. These receptors are most abundant in reticulocytes and present at much lower levels in young and mature red cells while virtually absent in senescent cells (33).

Relatively high density of NRs in young cells may contribute to the process that selectively removes young erythrocytes

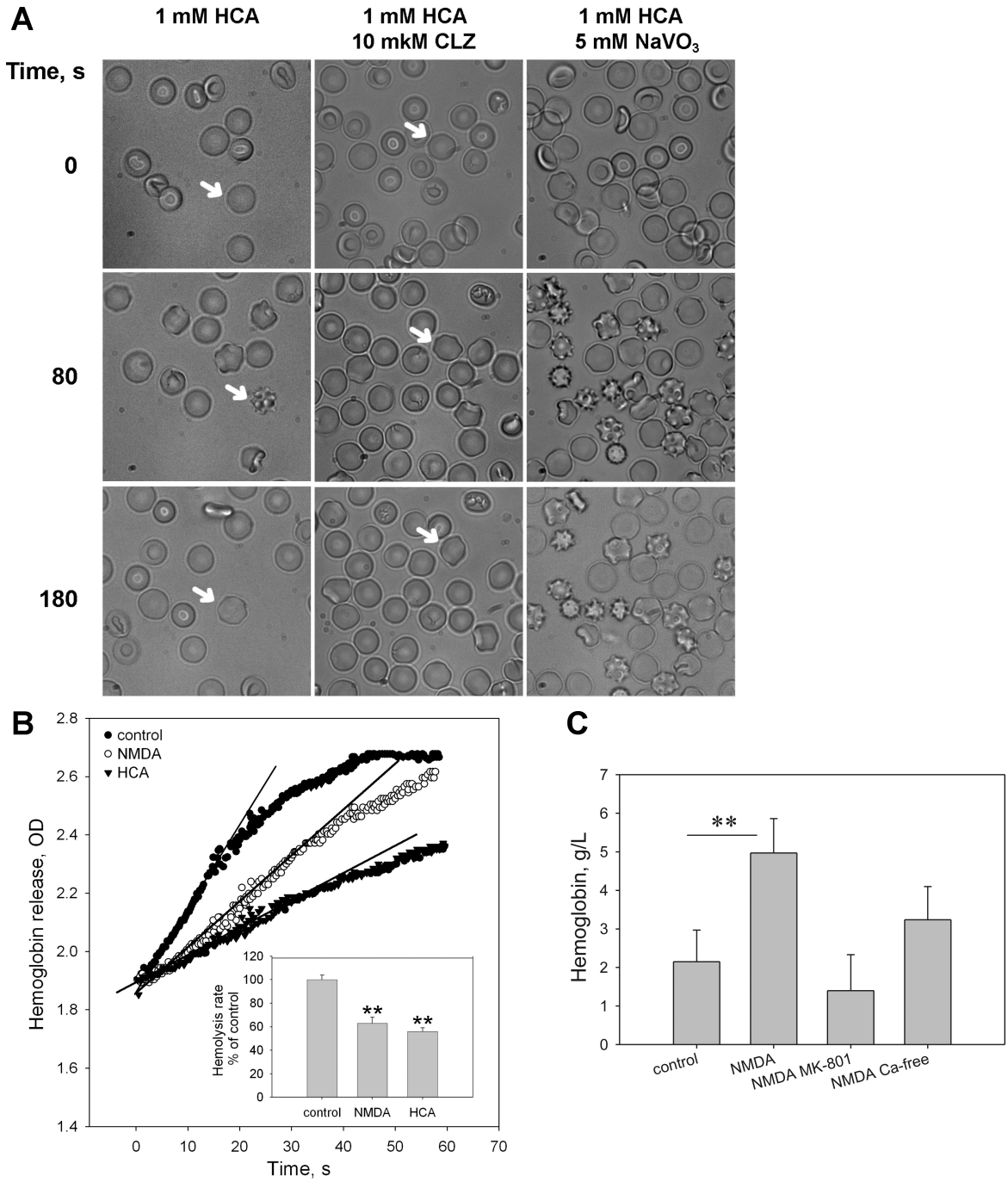

Fig. 6. Secondary changes in erythrocyte morphology, osmotic resistance, and resistance to shear stress caused by NR agonists. *A*: acute morphological alterations triggered by a high dose (1 mM) of NR agonist homocysteic acid (HCA) in the absence or in the presence of 10 μM clotrimazole or 5 mM Na_3VO_4. Images are taken from the cells before and 100 or 180 s after the addition of the HCA. Cells highlighted with arrows show characteristic reversible shape changes when exposed to HCA alone and or in the presence of clotrimazole. Inhibition of the Ca^{2+} pump with Na_3VO_4 facilitated the rate of echinocytic transformation and the number of responding cells compared with that in the presence of HCA alone as well as made these changes irreversible. *B*: osmotic resistance of rat erythrocytes treated with 1 mM HCA or NMDA. Osmotic resistance was assessed as a rate of hemolysis in response to acute hypoosmotic stress. Exposure of cells to agonists of the NR for 1 min caused a significant decrease in hemolytic rates calculated from the linear slopes of the plots of hemoglobin release. Shown are the representative hemoglobin liberation kinetics plots. *Inset*: statistical analysis of the rate of osmotic hemolysis for nine independent experiments; $^{**}P < 0.01$ compared with the nontreated control. *C*: shear stress-induced hemolysis in cells after a long-term exposure to NMDA. Accumulation of hemoglobin in the incubation medium during 1 h at 37°C in an Eppendorff Thermomixer (900 rpm shaking speed) was assessed in control cells and in the cells exposed to 100 μM NMDA ± 100 μM MK-801 in the presence or absence of 1 mM Ca^{2+} in the incubation medium. Data are means of seven independent experiments ± SE; $^{**}P < 0.01$.

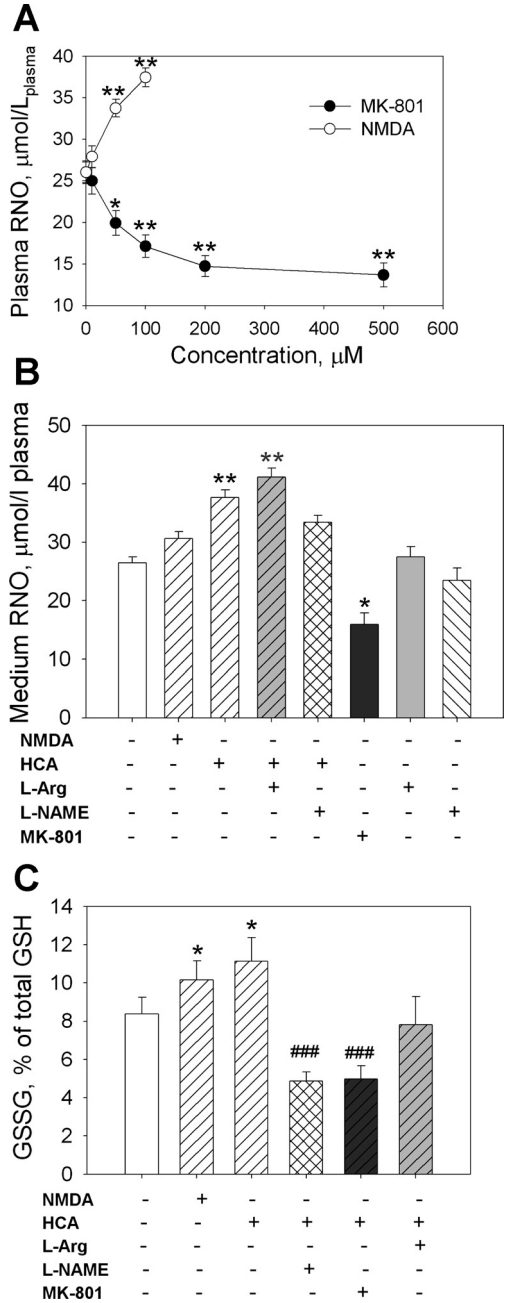

Fig. 7. Effect of the NR agonists and antagonist on the NO production and the intracellular redox state. *A*: total oxidized NO (RNO: NO_2^- + NO_3^-) levels in whole blood as a function of treatment with various concentrations of MK-801 or NMDA for 1 h. Data are means of five5 experiments ± SE; *$P < 0.05$ and **$P < 0.01$ compared with the basal levels of RNO in plasma. *B*: RNO levels in the incubation medium in which the RBC were exposed to the 100 μM of the NR agonists NMDA or HCA (right side-facing hatched bars) or 50 μM antagonist MK-801 (dark grey bar) in the presence or in the absence of either 100 μM L-arginine (grey bar) or nitro-L-arginine methyl ester (L-NAME) (left side-facing hatched bar) for 1 h. Combined treatment is represented as a combination of the corresponding bar filling. *$P < 0.05$ and **$P < 0.01$ compared with the untreated control (open bars). *C*: intracellular GSSG content in percentage of total GSH levels in erythrocytes treated similar as in *B*. Right side facing-hatched bars represent agonist-treated cells, left side-facing hatching stands for the L-NAME-treated ones, dark and light grey filling represents MK-801 and L-arginine exposure, respectively. The corresponding controls for the GSSG content in the cells treated with L-arginine, MK-801, or L-NAME alone are not shown and did not differ from the control shown as an open bar. Data are means of five independent experiments ± SE. *$P < 0.05$ compared with control (open bars) and ###$P < 0.001$ compared with the values in cells treated with HCA alone (right side-facing hatched bars).

when Epo receptors are dormant, which is known as neocytolysis (2, 12). In contrast to the common opinion that Ca^{2+} levels increase with red cell maturation and senescence (15), our data indicates that reticulocytes contain more Ca^{2+} than the either adult or senescent cells (Fig. 2). Thus Ca^{2+}-induced processes may control the rapid decrease in blood cell mass, whereas clearance of senescent cells is regulated by other factors (31). Assessing the effects that Epo has on the activation state of NR and intracellular Ca^{2+} levels may shed light on the mechanism(s) involved in selective clearance of reticulocytes and young erythrocytes during conditions of Epo deficiency and the potential effects of Epo on the "non-selective cation channels" described my Myssina et al. (35).

Accumulation of Ca^{2+} in the cells following treatment with NR agonists is a common mechanism demonstrating NMDA/HCA cytotoxicity in erythrocytes and neurons (28) (Figs. 2 and 3). Exposure of erythrocytes to NMDA or HCA gives rise to numerous Ca^{2+}-dependent responses. Downstream targets of the Ca^{2+}-sensitive signaling cascade have different Ca^{2+} sensitivity thresholds. Gardos channel activation requires 1–3 μM Ca^{2+} to reach half-activation (20). These channels remain closed under most physiological conditions and are only activated by maneuvers that result in intracellular Ca^{2+} accumulation (5). Activation of the Ca^{2+}-dependent, clotrimazole-sensitive K^+ influx can be observed in the presence of 50–100 μM NMDA, whereas treatment of the cells with MK-801 or clotrimazole shows no effect (Fig. 5). Changes in the intracellular Ca^{2+} trigger characteristic alterations in erythrocyte morphology (21, 22) resembling those we have observed in NMDA-treated cells (Fig. 6*B*). These reversible alterations in cell shape, which can be blocked by clotrimazole, reveal the result of Gardos channel activation.

De novo NO production by RBC-eNOS is Ca^{2+} dependent. Half-activation of eNOS requires 50–300 nM Ca^{2+} depending on the phosphorylation state of the enzyme (45). Thus threshold levels of intracellular Ca^{2+} for eNOS activation are lower than those for Gardos channel activation (1–3 μM). Inhibition of Ca^{2+} uptake via NRs by MK-801 compromises eNOS function as Ca^{2+} levels drop below 50–100 nM due to its removal from the cytosol by the Ca^{2+} pump (Fig. 7*A*). On the other hand, treatment of the cells with NMDA further stimulates NO production in the presence of L-arginine, which suggests that steady-state Ca^{2+} levels are insufficient to support function of the eNOS at maximal rates. Changes in the NO production by erythrocytes in turn are reported to affect deformability, redox state, and oxygen-carrying capacity of RBCs(33, 38).

In rat erythrocytes, alterations in activity of RBC-eNOS had an immediate effect on the intracellular redox balance. As shown before in mouse erythrocytes (33), activation of eNOS in rat RBCs by NR agonists was pro-oxidative under conditions of L-arginine deprivation as eNOS was forced into the $O_2^{\cdot -}$-generating mode (Fig. 6*C*). Similar effects were observed in mouse erythrocytes upon treatment with Epo (33). Oxidative stress triggered by NR activation may possibly contribute to an increased susceptibility of erythrocytes to shear stress-induced hemolysis after a long-term exposure to NMDA or HCA (Fig. 5*C*).

Taken together our findings indicate that an increase in the number or activity of NRs may cause oxidative stress, abnor-

mal volume regulation, and hemolysis. These events may contribute to the increased incidence of thrombosis and anemia that has been reported in patients with high concentration of HC, which can reach 200–300 μM (1, 8). Macrocytosis and abnormal RBC morphology are reported in patients with hyperhomocysteinemia (1) in which similar mechanisms as those described here may actually occur in vivo. So far the effect of HC on platelets has been suggested to be the only cause of thrombotic complications (34). If our observations on rat erythrocytes reflect the conditions in human red cells, these cells would also contribute to HC-induced thrombus formation and hemolytic anemia in patients with vitamin B12 and folate deficiency (50). The final impact of HC/HCA on the survival prognosis or mortality risk in hemodialysis patients was shown to increase by 3% per each additional 1 μM of HC in the plasma (9). The next step therefore would be to assess the levels of NRs in erythrocytes of healthy subjects and patients with various forms of anemia. This work is currently in progress.

ACKNOWLEDGMENTS

We thank Robert A. Jacobs for assistance with the revisions and editing of this manuscript.

GRANTS

This study was funded by the Swiss National Fund (SNF no. 31003B-112449 and 310030-124970) and the Zurich Center for Integrative Human Physiology to A. Bogdanova and the grant of the Saarland Ministry for Economy and Science (to L. Kaestner).

DISCLOSURES

No conflicts of interest are declared by the author(s).

REFERENCES

1. **Acharya U, Gau JT, Horvath W, Ventura P, Hsueh CT, Carlsen W.** Hemolysis and hyperhomocysteinemia caused by cobalamin deficiency: three case reports and review of the literature. *J Hematol Oncol* 1: 26, 2008.
2. **Alfrey CP, Fishbane S.** Implications of neocytolysis for optimal management of anaemia in chronic kidney disease. *Nephron Clin Pract* 106: c149–156, 2007.
3. **Andras IE, Deli MA, Veszelka S, Hayashi K, Hennig B, Toborek M.** The NMDA and AMPA/KA receptors are involved in glutamate-induced alterations of occludin expression and phosphorylation in brain endothelial cells. *J Cereb Blood Flow Metab* 27: 1431–1443, 2007.
4. **Bashir ZI, Alford S, Davies SN, Randall AD, Collingridge GL.** Long-term potentiation of NMDA receptor-mediated synaptic transmission in the hippocampus. *Nature* 349: 156–158, 1991.
5. **Bennekou P, Christophersen P.** Ion channels. In: *Red Cell Membrane Transport in Health and Disease*, edited by Bernhardt I and Ellory JC. Berlin: Springer, 2003, p. 139–152.
6. **Boldyrev AA, Johnson P.** Homocysteine and its derivatives as possible modulators of neuronal and non-neuronal cell glutamate receptors in Alzheimer's disease. *J Alzheimers Dis* 11: 219–228, 2007.
7. **Boldyrev AA, Kazey VI, Leinsoo TA, Mashkina AP, Tyulina OV, Johnson P, Tuneva JO, Chittur S, Carpenter DO.** Rodent lymphocytes express functionally active glutamate receptors. *Biochem Biophys Res Commun* 324: 133–139, 2004.
8. **Brattstrom L, Wilcken DE.** Homocysteine and cardiovascular disease: cause or effect? *Am J Clin Nutr* 72: 315–323, 2000.
9. **Buccianti G, Baragetti I, Bamonti F, Furiani S, Dorighet V, Patrosso C.** Plasma homocysteine levels and cardiovascular mortality in patients with end-stage renal disease. *J Nephrol* 17: 405–410, 2004.
10. **Castellanos M, Sobrino T, Pedraza S, Moldes O, Pumar JM, Silva Y, Serena J, Garcia-Gil M, Castillo J, Davalos A.** High plasma glutamate concentrations are associated with infarct growth in acute ischemic stroke. *Neurology* 71: 1862–1868, 2008.
11. **Chen H, Fitzgerald R, Brown AT, Qureshi I, Breckenridge J, Kazi R, Wang Y, Wu Y, Zhang X, Mukunyadzi P, Eidt J, Moursi MM.** Identification of a homocysteine receptor in the peripheral endothelium and its role in proliferation. *J Vasc Surg* 41: 853–860, 2005.
12. **De Santo NG, Cirillo M, Kirsch KA, Correale G, Drummer C, Frassl W, Perna AF, Di Stazio E, Bellini L, Gunga HC.** Anemia and erythropoietin in space flights. *Sem Nephrol* 25: 379–387, 2005.
13. **Divino Filho JC, Hazel SJ, Furst P, Bergstrom J, Hall K.** Glutamate concentration in plasma, erythrocyte and muscle in relation to plasma levels of insulin-like growth factor (IGF)-I, IGF binding protein-1 and insulin in patients on haemodialysis. *J Endocrinol* 156: 519–527, 1998.
14. **Dzubay JA, Jahr CE.** The concentration of synaptically released glutamate outside of the climbing fiber-Purkinje cell synaptic cleft. *J Neurosci* 19: 5265–5274, 1999.
15. **Foller M, Huber SM, Lang F.** Erythrocyte programmed cell death. *IUBMB life* 60: 661–668, 2008.
16. **Fowler B.** Homocysteine: overview of biochemistry, molecular biology, and role in disease processes. *Seminars Vasc Med* 5: 77–86, 2005.
17. **Genever PG, Wilkinson DJ, Patton AJ, Peet NM, Hong Y, Mathur A, Erusalimsky JD, Skerry TM.** Expression of a functional *N*-methyl-D-aspartate-type glutamate receptor by bone marrow megakaryocytes. *Blood* 93: 2876–2883, 1999.
18. **Gill S, Veinot J, Kavanagh M, Pulido O.** Human heart glutamate receptors–implications for toxicology, food safety, and drug discovery. *Toxicol Pathol* 35: 411–417, 2007.
19. **Gill SS, Pulido OM.** Glutamate receptors in peripheral tissues: current knowledge, future research, and implications for toxicology. *Toxicol Pathol* 29: 208–223, 2001.
20. **Grygorczyk R, Schwarz W.** Properties of the Ca^{2+}-activated K^+ conductance of human red cells as revealed by the patch-clamp technique. *Cell Calcium* 4: 499–510, 1983.
21. **Hagerstrand H, Danieluk M, Bobrowska-Hagerstrand M, Iglic A, Wrobel A, Isomaa B, Nikinmaa M.** Influence of band 3 protein absence and skeletal structures on amphiphile- and Ca(2+)-induced shape alterations in erythrocytes: a study with lamprey (*Lampetra fluviatilis*), trout (*Onchorhynchus mykiss*) and human erythrocytes. *Biochim Biophys Acta* 1466: 125–138, 2000.
22. **Hagerstrand H, Mrowczynska L, Salzer U, Prohaska R, Michelsen KA, Kralj-Iglic V, Iglic A.** Curvature-dependent lateral distribution of raft markers in the human erythrocyte membrane. *Mol Membr Biol* 23: 277–288, 2006.
23. **Hayashi H, Jarrett HW, Penniston JT.** Peripheral proteins and smooth membrane from erythrocyte ghosts. Segregation of ATP-utilizing enzymes into smooth membrane. *J Cell Biol* 76: 105–115, 1978.
24. **Herrmann M, Taban-Shomal O, Hubner U, Bohm M, Herrmann W.** A review of homocysteine and heart failure. *Eur J Heart Fail* 8: 571–576, 2006.
25. **Hitchcock IS, Skerry TM, Howard MR, Genever PG.** NMDA receptor-mediated regulation of human megakaryocytopoiesis. *Blood* 102: 1254–1259, 2003.
26. **Jasek MC, Griffith WH.** Pharmacological characterization of ionotropic excitatory amino acid receptors in young and aged rat basal forebrain. *Neuroscience* 82: 1179–1194, 1998.
27. **Kleinbongard P, Schulz R, Rassaf T, Lauer T, Dejam A, Jax T, Kumara I, Gharini P, Kabanova S, Ozuyaman B, Schnurch HG, Godecke A, Weber AA, Robenek M, Robenek H, Bloch W, Rosen P, Kelm M.** Red blood cells express a functional endothelial nitric oxide synthase. *Blood* 107: 2943–2951, 2006.
28. **Kloda A, Martinac B, Adams DJ.** Polymodal regulation of NMDA receptor channels. *Channels* 1: 334–343, 2007.
29. **Krizbai IA, Deli MA, Pestenacz A, Siklos L, Szabo CA, Andras I, Joo F.** Expression of glutamate receptors on cultured cerebral endothelial cells. *J Neurosci Res* 54: 814–819, 1998.
30. **Lipton SA, Kim WK, Choi YB, Kumar S, D'Emilia DM, Rayudu PV, Arnelle DR, Stamler JS.** Neurotoxicity associated with dual actions of homocysteine at the *N*-methyl-D-aspartate receptor. *Proc Natl Acad Sci USA* 94: 5923–5928, 1997.
31. **Lutz HU.** Innate immune and non-immune mediators of erythrocyte clearance. *Cell Mol Biol (Noisy-le-Grand, France)* 50: 107–116, 2004.
32. **Merle B, Itzstein C, Delmas PD, Chenu C.** NMDA glutamate receptors are expressed by osteoclast precursors and involved in the regulation of osteoclastogenesis. *J Cell Biochem* 90: 424–436, 2003.

33. **Mihov D, Vogel J, Gassmann M, Bogdanova A.** Erythropoietin activates nitric oxide synthase in murine erythrocytes. *Am J Physiol Cell Physiol* 297: C378–C388, 2009.
34. **Mohan IV, Jagroop IA, Mikhailidis DP, Stansby GP.** Homocysteine activates platelets in vitro. *Clin Appl Thromb Hemost* 14: 8–18, 2008.
35. **Myssina S, Huber SM, Birka C, Lang PA, Lang KS, Friedrich B, Risler T, Wieder T, Lang F.** Inhibition of erythrocyte cation channels by erythropoietin. *J Am Soc Nephrol* 14: 2750–2757, 2003.
36. **Nasstrom J, Boo E, Stahlberg M, Berge OG.** Tissue distribution of two NMDA receptor antagonists, [3H]CGS 19755 and [3H]MK-801, after intrathecal injection in mice. *Pharmacol Biochem Behav* 44: 9–15, 1993.
37. **Orlov SN, Kolosova IA, Cragoe EJ, Gurlo TG, Mongin AA, Aksentsev AL, SVK.** Kinetics and pecularities of thermal inactivation of volume-induced Na/H exchange, Na,K,2Cl cotransport and K,Cl contrasport in rat erythrocytes. *Biochim Biophys Acta* 1151: 186–192, 1993.
38. **Ozuyaman B, Grau M, Kelm M, Merx MW, Kleinbongard P.** RBC NOS: regulatory mechanisms and therapeutic aspects. *Trends Mol Med* 14: 314–322, 2008.
39. **Parsons CG, Danysz W, Quack G.** Glutamate in CNS disorders as a target for drug development: an update. *Drug News Perspect* 11: 523–569, 1998.
40. **Petrushanko I, Bogdanov N, Bulygina E, Grenacher B, Leinsoo T, Boldyrev A, Gassmann M, Bogdanova A.** Na-K-ATPase in rat cerebellar granule cells is redox sensitive. *Am J Physiol Regul Integr Comp Physiol* 290: R916–R925, 2006.
41. **Selhub J.** The many facets of hyperhomocysteinemia: studies from the Framingham cohorts. *J Nutr* 136: 1726S–1730S, 2006.
42. **Seshadri S, Beiser A, Selhub J, Jacques PF, Rosenberg IH, D'Agostino RB, Wilson PW, Wolf PA.** Plasma homocysteine as a risk factor for dementia and Alzheimer's disease. *N Engl J Med* 346: 476–483, 2002.
43. **Stabler SP, Marcell PD, Podell ER, Allen RH, Savage DG, Lindenbaum J.** Elevation of total homocysteine in the serum of patients with cobalamin or folate deficiency detected by capillary gas chromatography-mass spectrometry. *J Clin Invest* 81: 466–474, 1988.
44. **Tietze F.** Enzymic method for quantitative determination of nanogram amounts of total and oxidized glutathione: applications to mammalian blood and other tissues. *Anal Biochem* 27: 502–522, 1969.
45. **Tran QK, Leonard J, Black DJ, Nadeau OW, Boulatnikov IG, Persechini A.** Effects of combined phosphorylation at Ser-617 and Ser-1179 in endothelial nitric-oxide synthase on EC50(Ca2+) values for calmodulin binding and enzyme activation. *J Biol Chem* 284: 11892–11899, 2009.
46. **Tsai JC, Wang H, Perrella MA, Yoshizumi M, Sibinga NE, Tan LC, Haber E, Chang TH, Schlegel R, Lee ME.** Induction of cyclin A gene expression by homocysteine in vascular smooth muscle cells. *J Clin Invest* 97: 146–153, 1996.
47. **Tsai PJ, Huang PC.** Circadian variations in plasma and erythrocyte glutamate concentrations in adult men consuming a diet with and without added monosodium glutamate. *J Nutr* 130: 1002S–1004S, 2000.
48. **Tyulina OV, Prokopieva VD, Dodd RD, Hawkins JR, Clay SW, Wilson DO, Boldyrev AA, Johnson P.** In vitro effects of ethanol, acetaldehyde and fatty acid ethyl esters on human erythrocytes. *Alcohol Alcohol* 37: 179–186, 2002.
49. **Vander Jagt TA, Connor JA, Shuttleworth CW.** Localized loss of Ca2+ homeostasis in neuronal dendrites is a downstream consequence of metabolic compromise during extended NMDA exposures. *J Neurosci* 28: 5029–5039, 2008.
50. **Ventura P, Panini R, Emiliani S, Salvioli G.** Plasma homocysteine after insulin infusion in type II diabetic patients with and without methionine intolerance. *Exp Clin Endocrinol Diabetes* 112: 44–51, 2004.
51. **Yuzaki M, Connor JA.** Characterization of L-homocysteate-induced currents in Purkinje cells from wild-type and NMDA receptor knockout mice. *J Neurophys* 82: 2820–2826, 1999.

Paper 2

N-methyl-D-aspartate receptors in human erythroid precursor cells and in circulating red blood cells contribute to the intracellular calcium regulation

Asya Makhro*, Pascal Hänggi *, Jeroen S. Goede, Jue Wang, Andrea Brüggemann, Max Gassmann, Markus Schmugge, Lars Kaestner, Oliver Speer, and Anna Bogdanova.

* A. Makhro and P. Hanggi contributed equally to this work.

Am J Physiol Cell Physiol 305: C1123–C1138, 2013.
Submitted 31 January 2013; accepted in final form 16 September 2013

Contribution:

Makhro A. participated in study design, organization and discussion. Results showed on Figures 6, 7, 8, 9 were produced by Makhro A.

Am J Physiol Cell Physiol 305: C1123–C1138, 2013.
First published September 18, 2013; doi:10.1152/ajpcell.00031.2013.

N-methyl-D-aspartate receptors in human erythroid precursor cells and in circulating red blood cells contribute to the intracellular calcium regulation

Asya Makhro,[1,4]* Pascal Hänggi,[1,2,4]* Jeroen S. Goede,[3,4] Jue Wang,[5] Andrea Brüggemann,[6] Max Gassmann,[1,4] Markus Schmugge,[2,4,7] Lars Kaestner,[5] Oliver Speer,[2,4,7] and Anna Bogdanova[1,4]

[1]*Institute of Veterinary Physiology, Vetsuisse Faculty, University of Zurich, Zurich, Switzerland;* [2]*Division of Hematology, University Children's Hospital, Zürich, Switzerland;* [3]*University Hospital Zurich, Division of Hematology, Zurich, Switzerland;* [4]*Zurich Center for Integrative Human Physiology, University of Zurich, Zurich, Switzerland;* [5]*Institute for Molecular Cell Biology, Medical Faculty, Saarland University, Homburg/Saar, Germany;* [6]*Nanion Technologies, München, Germany; and* [7]*Children's Research Center, University Children's Hospital, Zürich, Switzerland*

Submitted 31 January 2013; accepted in final form 16 September 2013

Makhro A, Hänggi P, Goede JS, Wang J, Brüggemann A, Gassmann M, Schmugge M, Kaestner L, Speer O, Bogdanova A. *N*-methyl-D-aspartate receptors in human erythroid precursor cells and in circulating red blood cells contribute to the intracellular calcium regulation. *Am J Physiol Cell Physiol* 305: C1123–C1138, 2013. First published September 18, 2013; doi:10.1152/ajpcell.00031.2013.—The presence of *N*-methyl-D-aspartate receptor (NMDAR) was previously shown in rat red blood cells (RBCs) and in a UT-7/Epo human myeloid cell line differentiating into erythroid lineage. Here we have characterized the subunit composition of the NMDAR and monitored its function during human erythropoiesis and in circulating RBCs. Expression of the NMDARs subunits was assessed in erythroid progenitors during ex vivo erythropoiesis and in circulating human RBCs using quantitative PCR and flow cytometry. Receptor activity was monitored using a radiolabeled antagonist binding assay, live imaging of Ca^{2+} uptake, patch clamp, and monitoring of cell volume changes. The receptor tetramers in erythroid precursor cells are composed of the NR1, NR2A, 2C, 2D, NR3A, and 3B subunits of which the glycine-binding NR3A and 3B and glutamate-binding NR2C and 2D subunits prevailed. Functional receptor is required for survival of erythroid precursors. Circulating RBCs retain a low number of the receptor copies that is higher in young cells compared with mature and senescent RBC populations. In circulating RBCs the receptor activity is controlled by plasma glutamate and glycine. Modulation of the NMDAR activity in RBCs by agonists or antagonists is associated with the alterations in whole cell ion currents. Activation of the receptor results in the transient Ca^{2+} accumulation, cell shrinkage, and alteration in the intracellular pH, which is associated with the change in hemoglobin oxygen affinity. Thus functional NMDARs are present in erythroid precursor cells and in circulating RBCs. These receptors contribute to intracellular Ca^{2+} homeostasis and modulate oxygen delivery to peripheral tissues.

NMDA receptors; calcium; red blood cells; erythroid precursors

INTRACELLULAR CALCIUM IS A regulator of multiple processes in mammalian red blood cells (RBCs; Ref. 6). Functions of key glycolytic enzymes are calcium sensitive (e.g., Refs. 2, 36, 75). Increase in the intracellular calcium to 1 μM and more causes activation of Ca^{2+}-dependent K^+ channels (Gardos channels), loss of KCl from the cells, cell shrinkage, and dehydration (37). Along with the changes in cell volume and cation content, accumulation of Ca^{2+} was shown to facilitate intercellular adhesion (60). Upregulation of the intraerythrocytic Ca^{2+} results in activation of calpain and promotes cleavage of cytoskeletal proteins (actin, spectrin, ankyrin, and band 4.1 protein) as well band 3 protein and the plasma membrane Ca^{2+} pump (PMCA; Ref. 6). Thus the cell membrane becomes destabilized in RBCs upon Ca^{2+} overload. The changes in rheology associated with cell dehydration and proteolysis of cytoskeletal proteins are followed by the alteration of hemodynamics. Uncontrolled Ca^{2+} accumulation upon treatment of RBCs with Ca^{2+} ionophore A23187 was reported to cause phosphatidylserine (PS) exposure to the outer membrane leaflet (16). This process may contribute to enhanced RBC clearance by macrophages in patients with a number of diseases. Apart of PS exposure, high intracellular Ca^{2+} may promote oxidative stress due to the activation of NADPH oxidase and nitric oxide synthase in its uncoupled mode (20, 51). Whereas extracellular Ca^{2+} concentration in the plasma reaches 1.8 mM, the intracellular free Ca^{2+} level is precisely controlled and does not exceed 50–100 nM in healthy human RBCs (64). This impressive transmembrane gradient is maintained by an active Ca^{2+} extrusion via the PMCA and low passive permeability of the RBC plasma membrane for Ca^{2+} which is mainly mediated by ion channels (28). PMCA in RBCs has been well characterized, whereas our knowledge on the ion transport systems mediating Ca^{2+} uptake in human RBCs is rather limited. Among the transport systems contributing to Ca^{2+} uptake into human RBCs are several classes of cation channels (28). An increase in Ca^{2+} "leak" and the concomitant elevation of intracellular Ca^{2+} concentrations are typical for RBCs of patients with phosphofructokinase deficiency (75), thalassemia (7), and sickle cell disease (7, 70). The importance of electrogenic Ca^{2+} uptake pathway (P_{sickle}) in promoting sickle cell transformation upon deoxygenation has been acknowledged (8, 70, 72). The molecular identity of the nonselective cation channels, including those mediating P_{sickle}, remains unknown.

Recently, we have reported the presence of *N*-methyl-D-aspartate receptors (NMDARs) in the plasma membrane of rat RBCs and in the human erythroid precursor cell (EPC) line UT-7/Epo (38). These receptors are ligand-gated, nonselective cation channels showing a 10-fold preference for Ca^{2+} over Na^+ or K^+ (12).

These receptors are comprised of four subunits of which eight different isoforms coded by independent genes have been described (68). Subunits NR1 and NR3A and B are binding glycine or D-serine whereas NR2A, B, C, and D interact with glutamate and its homologues homocysteine, homocysteic acid

* A. Makhro and P. Hanggi contributed equally to this work.

Address for reprint requests and other correspondence: A. Bogdanova, Institute of Veterinary Physiology, Vetsuisse Faculty, and Zurich Center for Integrative Human Physiology (ZIHP), Univ. of Zurich, Winterthurerstrasse 260,, CH-8057 Zurich, Switzerland (e-mail: annab@access.uzh.ch).

(HCA), or NMDA. Subunit composition defines gating properties and ion preferences of the channel, as well as its affinity to the agonists and antagonists. Whereas channels composed of NR1-NR2A/B generate large currents and deactivate quickly, the channels built up by the NR1-NR2D generate smaller currents and are slow-deactivating (10). Physiological role of the "inhibitory" NR3 subunits making the receptors in the brain glutamate insensitive are not well defined (52). Local expression pattern vary within the brain (21, 40). Apart of that in the brain NMDARs have been shown to be expressed in a number of nonneuronal tissues including the bone and the kidney (42, 57). Subunit composition, physiological function, and regulation of activity of these "atypical glutamate receptors" in megakaryocytes (19, 24) and in rat RBCs (38) have been reported. In rat RBCs activation of the NMDARs by administration of agonists triggered Ca^{2+} accumulation whereas exposure of the cells to antagonists on the contrary reduced the intracellular Ca^{2+} levels (38). Furthermore, activation of the receptor by glutamate, NMDA, or HCA triggered opening of the Gardos channel followed by cell shrinkage as well as activation of the endothelial nitric oxide synthase (38).

Herein we report the presence of NMDARs in membranes of EPCs and circulating RBCs of healthy human subjects. We characterize subunit composition of the receptor and explore its function and contribution to the maintenance of intracellular Ca^{2+} homeostasis and in regulation of hemoglobin oxygen affinity.

DESIGN AND METHODS

Human subjects. Our subject pool consisted of 36 adult subjects (Caucasians, both genders, median age 32.5; range 25–49) with no history of hematological disorders. Five to ten milliliters of venous heparinized blood were obtained after informed, written consent, in accordance with the Declaration of Helsinki, at the Divisions of Hematology of the University Hospital and the Children's Hospital Zurich as well as at the Medical Faculty, Saarland University, Homburg/Saar, Germany and processed immediately. The Institutional Ethics Board of the University Hospital in Zurich and that of the Canton of Zurich as well as the Ethics committee of the medical association of the Saarland approved the study protocol.

RBC purification for flow cytometry and quantitative real-time PCR. Blood was washed three times with 10 ml of PBS containing 2 mM EDTA and separated in a Ficoll-Hypaque gradient (GE Healthcare, Glattbrug, Switzerland) to remove mononuclear cells and platelets. Reticulocytes were then filtered through a leuco-depletion filter (Purecell Neo; Pall, Basel, Switzerland). The leuco-depleted reticulocytes were washed and resuspended in PBS/EDTA. The purity grade of reticulocytes was assessed by an automated blood cell analyzer (Sysmex Digitana, Horgen, Switzerland), as well as by flow cytometry for surface expression of CD45 with fluorescence-labeled antibodies (Becton Dickinson, Rotkreuz, Switzerland). In addition, depletion of leukocytes and platelets and enrichment of late EPCs and reticulocytes were analyzed by quantitative real-time PCR (qPCR). The pan-leukocyte marker CD45 was used as a white blood cell (WBC) marker, and mRNAs encoding hemoglobin subunits were chosen to detect late EPCs and reticulocytes.

Ex vivo hematopoiesis. EPCs were cultured using a two-phase liquid system as described elsewhere (41, 42). At phase I mononuclear cells were isolated from peripheral blood according to the protocol provided by the GE Healthcare producing Ficoll-Paque PLUS and seeded in StemSpan SFEM Medium supplemented with a cytokine mix supplements CC100 StemSpan (StemCell Technologies, Grenoble, France) and penicillin/streptomycin. Cells were maintained in phase I medium at a density of $0.1–1 \times 10^6$ cells/ml for 5 days. Thereafter, nonadherent cells were reseeded in StemSpan SFEM Medium with 2% penicillin/streptomycin, 20 ng/ml SCF, 1 U/ml Epo, 5 ng/ml IL-3, 2 μM dexamethasone, and 1 μM β-estradiol and maintained in it for 6, 12, or 18 days.

mRNA isolation and qPCR. Total RNA was purified from cells by the TRIzol/glycogen/osopropanol. GRIN1, GRIN2A, GRIN2C, GRIN2D, GRIN3A, GRIN3B, and CD45 mRNAs, as well as control GAPDH mRNA, were quantified using the TaqMan Gene Expression Kits acquired from Applied Biosystems (Rotkreuz, Switzerland). The following primers were used: Hs02758991_g1 Gapdh: GTCCCCATCCCAACTCAGCCCCCAA; Hs00609557_m1 Grin1: TCATCTCCAGCCAGGTCTACGCCAT; Hs00168219_m1 Grin2a: GGAATGGGAAAAGGTGGGCAAGTGG; Hs00168230_m1 Grin2b: TGGGAAAGGGTGGGGAAGTGGAAAG; Hs01016626_m1 Grin2c: TGGCTTTCAGCAGGGGCATCTACAG; Hs00367969_m1 Grin2d: CAGCTCAAGGCAGGGAAGCTGGACG; Hs00370290_m1 Grin3a: ACATGACCCCAAGTTACATCATCCT; and Hs00367969_m1 Grin3b: GCTTCTTGGCACGGTTCCTGGCCAA.

Flow cytometry for detection of NMDAR abundance and distribution in EPCs. Staining of EPCs for the NMDAR subunit-specific antibodies was performed as follows. Cells were washed once with working solution (PBS supplemented with 0.1% BSA) and centrifuged for 30 s at 3,000 rpm. The supernatant was discarded and the cells resuspended in working solution and fixed with 0.05% glutaraldhyde solution prepared in PBS for 9 min. Cells were washed twice, supernatant was discarded, and cells were resuspended in Tween solution (working solution supplemented with 0.1% of NaN_3 and 0.1% of Tween20) to permeabilize them. Before the primary antibody was added, the EPCs were washed once and resuspended in working solution.

After incubation with primary antibodies for 15 min in the darkness at room temperature, the cells were washed once and exposed to the allophycocyanin-conjugated secondary antibodies for 15 min in the darkness. The following antibodies were used: IgG1 mouse anti human Anti-CD45 PerCP, clone 2D1 (BD, San Jose, CA) as a marker of WBCs; IgG2a mouse anti-human CD71, clone M-A712 FITC-conjugated (BD) as a marker of reticulocytes; anti-NMDAε3 (NR2C), goat polyclonal IgG, no. sc-1470; anti-NMDAε4 (NR2D), mouse monoclonal IgG, no. sc-178221; anti-NR3A (NR3A), goat polyclonal IgG no. sc-51160; and anti-NR3B, goat polyclonal IgG, no. sc-55731. All primary antibodies against the NMDAR subunits used were provided by Santa Cruz Biotechnology (Dallas, TX) and used at a final concentration of 0.2 μg/ml. Allophycocyanin-cojugated AffiniPure F(ab')2 Fragment Donkey Anti-Goat IgG, Code 705–136-147, and allophycocyanin-cojugated AffiniPure F(ab′)2 Fragment Goat Anti-Mouse IgG, Code 155–136-146 were used as secondary antibodies at 1:625 and 1:2500 dilutions, respectively.

Stained cells were washed once with the working solution supplemented with 1% formaldehyde and resuspended in an appropriated volume of the working solution, and fluorescence intensity was measured using the BD Biosciences FACSCalibur flow cytometer (BD Biosciences). Cells stained with the secondary antibodies alone were used as a negative control. Data were analyzed by using FCS express software (De Novo Software, Los Angeles, CA). All chemicals were provided by Sigma-Aldrich (St. Louis, MO).

Fractionation of RBCs on Percoll density gradient. Fractionation of RBCs into light (L), medium (M), and dense (D) fractions was performed in 90% isotonic Percoll solution prepared by mixing a 90-ml aliquot of sterile Percoll (GE Healthcare; density 1.130 g/ml) with 10 ml × 10 PBS (Sigma-Aldrich) and 11 ml × 1 PBS (Sigma-Aldrich). Blood or RBC suspension was prefiltered on cellulose filter to remove WBCs, platelets were as described elsewhere (5), and 1.0–1.5 ml was overlaid then over 12.5 ml isotonic Percoll and centrifuged using Sorvall RC 5C plus centrifuge equipped with a SM-24 rotor at 4°C for 30 min at 45,000 *g*. The obtained L, M, and D fractions of RBCs were collected and washed three times with the

incubation medium containing the following (mM): 145 NaCl, 4 KCl, 10 glucose, 10 Tris·HCl, 0.1 EDTA, and 0.1% BSA (pH 7.4 at room temperature). Therefore, the obtained RBCs were used for detection of the number of [^{3}H]MK-801 binding sites or for fluorescence live imaging. The amount of reticulocytes in L, M, and D fractions was 18.1 ± 8.2, 1.5 ± 4, and 0.89 ± 0.08% respectively, with mean reticulocyte counts of 1.9 ± 0.6%. Mean cell volume (MCV) of cells in fractions was 103.6 ± 1.9, 90.9 ± 0.7, and 82.6 ± 1.5 fl for the L, M, and D fraction, respectively, mean MCV being 86.5 ± 1.4 fl (means ± SD; Sysmex Digitana, Horgen, Switzerland).

Percoll solutions of lower density (82–86% Percoll) were used to monitor rapid changes in volume occurring within the M fraction containing the majority of mature RBCs in response to the NMDAR stimulation. Final ion composition in Percoll solution was adjusted to 145 mM NaCl, 5 mM KCl, 20 mM HEPES (pH 7.4 at room temperature), 10 mM glucose, and 2 mM $CaCl_2$. Control samples were agonists free. Stimulation of the NMDARs was performed by supplementation of Percoll solution with 200 μM of 1:1 NMDA-glycine mixture. Washed RBCs (0.5 ml packed cells per 12 mM of Percoll solution) were added to the Percoll solution, mixed with it and centrifuged for 2 min at 48,000 *g* at room temperature. Due to the interindividual variability in basal cell density and in the amplitude of responses, Percoll density was slightly adjusted for each of five healthy subjects tested to achieve better separation of the M fraction. In four out of five donors, the agonists-induced changes in RBC density developed within 2 min and were reversed already after 5 min of stimulation. In one subject the volume changes prevailed even 15 min after the onset of exposure to the agonists.

NMDAR activity measurements in circulating RBCs. Changes in the intracellular Ca^{2+} levels in RBCs caused by exposure to the NMDAR agonists or antagonists were monitored in L, M, and D fractions by means of microfluorescent live imaging using fluo-4 AM (Molecular Probes, Eugene, OR) as a marker (31). Loading of RBCs with the fluorescent dye (1–5 μM) was performed for 30 min at room temperature in the darkness. During loading, the cells were resuspended in the incubation medium supplemented with 0.1% BSA and 2 mM $CaCl_2$ to a density of ~4×10^6 cells/ml. Thereafter, the cells were placed in an imaging chamber and allowed to settle for 10 min. In experiments in which kinetics of responses of individual cells to the NMDA agonists and antagonists was monitored over time, the coverslip serving as a bottom of the imaging chamber was coated with polylysine to immobilize the cells. A series of images (bright field and fluorescent images excited at center wavelength of 480 nm with a half-width of 25 nm and a 510-nm longpass emission filter to reach maximal detection efficiency) were taken with a ×100 objective using Axiovert 200M microscope (Carl Zeiss, Jena, Germany). At least five images were taken before the addition of agonists or antagonists and used to calculate baseline levels of fluorescence. Solvent (incubation medium) addition was performed in control samples.

Calibration was performed using cells resuspended in calcium buffer containing 20–200 nM free Ca^{2+} (a set of $CaCl_2$-EGTA mixtures) in the presence of Ca^{2+} ionophore A23187 (10 μM) and the Ca^{2+} pump blocker sodium orthovanadate (4 mM). These cells were addressed to as calcium-clamped cells.

Analysis of the obtained images was performed using CellFinder program developed by Dr. M. Makhinya (Computer Vision Lab; ETH Zurich). This software was designed to detect the cell projection area as an indicator of cell volume, the average fluorescent intensity within this area corrected for the background fluorescence, and anisotropy (a longest to shortest diameter ratio).

Radiolabeled antagonist binding assay was used as an alternative approach to assess the number of active receptors per cell. [^{3}H]MK-801 is a specific NMDAR antagonist interacting with the channel pore of active receptors exclusively (18). The number of [^{3}H]MK-801 binding sites per cell in the absence or in the presence of a 200-fold excess of nonlabeled MK-801 was assessed for evaluation of specific and nonspecific binding.

Washed RBCs were incubated with [^{3}H]MK-801 (20 Ci/mmol; American Radiolabeled Chemicals) at a concentration of 5×10^{-7} mmol/ml (1 h, room temperature) in the presence of 300 μM NMDA and 100 μM Gly. Thereafter the cells were fractioned according to their density on 90% Percoll gradient (45,000 *g*, 30 min). L, M, and D fractions were collected, washed three times in *buffer 1* containing the following (in mM): 145 NaCl, 5 KCl, 10 glucose, 0.1 EDTA, 10 Tris·HCl (pH 7.4 room temperature) supplemented with 0.1% BSA, and lysed. One part of packed RBCs was mixed with 30 parts of lysis buffer containing 25 mM NaH_2PO_4 and 1 mM EDTA (pH 7.0 at 0°C) and incubated on ice for 30 min. Thereafter, RBC membranes were precipitated (45,000 *g* for 30 min at 4°C) and the amount of [^{3}H]MK-801 bound to the membranes was assessed using Packard 1600 TR liquid scintillation analyzer. The number of [^{3}H]MK-801 binding sites per cell was then calculated using the following equation:

$$N_{NR} = \frac{A_{cells}}{A_{sp}(MK-801) * N_A * N_{cells}}$$

N_{NR} is a number of NMDARs per cell, A_{cells} denoted activity of bound [^{3}H]MK-801 after nonspecific binding is subtracted [Bq] and A_{sp} stands for specific activity of the [^{3}H]MK-801 in [Bq/mmol], N_A is the Avogadro constant (6.022×10^{23} mol^{-1}), and N_{cells} are the amount of cells in the sample.

Whole cell currents were measured using a NPC-16 Patchliner (Nanion, Munich, Germany). The "pipette" solution contained the following (in mM): 50 KCl, 10 NaCl, 60 KF, 20 EGTA, and 10 HEPES (pH adjusted to 7.2 by KOH), while the bath solution contained the following (in mM): 140 NaCl, 4 KCl, 1 $MgCl_2$, 2 $CaCl_2$, 5 glucose, and 10 HEPES (pH adjusted to 7.4 by NaOH). NMDA, glycine, and MK-801 were added as indicated in the experiments. The pipette resistance was in the range of 3–5 MΩ, and the seal resistance was between 800 MΩ and 5 GΩ at a holding potential of −40 mV. Measurements were performed with fresh RBC samples from three healthy donors within 2–3 h after blood withdrawal.

pH measurements in RBCs and in RBC lysates. Shifts in the intracellular pH were monitored over 10 min using microfluorescence live imaging. RBC were washed three times in isotonic buffer containing the following (in mM): 15 NaCl, 5 KCl, 10 glucose, 20 HEPES-imidazol buffer, 0.1 EDTA, and 0.1% BSA. The cells were centrifuged and resuspended in the same buffer supplemented with 2 mM $CaCl_2$ and 2 μM of pH-sensitive fluorescent dye BCECF-AM and incubated for 45 min at 37°C in the darkness to achieve optimal dye loading. Some samples were supplemented with 50 μM of MIA during loading with the dye. The kinetics of the changes in BCECF fluorescence in response to the treatment with 300 μM of 1:1 NMDA-glycine mixture were recorded at 488-nm excitation and 535-nm emission wavelengths using Axiovert 200M fluorescent microscope (Zeiss). The images were taken in time laps mode at ×100 magnification at a constant rate of 1 frame per min. The obtained data were analyzed using CellFinder software. Fluorescent intensities were normalized to those at time zero (first frame) and expressed as changes compared with the readouts obtained for nontreated cells to correct for the BCECF photobleaching.

Calcium-induced changes in pH were monitored in fresh hemoglobin solution obtained by lysing 10 μl of packed RBCs in 5 ml of distilled water. Final hemoglobin concentration obtained that way was ~0.25 μM. Sodium chloride concentration was then adjusted to 150 mM, and 2,3-diphosphglycerate pentasodium salt (2-mM final concentration; Sigma) was added to it. These solutions were supplemented with various $CaCl_2$ doses (0–200 μM), and pH was measured at 37 ^{0}C using glass pH electrode of the ABL 700 blood analyzer (Radiometer). Thereafter, oxygen dissociation curves were recorded from these cell lysates as described below.

Hemoglobin oxygen dissociation curves. Oxygen affinity of hemoglobin was assessed using Hemox analyzer (TCS Scientific, New

Hope, PA). Measurements were performed in Ca^{2+}-clamped cells, in intact RBCs resuspended in buffer containing 2 mM $CaCl_2$, and in RBC lysates. Ten microliters of packed RBCs were added to 5 ml of buffer in the presence or absence of NMDAR agonists NMDA (300 μM) and glycine (100 μM). Oxygen dissociation curves were recorded at 30 or 37°C and P_{50} calculated from them using Hemox Analytical Software (HAS). Similar recordings were performed in cell lysates [10 μM of cells lysed in 5 ml H_2O supplemented with 150 mM NaCl, 2 mM 2,3-diphosphoglycerate (2,3-DPG), and various concentrations of $CaCl_2$] obtained as stated above after pH detection.

Statistical analysis. The obtained data were analyzed using GraphPad Instat v.3.0 (GraphPad Software,) and presented as means ± SE. Statistical significant differences were assessed using normality test followed by either one-way ANOVA test (when distribution was normal) or Kruskal-Wallis test (when normality of distribution cannot be confirmed) with the Bonferroni or Dunn's posttest correspondingly (accepted at $P < 0.05$).

RESULTS

Expression of the NMDAR subunits in erythroid progenitors during erythropoiesis. The number of functional NMDAR heterotetramers in the immortalized human erythroid cell line UT-7/Epo was estimated to be~350,000 copies per cell (38). We have then performed characterization of the expression pattern of NMDAR subunits during ex vivo erythropoiesis derived from peripheral stem cells and in circulating human RBCs. Subunit speciation of the NMDARs in human EPCs during their differentiation was monitored in the course of transformation from pluripotent precursor (*day 0*) cells through the proerythroblast (*day 6*) and basophilic and polychromatic erythroblast (*day 12*) stages to normoblasts and enucleated reticulocytes (*day 18*). Differentiation stages were verified morphologically (Fig. 1, *A–C*) as well as by expression of CD71 (Fig. 2). We have detected transcripts of the genes

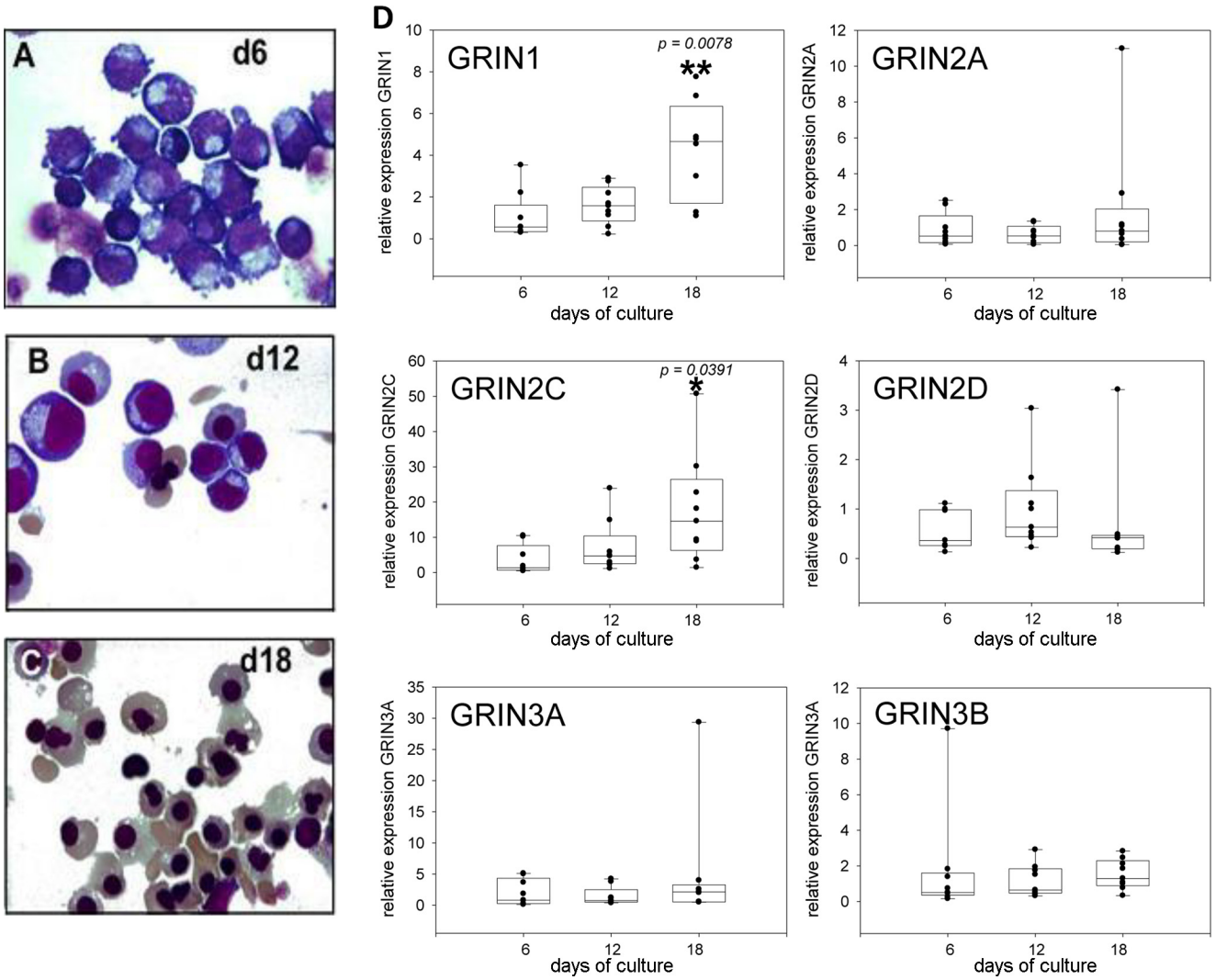

Fig. 1. Peripheral blood-derived erythroid cultures express *N*-methyl-D-aspartate receptor (NMDAR) subunits. Representative cytospins of erythroid cells on *day 6* (d6, *A*), *12* (d12, *B*), and *18* (d18, *C*). Cytospins were stained with May Grünwald Giemsa, and images were acquired with a Zeiss Axioskop2 microscope equipped with a Zeiss Plan-Apochromat ×63/1.4 oil immersion objective lens and a Zeiss AxioCam MRc digital camera. Images were recorded using Zeiss AxioVision AC release 4.5.0 software. *D*: relative amounts of the GRIN gene transcripts in erythroid precursor cells (EPCs) harvested at *day 6*, *12*, and *18* measured by TaqMan quantitative PCR. Values are represented as box plots of 9 erythroid cultures, each started with cells from a different donor. An overall comparison indicated significant increase in expression of GRIN1 and GRIN2C between the *days 6* and *18* in culture. *$P = 0.0391$; **$P = 0.0078$.

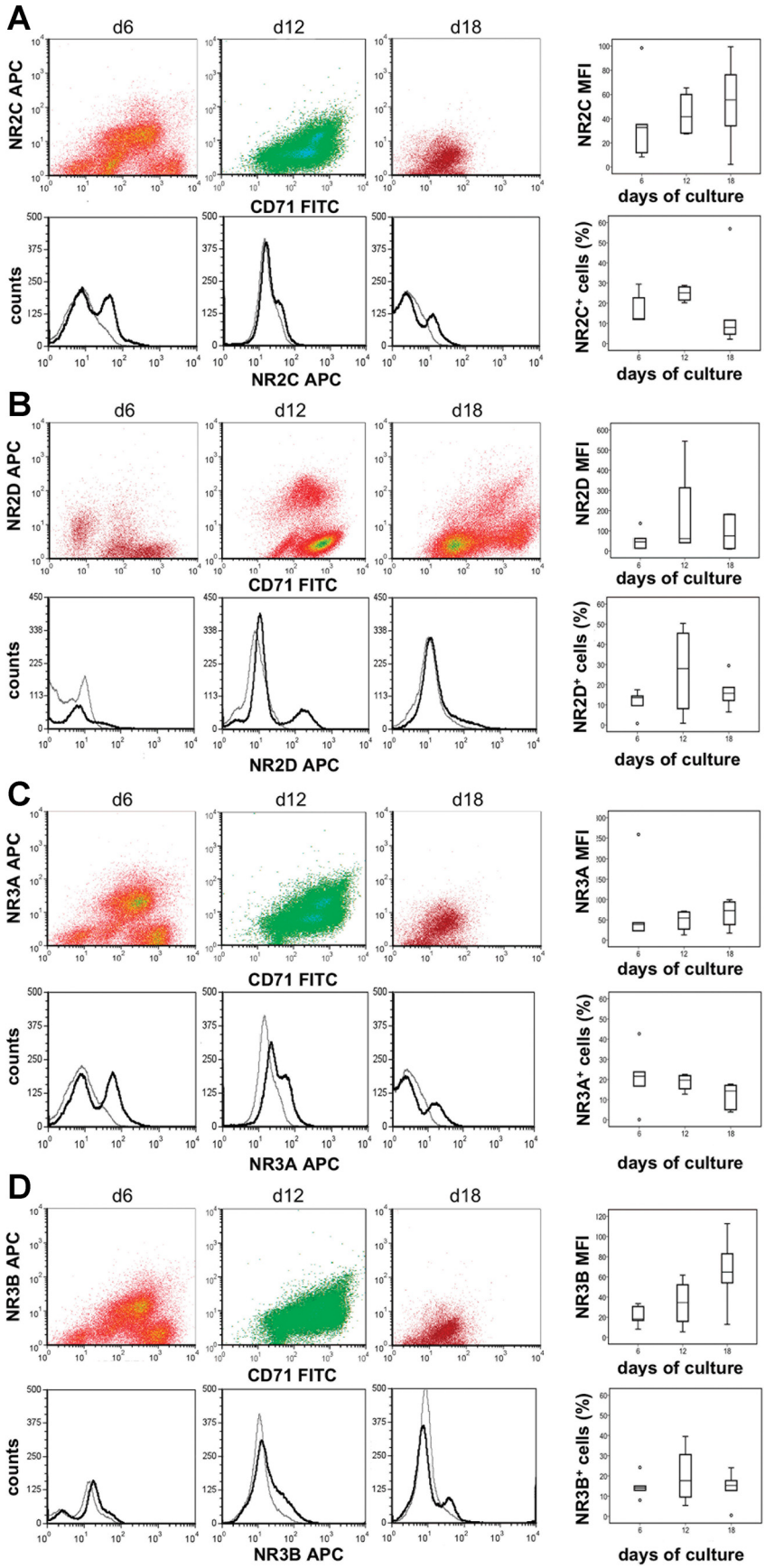

Fig. 2. Changes of protein levels of NMDAR subunits during erythropoiesis. Peripheral blood-derived erythroid cultures were analyzed by flow cytometry on *day 6* (d6), *12* (d12), and *18* (d18) after seeding. NMDAR subunit expression at various EPC differentiation states was assessed. Surface expression of CD71 (CD71 FITC) was used as a marker of EPCs in the presented dot blots. The number of cells expressing NMDAR subunits are shown as histograms. Grey plots show the signal obtained from staining with secondary APC-conjugated antibodies alone, and black plots show specific anti-NR-APC signal. The geometric mean fluorescence intensity (MFI) and the fraction of cells showing specific anit-NR-APC signal were analyzed from 60'000 cells each measurement and represented as box plots for the subunits NR2C (*A*), NR2D (*B*), NR3A (*C*), and NR3B (*D*). Values are represented as box plots of 9 erythroid cultures, each started with cells from a different donor ($n = 9$).

Table 1. *Expression of NMDAR subunits in WBCs*

Gene	ID*	Protein	ΔCt	ΔΔCt (fold mRNA expression compared with EPCs)
GRIN1	2902	NR1	19.8 ± 1.6	7.0
GRIN2A	2903	NR2A	15.8 ± 1.9	11.2
GRIN2B	2904	NR2B	18.8 ± 1.4	(Not expressed in EPCs)
GRIN2C	2905	NR2C	15.6 ± 1.8	0.7
GRIN2D	2906	NR2D	12.0 ± 0.9	11.0
GRIN3A	116443	NR3A	18.3 ± 2.3	1.0
GRIN3B	116444	NR3B	17.3 ± 1.6	10.8

Values are ± SE for 3 cultures, each started with cells from a different donor ($n = 3$). EPC, erythroid precursor cell. Relative amounts of transcripts of *N*-methyl-D-aspartate receptor (NMDAR) subunits were detected by TaqMan quantitative PCR. White blood cells (WBCs; predominantly monocytes) were obtained from mononuclear cells in culture and separated from the hematopoietic stem cells (HSC) at *day 3* of culturing as "adherent cell fraction." Individual values were normalized to GAPDH (ΔCt), and the individual fold change compared with the median ΔCt values of erythropoiesis at *day 6* was calculated (expΔΔCt, fold change in mRNA expression). Comparison with the values for mRNA expression in HSCs at *day 3* was not possible as too few cells were available at that time. GRIN2B expression in HSCs was fixed to 40 cycles. *NCBI gene ID.

GRIN1, GRIN2A, GRIN2C, GRIN2D, GRIN3A, and GRIN3B encoding NMDAR subunits NR1, NR2A, 2C, and 2D and NR3A and 3B in EPC at various stages of erythropoiesis (Fig. 1; Table 1). Relative expression of GRIN1 and GRIN2C mRNA increased substantially from *day 6* to *day 18* in culture ($P < 0.05$; Fig. 1*E*). A tendency to increased expression of GRIN2A, GRIN3A, and GRIN3B mRNA over 18 days in culture was detected but was not statistically significant (Fig. 1*E*). Maximal expression of GRIN2D mRNA was found in cells after 12 days in culture, whereas in 18-day-old cells the expression levels dropped to the values similar to those detected at *day 6* (Fig. 1*G*). No transcripts of GRIN2B were detected at any differentiation stage. In peripheral RBCs we were not able to detect any GRIN transcripts, indicating that those were eliminated during erythrocyte maturation (data not shown).

Protein levels of subunits NR2C, 2D, 3A, and 3B were measured using flow cytometry (Fig. 2). The number of erythroid cells in culture expressing NMDAR subunits varied between 10 and 30%. The number of erythroid cells expressing NR2C and NR2D increased during the basophilic and polychromatic cell stages and decreased again once cells matured towards normoblasts and reticulocytes (Fig. 2, *A* and *B*). However, the number of copies for these subunits was rather stable throughout the culture period as follows from the mean fluorescence intensity levels (Fig. 2, *A* and *B*). The subunit NR3A appeared to be expressed by an increasing proportion of cells throughout erythropoiesis; however, its expression decreased slightly (Fig. 2*C*). The number of cells expressing NR3B remained stable during the erythropoietic culture, whereas its expression increased slightly (Fig. 2*D*). Specifically during ex vivo differentiation, the GRIN2D levels of the median subunit per cell remained relatively unchanged from *day 6* (proerythroblast) with 186,000 (41,000–320,000) to *day 12* (basophilic erythroblast) with 140,000 (18,300–540,000) subunits per cell. Towards *days 18–24* in culture (polychromatic- and normoblast, and also reticulocytes), expression of the NR2D subunit dropped to 120,000 (4,100–240,000) subunits per cell. Thus the stable expression of GRIN2D mRNA during differentiation from myeloid progenitor towards the basophilic/polychromatic erythroblast was mirrored by a stable expression in GRIN2D protein levels. During differentiation towards erythrocytes the transcripts appear to become degraded, as they are not detected anymore, whereas NR2D protein is retained although at much lower levels (data not shown).

The importance of functional NMDARs in EPCs in the course of differentiation was explored. The kinetics of changes in the intracellular Ca^{2+} levels in EPCs in response to stimulation of the NMDARs with a mixture of NMDA and glycine (300 μM each) in the absence or presence of 50 μM MK-801 were monitored using fluorescence microscopy. Administration of NMDA/glycine to the cells at *day 12* resulted in acute increase in the intracellular Ca^{2+} levels as shown in Fig. 3*A*.

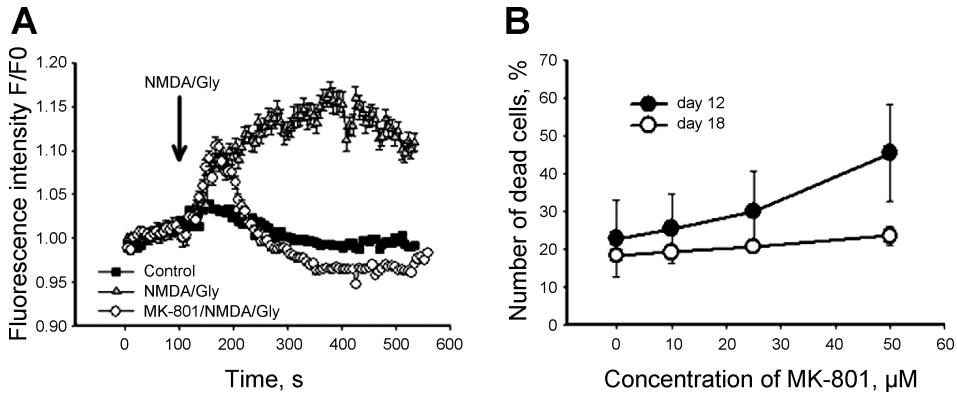

Fig. 3. NMDAR function in EPCs. *A*: cells on *day 12* were loaded with 3 μM fluo-4 AM for 45 min at 37°C in cell culture medium and thereafter fluorescence recordings were initiated using Axiovert 200M microscope in time-lapse mode at a frequency of one frame in 7 s. Cells were stimulated with 300 μM of NMDA/glycine 1 min after the onset of recordings and the changes in fluorescence followed for 10 min. Some cells were pretreated with 50 μM of MK-801 for 45 min before the imaging procedure. The antagonist was present in the cell culture medium during the imaging. The number of cells analyzed was 542 for control nontreated group (closed squares), 511 for the NMDA/Glycine-stimulated group (grey triangles), and 494 for the cells pretreated with MK-801 before the stimulation with antagonists (open circles). *B*: cells at *day 12* (closed circles) or at *day 18* (open circles) were exposed to various concentrations of MK-801 for 24 h and cellular viability was assessed thereafter using flow cytometry (FacsCalibur; BD). Nuclear staining of propidium iodide was used as a marker of cell death.

Whenever MK-801 was present in the incubation medium before the receptor activation, the response was biphasic. A transient and incomplete Ca^{2+} accumulation during the first 30 s upon NMDA/glycine addition was followed by a decrease in the intracellular Ca^{2+} significantly below the levels observed in control nontreated cells. On *day 18*, EPCs lost their sensitivity to NMDA/glycine and stimulation of the receptors did not result in any acute significant changes in the intracellular calcium along with higher intercellular variability in the intracellular Ca^{2+} levels and responsiveness to the stimulation (data not shown). The effects of long-term exposure on the EPCs to different concentrations of the pore blocking NMDAR antagonist MK-801 were explored. In line with the data on NMDA/Gly-sensitivity of the intracellular Ca^{2+} levels, exposure of EPCs at *day 12* to *50* μM MK-801 for 24 h resulted in significant increase of mortality whereas the cells at *day 18* were antagonist resistant (Fig. 3*B*).

NMDAR expression pattern in WBCs. To evaluate the impact of potential contaminations of myeloid progenitors in our culture systems and that of WBCs in our RBCs preparations, we used CD45 as a marker of myeloid and WBCs (45). We were unable to detect myeloid cells in our culture system after *day 6*. No WBCs were detected in purified RBCs, as shown previously (3). We have assessed the expression GRIN transcripts in adhesive WBCs separated at *day 2* from our erythroid culture. These cell preparations contained predominantly monocytes. Expression of GRIN1 in this myeloid cell population exceeded that in erythroid cells at *day 6* of the erythropoietic culture by 4.4-fold, that of GRIN2A by 6.5-fold, and that of GRIN2D by 9.8-fold whereas GRIN2C was 50% lower in WBCs than in erythroid progenitors (Table 1). Compared with erythropoietic cultures at *day 18*, WBCs expressed 0.6-fold less GRIN1, 3.8-fold more GRIN2A, 0.06-fold less GRIN2C, and 10.8-fold more GRIN2D compared with the levels in basophilic and polychromatic erythroblasts (Table 1).

These findings provided further evidence for the absence of myeloid cells or WBCs in erythroid cell culture. Expression profiles for NMDAR subunits GRIN1, GRIN2C, and GRIN3A in differentiated erythroid cells differed substantially from those in WBCs. Furthermore, WBCs appeared to express GRIN2B subunit whereas in erythroid cells the GRIN2B transcripts remained below detection level at any time in culture (Table 1).

NMDAR activity and intracellular Ca^{2+}concenrtation. In the following set of experiments, the activity of NMDAR was assessed in circulating RBCs. Changes in the intracellular calcium levels in RBCs upon treatment with agonists NMDA, glutamate, and HCA are shown in Fig. 4*A*. Increase in the intracellular Ca^{2+} levels, which was induced within minutes of exposure to the agonists, could be blocked by the pore-blocking antagonist interacting with the open receptor channel MK-801 (Fig. 4, *A* and *B*). Responses of individual cells to the NMDAR stimulation varied substantially (Fig. 4*C*). However, despite pronounced intercellular variability, the majority of cells responded to the treatment with the NMDAR agonists with acute Ca^{2+} uptake.

NMDAR-induced whole cell currents in RBCs. Calcium uptake following activation of the NMDAR was associated with an increase in whole cell currents across the RBC plasma membranes (Fig. 5). Changes in membrane conductance were assessed using automated patch clamp platform Patchliner (Nanion). Similar to the observations obtained using microfluorescence live imaging (Fig. 4*C*), sensitivity of the cells to agonists and antagonists varied markedly between individual cells. An increase in currents associated with exposure to the NMDA-glycine mixture was observed in 29.4% of cells. Currents induced by the treatment of cells with agonists could be blocked by the treatment of cells with MK-801. Examples of the NMDA-sensitive currents are shown in Fig. 5, *A* and *C*, and statistical analysis of the findings in responding cells is given in Fig. 5*E*. The appearance of the current-voltage (*I-V*) curves changes when the NMDAR is activated (green line in Fig. 5*D*) or when it is blocked (blue line in Fig. 5*D*). To relate the current traces to the other data in the paper the slope of the *I-V* curves was analyzed in the physiological relevant range between −30 and 0 mV (Fig. 5*D*). At stimulated NMDAR, the whole cell conductance is significantly increased compared with naïve RBCs (green column vs. red column in Fig. 5*E*). When the RBCs with activated NMDARs are treated with MK-801 to block NMDAR activity, the whole cell conductance is significantly decreased (green column vs. blue column in Fig. 5*E*).

NMDAR abundance in RBC fractions of high medium and low density. In the next sets of experiments RBCs were separated into fractions according to their density using Percoll density gradient centrifugation. D, M, and L fractions were isolated as shown in Fig. 6*A*. The basal activity of the receptor and total number of the functional NMDAR units was measured in each fraction using two independent approaches: radioactive antagonist binding assay and agonists/antagonists-induced changes in the intracellular calcium levels. Basal receptor activity was evaluated as the cells were allowed to interact with [^{3}H]MK-801 in plasma and then fractioned on Percoll gradient. The number of binding sites for radiolabeled antagonist per cell obtained that way reflected the number of NMDARs active in plasma-borne RBCs. The values for the [^{3}H]MK-801 binding to "activated" cells were obtained in the presence of saturating concentrations of NMDA in plasma and hence represented the total number of receptors. As shown in the Fig. 6*B*, the number of active receptors interacting with [^{3}H]MK-801 was maximal in the L fraction enriched with reticulocytes and young cells (see DESIGN AND METHODS). In this fraction, no further activation of the receptor could be caused by glutamate/NMDA supplementation of plasma. In contrast to that, the receptors in M and D fractions, although significantly lower in number, could be further activated by addition of agonist to plasma (Fig. 6*B*).

These experimental settings could give rise to artefacts due to the WBCs contamination (average of 5.6, 4.9, and 1.4 per 1,000 cells in the L, M, and D fractions; Ref. 45). To avoid the overestimation of the receptor activity in RBCs, we have used an alternative approach monitoring the agonist-induced Ca^{2+} uptake in individual RBCs of L, M, and D fractions isolated from blood of three healthy individuals by microfluorescence live imaging. Receptor activity in RBCs of these donors was assessed by [^{3}H]MK-801 binding and presented in the right panel of Fig. 6 (in red for *donor 1*, in green for *donor 2*, and in blue for *donor 3*). The observations obtained by means of microfluorescence imaging were in agreement with the ones generated using radiolabeled antagonist binding assay. Maximal amount of "responding" RBCs of each individual donor was present in the L fraction (Fig. 7*A*). Maximal amplitude of NMDA-induced Ca^{2+} uptake was recorded in the least dense

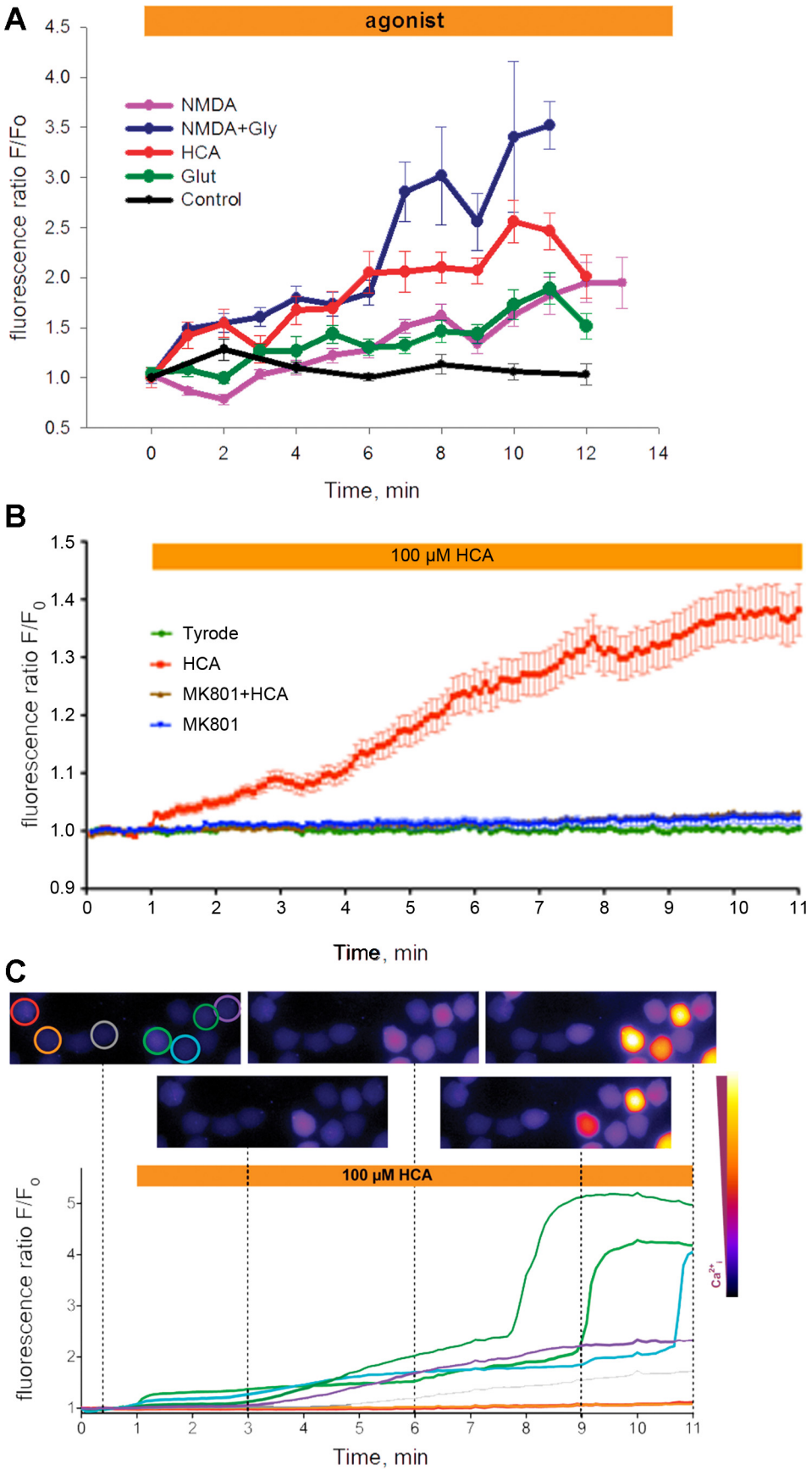

Fig. 4. Changes in the intracellular Ca^{2+} levels in red blood cells (RBCs) exposed to agonists and antagonist of NMDARs. *A*: an increase in the intracellular Ca^{2+} in response to administration of 100 μM NMDA, 100 μM NMDA + 100 μM glycine, 100 μM glutamate, or 50 μM homocysteic acid (HCA) was observed. Data are means of 34–80 single cell recordings ± SE. The orange bar on top of each panel schematically indicates the duration of exposure to the agonists. *B*: sensitivity of the HCA-induced Ca^{2+} uptake by RBCs to the NMDAR antagonist MK-801 (50 μM). Pretreatment with antagonist for 10 min abolished the effects of subsequent exposure to HCA. The green trace represents the average Ca^{2+}-sensitive fluorescent signal recordings for 444 unstimulated control HBA RBCs in Tyrode's solution. The red trace shows the F/F_o ratio for RBCs stimulated with NMDAR agonist HCA (100 μM) 1 min after the start of the recordings averaged from 776 single cell recordings. Preincubation of the cells with NMDAR antagonist MK-801 (100 μM) administered 10 min before the onset of the recordings did not affect the basal intracellular Ca^{2+} levels during 20 min of exposure (blue trace, average of 775 individual cell recordings), but effectively inhibited the HCA-sensitive Ca^{2+} influx, as depicted by the brown trace (average of 742 individual cell recordings). Each curve shows data from 9 independent measurements of 3 healthy donors ± SE. (*C*) A selection of traces from individual cells. The images above the diagram exemplify the original fluorescent images of cells at the time points indicated by the dotted lines. The false color coding scale is shown next to the original tracks of the changes in fluorescence intensity over time. The colors of traces correspond to those of the circles marking the individual cells in the leftmost image. The tremendous cell-to-cell variation is obvious in both the images and the traces.

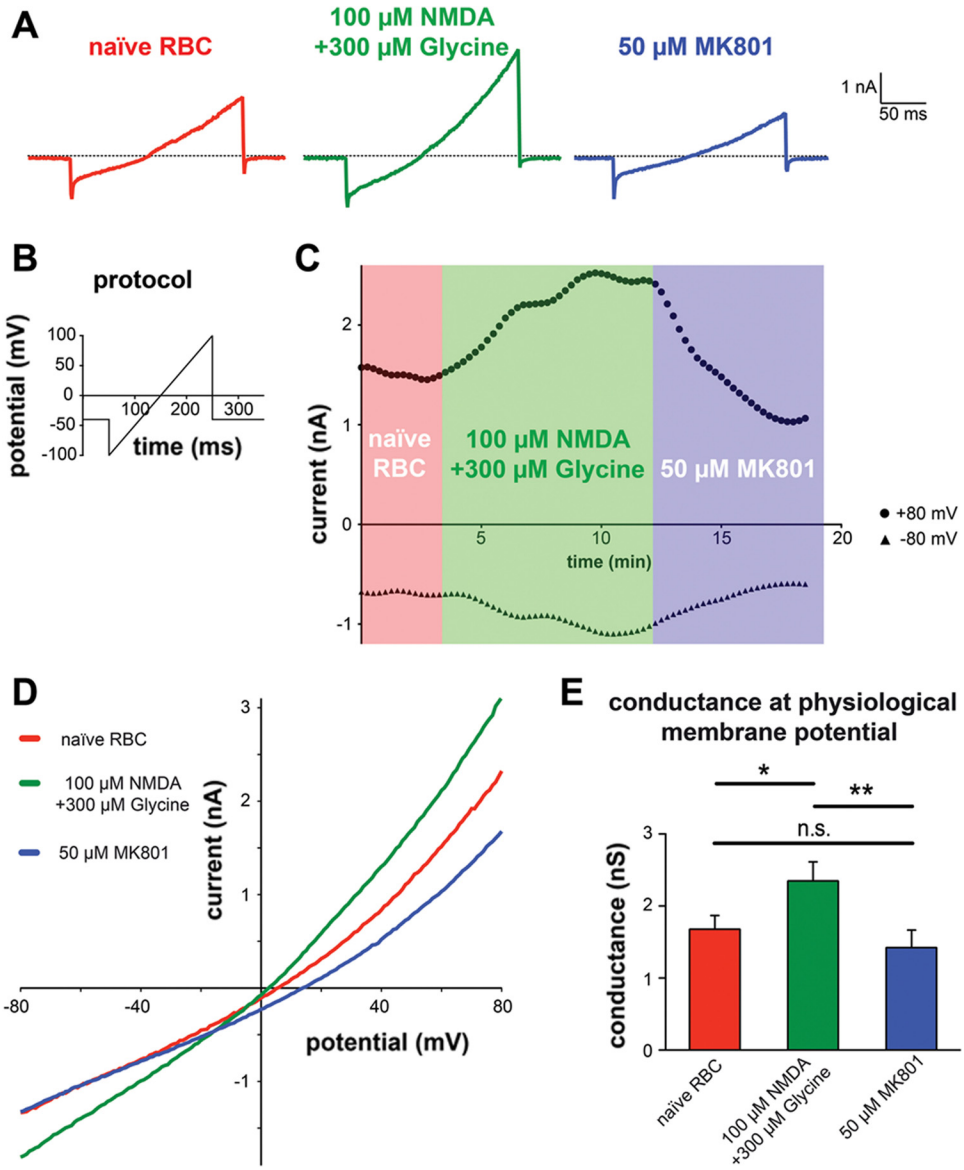

Fig. 5. Whole cell currents of RBC under activation and blocking of the NMDARs. Measurements as shown in *A* were performed on 56 gigasealed RBCs. However, for an observation period of 15–20 min only 34 cells were stable enough to allow analysis. 29% of the analyzed RBCs were classified as "responders." Similar in size fraction of responding cells was obtained in Ca^{2+} imaging experiments and when the number of NR2D subunits was assessed using flow cytometry. Responding cells were the RBCs showing an increase in conductance with the application of NMDA (100 μM) and glycine (300 μM) and a decrease when MK-801 was added. *A*: original current traces of an RBC under the conditions presented above the traces as a response to the voltage protocol given in *B*. The current-time (*I-t*) diagram in *C* depicts the temporal distribution of the currents at +80 and −80 mV over the experimental course starting with naïve RBC, application of NMDA and glycine for NMDAR activation and finally MK801 for NMDAR block as indicated. The current traces in *A* correspond to the time points at 2, 10, and 18 min, respectively in *C*. *D*: current-voltage (*I-V*) curves of the responding RBCs under the conditions indicated (data are mean of 10 measurements). The slope of the curves in the range between −30 and 0 mV was analyzed by linear regression and the results are presented in *E*, revealing significant differences in the whole cell conductance at the physiologically relevant membrane potential for the different experimental conditions. Significance was tested by comparing the slopes using a 2-way ANOVA test and is expressed as $*P < 0.05$, $**P < 0.01$, and n.s., $P > 0.05$.

fraction of RBCs of *donor 2*. Transient Ca^{2+} accumulation in RBCs was associated with a transient shrinkage of cells that could be caused by the activation of Gardos channel. Medium density fraction of the *donor 2* was also rich in responding RBCs and showing a transient reduction in cell volume in response to the NMDAR stimulation (Fig. 7*B*, *middle*).

We used Percoll density gradient to assess the amount of cells changing their volume in response to the NMDAR stimulation in the M fraction to which majority of RBCs belong (Fig. 6*A*). The density of Percoll solution used in these experiments was adjusted to resolve the changes in the M fraction. As shown in Fig. 7*D*, most of the cells forming M fraction migrated downwards in Percoll gradient 2 min after the onset of stimulation with 300 μM of 1:1 NMDA/glycine mixture. This increase in RBC density was transient and could not be detected 5 min after the onset of exposure to the NMDAR agonists in four out of five donors. Cells of the fifth donor remained dehydrated even after 15 min of exposure to the agonists. No volume changes were observed in RBCs of all donors suspended in nominally Ca^{2+}-free Percoll solution containing 0.1 mM EDTA supplemented with NMDA and glycine (data not shown).

In fraction D (Fig. 7*C*), the cells remained largely insensitive to the agonist treatment and showing modest transient increase in the intracellular Ca^{2+}. The obtained data revealed vast interindividual and intercellular variation in the number of functional receptor units and the amplitude of responses to the NMDAR agonists. Among typical morphological characteristics of responding cells are big volume (cell surface projection) and low density as L fraction is enriched with responding cells. Medium fraction also contains some of the responders, whereas D fraction is largely deprived of them.

The impact of NMDAR activation state on Gardos channel function. The following experiments were performed to assess the possible influence of NMDA-sensitive Ca^{2+} uptake on K^+ transport across the RBC membrane. Ouabain-resistant chloride-independent K^+ (^{86}Rb) influx was assessed at room temperature, as was the case for Ca^{2+} imaging presented in Fig. 7.

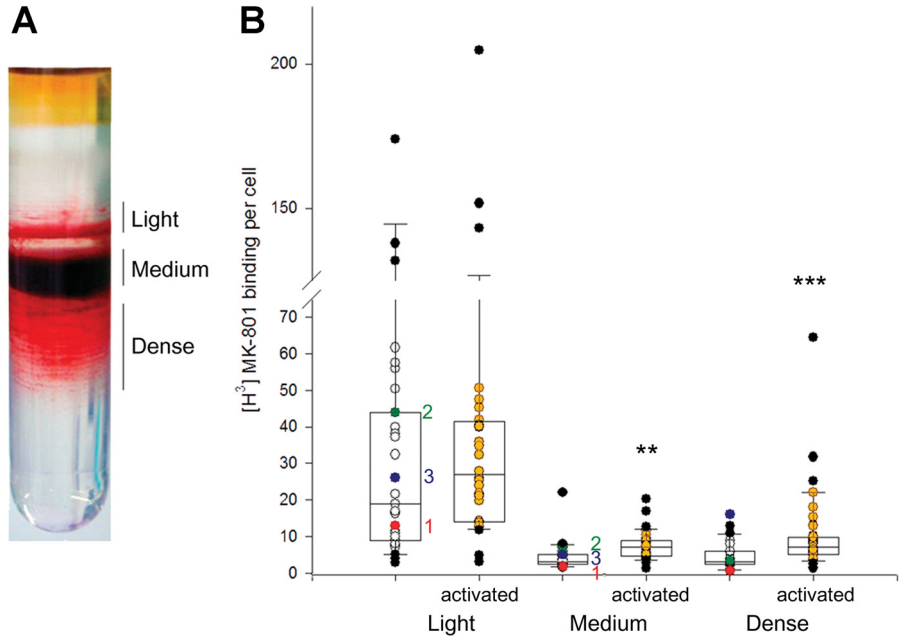

Fig. 6. Activity and abundance of the NMDAR units in light (L), medium (M), and dense (D) RBC fractions. Cells were incubated with radiolabeled [^{3}H]MK-801 in the absence or presence of saturating concentrations of NMDA (300 μM) and glycine (100 μM) added to plasma (activated cells, orange dots). Thereafter, the cells were separated according to their density into L, M, and D fractions on Percoll gradient as shown in *A*. *B*: presents binding of radio-labeled MK-801 to the activated NMDARs was then determined in RBCs in L, M, and D fractions. Non-specific binding was assessed in the presence of 200-fold excess of non-labeled MK-801 and subtracted from the obtained values. Thus the number of active NMDARs was obtained. Values obtained in plasma were shown as "basal receptor activity" in nonstimulated RBCs. Upon stimulation with agonists all receptors in cells were activated and therefore binding of [^{3}H]MK-801. Thus the number of [^{3}H]MK-801 binding sites within activated cells reflected total number of receptors in cells forming L, M, and D fractions. The measurements were performed in blood samples per cell collected from 31 healthy human subjects. Data are presented as box and whisker plots in which each dot represent a value obtained for an individual subject. Specifically marked in red (*1*), green (*2*), and blue (*3*) are the number of active receptors in blood samples of donors blood of which was used to generate data shown in Fig. 7. In L, M, and D fractions distribution of values for individual donors did not show normal Gaussian distribution and statistical analysis of the data was performed using nonparametric Kruskal-Wallis test with Dunn's posttest (**$P < 0.01$, and ***$P < 0.0001$ compared with the basal activity of the NMDAR in corresponding fraction).

No density fractioning was performed before flux measurements. As shown in Table 2, treatment of RBCs suspended in Ca^{2+}-containing but not in nominally Ca^{2+}-free incubation medium with 50 μM memantine caused reduction in unidirectional K^+ influx. Administration of 100 μM NMDA triggered the activation of clotrimazol-sensitive Ca^{2+}-dependent K^+ influx. In nonactivated cells, Gardos channels remained quiescent.

Effect of the NMDAR activation on hemoglobin oxygen affinity. The effect of the intracellular Ca^{2+} on oxygen binding to hemoglobin was tested. Intracellular free Ca^{2+} concentration was clamped as cells were treated with Ca^{2+} ionophore A23187, and extracellular concentration of free calcium ions was adjusted to 10–200 nM by using an EGTA-$CaCl_2$ buffer system. Oxygen dissociation curves were then measured and P_{O_2} required to achieve hemoglobin oxygen saturation of 50%, P_{50}, was assessed for the calcium-clamped RBCs. Calcium levels in clamped RBCs were assessed using microfluorescence imaging. As shown in Fig. 8, the fluorescent signal intensity of fluo-4 follows linearly the changes in the intracellular Ca^{2+} within the 10- to 200-nM interval (Fig. 8*A*). Intraerythrocytic Ca^{2+} levels in intact and NMDA-stimulated cells lies within this concentration range (triangle symbols). Oxygen affinity of Ca^{2+}-clamped cells drops (P_{50} increases from 2.28 ± 0.01 to 4.1 ± 0.27 kPa) as intracellular Ca^{2+} increased from 20 to 200 nM (Fig. 8*C*). Exposure of RBCs in suspension to 300 μM NMDA-100 μM glycine mixture was also associated with an increase in P_{50} (Fig. 8, *B* and *D*).

Acute transient RBC shrinkage triggered by exposure to the NMDAR agonists results in transient increase in the intracellular levels of 2,3-DPG and ATP due to the cytosolic water loss. Additional experiments were performed to explore if this factor contributed to a decrease in hemoglobin oxygen affinity. Oxygen dissociation curves were monitored in RBCs suspended in the medium containing 100 mM KCl/50 mM NaCl medium or in the presence of clotrimazol. The effect of NMDA/glycine on P_{50} was less pronounced but still preserved in both conditions, (3.04 ± 0.65 kPa in control vs. 3.16 ± 0.04 kPa in depolarizing high KCl medium, $P = 0.011$).

The effect of NMDAR agonists on the intracellular pH was assessed microscopically using proton-sensitive fluorescent dye BCECF-DA. Treatment of RBCs with NMDA/glycine resulted in a modest transient decrease in pH-dependent BCECF fluorescence indicating transient intracellular acidification (Fig. 8*F*). The signal we reported was underestimated as shrinkage following the NMDAR activation caused concentration of the fluorescent dye. This acidification reaction monitored in bicarbonate-free medium was insensitive to the inhibitor of Na^+/H^+ exchanger methyl isobutyl amiloride applied at the concentration of 50 μM. The ability of Ca^{2+} to cause the proton release from hemoglobin was explored as RBC lysates (Hb concentration of 0.25 μM, equilibrated with ambient air) were exposed to various concentrations of Ca^{2+}. Cell lysates prepared in 150 mM NaCl solution showed no changes in pH in response to Ca^{2+} administration. However, dose-dependent acidification was observed if cell lysates were exposed to Ca^{2+}

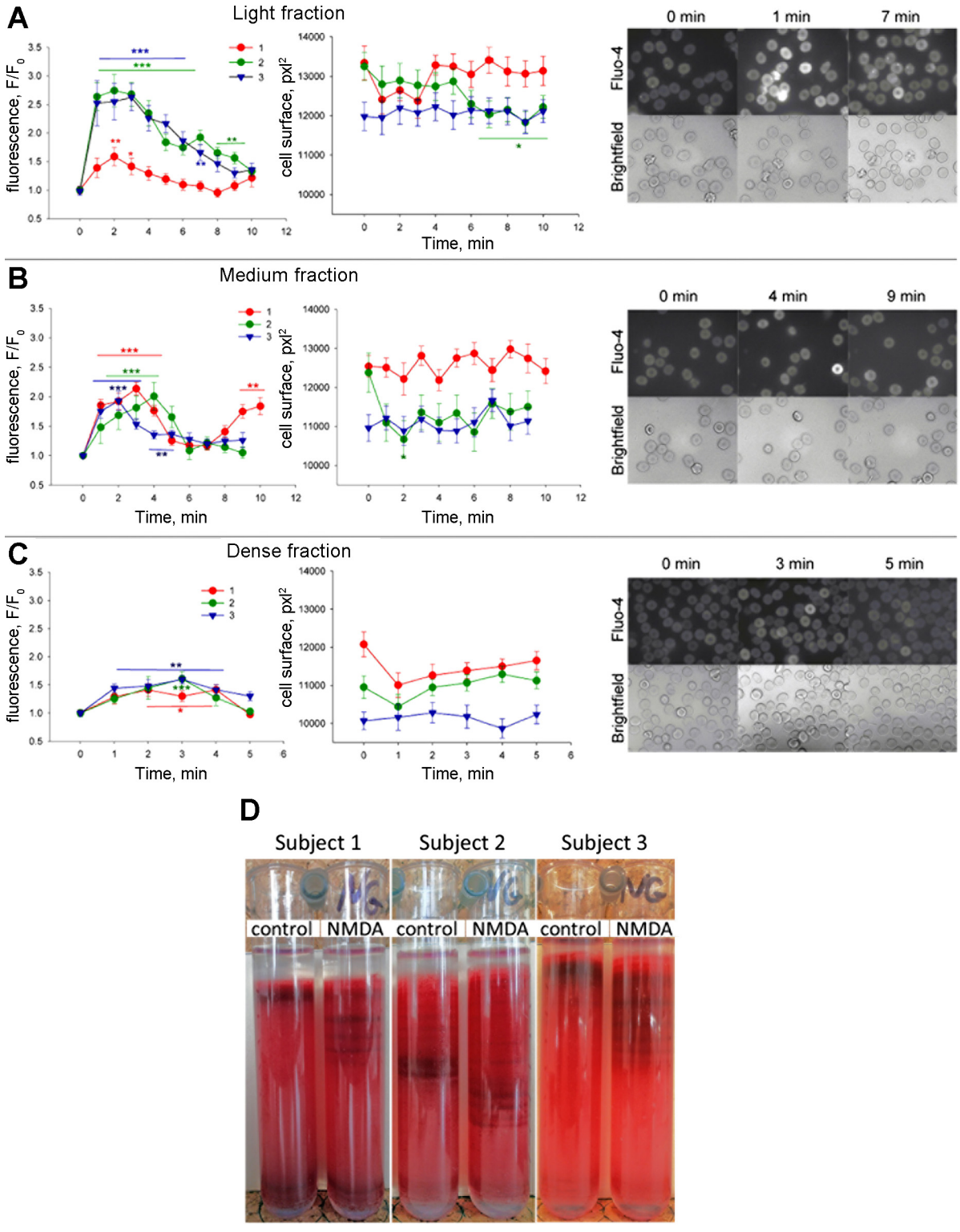

Fig. 7. Kinetics of Ca^{2+} uptake and volume changes in response to NMDAR activation in L, M, and D fractions. Intracellular calcium levels were assessed in RBCs forming L (*A*), M (*B*), and D (*C*) fractions after their separation on Percoll density gradient using fluorescent live cell imaging. The experiments were performed using blood of *subjects 1* (red), *2* (green), and *3* (blue). The values of [^{3}H]MK-801 binding obtained for RBCs of these subjects are highlighted in corresponding colors in Fig. 6. Presented in the left panels are quantification of Fluo-4 fluorescence intensity F upon stimulation with glutamate (300 μM) and glycine (100 μM) normalized to that at time zero in agonist-free medium (F_o). *Middle*: changes in cell projection area in the bright field images over the period of stimulation with the NMDAR agonists. The numbers of cells used for analysis varied from 13 to 35. Data are presented as mean ± SE. *Right*: representative fluorescent images at 3 points in time (before, 1, and 6 min after the stimulation) for the cells in L, M, and D fractions obtained from blood of subject 2 (green plots). Kruskal-Wallis test was performed to follow the changes in Ca^{2+} levels and cell surface (a marker of volume) after the receptor activation. *$P < 0.05$, ** and **$P < 0.01$ and ***$P < 0.001$ compared with time zero. *D*: shift of RBCs within the M fraction down the Percoll density gradient in response to 2 min of stimulation with 300 μM of 1:1 NMDA/glycine mixture in *donors 1*, *2*, and *3*.

Table 2. *Effects of NMDA and memantine on the unidirectional ouabain-insensitive Cl^- -independent K^+ ($^{86}Rb^+$) influx in Ca^{2+}-containing and Ca^{2+}-free medium*

Treatment	1.8 mM Ca^{2+}, mmol·l_{cells}^{-1}·h^{-1}	Ca^{2+}-free, mmol·l_{cells}^{-1}·h^{-1}
Control	0.0134 ± 0.0017	0.0176 ± 0.0029
Memantine	0.0056 ± 0.0012*	0.0162 ± 0.0015
Clotrimazol	0.0158 ± 0.0016	NA
NMDA	0.0201 ± 0.0017*	0.0160 ± 0.0008
NMDA-memantine	0.0102 ± 0.0059	0.0168 ± 0.0028
NMDA-clotrimazol	0.0126 ± 0.0023	NA

Values are means ± SE. *$P < 0.05$, in one-way ANOVA analysis with Dunnett multiple comparison posttest; NA, not assessed.

in the presence of 2 mM 2,3-DPG (Fig. 9). Exposure of 2,3-DPG alone to Ca^{2+} did not result in the changes in pH (Fig. 9). Oxygen binding to hemoglobin within RBC lysates was tested in the presence of 2,3-DPG and various concentrations of Ca^{2+}. As shown in Fig. 9 Ca^{2+}-induced proton release was associated with a dose-dependent rightward shift in oxygen binding curve, the effect observed in Ca^{2+}-loaded or NMDA-glycine stimulated RBCs (Fig. 8). Similar to that of pH, oxygen binding to hemoglobin in lysates remained calcium-insensitive in the absence of 2,3-DPG (data not shown).

DISCUSSION

Following up on our earlier observations on the presence of NMDARs in rat RBCs and in human myeloid cell line differentiating into erythroid progeny, UT-7/EPO (38), we have demonstrated that NMDAR subunits are expressed in human EPCs. Circulating human RBCs retain a limited number of functional receptor units compared with the EPCs. Mammalian RBCs may therefore be added to the list of cells possessing NMDARs along with neurons and a number of nonneuronal cells and tissues (22, 57). Expression of the GRIN transcripts coding for the NMDAR subunits was changing dynamically during erythropoiesis, as did the protein abundance. NMDARs appear to be essential for survival, particularly at the early stages of differentiation of precursor cells during erythropoiesis. Subunit composition of the erythroid receptors differed substantially between the erythroid progeny and WBCs.

Calcium uptake was reported to be of key importance for promoting differentiation and proliferation of EPCs at the stages of burst-forming units erythroid (BFU-E) colony-forming units erythroid (CFU-E; Refs. 43, 56). Increase in the intracellular Ca^{2+} is an integral part of signaling pathway activated by binding of erythropoietin to its receptor (44). Our data suggest that glutamate released from megakaryocytes (63)

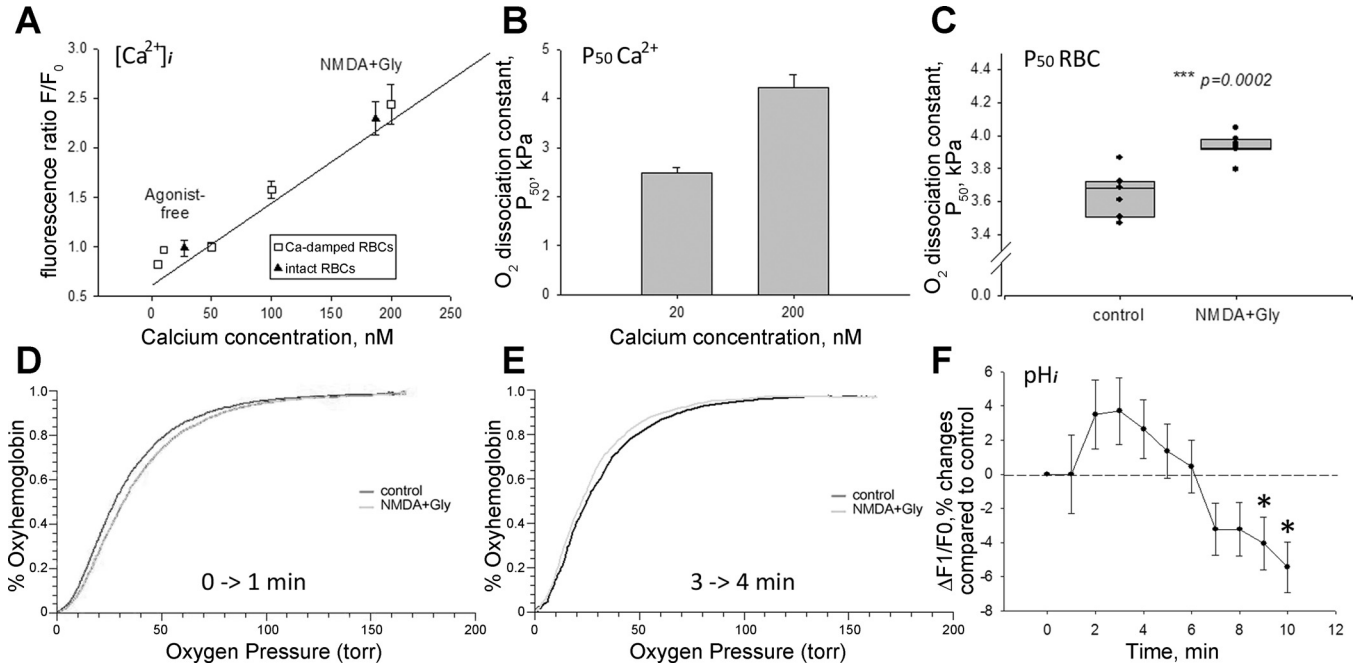

Fig. 8. Ca^{2+} sensitivity of hemoglobin oxygen affinity. Intracellular Ca^{2+} concentration in RBCs was clamped using A23187 and EGTA-$CaCl_2$ buffer to 5–200 nM. *A*: efficacy of clamping of intracellular Ca^{2+}, which was monitored as the change in fluorescence intensity of fluo-4 (open circles). Fluorescence intensity measured in cells clamped at 50 nM Ca^{2+} was chosen as F_o. Closed triangles show the fluorescence intensity of fluo-4 in native cells in the absence of presence of 300 μM NMDA/100 μM glycine, which were resuspended in buffer containing 1.8 mM $CaCl_2$. *B*: data on P_{50} detection obtained for the blood of one single donor on four occasions. Before the P_{50} detection RBCs were loaded with various concentrations of calcium (clamping at 20 or 200 nM free Ca^{2+}). Oxygen dissociation curves for calcium-clamped cells were recorded at 30°C. *C*: changes in P_{50} caused by exposing RBCs of 7 healthy donors to a mixture of NMDA (300 μM) and glycine (100 μM). Intact RBCs were resuspended in the medium containing 2 mM Ca^{2+} at 37°C and agonists added at the onset of oxygen dissociation curve recording. Each point represents P_{50} of one donor (mean of triple recordings). Also presented are median values with variance shown as whiskers. *D*: rightward shift in oxygen dissociation curve observed 1 min after the onset of stimulation with 300 μM of 1:1 mixture of NMDA/glycine at 37°C. *E*: opposite leftward shift in the same blood sample monitored between the 3d and 4th min of NMDAR stimulation. These reciprocal changes in P50 were associated with the opposite shifts in the intracellular pH over shown in *F*. RBCs of 4 different donors were used for measurements of the intracellular pH by means of microfluorescence live imaging. Due to the technical difficulties imaging was performed at room temperature. Shown are the differences in mean fluorescence intensity between the unstipulated control and cells exposed to the 300 μM of 1:1 mixture of NMDA/glycine. The number of cells analyzed at each time point ranged between 343 and 412. $P < 0.05$ resulting from Mann-Whitney test (normal distribution was not confirmed). ***$P = 0.0002$, *$P < 0.05$.

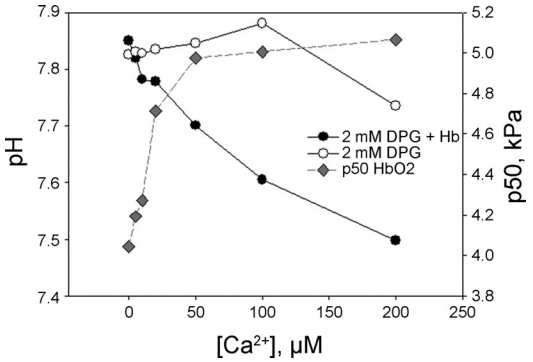

Fig. 9. Dose-dependent Ca^{2+}-induced changes in pH and in P_{50} measured in RBC lysates. Changes of pH and hemoglobin oxygen affinity in RBC lysates in the presence of 2,3-diphosphoglycerate (2,3-DPG). RBCs were lysed in the distilled water, and then NaCl was added to a final concentration of 150 mM with the final hemoglobin concentration 0.25 μM. 2,3-DPG (2 mM) and various concentrations of $CaCl_2$ were added and pH (closed circles) was measured at 37 ^{0}C for each sample in prior to the P_{50} measurements (grey diamonds). The impact of 2,3-DPG-Ca^{2+} interactions into the observed shifts in pH was assessed (open circles). Data shown are means of triplicate measurements form one representative donor. The experiment was repeated with blood of 3 different healthy individuals.

may contribute to the regulation of Ca^{2+} levels in EPCs at *day 12* corresponding to the stage of basophilic and polychromatic erythroblasts (Fig. 3*A*). The number of EPCs possessing NR2C, 2D, and 3A subunits is maximal at this stage (Fig. 2). Accordingly, the cells display high sensitivity to treatment with NMDAR agonists in our ex vivo erythropoietin system (Fig. 3*A*).

Ca^{2+} uptake is inhibited and differentiation and survival of EPCs is compromised in calcium-free medium (43, 56). Similar to that, inhibition of Ca^{2+} uptake by MK-801 in our ex vivo erythropoiesis system resulted in 45.5 ± 12.8% mortality of cells at the stage of basophilic and polychromatic erythroblasts (Fig. 3*B*). Cells at later differentiation stages (normoblasts at *day 18* and enucleated RBCs) are less or not at all damaged by MK-801.

Transient receptor potential channels TRPC2, 3, and 6 were suggested to mediate Ca^{2+} currents in EPCs (23, 67). However, observations on the activation of the TRPC channels by the downstream targets of erythropoietin [e.g., phospholipase C (PLC), and protein kinase C (PKC)] were exclusively reported in nonerythroid channel expressing systems (CHO and HEK cells). Similar to TRPCs, NMDARs were shown to be sensitive to the activation of PLC-inositol-3-phosphate kinase signaling cascade and targets of regulatory PKC-induced phosphorylation (39, 73). Thus both types of ligand-gated channels may coexist in membranes of EPCs (63).

Subunit composition of the erythroid NMDARs. From the data shown in this study, we conclude that human erythroid NMDARs are hetero-tetramers composed of NR1, NR2A, 2C, and 2D and NR3A and 3B subunits. Subunit composition of the erythroid NMDARs differs strikingly from that of the neuronal receptors. As follows from our observations, NR2D and NR2C are most abundant NMDAR subunits in EPCs and, most likely, in circulating RBCs. In the mammalian brain, this subunit shows particularly restricted temporal and spatial expression pattern. Very high levels of expression of NR2D in some areas of embryonic rat brain (precocious midline diencephalic structures and medial geniculate, anteroventral nucleus, and periaqueductal grey zones) drop down dramatically during postnatal period (49). In adult rodent brain, NR2D is only detected in cerebellum and Golgi structures (9, 47) and is highly expressed in motoneurons of the spinal cord (66). In bone marrow and in megakaryoblasts derived from $CD34^+$ precursor cells, the NR2D subunit was found along with NR1 and NR2A (19, 24). Among the characteristic features reported for the NR2D/NR1 heterodimers are reduced Mg^{2+} block, lower ion conductance and slow inactivation (15, 54). However, based on the available data obtained in transfected cells by other groups, one can suggest that the erythroid-specific receptor channels share at least some of these features, such as slow inactivation, since glutamate-binding NR2D subunit is highly abundant in these cells. Calcium accumulations observed upon activation of the receptor activity with glutamate, NMDA, and homocysteic acid that could be blocked by MK-801 (Fig. 4) are in line with this hypothesis (33, 46, 48). However, in erythroid precursors the glycine-binding NR3A and B subunits were highly expressed, whereas the expression of a common NR1 subunit was modest compared with that in the brain (Figs. 1 and 2). These subunits are known as "inhibitory subunits" in the brain as they are glutamate-insensitive but excited by glycine only (35). Currents induced by glycine in NR1/NR3 diheteromers are insensitive to MK-801 or memantine (58). This is not the case for the erythroid NMDARs, as the receptors respond to the pore-targeting antagonists in both EPCs and circulating RBCs. Thus the receptors are either NR1/NR2 heterodimers or are built up of all three subunit subtypes (NR1/NR2C, D/NR3 heterotetramers), although the existence of the latter has been questioned (69). Any speculations on the electrophysiological characteristics of erythroid NMDARs require verification upon detailed investigation.

Receptor function in circulating RBCs of healthy human subjects. NMDARs retained in circulating RBCs remain functional and keep responding to stimulation with glutamate, HCA, or NMDA as well as to the inhibition by MK-801 (Figs. 3–6). Calcium transport through the receptor is electrogenic, putting NMDARs in line with other calcium-transporting ion channels (Fig. 4). The number of such ion channels in RBC is rather limited and their molecular identity often remains unknown (28). Among the TRP channels, only TRPC6 is described in RBC (17). Furthermore, there is biochemical and functional evidence for a $Ca_V2.1$ channel (1, 71). There are numerous electrophysiological reports of Ca^{2+}-permeable channels that can be grouped in two categories: nonselective voltage activated cation channels (NSVAC; e.g., Refs. 4, 29) and receptor-mediated channels (e.g., Refs. 13, 25). Although the *I-V* curve for NSVAC in whole cell conductance mode (55) differs from that shown in Fig. 4*D*, NMDARs and NSVACs have one common property. Both channels share the hysteresis of whole cell current-voltage curves as their opening probability depends on the direction in which membrane potential changes occur (50).

The receptor-activated channels previously described in RBCs share some conductance properties with the channel described in Fig. 5 (13, 25). However, it is premature to make any conclusions on the molecular identity of these channels. Our findings strongly suggest that the currents presented in Fig. 5 are NMDAR mediated. Stimulation of RBCs with NMDA induced an increase in conductance whereas administration of the pore-blocking antagonist suppressed it. Asymmetrical alterations in conductance in response to NMDA treatment

suggest that is it may be channel mediated. The current measured is a superposition of NMDAR-channel current, currents mediated by other ion channels (e.g., those reported elsewhere; Refs. 11, 62), and a leak current. Channel-mediated components show a slight outward rectification and a positive reversal potential (Fig. 5*D*, blue *I-V* curve). Considering the composition of the bath and pipette solutions this could well be chloride channel activity (61). The contribution of the NMDAR channel can be estimated as the difference between putative fully activated channels (Fig. 5*D*, green trace) and the corresponding inhibited channels (Fig. 5*D*, blue trace). In the physiological relevant range between −30 and 0 mV, this difference amounts to a conductance of ~930 pS (Fig. 5*E*). The decreased current at negative membrane potentials in the presence of Mg^{2+} in the bath solution is another indication for the NMDAR identity of the channel (15).

So far channel-mediated Ca^{2+} uptake by RBC was always associated with pathophysiological conditions, such as clot formation (30, 74) or Ca^{2+}-induced clearance (34). To our knowledge, our study is the first one revealing possible physiological role of controlled transient Ca^{2+} uptake following the activation of NMDARs, namely the regulation of oxygen affinity of hemoglobin (Figs. 8 and 9).

Among endogenous regulators of the erythroid NMDAR activity are plasma-borne glutamate, glycine, D-serine, homocysteine, and HCA. The rodent NMDAR EC_{50} for glutamate is 96 ± 20 μM (26), being ~10 μM for HCA (53), and ~40 μM for glycine (38, 58). These data were obtained for the receptors in neurons and in artificial expression systems. These values are close to the EC_{50} for glutamate (88.2 μM) and homocysteic acid (21 μM) reported for the NMDARs in rat RBCs (38). Glutamate concentrations in plasma of healthy human subjects vary substantially depending on physical condition, exercises, gender, diet, and age, making up from 7 ± 1 μM (14) to 255 ± 26 μM (32). Local glutamate and glycine availability in vicinity of RBC membranes may exceed the bulk plasma levels due to high abundance of these amino acids in the cytosol (32). Homocysteine and HCA also contribute to the activation of erythroid NMDARs. Plasma total homocysteine levels ranges from 4.2 to 17.2 μM in healthy human subjects to up to 470 μM in patients with hyper-homocysteinemia (59).

Transient activation of the NMDARs by glutamate released from the exercising muscle (14) or obtained with meal (27) might also contribute to a transient increase in the intracellular Ca^{2+} promoting thereby oxygen release from hemoglobin (Fig. 8). The exact mechanism of a cross talk between calcium levels in RBCs and hemoglobin oxygen affinity remains to be studied in details.

Shrinkage (Fig. 8; Table 2) results in a rapid transient increase in 2,3-DPG levels in the cytosol, which in turn could stabilize hemoglobin in T state and promote oxygen release (Fig. 7, *B* and *D*). However, a shift in oxygen affinity of hemoglobin caused by the stimulation of the NMDARs was preserved in the presence of clotrimazol or in high KCl medium, conditions preventing Ca^{2+}-induced KCl and water loss from RBCs. The obtained data reveal that changes in the intracellular pH result from the shifts in protonation of hemoglobin (Fig. 8). The latter result in the 2,3-DPG-dependent alterations in P_{50} (Figs. 8 and 9). These observations are consistent with earlier reports on an increase in free Ca^{2+} concentration in the cytosol of RBCs undergoing deoxygenation in which hemoglobin gets protonated (65). Conformational changes responsible for these Ca^{2+}-induced changes in oxygen affinity of hemoglobin await further characterization.

Taken together, the obtained findings reveal the presence of functional NMDARs in EPCs and, at much lower levels, in circulating RBCs. The abundance and activity of these receptors in plasma membrane of RBCs and their progenitors are proportional to the intracellular Ca^{2+} levels. Among the downstream targets of Ca^{2+} accumulation are cell volume and hemoglobin oxygen affinity.

ACKNOWLEDGMENTS

We thank Maxim Makhinya for the excellent program CellFinder for intracellular calcium content estimation and morphometric analysis of RBCs he has written for us.

GRANTS

This study was supported by the Swiss National Science Foundation (No. 112 449 and 310030 124970/1 to A. Bogdanova), by Zurich Center for Integrative Human Physiology (cooperative grant to J. Goede, O. Speer, and A. Bogdanova), as well as by Hartmann Müller-Stiftung (to O. Speer and J. Goede). Financial support was provided by the Saarland Graduate School (to J. Wang).

DISCLOSURES

No conflicts of interest, financial or otherwise, are declared by the author(s).

AUTHOR CONTRIBUTIONS

Author contributions: A.M., P.H., J.W., A. Brüggemann, L.K., O.S., and A. Bogdanova performed experiments; A.M., P.H., J.W., A. Brüggemann, L.K., O.S., and A. Bogdanova analyzed data; A.M., P.H., J.S.G., J.W., A. Brüggemann, M.G., M.S., L.K., O.S., and A. Bogdanova interpreted results of experiments; A.M., P.H., J.W., L.K., O.S., and A. Bogdanova prepared figures; A.M., L.K., O.S., and A. Bogdanova drafted manuscript; A.M., J.S.G., A. Brüggemann, M.G., M.S., L.K., O.S., and A. Bogdanova edited and revised manuscript; A.M., P.H., J.S.G., J.W., A. Brüggemann, M.G., M.S., L.K., O.S., and A. Bogdanova approved final version of manuscript; J.S.G., M.S., L.K., O.S., and A. Bogdanova conception and design of research.

REFERENCES

1. **Andrews DA, Yang L, Low PS.** Phorbol ester stimulates a protein kinase C-mediated agatoxin-TK-sensitive calcium permeability pathway in human red blood cells. *Blood* 100: 3392–3399, 2002.
2. **Assouline-Cohen M, Beitner R.** Effects of Ca^{2+} on erythrocyte membrane skeleton-bound phosphofructokinase, ATP levels, and hemolysis. *Mol Genet Metab* 66: 56–61, 1999.
3. **Azzouzi I, Moest H, Winkler J, Fauchere JC, Gerber AP, Wollscheid B, Stoffel M, Schmugge M, Speer O.** MicroRNA-96 directly inhibits gamma-globin expression in human erythropoiesis. *PLoS One* 6: e22838, 2011.
4. **Bennekou P, Kristensen BI, Christophersen P.** The human red cell voltage-regulated cation channel. The interplay with the chloride conductance, the Ca(2+)-activated K(+) channel and the Ca(2+) pump. *J Membr Biol* 195: 1–8, 2003.
5. **Beutler E, West C, Blume KG.** The removal of leukocytes and platelets from whole blood. *J Lab Clin Med* 88: 328–333, 1976.
6. **Bogdanova A, Makhro A, Wang J, Lipp P, Kaestner L.** Calcium in red blood cells-a perilous balance. *Int J Mol Sci* 14: 9848–9872, 2013.
7. **Bookchin RM, Ortiz OE, Shalev O, Tsurel S, Rachmilewitz EA, Hockaday A, Lew VL.** Calcium transport and ultrastructure of red cells in beta-thalassemia intermedia. *Blood* 72: 1602–1607, 1988.
8. **Browning JA, Staines HM, Robinson HC, Powell T, Ellory JC, Gibson JS.** The effect of deoxygenation on whole-cell conductance of red blood cells from healthy individuals and patients with sickle cell disease. *Blood* 109: 2622–2629, 2007.
9. **Cull-Candy SG, Brickley SG, Misra C, Feldmeyer D, Momiyama A, Farrant M.** NMDA receptor diversity in the cerebellum: identification of subunits contributing to functional receptors. *Neuropharmacology* 37: 1369–1380, 1998.

10. **Cull-Candy SG, Leszkiewicz DN.** Role of distinct NMDA receptor subtypes at central synapses. *Sci STKE* 2004: re16, 2004.
11. **Desai SA, Bezrukov SM, Zimmerberg J.** A voltage-dependent channel involved in nutrient uptake by red blood cells infected with the malaria parasite. *Nature* 406: 1001–1005, 2000.
12. **Dingledine R, Borges K, Bowie D, Traynelis SF.** The glutamate receptor ion channels. *Pharmacol Rev* 51: 7–61, 1999.
13. **Duranton C, Huber SM, Lang F.** Oxidation induces a Cl(−)-dependent cation conductance in human red blood cells. *J Physiol* 539: 847–855, 2002.
14. **Durham WJ, Miller SL, Yeckel CW, Chinkes DL, Tipton KD, Rasmussen BB, Wolfe RR.** Leg glucose and protein metabolism during an acute bout of resistance exercise in humans. *J Appl Physiol* 97: 1379–1386, 2004.
15. **Erreger K, Chen PE, Wyllie DJ, Traynelis SF.** Glutamate receptor gating. *Crit Rev Neurobiol* 16: 187–224, 2004.
16. **Foller M, Huber SM, Lang F.** Erythrocyte programmed cell death. *IUBMB Life* 60: 661–668, 2008.
17. **Foller M, Kasinathan RS, Koka S, Lang C, Shumilina E, Birnbaumer L, Lang F, Huber SM.** TRPC6 contributes to the Ca(2+) leak of human erythrocytes. *Cell Physiol Biochem* 21: 183–192, 2008.
18. **Foster AC, Wong EH.** The novel anticonvulsant MK-801 binds to the activated state of the N-methyl-D-aspartate receptor in rat brain. *Br J Pharmacol* 91: 403–409, 1987.
19. **Genever PG, Wilkinson DJ, Patton AJ, Peet NM, Hong Y, Mathur A, Erusalimsky JD, Skerry TM.** Expression of a functional N-methyl-D-aspartate-type glutamate receptor by bone marrow megakaryocytes. *Blood* 93: 2876–2883, 1999.
20. **George A, Pushkaran S, Konstantinidis DG, Koochaki S, Malik P, Mohandas N, Zheng Y, Joiner CH, Kalfa TA.** Erythrocyte NADPH oxidase activity modulated by Rac GTPases, PKC, and plasma cytokines contributes to oxidative stress in sickle cell disease. *Blood* 121: 2099–2107, 2013.
21. **Goebel DJ, Poosch MS.** NMDA receptor subunit gene expression in the rat brain: a quantitative analysis of endogenous mRNA levels of NR1Com, NR2A, NR2B, NR2C, NR2D and NR3A. *Brain Res Mol Brain Res* 69: 164–170, 1999.
22. **Hinoi E, Takarada T, Ueshima T, Tsuchihashi Y, Yoneda Y.** Glutamate signaling in peripheral tissues. *Eur J Biochem* 271: 1–13, 2004.
23. **Hirschler-Laszkiewicz I, Tong Q, Conrad K, Zhang W, Flint WW, Barber AJ, Barber DL, Cheung JY, Miller BA.** TRPC3 activation by erythropoietin is modulated by TRPC6. *J Biol Chem* 284: 4567–4581, 2009.
24. **Hitchcock IS, Skerry TM, Howard MR, Genever PG.** NMDA receptor-mediated regulation of human megakaryocytopoiesis. *Blood* 102: 1254–1259, 2003.
25. **Huber SM, Gamper N, Lang F.** Chloride conductance and volume-regulatory nonselective cation conductance in human red blood cell ghosts. *Pflügers Arch* 441: 551–558, 2001.
26. **Jasek MC, Griffith WH.** Pharmacological characterization of ionotropic excitatory amino acid receptors in young and aged rat basal forebrain. *Neuroscience* 82: 1179–1194, 1998.
27. **Jinap S, Hajeb Glutamate P.** Its applications in food and contribution to health. *Appetite* 55: 1–10, 2010.
28. **Kaestner L.** Cation channels in erythrocytes–historical and future perspective. *Open Biol J* 4: 27–34, 2011.
29. **Kaestner L, Christophersen P, Bernhardt I, Bennekou P.** The non-selective voltage-activated cation channel in the human red blood cell membrane: reconciliation between two conflicting reports and further characterisation. *Bioelectrochemistry (Amsterdam, Netherlands)* 52: 117–125, 2000.
30. **Kaestner L, Tabellion W, Lipp P, Bernhardt I.** Prostaglandin E2 activates channel-mediated calcium entry in human erythrocytes: an indication for a blood clot formation supporting process. *Thromb Haemost* 92: 1269–1272, 2004.
31. **Kaestner L, Tabellion W, Weiss E, Bernhardt I, Lipp P.** Calcium imaging of individual erythrocytes: problems and approaches. *Cell Calcium* 39: 13–19, 2006.
32. **Kiessling K, Roberts N, Gibson JS, Ellory JC.** A comparison in normal individuals and sickle cell patients of reduced glutathione precursors and their transport between plasma and red cells. *Hematol J* 1: 243–249, 2000.
33. **Kutsuwada T, Kashiwabuchi N, Mori H, Sakimura K, Kushiya E, Araki K, Meguro H, Masaki H, Kumanishi T, Arakawa M, Mishina M.** Molecular diversity of the NMDA receptor channel. *Nature* 358: 36–41, 1992.
34. **Lang F, Lang KS, Wieder T, Myssina S, Birka C, Lang PA, Kaiser S, Kempe D, Duranton C, Huber SM.** Cation channels, cell volume and the death of an erythrocyte. *Pflügers Arch* 447: 121–125, 2003.
35. **Low CM, Wee KS.** New insights into the not-so-new NR3 subunits of N-methyl-D-aspartate receptor: localization, structure, and function. *Mol Pharmacol* 78: 1–11, 2010.
36. **Magnani M, Serafini G, Stocchi V.** Effects of Ca^{2+} and lipoxygenase inhibitors on hexokinase degradation in rabbit reticulocytes. *Mol Cell Biochem* 85: 3–7, 1989.
37. **Maher AD, Kuchel PW.** The Gardos channel: a review of the Ca^{2+}-activated K^+ channel in human erythrocytes. *Int J Biochem Cell Biol* 35: 1182–1197, 2003.
38. **Makhro A, Wang J, Vogel J, Boldyrev AA, Gassmann M, Kaestner L, Bogdanova A.** Functional NMDA receptors in rat erythrocytes. *Am J Physiol Cell Physiol* 298: C1315–C1325, 2010.
39. **Mandal M, Yan Z.** Phosphatidylinositol (4,5)-bisphosphate regulation of N-methyl-D-aspartate receptor channels in cortical neurons. *Mol Pharmacol* 76: 1349–1359, 2009.
40. **Masu M, Nakajima Y, Moriyoshi K, Ishii T, Akazawa C, Nakanashi S.** Molecular characterization of NMDA and metabotropic glutamate receptors. *Ann NY Acad Sci* 707: 153–164, 1993.
41. **Migliaccio G, Migliaccio AR, Druzin ML, Giardina PJ, Zsebo KM, Adamson JW.** Long-term generation of colony-forming cells in liquid culture of CD34+ cord blood cells in the presence of recombinant human stem cell factor. *Blood* 79: 2620–2627, 1992.
42. **Migliaccio G, Sanchez M, Masiello F, Tirelli V, Varricchio L, Whitsett C, Migliaccio AR.** Humanized culture medium for clinical expansion of human erythroblasts. *Cell Transplant* 19: 453–469, 2010.
43. **Miller BA, Cheung JY.** Mechanisms of erythropoietin signal transduction: involvement of calcium channels. *Proc Soc Exp Biol Med* 206: 263–267, 1994.
44. **Miller BA, Cheung JY, Tillotson DL, Hope SM, Scaduto RC Jr.** Erythropoietin stimulates a rise in intracellular-free calcium concentration in single BFU-E derived erythroblasts at specific stages of differentiation. *Blood* 73: 1188–1194, 1989.
45. **Minetti G, Egee S, Morsdorf D, Steffen P, Makhro A, Achilli C, Ciana A, Wang J, Bouyer G, Bernhardt I, Wagner C, Thomas S, Bogdanova A, Kaestner L.** Red cell investigations: art and artefacts. *Blood Rev* 27: 91–101, 2013.
46. **Mishina M, Mori H, Araki K, Kushiya E, Meguro H, Kutsuwada T, Kashiwabuchi N, Ikeda K, Nagasawa M, Yamazaki M, Masaki H, Yamakura T, Morita T, Sakimura K.** Molecular and functional diversity of the NMDA receptor channel. *Ann NY Acad Sci* 707: 136–152, 1993.
47. **Misra C, Brickley SG, Farrant M, Cull-Candy SG.** Identification of subunits contributing to synaptic and extrasynaptic NMDA receptors in Golgi cells of the rat cerebellum. *J Physiol* 524: 147–162, 2000.
48. **Misra C, Brickley SG, Wyllie DJ, Cull-Candy SG.** Slow deactivation kinetics of NMDA receptors containing NR1 and NR2D subunits in rat cerebellar Purkinje cells. *J Physiol* 525: 299–305, 2000.
49. **Monyer H, Burnashev N, Laurie DJ, Sakmann B, Seeburg PH.** Developmental and regional expression in the rat brain and functional properties of four NMDA receptors. *Neuron* 12: 529–540, 1994.
50. **Nowak LM, Wright JM.** Slow voltage-dependent changes in channel open-state probability underlie hysteresis of NMDA responses in Mg(2+)-free solutions. *Neuron* 8: 181–187, 1992.
51. **Ozuyaman B, Grau M, Kelm M, Merx MW, Kleinbongard P.** RBC NOS: regulatory mechanisms and therapeutic aspects. *Trends Mol Med* 14: 314–322, 2008.
52. **Paoletti P, Neyton J.** NMDA receptor subunits: function and pharmacology. *Curr Opin Pharmacol* 7: 39–47, 2007.
53. **Patneau DK, Mayer ML.** Structure-activity relationships for amino acid transmitter candidates acting at N-methyl-D-aspartate and quisqualate receptors. *J Neurosci* 10: 2385–2399, 1990.
54. **Qian A, Johnson JW.** Permeant ion effects on external Mg^{2+} block of NR1/2D NMDA receptors. *J Neurosci* 26: 10899–10910, 2006.
55. **Rodighiero S, De Simoni A, Formenti A.** The voltage-dependent non-selective cation current in human red blood cells studied by means of whole-cell and nystatin-perforated patch-clamp techniques. *Biochim Biophys Acta* 1660: 164–170, 2004.
56. **Schaefer A, Magocsi M, Marquardt H.** Signalling mechanisms in erythropoiesis: the enigmatic role of calcium. *Cell Signal* 9: 483–495, 1997.

57. **Skerry TM, Genever PG.** Glutamate signalling in non-neuronal tissues. *Trends Pharmacol Sci* 22: 174–181, 2001.
58. **Smothers CT, Woodward JJ.** Pharmacological characterization of glycine-activated currents in HEK 293 cells expressing N-methyl-D-aspartate NR1 and NR3 subunits. *J Pharmacol Exp Ther* 322: 739–748, 2007.
59. **Stabler SP, Marcell PD, Podell ER, Allen RH, Savage DG, Lindenbaum J.** Elevation of total homocysteine in the serum of patients with cobalamin or folate deficiency detected by capillary gas chromatography-mass spectrometry. *J Clin Invest* 81: 466–474, 1988.
60. **Steffen P, Jung A, Nguyen DB, Muller T, Bernhardt I, Kaestner L, Wagner C.** Stimulation of human red blood cells leads to Ca^{2+}-mediated intercellular adhesion. *Cell Calcium* 50: 54–61, 2011.
61. **Thomas SL, Bouyer G, Cueff A, Egee S, Glogowska E, Ollivaux C.** Ion channels in human red blood cell membrane: actors or relics? *Blood Cells Mol Dis* 46: 261–265, 2011.
62. **Thomas SL, Egee S, Lapaix F, Kaestner L, Staines HM, Ellory JC.** Malaria parasite Plasmodium gallinaceum up-regulates host red blood cell channels. *FEBS Lett* 500: 45–51, 2001.
63. **Thompson CJ, Schilling T, Howard MR, Genever PG.** SNARE-dependent glutamate release in megakaryocytes. *Exp Hematol* 38: 504–515, 2010.
64. **Tiffert T, Bookchin RM, Lew WL.** Calcium homeostasis in normal and abnormal human red cells. In: *Red Cell Membrane transport in Health and Disease*, edited by Bernhardt I, Ellory JC. Berlin, Germany: Springer, 2003, p. 373–405.
65. **Tiffert T, Etzion Z, Bookchin RM, Lew VL.** Effects of deoxygenation on active and passive $Ca^{2}+$ transport and cytoplasmic Ca^{2+} buffering in normal human red cells. *J Physiol* 464: 529–544, 1993.
66. **Tolle TR, Berthele A, Zieglgansberger W, Seeburg PH, Wisden W.** The differential expression of 16 NMDA and non-NMDA receptor subunits in the rat spinal cord and in periaqueductal gray. *J Neurosci* 13: 5009–5028, 1993.
67. **Tong Q, Chu X, Cheung JY, Conrad K, Stahl R, Barber DL, Mignery G, Miller BA.** Erythropoietin-modulated calcium influx through TRPC2 is mediated by phospholipase Cγ and IP3R. *Am J Physiol Cell Physiol* 287: C1667–C1678, 2004.
68. **Traynelis SF, Wollmuth LP, McBain CJ, Menniti FS, Vance KM, Ogden KK, Hansen KB, Yuan H, Myers SJ, Dingledine R.** Glutamate receptor ion channels: structure, regulation, and function. *Pharmacol Rev* 62: 405–496, 2010.
69. **Ulbrich MH, Isacoff EY.** Rules of engagement for NMDA receptor subunits. *Proc Natl Acad Sci USA* 105: 14163–14168, 2008.
70. **Vandorpe DH, Xu C, Shmukler BE, Otterbein LE, Trudel M, Sachs F, Gottlieb PA, Brugnara C, Alper SL.** Hypoxia activates a Ca2+-permeable cation conductance sensitive to carbon monoxide and to GsMTx-4 in human and mouse sickle erythrocytes. *PLoS One* 5: e8732, 2010.
71. **Wagner-Britz L, Wang J, Kaestner L, Bernhardt I.** Protein kinase Calpha and P-type Ca channel CaV2.1 in red blood cell calcium signalling. *Cell Physiol Biochem* 31: 883–891, 2013.
72. **Weiss E, Rees DC, Gibson JS.** Role of calcium in phosphatidylserine externalisation in red blood cells from sickle cell patients. *Anemia* 2011: 379894, 2010.
73. **Xiao Z, Jaiswal MK, Deng PY, Matsui T, Shin HS, Porter JE, Lei S.** Requirement of phospholipase C and protein kinase C in cholecystokinin-mediated facilitation of NMDA channel function and anxiety-like behavior. *Hippocampus*, 2011.
74. **Yang L, Andrews DA, Low PS.** Lysophosphatidic acid opens a Ca(++) channel in human erythrocytes. *Blood* 95: 2420–2425, 2000.
75. **Zancan P, Sola-Penna M.** Calcium influx: a possible role for insulin modulation of intracellular distribution and activity of 6-phosphofructo-1-kinase in human erythrocytes. *Mol Genet Metab* 86: 392–400, 2005.

Paper 3

Red blood cells of sickle cell disease patients exhibit abnormally high abundance of N-methyl D-aspartate receptors mediating excessive calcium uptake

Pascal Haenggi*, Asya Makhro*, Max Gassmann, Markus Schmugge, Jeroen S. Goede, Oliver Speer and Anna Bogdanova.

*Denotes equal contribution of the authors.

Br J Haematol. 2014 Jul 18. Doi: 10.1111/bjh.13028. [Epub ahead of print]

Received 6 February 2014; accepted for publication 29 May 2014

Contribution:

Makhro A. proposed the hypothesis for the study. Results showed on Figures 1, 2, 3, 4, S2-S8 and Table 2 were produced by Makhro A.

bjh research paper

Red blood cells of sickle cell disease patients exhibit abnormally high abundance of N-methyl D-aspartate receptors mediating excessive calcium uptake

Pascal Hänggi,[1,2]* Asya Makhro,[2,3]* Max Gassmann,[2,3] Markus Schmugge,[4] Jeroen S. Goede,[1,2]* Oliver Speer[2,4] and Anna Bogdanova[2,3]*

[1]Division of Haematology, University Hospital Zurich, [2]Zurich Centre for Integrative Human Physiology (ZIHP), University of Zurich, [3]Institute of Veterinary Physiology, University Children's Hospital, and [4]Division of Haematology, University Children's Hospital, Zürich, Switzerland

Received 6 February 2014; accepted for publication 29 May 2014

Correspondence: PD Dr Anna Bogdanova, Institute of Veterinary Physiology, and Zurich Centre for Integrative Human Physiology (ZIHP), University of Zurich, Winterthurerstrasse 260, CH-8057 Zurich, Switzerland.
E-mail: annab@access.uzh.ch
*Denotes equal contribution of the authors.

Summary

Recently we showed that N-methyl D-aspartate receptors (NMDARs) are expressed in erythroid precursors (EPCs) and present in the circulating red blood cells (RBCs) of healthy humans, regulating intracellular Ca^{2+} in these cells. This study focuses on investigating the possible role of NMDARs in abnormally high Ca^{2+} permeability in the RBCs of patients with sickle cell disease (SCD). Protein levels of the NMDAR subunits in the EPCs of SCD patients did not differ from those in EPCs of healthy humans. However, the number and activity of the NMDARs in circulating SCD-RBCs was substantially up-regulated, being particularly high during haemolytic crises. The number of active NMDARs correlated negatively with haematocrit and haemoglobin levels in the blood of SCD patients. Calcium uptake via these non-selective cation channels was induced by RBC treatment with glycine, glutamate and homocysteine and was facilitated by de-oxygenation of SCD-RBCs. Oxidative stress and RBC dehydration followed receptor stimulation and Ca^{2+} uptake. Inhibition of the NMDARs with an antagonist memantine caused re-hydration and largely prevented hypoxia-induced sickling. The EPCs of SCD patients showed higher tolerance to memantine than those of healthy subjects. Consequently, NMDARs in the RBCs of SCD patients appear to be an attractive target for pharmacological intervention.

Keywords: red blood cells, calcium, sickle cell disease, N-methyl D-aspartate receptors, memantine.

Sickle cell disease (SCD) is a well-known one-gene disease. A point mutation in position 6 of the beta-globin chain gives rise to polymerization of deoxyhaemoglobin S (HbS), loss of deformability and increase in cell adhesion. Haemolysis, vaso-occlusive and pain crises are hallmarks of this disease. Gene therapy and bone marrow transplantation are the optimal, but rarely available and very expensive treatment strategies for this group of patients (Locatelli *et al*, 2013; Chandrakasan & Malik, 2014). Treatment with hydroxycarbamide (HC), which aims to increase haemoglobin F levels in RBCs, is part of the current standard care (Manwani & Frenette, 2013). This therapy significantly decreases the incidence and severity of pain crises and can be combined with regular blood transfusions. Further management includes symptomatic care, such as iron chelation, antibiotic treatment and psycho-social support. However, not all patients respond equally well to HC treatment. Thus, there is a standing need for novel treatment strategies.

Extensive experimental efforts have resulted in the suggestion of a number of novel potential targets for pharmacological intervention. Inhibition of the Gardos channel with the selective blocker Senicapoc (ICA-17043; Neusentis, Cambridge, UK) was used in a clinical trial aiming to reduce dehydration, which promotes haemoglobin S (HbS) polymerization. (Eaton & Hofrichter, 1990). This strategy alone suppressed haemolysis but failed to decrease the incidence of pain and vaso-occlusive crises (Ataga & Stocker, 2009). Inhibition of the calcium-dependent cysteine protease μ-calpain, was recently suggested as an attractive clinical strategy to reduce proteolysis and thereby suppress premature clearance and lysis of RBCs carrying human haemoglobin S (De Franceschi *et al*, 2013). Further suggestions include protec-

doi:10.1111/bjh.13028

tion of RBCs from oxidative stress by blocking NADPH oxidases (NOXes) which generate superoxide anions and are particularly abundant in the RBCs of SCD patients (George *et al*, 2013). Pathological hyperactivation of Gardos channels, μ-calpain and NOXes in diseased RBCs are not directly triggered by mutated HbS expression. However, all three proteins are known to respond to the up-regulation of the intracellular Ca^{2+} levels which were reported in the RBCs of SCD patients (Bogdanova *et al*, 2013). Furthermore, calcium overload is known to increase the adherence of RBCs to vascular endothelium in SCD patients (Hebbel *et al*, 1980; Mohandas & Evans, 1985). The steady-state passive channel-mediated permeability of red cell membranes for Ca^{2+} in healthy humans is very low (*c.* 50 μmol/($l_{packed\ cells}$•h)). Thus, even a minor increase in Ca^{2+} uptake due to the activation of one or several types of ion channels is associated with a substantial transient increase in intracellular Ca^{2+}. In SCD-RBCs abnormally high Ca^{2+} uptake is mediated by a conductive transport pathway known as P_{sickle}. This pathway is activated by deoxygenation, shear stress and a number of other stimuli (Bookchin & Lew, 1981) and, when activated, results in a 6- to 10-fold increase in intracellular free Ca^{2+} levels (Tiffert *et al*, 2003). The molecular identity of ion channel(s) mediating P_{sickle} remains unknown. Identification and characterization of these channel(s) is of key importance. Inhibition of the P_{sickle} pathway and the consecutive decrease in intracellular Ca^{2+} levels will cause inhibition of Gardos channels, μ-calpain, and NOXes. We have recently shown that N-methyl D-aspartate receptors (NMDARs) are involved in Ca^{2+} uptake by the RBCs of healthy humans (Makhro *et al*, 2013). These ionotropic glutamate receptors are non-selective cation channels requiring glutamate and glycine for their activation. They are known to mediate synaptic Ca^{2+} uptake in the brain (Paoletti *et al*, 2013). This study focuses on the involvement of NMDARs in the control of intracellular Ca^{2+} levels in SCD-RBCs. We have been able to follow the abundance and activity of NMDARs in erythroid precursor cells and in the circulating RBCs of SCD patients. Pathological hyperactivation of the NMDARs monitored in SCD-RBCs resulted in an increase in membrane permeability for Ca^{2+}. Haemolytic crises were associated with further up-regulation in receptor activity. Correlation of NMDAR activity with red cell number and C-reactive protein levels in plasma suggests that NMDAR is an active player in regulating red cell properties and life span in SCD patients.

Subjects and methods

A detailed description of materials and methods is available as a supplementary file.

Patients and healthy subjects

Our subject pool consisted of 16 adult patients (21–44 years old) with symptomatic SCD and 31 age-matched healthy adult subjects with no history of SCD. The group of 16 SCD patients consisted of 9 subjects with HbS/HbS, 3 patients with HbS/HbC, 3 with HbS/β-thalassaemia and one patient with HbS/HbD genotype. All patients experience mild and severe SCD crises, and show chronic haemolytic anaemia and persisting reticulocytosis. Blood samples were collected after obtaining informed consent from the subjects. The study was approved by the Ethics Commission of the Canton of Zurich and was performed in accordance with the declaration of Helsinki. General information on the patients is presented in Table I.

Protein abundance of the GluN1 subunit of the NMDAR in SCD-RBC membranes

Immunoblotting was used to explore the alterations in protein abundance of the GluN1 subunit in membrane fractions obtained from the SCD-RBCs and cells of healthy donors after centrifugation on 90% isotonic Percoll gradient (Lutz *et al*, 1992). Blood or pre-filtered RBC suspension was used for fractionation, and membrane preparation from cells forming the light (L), medium (M) and dense (D) fractions of RBCs was obtained (see Fig 1A). Immunoblotting was performed using mouse monoclonal antibodies against the GluN1 subunit on the NMDAR (#MAB1586 Millipore, Temecula, CA) as well as rabbit polyclonal antibodies against total actin (#A2066, Sigma-Aldrich, St. Louis, MO, USA). Rat cortex lysate was used as a positive control, and total actin as a loading control.

NMDAR activity in SCD-RBCs

The number of active receptors per cell was detected using radiolabelled antagonist binding assay as described earlier (Makhro *et al*, 2013). Blood samples were incubated with [^{3}H]MK-801 (740 GBq/mmol, Perkin Elmer, Boston, MA) with subsequent fractionation on Percoll gradient. The potential impact of white blood cells (WBCs) on the [^{3}H]MK-801 binding assay in RBCs in fractions was assessed, as binding of the radiolabelled antagonist was tested in blood samples with and without filtration through a cellulose column. As filtration resulted in a substantial increase in the number of [^{3}H]MK-801 binding sites due to the shear stress filtration step, it was avoided in cases when basal activity of the erythrocytic NMDARs in plasma was determined. Microfluorescence live imaging was used to confirm the data on receptor activity and abundance obtained using [^{3}H]MK-801 binding assay.

Ca^{2+} uptake through NMDARs as a function of oxygenation of SCD-RBCs

Changes in the intracellular Ca^{2+} levels in RBCs upon treatment with agonists (300 μmol/l of NMDA, glutamate or homocysteine mixed with 100 μmol/l glycine) and/or antagonist

Table I. Clinical characteristics of sickle cell disease patients.

	Patient 1	Patient 2	Patient 3	Patient 4	Patient 5	Patient 6	Patient 7	Patient 8	Patient 9	Patient 10	Patient 11	Patient 12	Patient 13	Patient 14	Patient 15	Patient 16
Age (years)	39	24	44	28	26	37	41	27	38	22	31	24	24	36	35	21
Disease	HbS/ HbS	HbS/ HbS	HbS/HbS + hom α^+-thal.	HbS/β-thal. minor + het α^+-thal.	HbS/ HbC	HbS/ HbS	HbS/β-thal. minor	HbS/ HbS	HbS/ HbS	HbS/ HbS	HbS/ HbC	HbS/ HbD	HbS/ HbS	HbS/ HbC	HbS/ HbS	HbS/ HbS
Hb (g/l)	95	91	86	82	105	77	108	80	97	102	104	114	81	119	68	95
Reticulocytes (%)	20·8	12·5	11·9	6·4	6·0	10·7	7·0	32·0	16·8	4·7	4·2	3·83	7·3	4·4	11·4	9·5
MCV (fl)	86·9	92·8	76·6	62·8	80·8	89·2	69·2	96·4	86·0	106·5	81·3	113·6	94·7	74·5	81·1	78·2
LDH (u/l ULN: 420)	979	583	856	582	543	463	642	463	1003	754	419	1094	841	650	887	707
Repeated crisis	Yes	Yes	Yes	Yes	Yes	Yes	Yes	Yes	Yes	Yes	No	No	Yes	Yes	Yes	Yes

Hb, haemoglobin; MCV, men cell volume; LDH, lactate dehydrogenase; ULN, upper limit of normal.
Patients with HbS/HbS: 9.
Patients with HbS/HbC: 3.
Patients with HbS/thal: 3.
Patients with HbS/HbD: 1.

(memantine, 50 μmol/l) of the NMDARs were monitored using the fluo-4 AM dye, as described elsewhere (Makhro *et al*, 2013). RBCs were loaded with 5 μmol/l of the dye for 30 min at room temperature. Incubation medium contained 145 mmol/l NaCl, 5 mmol/l KCl, 1 mmol/l $CaCl_2$, 0·15 mmol/l $MgCl_2$,10 mmol/l Tris-HCl (pH 7·4), 10 mmol/l glucose and 0·1% bovine serum albumin. The effect of hypoxia on cell shape and Ca^{2+} content was tested in the RBCs of SCD patients. The cells were loaded with fluo-4 AM and exposed to 15% O_2 (normoxia) or 0·5% O_2 (hypoxia), 5% CO_2, balanced with N_2 for 10 min, with or without supplementation of the NMDAR antagonist memantine (100 μmol/l) and/or 300 μmol/l NMDA/100 μmol/l glycine mixture. Calcium uptake, cell surface projection and anisotropy as markers of cell volume and sickle cell transformation were then measured microscopically and analysed using CellFinder® (Dr. M. Makhinya, Computer Vision Laboratory, Zürich, Switzerland) as described (Makhro *et al*, 2013).

NMDARs in control of SCD-RBC density, K^+ content and intracellular reduced (GSH) and oxidized (GSSG) glutathione levels

The changes in red cell density upon activation or inhibition of the NMDARs were measured in blood from four selected SCD patients using centrifugation in Percoll density gradient in the presence or absence of NMDA or memantine. Together with mean cell volume (MCV), haematocrit and cell water content, distribution in Percoll gradient was used as an indication of dehydration-rehydration. Changes in the intracellular K^+ content in oxygenated and deoxygenated SCD-RBCs were monitored using flame photometry, and unidirectional chloride-independent K^+ influx was measured using ^{86}Rb as a tracer, as described elsewhere (Makhro *et al*, 2013). The effects of an NMDA/glycine mixture and memantine on the intraerythrocytic GSH:GSSG balance was tested using Ellman's reagent (5,5′-dithio-bis-[2-nitrobenzoic acid]). Proteins were precipitated with 5% trichloroacetic acid and removed; non-protein reduced thiols assessed with or without pre-treatment with glutathione reductase and NADPH, as described elsewhere (Tietze, 1969; Bogdanova *et al*, 2003).

Ex vivo *erythropoiesis and expression of NMDARs in erythroid precursor cells*

Mononuclear cells were isolated from the peripheral blood of healthy people and SCD patients and cultured *ex vivo*, using a 2-phase StemSpan liquid system. After seeding in serum-free expansion medium (SFEM) supplemented with a cytokine mix and penicillin/streptomycin the cells were cultured in it for 5 d. Thereafter non-adherent cells were reseeded and maintained for up to 21 d in StemSpan SFEM with 2% penicillin/streptomycin, 20 ng/ml stem cell factor, 1 u/ml erythropoietin and 5 ng/ml interleukin 3. At day 5, 2 μmol/l dexamethasone and 1 μmol/l β-estradiol were added. During

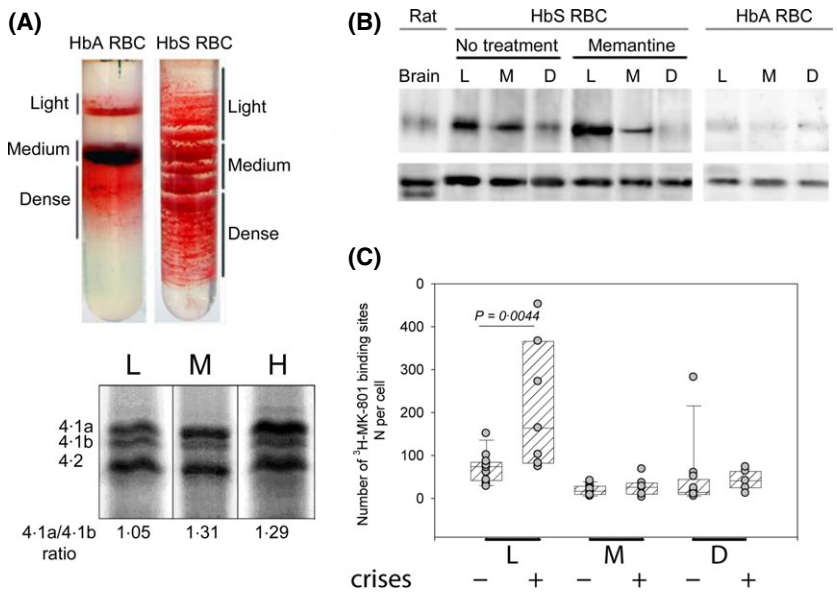

Fig 1. The abundance and activity of NMDARs is altered in the RBCs of SCD patients compared to that in the cells of healthy humans. (A) Separation of RBCs from a healthy donor (HbA) and SCD patient (HbS) into the light (L), medium (M) and dense (D) fractions on Percoll gradient and protein 4·1a/b ratio in cells forming the L, M and D fraction of the SCD patient. (B) Relative abundance of GluN1 subunit protein in the membranes of RBCs forming the L, M and D fraction of a healthy subject (HbA) and a SCD patient (HbS) with or without pre-treatment with memantine (100 μmol/l, 1 h) and in rat cerebellar protein extract. (C) The number of active NMDARs per cell in RBCs of L, M and D fractions of SCD patients during asymptomatic periods and during crises. The means ± SEM for 9 patients are shown. Circles denote individual values. NMDAR, N-methyl D-aspartate receptor; SCD, sickle cell disease; RBCs, red blood cells.

that time the cells progressed from pluripotent cells to pro-erythroblasts, to basophilic and polychromatic erythroblasts and finally, to normoblasts and enucleated reticulocytes (Makhro *et al*, 2013). High performance liquid chromatography (HPLC) was used to verify globin synthesis in fully differentiated cells. The preferential production of HbA/A2 or HbS in reticulocytes was measured in cells derived from the $CD34^+$ cells using HPLC (Figure S1). Expression of *GRIN* genes was monitored in the course of differentiation of EPCs (at days 6, 12 and 18 in culture) using TaqMan® Gene Expression Kits containing specific primers. Protein levels of NMDAR subunits were assessed in EPCs using flow cytometry. CD45 (Anti-CD45 peridinin chlorophyll [PerCP], clone 2D1, BD, San Jose, CA, USA) was used as a WBC marker and CD71 (clone M-A712 fluorescein isothiocyanate [FITC]-conjugated, BD, San Jose, USA) as reticulocyte marker. Abundance of the NMDAR subunits GluN2C (anti-NMDAε3 (NR2C), goat polyclonal IgG, sc-1470); GluN2D (anti-NMDAε4 (NR2D), mouse monoclonal IgG, sc-178221); GluN3A (anti-NR3A (NR3A), goat polyclonal IgG sc-51160) was measured in EPCs at various stages of differentiation. Stained cells were fixed with 1% formaldehyde and fluorescence intensity was measured using the BD Biosciences FACSCalibur flow cytometer (BD Biosciences, San Jose, USA). Memantine toxicity was probed for the EPCs of healthy donors and SCD patients after 6, 12 or 18 d in culture. Cells were exposed to 0·01–1 mmol/l memantine for 24 h and cell mortality monitored by flow cytometry, using propidium iodide (PI) nuclear staining.

Statistical analysis

The data obtained were analysed using GraphPad Instat v.3·0 (GraphPad Software, Inc., La Jolla, CA) and presented as means ± standard error of the mean (SEM) if not stated otherwise. Statistically significant differences were assessed using a one-way analysis of variance (ANOVA) test with the Bonferroni post-test, when a normal distribution test was passed, or, if normal distribution was not confirmed, with a Kruskal Wallis test with Dunn's *post-test* and accepted at $P < 0·05$. Pearson product-moment correlation coefficients were used to assess covariance between the NMDAR activity in RBC fractions and the appearance of blood markers of haemolytic events.

Results

Presence and activity of NMDARs in circulating RBCs of SCD patients during stable periods and in crises

Immunoblotting was used to assess the protein levels of the obligatory GluN1 subunit in membrane fractions prepared from light (L), medium (M) and dense (D) fractions of RBCs of healthy people and SCD patients (Fig 1A). The L fractions of both healthy and SCD-RBCs were enriched with young cells and reticulocytes as follows from cytological estimation using Sysmex (182 ± 82‰ reticulocytes (mean ± standard deviation [SD]) in healthy human samples and 243‰ in the SCD sample shown in Fig 1B) and the

band 4·1a/b ratio (Fig 1A). For SCD-RBCs the L fraction was highly enriched with GluN1 and showed higher receptor activity per cell in RBCs (Fig 1B and Table II). The receptor activity in all fractions of the RBCs of asymptomatic SCD patients exceeded that in cells of healthy donors by 50% and more (Table II). Notably, HC treatment had no effect on the receptor function in SCD-RBCs (Table II). The number of active receptors per cell was similar in RBCs of homozygous HbSS patients and those presented with compound HbS-β thalassaemia (data not shown). Activity of the NMDARs in the L-fraction of SCD-RBCs increased substantially during the crises compared to the asymptomatic values (Fig 1C).

Furthermore, the activity of NMDARs in SCD-RBCs appears to be intimately related to the severity of patients' condition. Up-regulation of the NMDAR activity of mature SCD-RBCs forming the M fraction correlated negatively with haemoglobin and haematocrit levels and positively with plasma lactate dehydrogenase (LDH) and C-reactive protein content (Fig 2). These observations suggest that hyper-activation of NMDARs was associated with onsets of haemolytic events. Furthermore, receptor activity in cells forming fractions L (younger cells) and D (terminally dehydrated cells) correlated positively with neutrophil counts in blood (data not shown). It is noteworthy that all patients studied showed only mild neutrophilia and neutrophil counts did not exceed 12–14 $\times$ 10^9/l.

Effect of NMDAR agonists and antagonists on intracellular Ca^{2+} levels, cell volume and ion content

The role of the NMDAR activation state in the maintenance of intracellular Ca^{2+} levels, RBC volume and redox state was explored *ex vivo*.

RBCs of SCD patients loaded with the calcium-sensitive dye fluo-4 AM responded to treatment with the agonists NMDA and glycine (300 and 100 μm respectively), with an acute temporary increase in intracellular Ca^{2+}. Exposure of the SCD-RBCs to memantine (50 μmol/l) caused a modest decrease in Ca^{2+}-sensitive fluorescence (Fig 3A,C, Figures S2 and Supplementary Animated Figures S3-S8). Uptake of Ca^{2+} triggered the activation of Ca^{2+}-sensitive Gardos channels, K^+ loss, and cell shrinkage. Passive K^+ flux through the membranes of SCD-RBCs substantially exceeding that in the RBCs of healthy humans could be further facilitated by the NMDAR agonists, and partially suppressed by the receptor antagonist memantine (Fig 3B). Inhibition or stimulation

Table II. NMDAR activity in light, medium and dense fractions of RBCs of healthy people and SCD patients off or on hydroxycarbamide treatment.

Fraction	Healthy subjects (n = 31)	SCD patients Off-HC (n = 11)	SCD patients On-HC (n = 6)
Light (L)	34·9 ± 7·5	69 ± 11**	72 ± 17**
Medium (M)	4·1 ± 0·7	22 ± 6***	16 ± 3***
Dense (D)	4·3 ± 0·6	30 ± 11***	12 ± 2***

NMDAR, N-methyl D-aspartate receptor; SCD, sickle cell disease; HC, hydroxycarbamide.
**Denotes $P < 0·01$ and ***stands for $P < 0·001$ when compared with healthy control subjects.

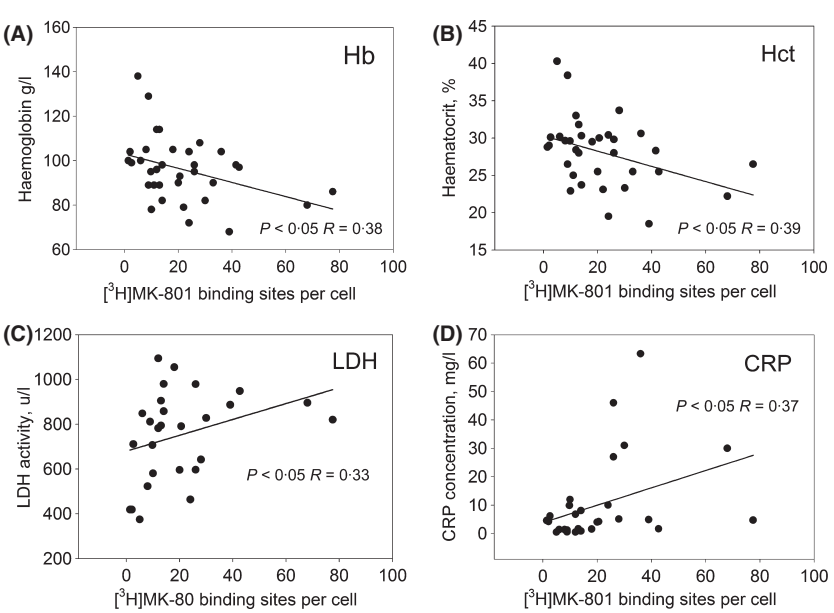

Fig 2. Correlation between the NMDAR activity in the M fraction of SCD-RBCs and markers of haemolysis [haemoglobin (A), haematocrit (B) and lactate dehydrogenase in plasma (C) and inflammation [C-reactive protein (D)]]. Covariance analysis of the receptor activity and the markers of haemolysis and inflammation was performed using Pearson product-moment correlation coefficients for the 34 blood samples taken from 16 patients on different occasions during asymptomatic periods and during haemolytic crises. HB, haemoglobin, Hct, haematocrit; LDH, lactate dehydrogenase; CRP, C-reactive protein.

of the NMDARs resulted in the re-distribution of RBCs in Percoll gradient. Interestingly, the cells containing more receptors underwent dehydration as soon as they were exposed to shear stress while passing through the Percoll, as follows from Fig 1B. These GluN1-enriched cells moved down the Percoll gradient to the D fraction. In line with this observation, filtration of RBCs through the cellulose column was associated with an increase in the NMDAR activity detected using ^{3}H-MK-801 binding assay (data not shown). Dehydration induced by passing through the Percoll gradient could be abolished by the pre-treatment of blood samples with memantine prior to the separation. Memantine-treated cells showed a maximum of GluN1 levels associated with the L fraction, whereas the D fraction was almost deprived of GluN1 (Fig 1B).

Incubation of whole blood from asymptomatic SCD patients with NMDA resulted in further dehydration of cells, which were then shifted down the gradient (Fig 3D). Treatment of blood with memantine, on the other hand, induced re-hydration and a corresponding upward shift within the Percoll gradients (Fig 3D). Monitoring of the kinetics of the morphological responses to the stimulation of the NMDARs in SCD-RBCs in the absence or presence of memantine was performed microscopically. The cells were pre-incubated with saturating concentrations of glutamate and glycine with or without memantine in a Ca^{2+}-free medium. During the recording, Ca^{2+} (final concentration 1.8 mM) was administered to the medium and the changes in cellular morphology monitored over 12 min. The corresponding Supplementary Animated Figures S3-S8, can be viewed online in the supplementary section. These video files show substantial reduction or complete abolishment of echinocytic transformation in the cells pre-treated with memantine before exposure to calcium.

The oxidative stress characteristic of SCD-RBCs was monitored as a four-fold increase in the intracellular oxidized glutathione (GSSG) levels over the GSSG content of RBCs in healthy human subjects. Further accumulation of GSSG was observed upon stimulation of NMDARs in SCD-RBCs with NMDA. Inhibition of the NMDARs with memantine prevented an oxidative burst triggered by NMDA (Fig 3E).

NMDARs and sickle cell transformation caused by deoxygenation

Polymerization of deoxygenated HbS was induced *ex vivo* by equilibration of SCD-RBCs with a humidified gas phase containing 5% CO_2 and 0·5% O_2 in Eschweiler tonometers. These oxygen levels have been recorded in some areas in the brain (Erecinska & Silver, 2001). Cells exposed to a gas phase supplemented with 15% O_2 served as the normoxic control, mimicking pO_2 in human lungs under normoxic conditions (13·3 kPa). At the onset of deoxygenation, the NMDARs in SCD-RBCs were either stimulated with NMDA (300 μmol/l) and glycine (100 μmol/l) or suppressed with memantine (50 μmol/l). Following 2 min of equilibration with the gas phase, the cells were incubated under normoxic or hypoxic conditions for 15 min. Thereafter RBC morphology (Fig 4A–D,F,G and Figure S2), intracellular Ca^{2+} (Fig 4E) and the intracellular ion content (Fig 4H) were assessed.

Deoxygenation of SCD-RBCs resulted in characteristic alterations in cell morphology, including the formation of drepanocytes (indicated with arrows in Fig 4B,C), "holy leaf", and "granular" cells (Figure S2C) and echinocytes (Fig 4 and Figure S2C). Quantitatively, these changes were assessed as an increase in anisotropy (Fig 4G, Figure S2A). Intracellular Ca^{2+} accumulation was induced by deoxygenation, as exemplified in Fig 4B–D and quantified in Fig 4E. Intake of Ca^{2+} triggered loss of K^+ (Fig 4H) and a decrease in cellular projection areas, signifying dehydration and shrinkage (Fig 4F, Fig S2B). The presence of extracellular Ca^{2+} was critical for initiating Ca^{2+}-driven dehydration which in turn facilitated polymerization of deoxy-HbS (Figure S2A). Chelation of the intracellular Ca^{2+} with 1,2-bis(o-aminophenoxy)ethane-N,N,N′,N′-tetraacetic acid (BAPTA) in addition to omission of the extracellular Ca^{2+} further reduced sickling and shrinking of hypoxic SCD-RBCs (Figure S2A).

Polymerization rate of deoxy-HbS is inversely related to the Hb concentration to an extremely high power (Hebbel, 2009). Stimulation of the NMDARs with NMDA and glycine aggravated the morphological changes induced by deoxygenation, including impressive induction of echinocytosis and RBC fragmentation (Fig 4D). Potassium loss from the oxygenated agonists'-treated SCD-RBCs reached its maximum and could not be further stimulated by hypoxia (Fig 4H). Some of the cells were showing signs of irreversible HbS polymerization ("holy leaf" appearance) even under normoxic conditions (Figure S2C). Memantine administration effectively prevented hypoxia-induced sickling and echinocytosis (Fig 4C,G). A decrease in Ca^{2+} uptake by deoxygenated cells was observed upon memantine treatment followed by the suppression of hypoxia-induced K^+ loss and dehydration (Fig 4H and F respectively).

Subunit composition of NMDARs and their expression in erythroid precursor cells of patients (SCD-EPCs)

Previously we explored the expression profile of *GRIN* genes in EPCs derived from healthy human blood (Makhro *et al*, 2013). A similar approach was used to monitor the presence of transcripts of *GRIN* genes and changes in protein levels of all subunits of the NMDARs in SCD-EPCs. Pluripotent mononuclear cells were isolated from the peripheral blood of healthy subjects and patients. These cells were cultured to obtain pro-erythroblasts (day 6), basophilic and polychromatic erythroblasts (day 12) or normoblasts and enucleated reticulocytes (day 18). Expression profiles obtained for the transcripts of *GRIN1, GRIN2A, GRIN2C, GRIN2D, GRIN3A* and *GRIN3B* in SCD-EPCs at each differentiation stage are shown in Fig 5. The expression of *GRIN1* and *GRIN2C* tran-

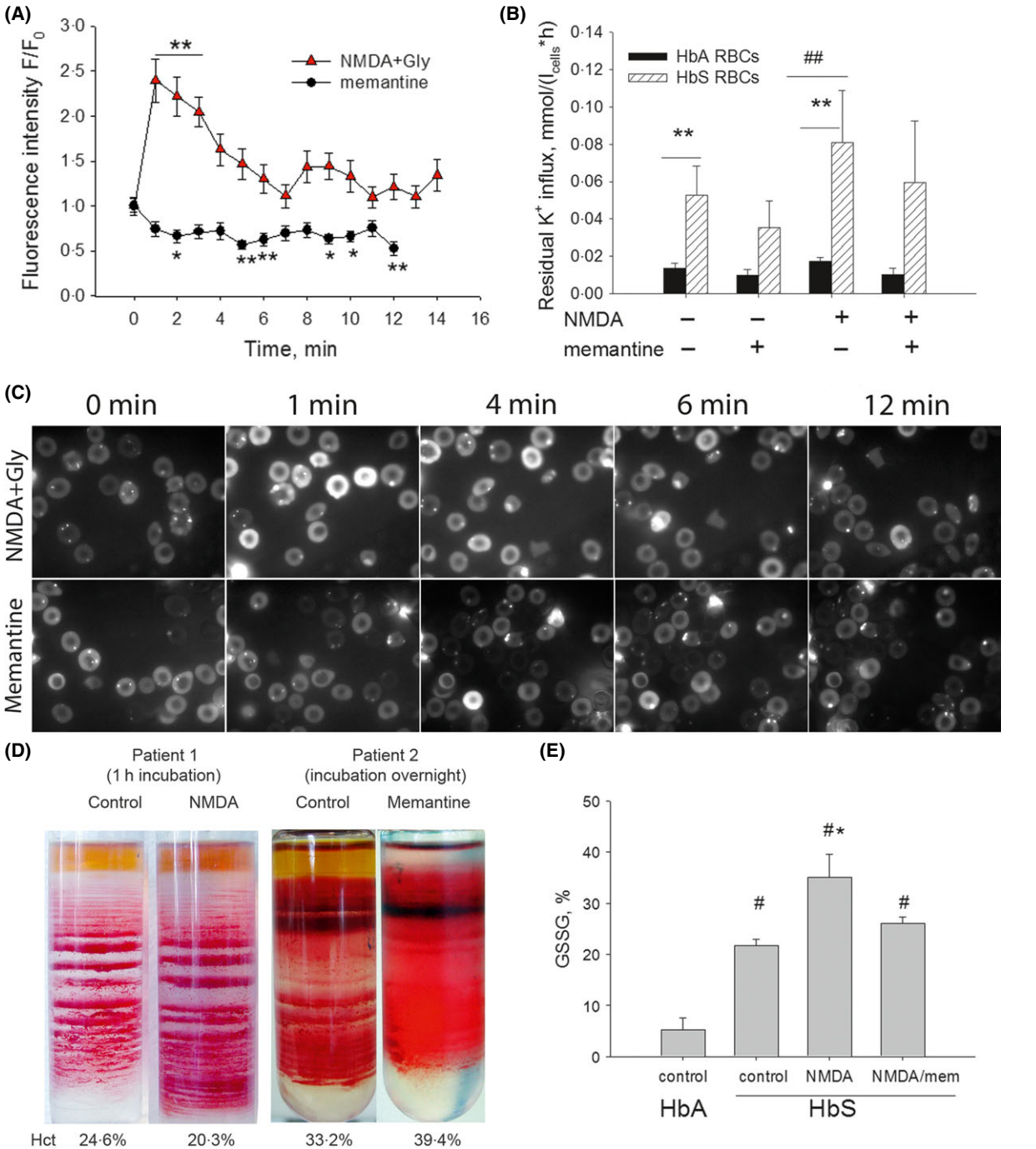

Fig 3. Intracellular Ca^{2+} and oxidized glutathione levels, cell density, and residual K^+ flux in SCD-RBCs upon activation (300 μmol/l glutamate and 100 μmol/l glycine) or inhibition (100 μmol/l memantine) of the NMDARs. (A) Kinetics of changes in the intracellular Ca^{2+} in SCD-RBCs (fluorescence intensity at each time-point (F) normalized to the average signal intensity at time zero (Fo)). Number of cells analysed per time point ranges from 24 to 42. * denotes $P < 0{\cdot}05$ and ** stands for $P < 0{\cdot}01$ when compared to the signal at time zero. (B) Chloride-independent ouabain-insensitive unidirectional K^+ influx into the RBCs of healthy humans and SCD patients. ** indicates $P < 0{\cdot}01$ when fluxes were compared between the HbA and HbS-RBCs under the same conditions. Data are means of six independent experiments ± SD. ## denotes $P < 0{\cdot}01$ for the K^+ fluxes in SCD-RBCs treated with either memantine or NMDA/Gly. (C) Representative experiments showing the alterations in Ca^{2+}-sensitive fluo-4 fluorescent signal intensity in response to NMDA/Gly or memantine treatment quantified in panel A. (D) Distribution of SCD-RBCs in Percoll gradient after pre-treatment of whole blood with either 300 μmol/l NMDA or 100 μmol/l memantine. Numbers below the images indicate the corresponding haematocrit values. (E) Oxidized glutathione (GSSG) content of RBCs exposed to agonists in the presence or absence of memantine for 30 min. # denotes $P < 0{\cdot}05$ compared to the values in the RBCs of healthy humans (HbA-control). *stands for $P < 0{\cdot}05$ compared to control levels in SCD-RBCs (HbS-control). NMDA, N-methyl D-aspartate; SCD, sickle cell disease; RBCs, red blood cells; Gly, glycine.

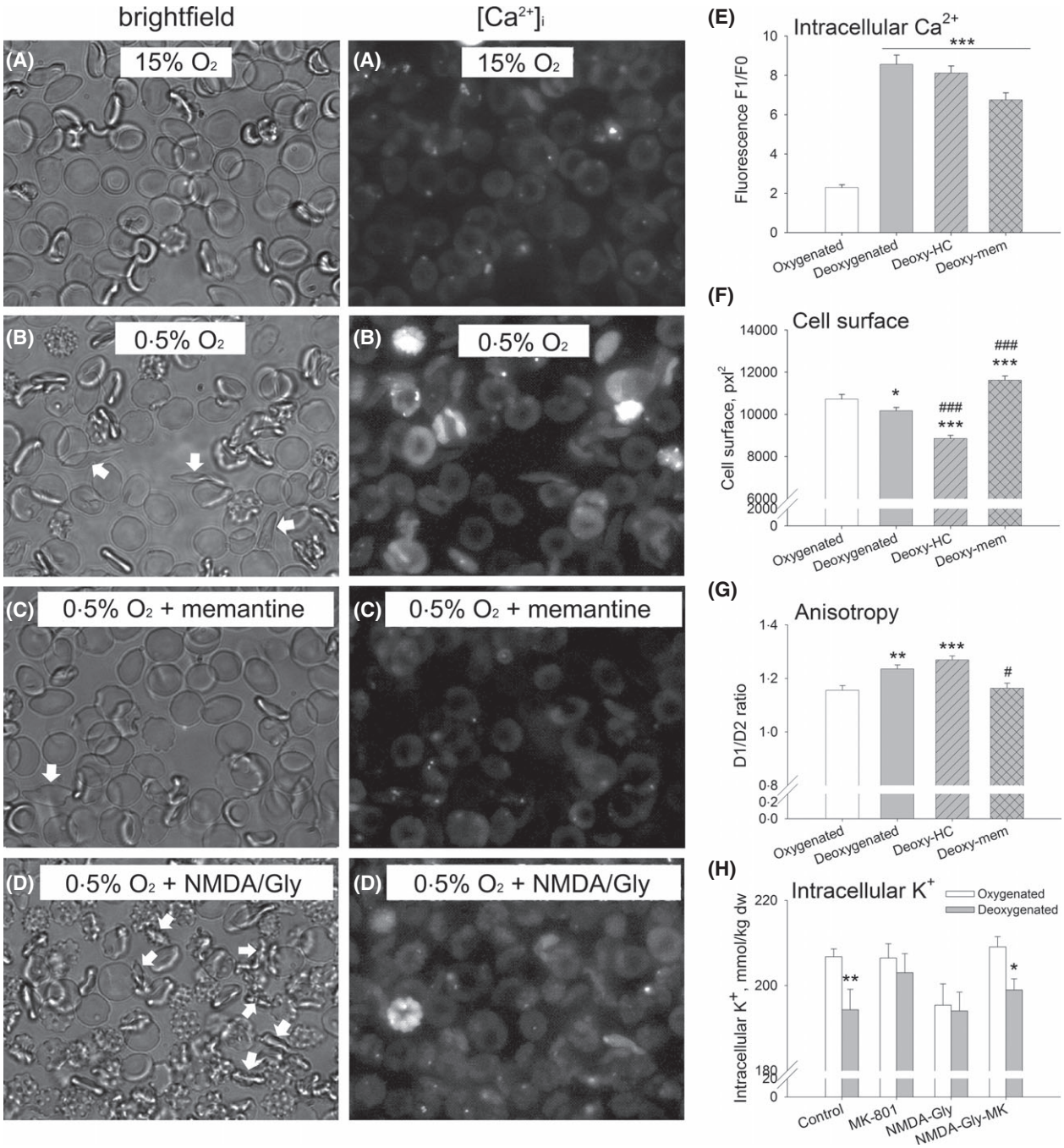

Fig 4. Responses of SCD-RBCs to deoxygenation in the presence of the NMDAR agonists (300 μmol/l NMDA/100 μmol/l glycine) and antagonist (50 μmol/l memantine). RBCs in suspension were exposed to either 15% or 0·5% O_2 in gas phase in Eschweiler tonometers (15 min, 37°C). Shown are (A-D) the representative images of erythrocytes in different conditions, cell morphology and intracellular Ca^{2+} levels; (E) quantification of the changes in the intracellular Ca^{2+} levels; (F) alterations in RBC projection area; (G) changes in anisotropy as a marker of sickle cell transformation in deoxygenated SCD-RBCs and (H) changes in the intracellular K^+ concentration. NMDA, N-methyl D-aspartate; SCD, sickle cell disease; RBCs, red blood cells; Gly, glycine.

scripts in healthy subjects increased progressively during *ex vivo* differentiation. Peak levels of *GRIN2D* transcripts were found at the stage of basophilic and polychromatic erythroblasts (12 d). In SCD-EPCs these stage-dependent variations in expression levels of all *GRIN* genes were blunted. No significant changes in NMDAR transcript levels were detected during differentiation. Compared to healthy controls, relative expression of *GRIN3B* was significantly higher in SCD throughout erythropoiesis. Similar to those in EPCs of healthy humans (Makhro *et al*, 2013), transcripts of *GRIN2B* in EPCs obtained from SCD patients were below the detection threshold at any differentiation stage.

Protein levels per cell and the number of cells expressing GluN2C, 2D, 3A and 3B were assessed in EPCs during differentiation. On average, the percentage of cells expressing the NMDA subunits varied from *c.* 10% for pro-erythroblasts to 20–40% at the later differentiation stages, independent of the presence of the *HBB* E6V mutation (HbS gene) (Fig 6A,C,D, and E). The number of copies of the dominant GluN2D and 3B subunits per cell, expressed as the mean fluorescence intensity, were the highest at the normoblastic stage (Figs 6D and 3B). A tendency towards an increased number of cells expressing GluN3A and 3B subunit in the EPCs of SCD patients was observed at the stage of basophilic and polychromatic erythroblasts (Fig 6E and G). However, this tendency did not reach statistical significance and was not preserved at the normoblastic stage. All in all, the protein levels for all subunits at each differentiation stage tested did not differ between the EPCs of healthy humans and those of SCD patients. This observation suggests that the striking enrichment of the circulating SCD-RBCs with NMDARs resulted from the disturbed clearance of the receptors from reticulocytes.

Sensitivity of the EPCs to memantine exposure was tested as a function of antagonist concentration. As shown in Fig 7, memantine was well-tolerated by both the EPCs of control subjects and those of SCD patents within a pharmacologically relevant concentration range (1–50 μmol/l). At higher concentrations (0·1–1 mmol/l) the highest mortality rate was observed in control EPCs at the pro-erythroblast stage (6 d in culture, Fig 7A). The EPCs of SCD patients showed maximal sensitivity to high doses of memantine only at the stage of polychromatic erythroblasts (12 d in culture, Fig 7B), being generally more tolerant to memantine than the cells of healthy humans. Cell death was accompanied by characteristic changes in morphology, including a high degree of vacuolization and vesiculation (Fig 7C).

Discussion

The present study indicates that an abnormally great abundance of functional NMDARs is characteristic of the circulating RBCs of SCD patients (Fig 1, Table II). Hyperactivation of the NMDARs in RBCs was associated with the severity of haemolytic events, as the number of active receptors in the majority of cells forming M fraction correlated negatively with haemoglobin/haematocrit levels and positively with plasma LDH (Fig 2). Induction of HbS polymerization *in vitro* by exposing the RBCs of SCD patients to low oxygen

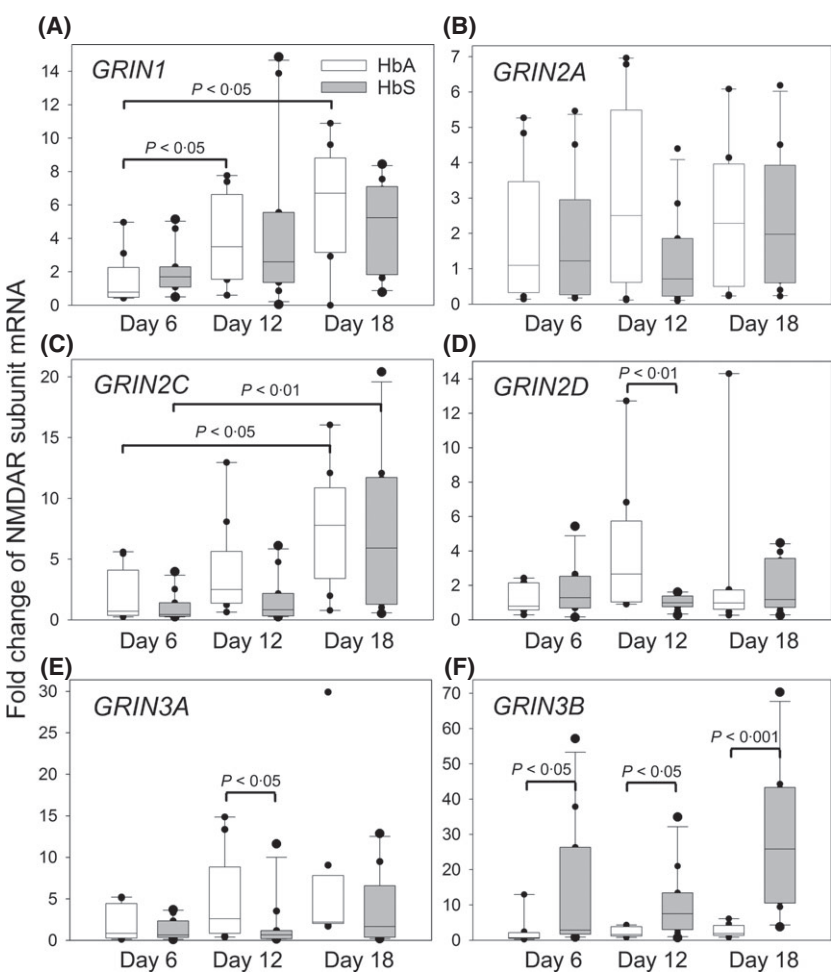

Fig 5. Expression of NMDAR subunits during erythropoiesis**.** (A-F) relative amounts of the different NMDAR isotypes (as indicated). Cells were harvested and analysed at days 6, 12 and 18, transcripts were measured by TaqMan real time polymerase chain reaction. Values are represented as box plots of 9 erythroid cultures from healthy subjects (open boxes, $n = 9$) and 10 erythroid cultures from SCD (grey boxes, $n = 10$), each started with cells from a different donor. An overall comparison indicated significant differences between days of culture only for the expression of *GRIN2C* ($P < 0·05$) and *GRIN1* ($P < 0·05$).

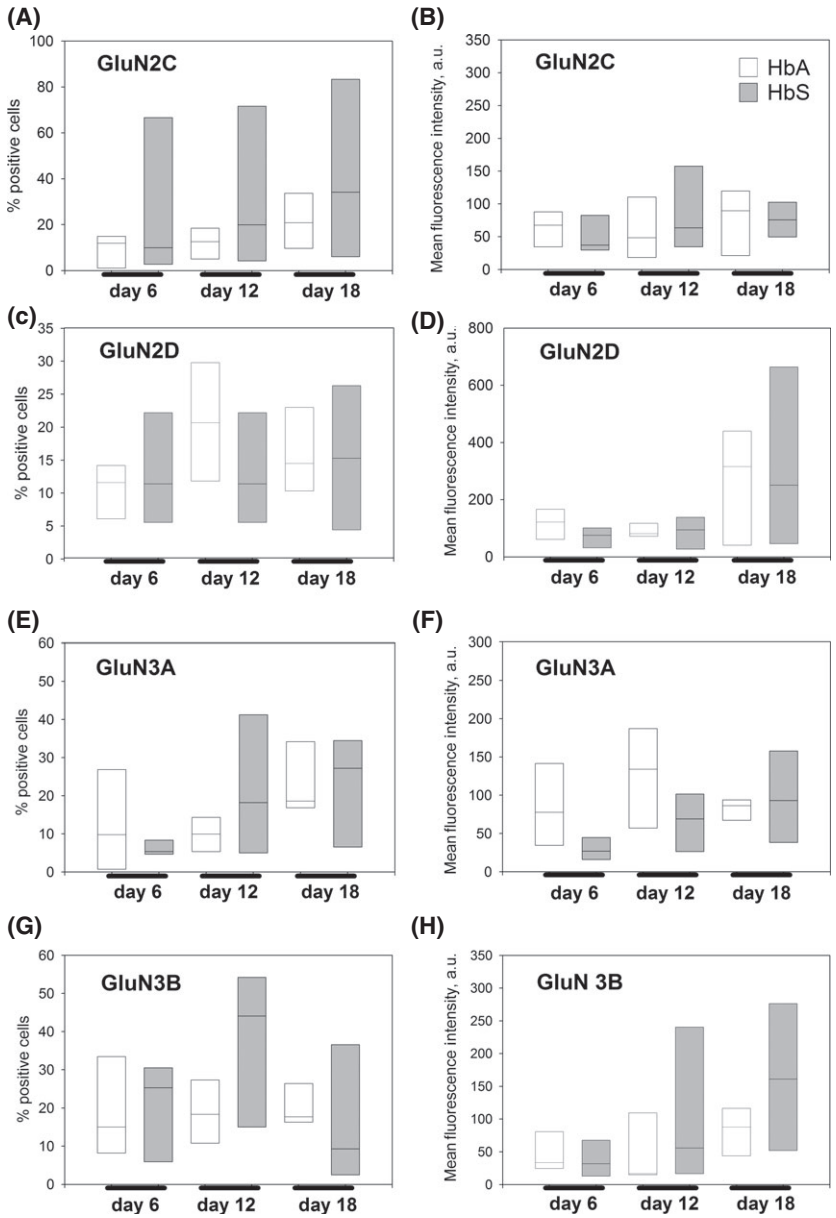

Fig 6. Protein levels of GluN2C, 2D, 3A and 3B in EPCs at various differentiation stages. Shown are the numbers of cells in which fluorescent signal from the corresponding antibodies was detected by means of flow cytometry (A, C, E, G) and the mean intensity of this signal per cell (B, D, F, H). Numbers above boxes represent medians of the corresponding signal in EPC cultures obtained from healthy control subjects. Cells were harvested and analysed at day 6, 12 and 18. Data were obtained from cultures grown from $CD34^+$ cells of four different SCD patients (open boxes) and six healthy subjects (grey boxes). EPCs, erythroid precursors; AU, arbitrary units.

levels revealed that hypoxia-induced Ca^{2+} uptake, dehydration and the polymerization rate itself could be substantially slowed down in the presence of the NMDAR antagonist memantine (Fig 4). Activation of the NMDARs with NMDA and glycine, on the other hand, could induce a complex cell response resembling that occurring during crises, including some sickle cell transformation Ca^{2+} uptake, K^+ and water loss and oxidative stress (Fig 3).

Taken together, all these findings suggest that inhibition of the NMDARs may be beneficial as it hits multiple calcium-sensitive targets, preventing the dehydration, sickling and oxidation associated with haemolytic crises in SCD patients (Bogdanova *et al*, 2013). The design of the present *ex vivo* study did not allow testing for the long-term effects of memantine supplementation on SCD-RBCs, such as changes in calpain activity, or changes in the adherence of SCD-RBCs to the endothelial layer. The lack of active NMDARs in the circulating C57B6 mouse red blood cells was documented by using [^{3}H]MK-801 binding assay (A. Makhro and A. Bogdanova, unpublished observations). This observation limits us to the use of human cells in the future, making mouse models of SCD useless for such a long-term study.

We have previously shown that the number of NMDARs and the amplitude of response to the stimulation of NMDARs in the RBCs of healthy humans is particularly high in the light fraction enriched with reticulocytes and young cells (Makhro *et al*, 2013). Similarly, the number of copies of GluN1 and the number of active receptors assessed as the [^{3}H]MK-801 binding sites per cell is maximal in the upper light fraction of SCD-RBCs (Table II, Fig 1B, C). As reported by Bookchin *et al* (1991), the reticulocytes of SCD patients

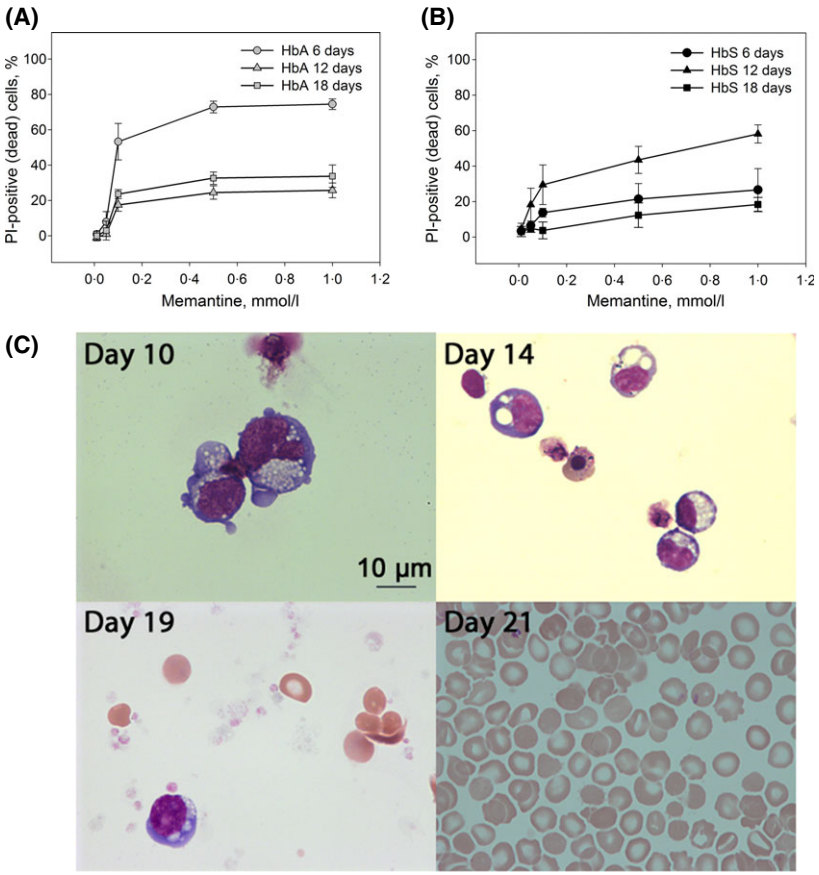

Fig 7. Memantine and MK-801 toxicity studies performed for healthy human-derived EPCs and SCD-EPCs at days 6, 12 and 18 in culture. The EPCs were exposed to memantine added to the culturing medium at concentrations of 10 μmol/l-1 mmol/l for 24 h (A,B). Thereafter the cells were harvested and mortality assessed using propidium iodide staining. Data are the means of four cultures obtained from four independent healthy subjects or HbSS patients ± SD. (C) SCD-EPCs were treated with 0·5 mmol/l MK-801 for 12 h at the various differentiation stages. Vacuolization is present at days 14 and 19 and indicates apoptosis. Cells at the early stage of erythropoiesis (day 10) are less sensitive to MK-801 treatment and mature RBCs (day 21) are completely resistant. SCD, sickle cell disease; EPCs, erythroid precursors.

show maximal susceptibility to dehydration and sickling. This paradoxic predisposition of young cells to premature clearance may be caused at least in part by higher susceptibility to calcium overload resulting from hyperactivation of NMDARs.

Substantial up-regulation of NMDAR abundance and activity in SCD-RBCs was observed in all RBC fractions, being particularly high in the L fraction (Table II). A further increase in the number of active receptors in the L fraction of SCD-RBCs was detected in patients showing symptoms of haemolytic crises manifested as a decrease in haematocrit, and the onset of a pain crisis (Fig 1C). These observations suggest that the greater abundance and activity of NMDARs may be associated with the onset of crises. Dissection of the factors involved in hyperactivation of the NMDARs in RBCs of patients with SCD during the crisis is of key importance. Plasma glutamate and glycine levels are determinants of NMDAR activity in RBCs. Increased levels of glycine and a *c.* 3·5-fold increase in the intraerythrocytic levels of both agonists have been reported for SCD patients during asymptomatic periods (Kiessling *et al*, 2000). No data for plasma amino acid composition during crises are currently available. One can expect that haemolysis would be associated with the release of these excitatory amino acids, resulting in progressive activation of the receptors in RBCs.

Mechanisms that control NMDAR abundance in the RBCs of SCD patients await further in-depth characterization, which is beyond the scope of this study. Although relatively high, the number of receptors per cell in circulating SCD-RBCs is within the 10^2 range and is thus not comparable with that in EPCs, which range from 10^5 to 10^3 receptor copies per cell (Makhro *et al*, 2010, 2013). Terminal stages of EPC differentiation are clearly associated with massive clearance of the receptors from the plasma membrane. Even a slight disturbance in clearance efficiency would result in significant up-regulation of the number of NMDARs remaining in membranes of circulating RBCs. The mechanisms involved in clearance of NMDARs in EPCs have not yet been studied. Unusually high levels of membrane-bound haemoglobin resulting from its higher affinity to the cytosolic domain of band 3 protein may at least partly explain the inclmplete clearance of the receptors (Rotter *et al*, 2010).

The conductive pathway involved in the increased permeability of the membranes of SCD-RBCs to cations, including calcium ions, is known as P_{sickle}. Analysis of the properties and pharmacological profile of P_{sickle} suggests that the current is mediated by more than one channel type. Among the hallmarks of P_{sickle} are activation upon deoxygenation (Browning *et al*, 2007; Vandorpe *et al*, 2010) and filtration (shear stress) (Brain *et al*, 2004), permeability for K^+, Na^+ and Ca^{2+} (Bookchin & Lew, 1981), sensitivity to Zn^{2+} and

stilbene disulfonate (DIDS) (Joiner, 1990; Browning *et al*, 2007), voltage- and pH-dependence (Joiner *et al*, 1993). These properties are shared by NMDARs. We have demonstrated that NMDAR function in the RBCs of SCD patients is oxygen-dependent (Fig 4). Sensitivity to 4,4′- diisothiocyanostilbene-2,2′-disulfonic acid (DIDS) (Tauskela *et al*, 2003) and voltage-dependence were demonstrated in the NMDARs in neurons. Sensitivity of NMDARs to Zn^{2+} appears to be particularly interesting in view of reports that 1 year of zinc sulphate supplementation was found to reduce the incidence of pain crises and infections in SCD patients in several clinical trials (Swe *et al*, 2013). Whether this beneficial action of Zn^{2+} is, at least in part, mediated by suppression of the NMDARs remains to be confirmed.

We have demonstrated the sensitivity of NMDARs in SCD-RBCs to filtration as a manifestation of shear stress (Fig 1B, and text). These receptors have been shown to be mechano-sensitive (Paoletti & Ascher, 1994; Singh *et al*, 2012). Other features of P_{sickle}, such as sensitivity to Gd^{3+}, CO and to a toxin produced by the tarantula spider GsMTx-4 (Vandorpe *et al*, 2010) have not been tested for NMDARs. NMDAR function is known to be highly sensitive to changes in pH, but the optimal pH range for the NMDARs in the brain differs from that of P_{sickle}. These are the indications that Cav2·1 channels and voltage-dependent anion channels (VDACs) may contribute to P_{sickle} along with NMDARs, each responding to a characteristic set of stimuli related to stress and inflammation (Kaestner, 2011).

Our observations clearly show that the inhibition of NMDARs hits multiple targets in RBCs. In addition, memantine has recently been reported to effectively suppress neuropathic pain after surgery (Morel *et al*, 2013). Failure to reduce the number and severity of acute pain episodes was the reason for the negative outcome of several trials in which a Gardos channel blocker, the anti-adhesion drug poloxamer 188, and inhaled nitric oxide were used in treatment of patients with SCD (Gee, 2013). A combination of the prevention of haemolytic crises and reduction in vaso-occlusive events with potential effective pain management makes memantine an attractive candidate for therapy of SCD.

The number of patients with SCD is growing rapidly in Switzerland and other European countries due to the increasing flow of migrants from Africa and Asia to Europe (Schmugge *et al*, 2008). Currently, most of the SCD patients in Switzerland are children. Moreover, when proven efficient in treatment of SCD, calcium-lowering therapy could be extended for treatment of other types of rare hereditary forms of anaemia associated with abnormal intracellular Ca^{2+} levels, such as thalassaemia, phosphofructokinase deficiency and others.

Authorship

P.H. and O.S. performed research shown in Figs 5–7; A.M. produced data for the Figs 1 and 3A,C,D and Table II; A.B. generated data for Figs 3C, 4, and Figures S2 and animation figures; J.S.G. and M.S. provided blood and information on the SCD patients. J.S.G. produced the data shown in Fig 2. All authors contributed to data analysis, discussion and writing of the manuscript.

Acknowledgements

This study was supported by a ZIHP cooperative grant (to J.S.G, O.S. and A.B.), funded by the European Community's Seventh Framework Programme (FP7/2007-2013) under Grant Agreement No. 602121, the CTI/Lyfjos GmbH grant and the Vontobel Foundation (to A.B.), and supported by the Hartmann Müller-Stiftung (to O.S.). The authors state that there is no conflict of interests to disclose. We gratefully acknowledge technical assistance of Nikolay Bogdanov and cordially thank Dr Heather Murray for careful proof-reading and language editing.

Supporting Information

Additional Supporting Information may be found in the online version of this article:

Data S1. Subject and methods**.**

Fig S1. Quantification of HbA, HbF, HbA1C, HbA2 and HbS of the total haemoglobin at reticulocyte stage of erythropoietic maturation (day 21).

Fig S2. The role of intra- and extracellular $Ca2^{+}$ in facilitation of HbS polymerisation and SCD-RBC shrinkage.

Fig S3. Experiment 1 Control: HbSS control 1 BF (bright field)/HbSS control 1 Ca (green channel).

Fig S4. Experiment 2 Control: HbSS control 2 BF (bright field)/HbSS control 2 Ca (green channel).

Fig S5. Experiment 3 Control HbSS control 3 BF (bright field)/HbSS control 3 Ca (green channel).

Fig S6. Experiment 1 Memantine-pretreated cells: HbSS memantine 1 BF (bright field)/HbSS memantine 1 Ca (green channel).

Fig S7. Experiment 2 Memantine-pretreated cells: HbSS memantine 2 BF (bright field)/HbSS memantine 2 Ca (green channel).

Fig S8. Experiment 3 Memantine-pretreated cells: HbSS memantine 3 BF (bright field)/HbSS memantine 3 Ca (green channel).

References

Ataga, K.I. & Stocker, J. (2009) Senicapoc (ICA-17043): a potential therapy for the prevention and treatment of hemolysis-associated complications in sickle cell anemia. *Expert Opinion on Investigational Drugs*, **18**, 231–239.

Bogdanova, A.Y., Ogunshola, O.O., Bauer, C. & Gassmann, M. (2003) Pivotal role of reduced glutathione in oxygen-induced regulation of the Na(+)/K(+) pump in mouse erythrocyte membranes. *Journal of Membrane Biology*, **195**, 33–42.

Bogdanova, A., Makhro, A., Wang, J., Lipp, P. & Kaestner, L. (2013) Calcium in red blood cells-a

perilous balance. *International Journal of Molecular Sciences*, **14**, 9848–9872.

Bookchin, R.M. & Lew, V.L. (1981) Effect of a 'sickling pulse' on calcium and potassium transport in sickle cell trait red cells. *Journal of Physiology*, **312**, 265–280.

Bookchin, R.M., Ortiz, O.E. & Lew, V.L. (1991) Evidence for a direct reticulocyte origin of dense red cells in sickle cell anemia. *Journal of Clinical Investigation*, **87**, 113–124.

Brain, M.C., Pihl, C., Robertson, L. & Brown, C.B. (2004) Evidence for a mechanosensitive calcium influx into red cells. *Blood Cells, Molecules, & Diseases*, **32**, 349–352.

Browning, J.A., Staines, H.M., Robinson, H.C., Powell, T., Ellory, J.C. & Gibson, J.S. (2007) The effect of deoxygenation on whole-cell conductance of red blood cells from healthy individuals and patients with sickle cell disease. *Blood*, **109**, 2622–2629.

Chandrakasan, S. & Malik, P. (2014) Gene Therapy for Hemoglobinopathies: the State of the Field and the Future. *Hematology/oncology Clinics of North America*, **28**, 199–216.

De Franceschi, L., Franco, R.S., Bertoldi, M., Brugnara, C., Matte, A., Siciliano, A., Wieschhaus, A.J., Chishti, A.H. & Joiner, C.H. (2013) Pharmacological inhibition of calpain-1 prevents red cell dehydration and reduces Gardos channel activity in a mouse model of sickle cell disease. *FASEB Journal*, **27**, 750–759.

Eaton, W.A. & Hofrichter, J. (1990) Sickle cell hemoglobin polymerization. *Advances in Protein Chemistry*, **40**, 63–279.

Erecinska, M. & Silver, I. (2001) Tissue oxygen tension and brain sensitivity to hypoxia. *Respiration Physiology*, **128**, 263–276.

Gee, B.E. (2013) Biologic complexity in sickle cell disease: implications for developing targeted therapeutics. *ScientificWorldJournal*, **2013**, 694146.

George, A., Pushkaran, S., Konstantinidis, D.G., Koochaki, S., Malik, P., Mohandas, N., Zheng, Y., Joiner, C.H. & Kalfa, T.A. (2013) Erythrocyte NADPH oxidase activity modulated by Rac GTPases, PKC, and plasma cytokines contributes to oxidative stress in sickle cell disease. *Blood*, **121**, 2099–2107.

Hebbel, R.P. (2009) Chapter 42 Pathobiology of sickle cell disease. In: Hematology. Basic Principles and Practice. (ed. by Hoffma, R., Benz, E.J., Shattil, S.J., Furie, B., Silberstein, L.E., McGlave, P. & Heslop, H.), pp. 565–576. Churchill Livingstone Elsevier, Philadelphia, PA.

Hebbel, R.P., Yamada, O., Moldow, C.F., Jacob, H.S., White, J.G. & Eaton, J.W. (1980) Abnormal adherence of sickle erythrocytes to cultured vascular endothelium: possible mechanism for microvascular occlusion in sickle cell disease. *Journal of Clinical Investigation*, **65**, 154–160.

Joiner, C.H. (1990) Deoxygenation-induced cation fluxes in sickle cells: II. Inhibition by stilbene disulfonates. *Blood*, **76**, 212–220.

Joiner, C.H., Morris, C.L. & Cooper, E.S. (1993) Deoxygenation-induced cation fluxes in sickle cells. III. Cation selectivity and response to pH and membrane potential. *American Journal of Physiology*, **264**, C734–C744.

Kaestner, L. (2011) Cation channels in erythrocytes - historical and future perspective. *The Open Biology Journal*, **4**, 27–34.

Kiessling, K., Roberts, N., Gibson, J.S. & Ellory, J.C. (2000) A comparison in normal individuals and sickle cell patients of reduced glutathione precursors and their transport between plasma and red cells. *Hematology Journal*, **1**, 243–249.

Locatelli, F., Kabbara, N., Ruggeri, A., Ghavamzadeh, A., Roberts, I., Li, C.K., Bernaudin, F., Vermylen, C., Dalle, J.H., Stein, J., Wynn, R., Cordonnier, C., Pinto, F., Angelucci, E., Socie, G., Gluckman, E., Walters, M.C., Rocha, V. & Eurocord, European, B. & Marrow Transplantation, g. (2013) Outcome of patients with hemoglobinopathies given either cord blood or bone marrow transplantation from an HLA-identical sibling. *Blood*, **122**, 1072–1078.

Lutz, H.U., Stammler, P., Fasler, S., Ingold, M. & Fehr, J. (1992) Density separation of human red blood cells on self forming Percoll gradients: correlation with cell age. *Biochimica et Biophysica Acta*, **1116**, 1–10.

Makhro, A., Wang, J., Vogel, J., Boldyrev, A.A., Gassmann, M., Kaestner, L. & Bogdanova, A. (2010) Functional NMDA receptors in rat erythrocytes. *American Journal of Physiology. Cell Physiology*, **298**, C1315–C1325.

Makhro, A., Hanggi, P., Goede, J.S., Wang, J., Bruggemann, A., Gassmann, M., Schmugge, M., Kaestner, L., Speer, O. & Bogdanova, A. (2013) N-methyl D-aspartate (NMDA) receptors in human erythroid precursor cells and in circulating red blood cells contribute to the intracellular calcium regulation. *American Journal of Physiology. Cell Physiology*, **305**, C1123–C1138.

Manwani, D. & Frenette, P.S. (2013) Vaso-occlusion in sickle cell disease: pathophysiology and novel targeted therapies. *Blood*, **122**, 3892–3898.

Mohandas, N. & Evans, E. (1985) Sickle erythrocyte adherence to vascular endothelium. Morphologic correlates and the requirement for divalent cations and collagen-binding plasma proteins. *Journal of Clinical Investigation*, **76**, 1605–1612.

Morel, V., Etienne, M., Wattiez, A.S., Dupuis, A., Privat, A.M., Chalus, M., Eschalier, A., Daulhac, L. & Pickering, G. (2013) Memantine, a promising drug for the prevention of neuropathic pain in rat. *European Journal of Pharmacology*, **721**, 382–390.

Paoletti, P. & Ascher, P. (1994) Mechanosensitivity of NMDA receptors in cultured mouse central neurons. *Neuron*, **13**, 645–655.

Paoletti, P., Bellone, C. & Zhou, Q. (2013) NMDA receptor subunit diversity: impact on receptor properties, synaptic plasticity and disease. *Nature Reviews Neuroscience*, **14**, 383–400.

Rotter, M.A., Chu, H., Low, P.S. & Ferrone, F.A. (2010) Band 3 catalyzes sickle hemoglobin polymerization. *Biophysical Chemistry*, **146**, 55–59.

Schmugge, M., Speer, O., Ozsahin, A.H. & Martin, G. (2008) Die Sichelzellerkrankung in der Schweiz. Teil 1: pathophysiologie, Klinik. *Schweiz Med Forum*, **8**, 582–586.

Singh, P., Doshi, S., Spaethling, J.M., Hockenberry, A.J., Patel, T.P., Geddes-Klein, D.M., Lynch, D.R. & Meaney, D.F. (2012) N-methyl-D-aspartate receptor mechanosensitivity is governed by C terminus of NR2B subunit. *Journal of Biological Chemistry*, **287**, 4348–4359.

Swe, K.M., Abas, A.B., Bhardwaj, A., Barua, A. & Nair, N.S. (2013) Zinc supplements for treating thalassaemia and sickle cell disease. *Cochrane Database Systematic Review*, **6**, CD009415.

Tauskela, J.S., Mealing, G., Comas, T., Brunette, E., Monette, R., Small, D.L. & Morley, P. (2003) Protection of cortical neurons against oxygen-glucose deprivation and N-methyl-D-aspartate by DIDS and SITS. *European Journal of Pharmacology*, **464**, 17–25.

Tietze, F. (1969) Enzymic method for quantitative determination of nanogram amounts of total and oxidized glutathione: applications to mammalian blood and other tissues. *Analytical Biochemistry*, **27**, 502–522.

Tiffert, T., Bookchin, R.M. & Lew, W.L. (2003) Calcium homeostasis in normal and abnormal human red cells. In: Red Cell Membrane transport in Health and Disease (eds by Bernhardt, I. & Ellory, J.C.), pp. 373–405. Springer, Berlin.

Vandorpe, D.H., Xu, C., Shmukler, B.E., Otterbein, L.E., Trudel, M., Sachs, F., Gottlieb, P.A., Brugnara, C. & Alper, S.L. (2010) Hypoxia activates a $Ca2^{+}$-permeable cation conductance sensitive to carbon monoxide and to GsMTx-4 in human and mouse sickle erythrocytes. *PLoS ONE*, **5**, e8732.

Paper 4 (manuscript draft)

Cardiac N-methyl D-aspartate receptors as a pharmacological target

Asya Makhro, Dmitry Kosenkov, Colin Schwarzwald, Giuseppe Faggian, Max Gassmann, Anna Bogdanova

Contribution:

Makhro A. produced all the data in that study and participated in the study design.

Cardiac N-methyl D-aspartate receptors as a pharmacological target

Asya Makhro, Dmitry Kosenkov, Colin Schwarzwald, Giuseppe Faggian, Max Gassmann, Anna Bogdanova*

Institute of Veterinary Physiology (A.M., M.G, and A.B.), and Equine Department (C.S.), Vetsuisse Faculty and the Center for Integrative Human Physiology, University of Zurich, Zurich Switzerland; (C.S., M.G. and A.B.); and Division of Cardiac Surgery, University of Verona Medical School, Verona, Italy (G.F. and D.K.)

Key words: NMDA receptor, rat heart, ECG, arrhythmia, isolated blood-perfused heart

Corresponding author:

Dr Anna Bogdanova

University of Zurich, Vetsuisse Faculty

Institute of Veterinary Physiology

Winterthurerstrasse 260

CH-8057 Zurich

Switzerland

E-mail: annab@access.uzh.ch

Tel: +41 44 6358811

Fax: +41 44 6358932

Word count: 5648

Abstract

Aims: This study focuses on the cardiac N-methyl D-aspartate receptors (NMDARs) as a target for endogenous and synthetic agonists and antagonists.

Methods and Results: Using isolated perfused rat hearts, we have shown that intracoronary administration of agonists and antagonists of the NMDAR have a pronounced effect on autonomous heart function. Perfusion of rat hearts with autologous blood supplemented with NMDAR agonists was associated with induction of tachycardia, sinus arrhythmia and ischemia. Intracoronary administration of the NMDAR antagonists exerted an anti-arrhythmic effect and resulted in bradycardia and improvement of capillary perfusion. Half-maximal increase in heart rate and heart rate variability occurred in the presence of 150 and 270 μM glutamate/glycine mixture respectively. Action of the NMDAR antagonists on autonomous heart function differed strikingly from that of the L-type Ca^{2+} channel blockers verapamil and diltiazem. [^{3}H]-MK-801 displacement studies performed for eliprodil, Ro25-6981, memantine, ketamine, and MK-801 in rat heart tissue sections and in isolated sarcolemmal membranes proved selectivity of [^{3}H]-MK-801 interaction with cardiac NMDARs. Subunit composition of cardiac NMDARs was explored. Transcripts of the GluN3A and GluN2D were found in all heart chambers, whereas expression of GluN1 and GluN2A,C were restricted to the atria. Expression of the GluN2B protein in ventricles increased markedly with age of the animals. Subunit composition and unusual pharmacological characteristics reveal the unique features of cardiac NMDARs.

Conclusions: The obtained data reveal that NMDARs are expressed in rat heart contributing to the autonomic heart rate regulation and the function of the cardiac conduction system.

Introduction

The role of N-methyl D-aspartate receptors (NMDARs) in brain development, cognitive function and progression of neurological disorders cannot be overestimated. These ligand-gated cation channels formed by glycine-binding (GluN1 and GluN3A/B) and glutamate-binding (GluN2A, B, C and D) subunits show high preference for Ca^{2+} [1]. Gating properties, conductance, deactivation kinetics as well as responses to inhibitors and allosteric modulators vary greatly depending on the subunit composition of the receptor complex[2]. The pivotal importance of this class of ionotropic glutamate receptors in the brain gave rise to a rapid progress in pharmacology during the past 30 years and resulted in development of numerous antagonists targeting specific subunits that form the receptor or specific binding sites[3]. These compounds are currently used for medication of patients with Alzheimer's disease, Huntington's disease, and various forms of dementia. Some of them are broadly used as anaesthetics and others were tested for treatment of epilepsy and stroke[4]. Each antagonist used to target the NMDARs in the central nervous system has been shown to produce multiple systemic effects. In particular, compounds targeting 1-(1-phenylcyclohexyl)piperidine (phencyclidine, PCP)-binding site within the receptor channel pore (e.g. memantine, ketamine, and MK-801) were reported to act as antiarrhythmic drugs in animal models[5-7]. The PCP-targeting antagonist aptiganel HCl decreased the incidence of arrhythmia, suppressed premature ventricular complexes (PVCs) and reduced the S-T interval depression in human patients affected by stroke [4]. Eliprodil, another NMDAR antagonist interacting selectively with the glutamate-binding GluN2B subunit, was shown to modulate oxygen consumption in the heart[8, 9] and cause prolongation of the rate-corrected QT interval (QTc) in human subjects at high doses[4]. Initially, all the changes in the heart function triggered by the NMDAR agonists and antagonists were attributed to the action of these compounds on the central and peripheral nervous system. Indeed, microinjections of NMDA

or glutamate directly into nucleus tractus solitaries caused bradycardia and reduced arterial pressure in rats. These effects were inhibited by the receptor antagonists MK-801 and AP5[10, 11]. The GluN1, GluN2A, and GluN2B subunits were detected in vagal preganglionic neurons projecting to the rat heart[12].

However, the effects of agonists and antagonists of the NMDARs were retained in denervated hearts. MK-801 in rat and ketamine in guinea pig spontaneously beating right atria caused a dose-dependent reduction in heart rate (HR) and contractile force[13,14]. Similar negative inotropic and chronotropic effects were observed in isolated hearts from rabbits and guinea pigs perfused with Krebs-Ringer or Tyrode buffer supplemented with ketamine[15, 16]. Recently, expression of the GluN1 and GluN2B subunits of the NMDARs was confirmed in heart tissue of several mammalian species[17-19]. However, detailed characterisation of autonomous heart responses to the NMDAR agonists and antagonists was lacking. Subunit composition of cardiac NMDAR complexes, pharmacology of cardiac NMDARs, and kinetics of responses of the heart to the alterations in receptor activity remained unidentified. This study presents detailed characterization of autonomous responses of the isolated blood-perfused rat heart to agonists and antagonists of the NMDARs. Using autoradiography and qPCR the heart was mapped for the NMDAR activity and subunit composition and the specific interaction of antagonists with cardiac NMDARs was explored. The obtained results indicate that cardiac NMDARs actively participate in regulation of HR and heart rate variability (HRV).

Materials and methods[#]

([#]For more details on the methods and protocol see the supplementary Method section).

Animals

Wistar rats of both sexes, aged from 3 months to 2 years, were used for the study. Animals were

purchased from Janvier (Le Genest Saint Isle, France). All animal experiments were approved by the Veterinary Office of the canton Zurich and performed in accordance with Swiss animal protection laws and institutional guidelines that comply with guidelines of the American Physiological Society and the Institute of Laboratory Animal Resources.

Ex vivo blood-perfused rat-heart model

Animals were anesthetized using 3% isoflurane in O_2/N_2O mixture (800 mL/min), heparinized intravenously (5000 U/kg), and 8-10 mL blood were collected from the caudal vena cava. The hearts were collected immediately thereafter and chilled in ice-cold perfusion buffer. The hearts were then perfused retrograde via the aorta with autologous rat blood or washed human erythrocytes suspensions to maintain optimal oxygen delivery to the tissue and to achieve intracoronary delivery of the compounds used. Human blood was collected from healthy donors at the University Hospital Zurich following written consent. Blood collection was approved by the cantonal ethic committee and conformed to the principles outlined in the Declaration of Helsinki. Haemoglobin oxygen saturation was maintained at 87-90%. Stock solutions of the NMDAR agonists (N-methyl D-aspartate (NMDA), glutamate, glycine, homocysteic acid, D-serine), and NMDAR antagonists (phencyclidine-targeting blockers (PCPBs): memantine, MK-801, ketamine; polyamine binding site-targeting antagonists (PAAs): eliprodil, Ro25-6981; and $ZnCl_2$) were used for intracoronary perfusion. L-type calcium channel blockers (CCBs) diltiazem and verapamil were always used at concentrations 10 µM and 5 µM respectively. Concentrations of the NMDAR agonists and antagonists were chosen based on the affinities and IC50 values reported for the neuronal NMDARs[20, 21]. Each of the antagonists chosen for the study was not absolutely specific, but NMDARs were the only receptors shared by all the compounds tested, whereas the other targets were not always overlapping (Table 1 and supplementary Table 1). All compounds were

administered 20 min after the onset of blood perfusion and applied for 40 min if not stated otherwise.

Evans Blue was added intracoronary and efficacy of capillary perfusion in ventricular tissue was monitored as stated elsewhere[22] in the presence or absence of 300 μM HCA or 50 μM of memantine in blood.

Classical Langendorff model

Changes in heart rate and heart rate variability were monitored as a function of glutamate and glycine concentration in Krebs-Henseleit solution. These experiments were performed to assess the action of physiological doses of agonists on autonomous heart function and EC50 detection.

ECG recordings, heart rate, and heart rate variability

ECG electrodes were fixed vertically on either side of the hearts so that the resulting recordings corresponded to the aVL projection. Heart rate (HR) was calculated from the RR intervals extracted from the ECG using MLS360/7 ECG Analysis Module of the LabChart7 Pro Software, ADInstruments Ltd, and manually corrected for artefacts. Heart rate variability (HRV) was assessed using time-domain analysis of consecutive artefact-free RR intervals. The values averaged over the last 5 minutes of the 20 min restitution period were used as controls and compared with the readouts averaged over the period between the 10^{th} and 15^{th} minute after the onset of treatment. This approach, i.e. comparing HR and HRV before and after treatment, allowed minimising the contribution of heart-to-heart variability into the observed effects of tested compounds on HR and HRV. HR as well as ECG recorded from the isolated rat hearts perfused with autologous rat blood (Fig S2H) or washed human red cell suspension was stable over the first two hours of perfusion despite certain variability in absolute values between the individual hearts.

mRNA isolation and qPCR analysis

RNA was isolated from the rat brain, left and right ventricles, septum, left and right atria and a region containing mitral, tricuspid, aortic and pulmonary valves as described elsewhere [23]. cDNA was synthesized from RNA samples by "High Capacity RNA-to-cDNA Master Mix", Applied Biosystems. "TaqMan® Gene Expression Master Mix". Sixty cycles at 95°C for 15 s and 60°C for 1 min were performed using 7500 Fast Real-Time PCR System, Applied Biosystems. Rat GAPDH was used as a reference. Triplicate readings were taken and the average was calculated. The results were normalised to a randomly selected value obtained for the control sample, which was accepted as equal to 1.

Protein detection by Western Blotting

Rat hearts were homogenized and proteins were separated on 7.5% acrylamide gel and transferred to nitrocellulose membrane. Staining performed with mouse monoclonal anti-GluN1 antibody, and rabbit polyclonal anti-GluN2C antibodies (NB300-118 and NB300-107, Novus Biologicals), rabbit polyclonal anti-GluN2A and mouse monoclonal anti-GluN2B antibodies (ab14596 and ab28373, Abcam) and the corresponding secondary antibodies.

Isolation of sarcolemmal membranes (SM) and detection of K_i for MK-801, ketamine, memantine, eliprodil and Zn^{2+} using [^{3}H]-MK-801 displacement approach

SM fraction was isolated from rat atrial and ventricular tissue according to the protocol described elsewhere[24]. Membranes were pre-incubated with 3 nM [^{3}H]-MK-801 and thereafter exposed to MK-801, memantine, eliprodil or Zn^{2+} at various concentrations for 60 min. Thereafter membranes were sedimented on a nitrocellulose filter and washed twice with 5 ml of assay buffer. Filters with sedimented membranes were then dissolved in the scintillation fluid and the amount of [^{3}H]-MK-

801 bound to the membranes was assessed using TRI-CARB liquid scintillation analyser (Packard, Canada).

Autoradiography

Autoradiography was performed as described elsewhere[25] to detect the active NMDAR complexes in intact hearts and in cryosections. Radiolabeled [^{3}H]-MK-801 was administered intracoronary and allowed to circulate for 100 min. Extraction of the [^{3}H]-MK-801 from plasma by the myocardium was monitored using liquid scintillation analyzer (Fig S1B). Localisation of the bound [^{3}H]-MK-801 within the heart was assessed in 10 μm cross-sections through the whole organ using X-ray Kodak film. The film was developed after 2 months of exposure and the obtained images digitalized and analyzed using MCID Image analysis software (InterFocus Imaging Ltd, Cambridge, UK).

A similar approach was used to detect [^{3}H]-MK-801 binding and assess displacement efficiency of MK-801 and other antagonists in the 20 μm-thick cryosections of rat hearts and rat brain. Sections were rinsed in sucrose buffer, air-dried and incubated with 30 nM [^{3}H]-MK-801 (20.5 Ci/mmol) in the presence of 300 μM NMDA and 300 μM glycine. After 20 min of incubation, the sections were washed free from non-bound antagonist and exposed to the film for 1 month. Displacement efficacy was tested. Non-specific binding tests were performed in which [^{3}H]-MK-801 binding to the cryosections was assessed in the presence of non-labelled MK-801, memantine, eliprodil or Ro-25-6981 (200 μM each), or ketamine (4 mM).

Statistical analysis

Data are presented as means±SEM if not stated otherwise. Data analysis and statistics were performed using GraphPad Instat Software. Normality test was performed followed by one-way Analysis of Variance (ANOVA) test followed by the Bonferroni or Dunnett Multiple Comparisons post-tests. The level of significance was accepted at $p<0.05$.

Results

Heart rate (HR)

Intracoronary administration of the NMDAR agonists (NMDA, glutamate, homocysteic acid) resulted in tachycardia developing within the first few minutes and reaching a plateau after 10 min of treatment (Fig 1A,F, S2A). Intracoronary supplementation of NMDAR antagonists belonging to PCPBs (MK-801, memantine, ketamine; Fig1B,F,S2C) and PAAs (eliprodil, Ro25-6981; Fig 1C,F, S2D) produced acute bradycardic response within 2-3 min which reached 30-40% of initial HR at the end of 40 min exposure. The degree of bradycardia was proportional to the antagonists concentration (Fig S5). Partial additively in effects was observed when 50 μM of MK-801 was administered subsequently after Ro25-6981 (Fig S2D) or eliprodil (data not shown) supplementation. Treatment with $ZnCl_2$ resulted in tachycardia, produced PVCs and was pro-arrhythmogenic (Table 2, Fig 1D,S3). Due to the similarities in responses to the individual agonists (Fig 1A) PCPBs (Fig 1B), PAAs (Fig 1C) and CCBs (Fig 1E), results were pooled together for further analysis (Fig 1F-I, Table 2).

Hearts perfused with Krebs-Henseleit saline developed dose-dependent tachycardia when treated intracoronary with equal concentrations of glutamate and glycine. Half-maximal response was observed at a concentration of 149 μM (Fig 2 A,B). Furthermore, stimulation of the NMDARs with glutamate and glycine produced a dose-dependent increase in heart rate variability (EC50 271 μM, Fig S3, B). No further changes in HR were observed above 1 mM of glutamate and glycine. Less potent, but more NMDAR-specific agonists NMDA (glutamate analogue) and D-serine (glycine analogue) were causing tachycardia although at doses significantly exceeding those of glutamate and glycine (EC50 of 1.55 and 2.1 mM for NMDA and D-serine respectively, Fig 2C).

The agonist-induced tachycardic response was not reversed after the 15 min of perfusion with the agonists-free buffer (Fig 2B). Flattening or inversion of ST segment on ECG recordings was consistent with the myocardium becoming ischemic upon stimulation of the receptors with agonists (Fig 2B,D). This observation was in line with results obtained on blood-perfused heart in which tachycardia and arrhythmia was associated with a decrease of ST segment amplitude (Fig 1A). Using Evans Blue capillary perfusion was visualised in ventricular tissue upon hyperactivation or inhibition of the cardiac NMDARs by HCA and memantine respectively. The number of perfused capillaries recognised by Evans Blue fluorescent signal was drastically reduced in ventricular tissue exposed to HCA and significantly improved upon administration of memantine (Fig 2C). These changes were associated with the onset or suppression of tachycardia and arrhythmia (Fig 2B,C, Fig S3B).

Heart rate variability (HRV)

Persisting stimulation of the cardiac NMDARs with agonists was associated with an increase in HRV (Table 2, Fig 2 A, D, Fig S2-S4). Increase in HRV was directly proportional to the dose of agonists present in the circulation with a half-maximal effect observed at 271 μM (Fig 2A,C). Spontaneous sinus arrhythmia observed in ~ 35% of harvested hearts exposed to a brief episode of global ischemia-reperfusion could be suppressed by treatment with PCPBs and PAAs. The anti-arrhythmic action of antagonists was reflected by a decrease in SD1, SD2, SDNN, and RMSDD (for abbreviations see Supplementary Methods section) back to the values observed in rhythmic hearts (Table 2). Representative Poincaré plots confirmed induction of sinus arrhythmia in autonomously beating hearts by the NMDAR agonists (Fig S4A-C). The action of Zn^{2+} ions generally mimicked

that of the NMDAR agonists (Fig 1D, Table 1). Tachyarrhythmia caused by exposure to Zn^{2+} could not to be reversed by the subsequent MK-801 administration (Fig S2F).

In contrast to the NMDAR antagonists, CCBs had a pronounced pro-arrhythmic effect in autonomously beating rat hearts (Table 2, FigS3D, S4H-E).

ECG

In blood-perfused as well as in RBC-perfused and KH-perfused hearts hyperactivation of the NMDARs with any agonist was associated with lowering or reversion of the ST segment (Figs 1A,2D). PCPBs MK-801 and memantine, or ketamine significantly increased QTc interval, while PR and QRS intervals were not changed (Fig 1B,G,H,I). Similar to that in RBC-perfused setup supplemented with NMDA and D-serine MK-801 produced biphasic dose-dependent bradycardic response (apparent IC50=40 μM) which was associated with the prolongation of PR, QRS and QTc intervals in the presence of agonists NMDA and D-serine (Fig. S5). Prolongation of QTc was not observed if Zn^{2+} (50 μM) was present in blood along with MK-801 (Fig 1D). Zinc alone did not alter ECG intervals despite is pro-arrhythmogenic action. GluN2B-specific PAAs did not alter QTc intervals significantly, but have prolonged QRS duration (Fig 1C,H,I).

Intracoronary administration of the CCBs resulted in disappearance of P-waves on the ECG (sinus arrest or sinus exit block) and induction of marked sinus arrhythmia (Fig S3E). Bradycardia (Fig 1F, S2F) and increase in RR intervals in the hearts exposed to the CCBs (Fig 1A) was associated with a pronounced decrease in QTc interval (Fig 1E,I).

Cardiac NMDAR pharmacology and localisation

Two approaches were used to assess the receptor activity and its pharmacological profile. Isolated SM fraction was pre-incubated with [^{3}H]-MK-801 and thereafter displacement of the bound

antagonist with various concentrations of non-radiolabeled MK-801 revealing that at least 90% of specific [^{3}H]-MK-801 binding to the SM. Similar dose-dependent [^{3}H]-MK-801 displacement experiments were performed for ketamine, memantine and Zn^{2+}. The IC50 values and the representative curves where [^{3}H]-MK-801 displacement efficiency was plotted against the concentration of non-labelled antagonists in semi-logarithmic coordinates and fitted using single or dual sigmoid functions are shown in Fig 3. In atrial SM, two types of binding sites with high ($IC50_1$ 15±4 nM) and low ($IC50_2$>1 µM) affinities were detected for MK-801, whereas memantine displaced [^{3}H]-MK-801 at a single binding site (IC50 37±9 nM). The $IC50_1$ for the NMDAR antagonists in ventricular SM made up (in nM): 1.8±0.3 for MK-801, 1.3±0.4 for memantine, and 1206±417 for ketamine (Fig 3B). Binding of MK-801 was altered in NMDARs pre-treated with 50 µM of eliprodil (Fig 3C). Treatment of the SM with Zn^{2+} increased [^{3}H]-MK-801 binding rate to the membranes at low nanomolar (e.g. 2 nM) concentration and antagonised [^{3}H]-MK-801 binding at higher doses (e.g. 50 µM, inset of Fig 3D).

Localisation of active cardiac NMDAR units within the rat heart chambers was explored using autoradiography. When administered intracoronary, [^{3}H]-MK-801 was gradually extracted from blood (Fig S1) as it interacted with the myocardium. In young hearts, maximal signal from the bound [^{3}H]-MK-801was obtained from the atria, when in old hearts [^{3}H]-MK-801 mostly bound within the ventricles and septum (Fig 4A). Antagonist displacement studies similar to those in SLM were performed using heart cryosections. Incubation of heart tissue with [^{3}H]-MK-801 revealed substantial specific binding of the radiolabeled antagonist to the cardiac as well as to the neuronal NMDARs. The bound [^{3}H]-MK-801 could be successfully displaced by non-labelled PCPBs like MK-801, memantine, ketamine as well as by PAAs as eliprodil and Ro25-6981 (Fig 4B,C). The PAAs antagonized [^{3}H]-MK-801 binding to the heart, but not to the brain cryosections (Fig 4B,C).

Targets of the NMDAR agonists and antagonists in the heart

Expression pattern of GluN (GRIN) genes encoding NMDAR subunits were assessed in the rat brain and in rat heart chambers, septum, and in the valvular region using RT-PCR. As shown in the Table 3, GluN1 and GluN2A were expressed in atria only, whereas transcripts of GluN2B and 2D, and that of GluN3A genes were detected in all regions of the heart. GluN2C was only detected in septum and in the left atrium. In adult rat brain, prominent expression of the GluN1, 2A and 2B was found. In rat heart most abundant were the transcripts coding for the glutamate-binding GluN2D and glycine-binding GluN3A subunits of the receptor. In cardiomyocytes isolated from ventricular tissue and septum, GluN2B, GluN2D, and GluN3A transcripts were detected. In fibroblasts obtained from the same areas in the heart, transcripts of GRIN genes remained below detection limit. (Table 3).

The presence of the NMDAR subunits at the protein level in whole heart homogenate was explored using immunoblotting. Total rat brain protein extracts were used as a positive control. Cardiac GluN1, GluN2A, 2B and 2C subunits recognised by the corresponding antibodies appeared to be similar to those in the brain (Fig 4D). The signal for GluN2D subunit was identical for in rat brain and heart-derived protein, but its weight (170 kDa) was somewhat higher than 135 kDa reported for this subunit (data not shown). In agreement with [^{3}H]-MK-801 binding studies (Fig 4A), the abundance of GluN2B subunit protein in ventricular tissue increased with age (Fig 4E).

Discussion

The importance of cardiac NMDARs activation state in autonomous control of HR and HRV, function of conductive system (QRS intervals), and ventricular repolarisation (QT) is a major finding of the present study.

Our data indicates that a substantial number of the cardiac NMDARs are active in blood-perfused rat heart. Their activity is maintained by endogenous agonists of which glutamate (35-200 μM) and glycine (180-310 μM)[26-29] are most abundant in plasma and the most potent activators of the cardiac

NMDARs (Fig 2A). Glutamate EC50 concentration reported for the neuronal NMDARs is 100 μM[30] whereas for the HR response the EC50 was 149 μM (Fig 2A). Recordings of ionic currents mediated by the NMDARs are required to assess EC50 of the cardiac NMDARs more precisely. Paracrine release of glutamate from the cardiac muscle where it is highly abundant (30 $\mu mol/_{mg}protein$), hemolysis, and other processes causing alterations of plasma glutamate levels may thus contribute to the development of tachycardia and arrhythmia. Glutamate is currently extensively used as an essential component of cardioplegic solution, where its concentrations may exceed 20 mM. Exogenous glutamate is effectively extracted by cardiomyocytes, and taken into the mitochondria where it is fed into the tricarboxylic acid cycle via malate-aspartate shuttle supporting respiration, particularly in ischemic heart[31]. In rats, these supra-physiological glutamate concentrations were shown to acutely reduce infarct size during the first minutes of reperfusion, but did not improve hemodynamic recovery[24, 32]. Our observations suggest that exogenous glutamate has more than one target, acting on the pacemaker function (HR, Table 2), conductive system (QRS interval, Fig 1H) and ventricular repolarisation (QT interval, Fig 1I) along with facilitation of mitochondrial respiration.

Pharmacological profile for cardiac NMDARs was assessed using [^{3}H]-MK-801 displacement approach. Biphasic dose-response curves obtained for PCPBs interaction with sarcolemmal membranes (Fig 3A,B) were similar to those reported for the neuronal NMDARs earlier on (see references to the supplementary Table 1). GluN2B-specific PAAs eliprodil and Ro25-6981 were equally efficient in displacement of [^{3}H]-MK-801 (Fig 4B,C, Fig3C) and producing bradycardia as were PCPBs (Fig1F, Fig S2, S3A). The absolute IC_{50} values obtained for neuronal and cardiac NMDARs using [^{3}H]-MK-801 displacement in membranes are not always within the same range (Table 1). Affinity of the cardiac NMDARs to memantine is three orders of magnitude higher than that of neuronal receptors (Table 1). This suggests that cardiac NMDARs, not the neuronal receptors

are the primary target of memantine in rats. Whether this hold true for patients with Alzheimer's disease remains to be explored. Furthermore, rat cardiac NMDARs respond to ketamine which is commonly used in veterinary practice.

Differences in receptor-antagonists interactions reflect variance in subunit composition of the cardiac and neuronal NMDARs. Whereas adult rat neuronal NMDARs are composed of GluN1, 2A and 2C, cardiac NMDARs are built of GluN3A, GluN2D, GluN2B is less abundant, and GluN1, 2A, and 2C are present at low levels in certain areas of the heart only (Table 3). These molecular settings explain the dual (pro-agonistic at low doses and antagonistic at high concentrations) action of Zn^{2+} on the cardiac NMDARs (Fig 3D). Earlier the stimulatory effect of Zn^{2+} on the receptors composed of GluN3A-GluN1 and its inhibition by interaction with the GluN2B subunits was reported [15, 32].

Anti-arrhythmic properties of the PCPBs were associated with a prolongation of QTc intervals (Fig 1D,F). This is not the case for the PAAs targeting the GluN2B subunit (Fig 1C,D,G). Expression of this subunit appeared to be amplified with aging, suggesting that antiarrhythmic effects of PAAs will be more pronounced in senescent rat hearts (Fig 4E). Reduction in abundance of this subunit in adult and senescent brain (Fig 4E, and[33, 34]) makes eliprodil action in adult rats largely restricted to the cardiac NMDARs. In contrast to the CCBs, NMDAR antagonists are anti-arrhythmic whereas verapamil and ditiazem were pro-arrhythmic, producing a HRV pattern resembling 2nd degree AV block or sinus exit block (Figs S3E and S4H,I).

One more striking observation is a potent cardioprotective effect of NMDAR antagonists related to the improvement of capillary perfusion (Fig 2E). Hyperactivation of the NMDARs due to the hypoxia-induced glutamate release contribute to brain oedema, which is in part caused by the suppression of Na,K-ATPase [35, 36]. Administration of antagonists (both PCPBs and PAAs) has been

shown to reduce brain oedema associated with deoxygenation[37, 38]. Detailed mechanisms involved in NMDAR-driven control of cardiomyocyte volume regulation await further investigation.

Taken together, these findings indicate that the NMDAR agonists and antagonists are potent modulators of autonomous rat heart function. The observed responses are clearly distinct from those produced by the CCBs and are mediated by a set of cardiac NMDARs. The obtained results turn cardiac NMDARs into potentially interesting targets for prevention and treatment of malignant arrhythmias and heart failure.

Funding

This study was supported by the SNF grants 1112 449 and 310030_124970/1 to AB

Acknowledgements

We thank Dr. Katharyn Mitchell for careful proofreading of the manuscript and Alexander Kosenkov for his help with analysis of autoradiogaphic images.

Conflict of interests: none declared

References

1. Paoletti P, Bellone C, Zhou Q. NMDA receptor subunit diversity: impact on receptor properties, synaptic plasticity and disease. *Nat Rev Neurosci* 2013;**14**:383-400.
2. Van Donden AM, ed. Biology of the NMDA Receptor. Boca Raton (FL): CRC Press, 2009.
3. Santangelo RM, Acker TM, Zimmerman SS, Katzman BM, Strong KL, Traynelis SF*, et al.* Novel NMDA receptor modulators: an update. *Expert Opin Ther Pat* 2012;**22**:1337-1352.
4. Herrling PL, ed. Excitatory Amino Acids - Clinical Results with Antagonists. San Diego London Boston Academic Press, 1997.
5. Baczko I, Lepran I, Papp JG. Influence of anesthetics on the incidence of reperfusion-induced arrhythmias and sudden death in rats. *J Cardiovasc Pharmacol* 1997;**29**:196-201.
6. Hageman GR, Simor T. Attenuation of the cardiac effects of cocaine by dizocilpine. *Am J Physiol* 1993;**264**:H1890-1895.
7. D'Amico M, Di Filippo C, Rossi F. Arrhythmias induced by myocardial ischaemia-reperfusion are sensitive to ionotropic excitatory amino acid receptor antagonists. *Eur J Pharmacol* 1999;**366**:167-174.

8. Catelli M, Monassier L, Feldman J, Tibirica E. Cardiovascular effects of chronic ifenprodil in a model of central sympathetic stimulation. *Fundam Clin Pharmacol* 2000;**14**:587-592.
9. Monassier L, Riehl V, Lienhard JP, Tibirica E, Feldman J, Bousquet P. Effects of ifenprodil and baclofen on exercise-induced increase of myocardial oxygen demand in normotensive rats. *J Pharmacol Exp Ther* 1999;**290**:1188-1194.
10. Canesin RO, Bonagamba LG, Machado BH. Bradycardic and hypotensive responses to microinjection of L-glutamate into the lateral aspect of the commissural NTS are blocked by an NMDA receptor antagonist. *Brain Res* 2000;**852**:68-75.
11. Tian B, Hartle DK. Cardiovascular effects of NMDA and MK-801 infusion at area postrema and mNTS in rat. *Pharmacol Biochem Behav* 1994;**49**:489-495.
12. Corbett EK, Saha S, Deuchars J, McWilliam PN, Batten TF. Ionotropic glutamate receptor subunit immunoreactivity of vagal preganglionic neurones projecting to the rat heart. *Auton Neurosci* 2003;**105**:105-117.
13. Huang CF, Su MJ. Positive inotropic action of NMDA receptor antagonist (+)-MK801 in rat heart. *Journal of biomedical science* 1999;**6**:387-398.
14. Sekino N, Endou M, Hajiri E, Okumura F. Nonstereospecific actions of ketamine isomers on the force of contraction, spontaneous beating rate, and Ca2+ current in the guinea pig heart. *Anesth Analg* 1996;**83**:75-80.
15. Stowe DF, Bosnjak ZJ, Kampine JP. Comparison of etomidate, ketamine, midazolam, propofol, and thiopental on function and metabolism of isolated hearts. *Anesth Analg* 1992;**74**:547-558.
16. Aya AG, Robert E, Bruelle P, Lefrant JY, Juan JM, Peray P*, et al.* Effects of ketamine on ventricular conduction, refractoriness, and wavelength: potential antiarrhythmic effects: a high-resolution epicardial mapping in rabbit hearts. *Anesthesiology* 1997;**87**:1417-1427.
17. Seeber S, Humeny A, Herkert M, Rau T, Eschenhagen T, Becker CM. Formation of molecular complexes by N-methyl-D-aspartate receptor subunit NR2B and ryanodine receptor 2 in neonatal rat myocard. *J Biol Chem* 2004;**279**:21062-21068.
18. Gill S, Goldstein T, Situ D, Zabka TS, Gulland FM, Mueller RW. Cloning and characterization of glutamate receptors in Californian sea lions (Zalophus californianus). *Mar Drugs* 2010;**8**:1637-1649.
19. Gill S, Veinot J, Kavanagh M, Pulido O. Human heart glutamate receptors - implications for toxicology, food safety, and drug discovery. *Toxicol Pathol* 2007;**35**:411-417.
20. Koller M, Urwyler S. Novel N-methyl-D-aspartate receptor antagonists: a review of compounds patented since 2006. *Expert Opin Ther Pat* 2010;**20**:1683-1702.
21. Paoletti P, Neyton J. NMDA receptor subunits: function and pharmacology. *Curr Opin Pharmacol* 2007;**7**:39-47.
22. Vogel J, Waschke KF, Kuschinsky W. Flow-independent heterogeneity of brain capillary plasma perfusion after blood exchange with a Newtonian fluid. *Am J Physiol* 1997;**272**:H1833-1837.
23. Rio DC, Ares M, Jr., Hannon GJ, Nilsen TW. Guidelines for the use of RNA purification kits. *Cold Spring Harb Protoc* 2010;**2010**:pdb ip79.
24. Povlsen JA, Lofgren B, Rasmussen LE, Nielsen JM, Norregaard R, Kristiansen SB*, et al.* Cardioprotective effect of L-glutamate in obese type 2 diabetic Zucker fatty rats. *Clin Exp Pharmacol Physiol* 2009;**36**:892-898.
25. Bowery NG, Wong EH, Hudson AL. Quantitative autoradiography of [3H]-MK-801 binding sites in mammalian brain. *Br J Pharmacol* 1988;**93**:944-954.
26. Henriksson J. Effect of exercise on amino acid concentrations in skeletal muscle and plasma. *J Exp Biol* 1991;**160**:149-165.
27. Kiessling K, Roberts N, Gibson JS, Ellory JC. A comparison in normal individuals and sickle cell patients of reduced glutathione precursors and their transport between plasma and red cells. *Hematol J* 2000;**1**:243-249.

28. Castellanos M, Sobrino T, Pedraza S, Moldes O, Pumar JM, Silva Y*, et al.* High plasma glutamate concentrations are associated with infarct growth in acute ischemic stroke. *Neurology* 2008;**71**:1862-1868.
29. Kuribayashi N, Matsuzaki H, Hata H, Yoshida M, Sonoki T, Nagasaki A*, et al.* Multiple myeloma associated with serum amino acid disturbance and high output cardiac failure. *Am J Hematol* 1998;**57**:77-81.
30. Jasek MC, Griffith WH. Pharmacological characterization of ionotropic excitatory amino acid receptors in young and aged rat basal forebrain. *Neuroscience* 1998;**82**:1179-1194.
31. Nielsen TT, Stottrup NB, Lofgren B, Botker HE. Metabolic fingerprint of ischaemic cardioprotection: importance of the malate-aspartate shuttle. *Cardiovasc Res* 2011;**91**:382-391.
32. Lofgren B, Povlsen JA, Rasmussen LE, Stottrup NB, Solskov L, Krarup PM*, et al.* Amino acid transamination is crucial for ischaemic cardioprotection in normal and preconditioned isolated rat hearts--focus on L-glutamate. *Exp Physiol* 2010;**95**:140-152.
33. Nankai M, Klarica M, Fage D, Carter C. Evidence for native NMDA receptor subtype pharmacology as revealed by differential effects on the NMDA-evoked release of striatal neuromodulators: eliprodil, ifenprodil and other native NMDA receptor subtype selective compounds. *Neurochem Int* 1996;**29**:529-542.
34. Dos-Anjos S, Martinez-Villayandre B, Montori S, Perez-Garcia CC, Fernandez-Lopez A. Early modifications in N-methyl-D-aspartate receptor subunit mRNA levels in an oxygen and glucose deprivation model using rat hippocampal brain slices. *Neuroscience* 2009;**164**:1119-1126.
35. Nilsson GE, Lutz PL. Anoxia tolerant brains. *J Cereb Blood Flow Metab* 2004;**24**:475-486.
36. Bulygina ER, Lyapina LY, Boldyrev AA. Activation of glutamate receptors inhibits Na/K-ATPase of cerebellum granule cells. *Biochemistry (Mosc)* 2002;**67**:1001-1005.
37. Xiao F, Pardue S, Arnold T, Carden D, Alexander JS, Monroe J*, et al.* Effect of ifenprodil, a polyamine site NMDA receptor antagonist, on brain edema formation following asphyxial cardiac arrest in rats. *Resuscitation* 2004;**61**:209-219.
38. Gorgulu A, Kins T, Cobanoglu S, Unal F, Izgi NI, Yanik B*, et al.* Reduction of edema and infarction by Memantine and MK-801 after focal cerebral ischaemia and reperfusion in rat. *Acta neurochirurgica* 2000;**142**:1287-1292.

Figure legends

Figure 1. The effects of agonists and antagonists on HR and ECG in autonomously beating rat heart. A: Waterfall diagrams of the changes in ECG in agonist-treated heart (300 µM of each). B: Responses to the PCPBs (MK-801 (50 µM), memantine (50 µM), ketamine (1 mM)). C: Responses to the PAAss (eliprodil, Ro25-6981,(60 µM)). D: Responses to $ZnCl_2$ (50 µM). E: Responses to the CCBs (Diltiazem (10 µM), Verapamil (5 µM)). Statistics on the HR (F), PR (G), QRS (H), and QTc (I) intervals for all the compounds used. Presented are box plots (medians, of 6-25 experiments and variance) of the values of the respective intervals overlaid with dots representing the values recorded

for individual hearts. Paired t-test was used for statistical analysis. "ns" stands for not significantly different, and *, ** and *** denote $p<0.05$, 0.01 and $p<0.001$, respectively.

Figure 2. Dose dependence and reversibility of action of the NMDAR agonists and antagonists on the autonomous heart function. A: HR and HRV (assessed as and RMSSD, for details see Supplementary materials) in KH-perfused rat heart as a function of (Glu+Gly) concentration. . EC50 values ± SD are shown (N=4). B: original recording of the acute HR changes caused by Glu+Gly and MK-801 in KH-perfused rat heart. C: Acute changes in RR interval caused by intracoronary administration of specific NMDAR antagonists NMDA and D-serine in RBC-perfused rat heart. D: Partially reversible pro-arrhythmogenic action of 500 µM of (Glu+Gly) in KH-perfused heart. Shown as insets are the changes in ECG shape averaged for the highlighted time intervals E: Evans blue staining for the perfused capillaries in frozen sections of ventricular tissue of rat heart perfused with autologous blood without (control) or with either 300 µM of HCA or 50 µM MK-801. Shown are representative images obtained in 4 animals per group.

Figure 3 Dose dependent displacement of [^{3}H]-MK-801 by other NMDAR antagonists in atrial and ventricular SMs. Dose-dependent displacement of [^{3}H]-MK-801 by PCPBs in artial (A) or ventricular (B) SMs. C: Displacement of [^{3}H]-MK-801 by MK-801 in the presence or absence of eliprodil in ventricular SM D: Dual effect of Zn^{2+} on the NMDAR activity in ventricular SMs. Inset shows [^{3}H]-MK-801 binding rate to the SMs in the presence of 2 nM or 50 µM $ZnCl_2$

Figure 4. Local heterogeneity and subunit composition of cardiac NMDAR. **A**: Receptor activity in blood-perfused young (1.5 months old) and old (1.5 years old) rat heart chambers visualized using [3H]-MK-801 localization (autoradiography). B**:** Quantification of autoradiographic images obtained in [3H]-MK-801 displacement studies. Data are means ±SD from 4-6 sections. 0 stands for control, NG for NMDA-glycine-treated sections, MK, Mem, Ket Ro25/Eli standing for MK-801,

memantine, ketamine, Ro25-6981 and eliprodil. One-way two-tailed ANOVA with Dunnett post-test were used for statistical analysis. C: Representative autoradiographic images from rat heart and brain sections obtained in antagonist displacement study. False scale is showing the colour coding of the signal strength. D: Results of immunoblotting for the GluN1, GluN2A, 2B and 2C in brain and heart homogenates are shown in panel. E. Changes in abundance of the NR2B subunit in rat heart with ageing from 0.5 months to 18 month

Table 1

NMDAR antagonists, IC50 for selected targets

	Ketamine	MK-801	Memantine	Eliprodil
ACh receptors	6-15 μM	21 μM	1 - 7 - 11 μM	-
Opiate receptors	27 μM	-	-	27 μM
5-HT receptors	3-30 μM	-	~1 μM	-
Ca^{2+} channels	33 μM	-	-	-
K^+/Na^+ channels	1-20μM	?	-	-
Neuronal NMDA receptors	10 - 40 ->100 μM	10-40 nM	1 μM	1-10 μM
[^{3}H]MK-801 displacement in neurons	1-2.5 μM	2-14 nM	0.4-0.7 μM	
[^{3}H]MK-801 displacement rat in atria	*na*	15.0±4.0 nM, N=15	36.8±9.2 nM, N=15	*na*
[^{3}H]MK-801 displacement rat in ventricles	1.2 ± 0.4 μM, N=6	1.8 ± 0.3 nM, N=7	1.3 ± 0.4 nM, N=5	6.2 ± 1.7*^{ǂ} nM, N=7

^{ǂ}– displacement by MK-801 in a presence of 50 μM eliprodyl. * - $p<0.05$ vs MK-801.

Details and references are presented in supplementary table 1.

Table 2. Time domain analysis of the heart rate variability for autonomously beating rat hearts exposed to the agonists and antagonists of the NMDARs or to the L-type Ca^{2+} channel blockers

	NN_{max}	NN_{min}	NN_{mean}	SDNN	RMSSD	SD1	SD2	N
Baseline: normal	297.4±16.1	209.7±17.8	266.8±13.0	5.5±0.9	4.58±0.79	2.37±0.44	2.94±0.39	25
Baseline: arrhythmia	696.1±95.1***	188.3±22.6	311.0±18.3*	33.2±4.2***	40.0±6.7***	22.9±5.0***	27.5±5.1***	15
Normal before agonists	300.9±29.7	179.8±32.7	265.6±20.7	5.4±1.4	4.98±1.2	2.1±0.5	3.0±0.6	7
Normal after agonists	386.4±53.2	189.8±37.2	272.8±21.2	20.8±6.8	20.21±7.95	25.7±12.6*	24.6±10.9***	7
Arrhythmia before agonists	633.0±122.0	150.3±20.3	347.3±20.6	35.1±6.1	41.8±12.4	7.53±0.9	13.6±1.4	5
Arrhythmia after agonists	802.0±297.5	234.78±40.42	336.89±15.43	40.44±9.28	51.27±13.66	17.3±1.83	29.27±2.53	5
Normal before antagonists	305.68±22.88	236.79±21.8	277.7±17.6	5.3±1.3	3.9±1.0	2.8±1.1	3.3±0.9	13
Normal after antagonists	370.1±29.86**	329.6±22.2***	346.6±25.1***	4.2±1.2	3.02±0.94	4.24±1.86	5.68±1.84	13
Arrhythmia before antagonists	773.54±138.6	219.09±32.39	296.1±26.6	33.2±6.3	40.77±9.26	33.05±6.49*	31.29±6.42*	9
Arrhythmia after antagonists	423.26±31.86*	246.76±29.74	349.4±32.13*	9.48±1.77**	10.42±2.38*	8.31±3.1**	10.2±2.2**	9
Normal before Zn^{2+}	398.68±37.06	347.15±42	379.57±36.41	6.51±0.91	4.68±1.69	2.81±1.06	5.41±1.02	10
Zn^{2+}	557.4±136.9	241.0±65.3*	343.4±35.9*	28.0±8.0	30.6±18.2	27.6±17.1	22.6±9.9	10
Zn^{2+} and MK 801	478.4±78.8	268.7±34.8	345.8±33.0	19.0±7.4	13.8±5.9	5.8±1.6	1.9±0.6	10
Normal before L-type blockers	349.7±52.6	210.2±9.6	259.3±23.7	4.9±0.9	5.9±1.5	2.2±0.8	3.1±0.4	6
Normal after L-type blockers	543.5±40.2	334.7±90.8	465.4±55.4*	38.4±16.9	51.7±27.0	35.9±16.7	41.8±15.7	6
Arrhythmia, before L-type blockers	1339.0±450.3	206.2±67.2	319.7±20.4	42.8±13.6	61.3±17.8	38.0±19.6	34.0±21.6	4
Arrhythmia, L-type blockers	835.3±338.1	261.1±65.9	410.9±43.1	58.3±36.8	72.01±42.1	36.8±34.5	53.8±50.0	4

Agonists (300 μM NMDA, homocysteic acid, glutamate) and antagonists (MK-801 or memantine (50 μM); ketamine (1 mM); Ro25-6981 r eliprodil (60 μM); 50 μM $ZnCl_2$, and L-type Ca^{2+} channel blockers (diltiazem (10 μM) or verapamil (5 μM)). Shown in the table are the maximal NN interval within 5 min period (NNmax), minimal NN intervals (NNmin), means of NN intervals (NNmean), standard deviation of NN intervals (SDNN), square root of the mean squared difference of adjacent NN (RMSSD; quantitative characteristics of the Poincaré plots (SD1 and SD2). All values are presented as means ±SE. *p<0.05, **p<0.01, ***p<0.005.

Table 3. Local pattern of NMDAR subunits' expression in rat heart (Δct, GAPDH expression used for normalisation)

Tissue/ cells	*GluN1*	*GluN2A*	*GluN2B*	*GluN2C*	*GRIN2D*	*GluN3A*	*GluN3B*
Brain	**6.18**	**6.42**	6.55	8.42	10.77	8.69	18.62
Septum	-	-	20.9±0.6	21.1±1.0	15.6±1.9	19.1±0.6	-
LV	-	-	20.2±1.9	-	15.2±2.6	17.7±2.6	-
RV	-	-	19.8±2.1	-	15.4±2.9	17.6±3.4	-
LA	20.2±1.4	20.6±0.6	21.1±1.2	20.3±1.8	14.9±1.1	18.2±1.0	-
RA	18.3±1.0	19.1±1.1	19.0±1.0	-	15.3±1.9	18.3±4.1	-
Valves	-	-	20.4±1.8	-	13.6±2.6	11.9±4.2	-
ARCs	-	-	21.5±0.6	-	18.5±0.5	22.0±0.03	-

Presented are values obtained for whole brain homogenate (Brain), various areas of the heart: septum, left and right ventricles (LV and RV), left and right atria (LA and RA), and valvular region (Valves), as well as in fresh-isolated adult ventricular rat cardiomyocytes (ARCs). Presented are means ± SD for 42 hearts and 3 brains. Cells were isolated from 3 different hearts. Hyphen indicates the levels below detection limits (60 cycles).

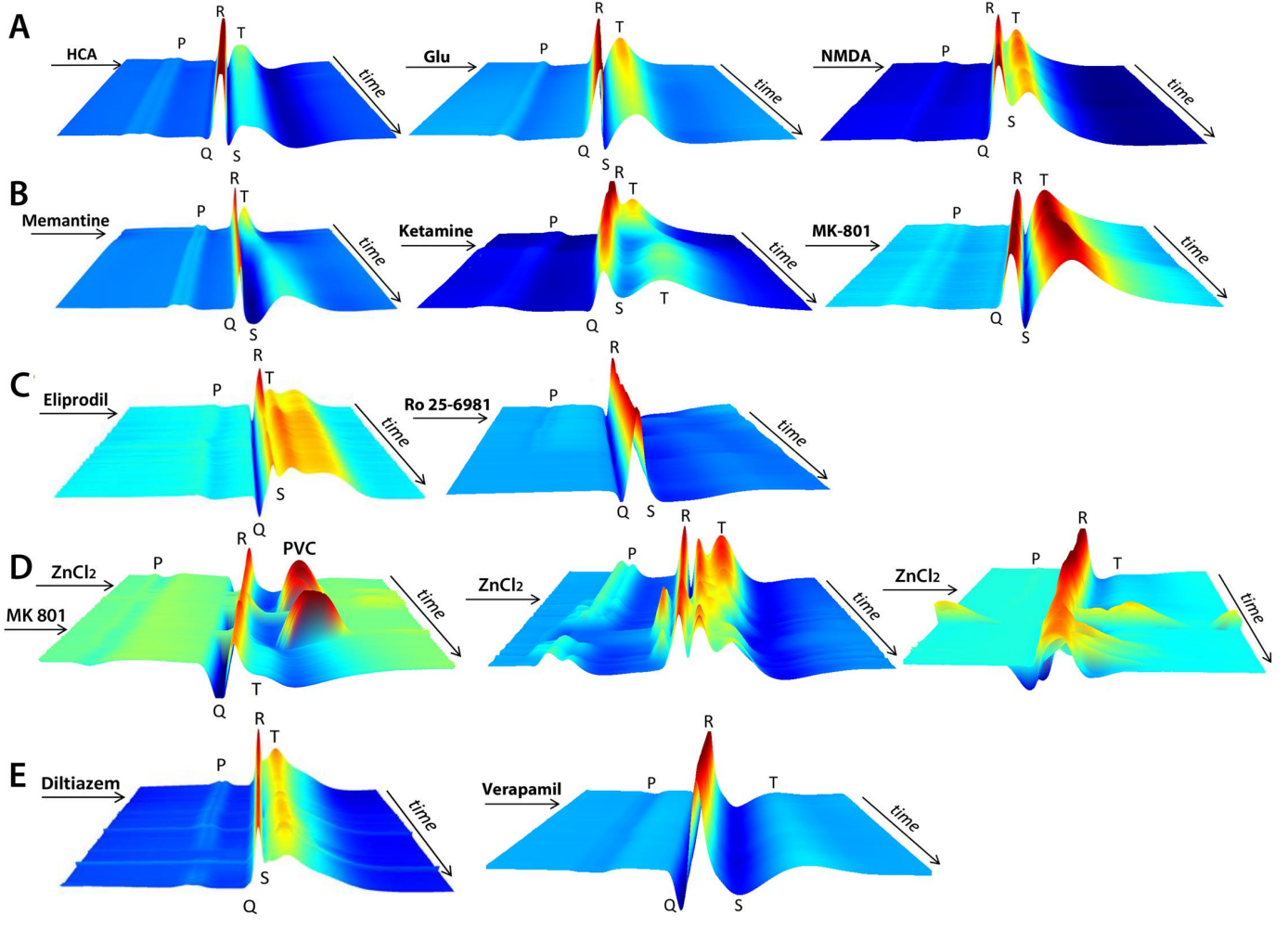
A
HCA
Glu
NMDA
B
Memantine
Ketamine
MK-801
C
Eliprodil
Ro 25-6981
D
ZnCl2
MK 801
PVC
E
Diltiazem
Verapamil
P
Q
R
S
T
time

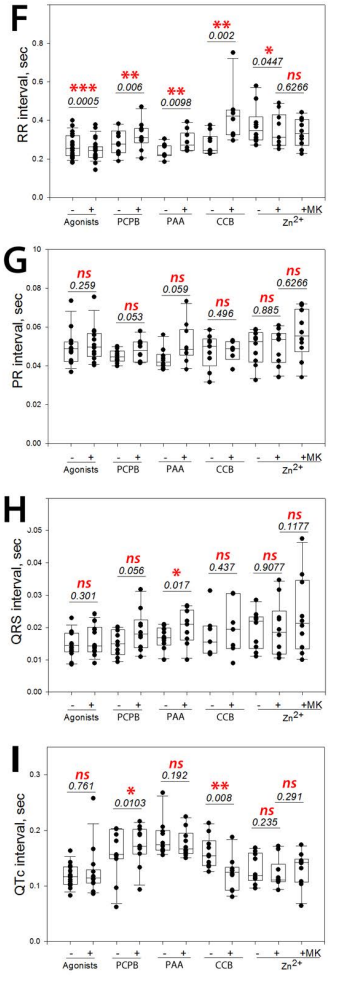
F
RR interval, sec
G
PR interval, sec
H
QRS interval, sec
I
QTc interval, sec
Agonists
PCPB
PAA
CCB
Zn2+
+MK

Figure 1.

Figure 2.

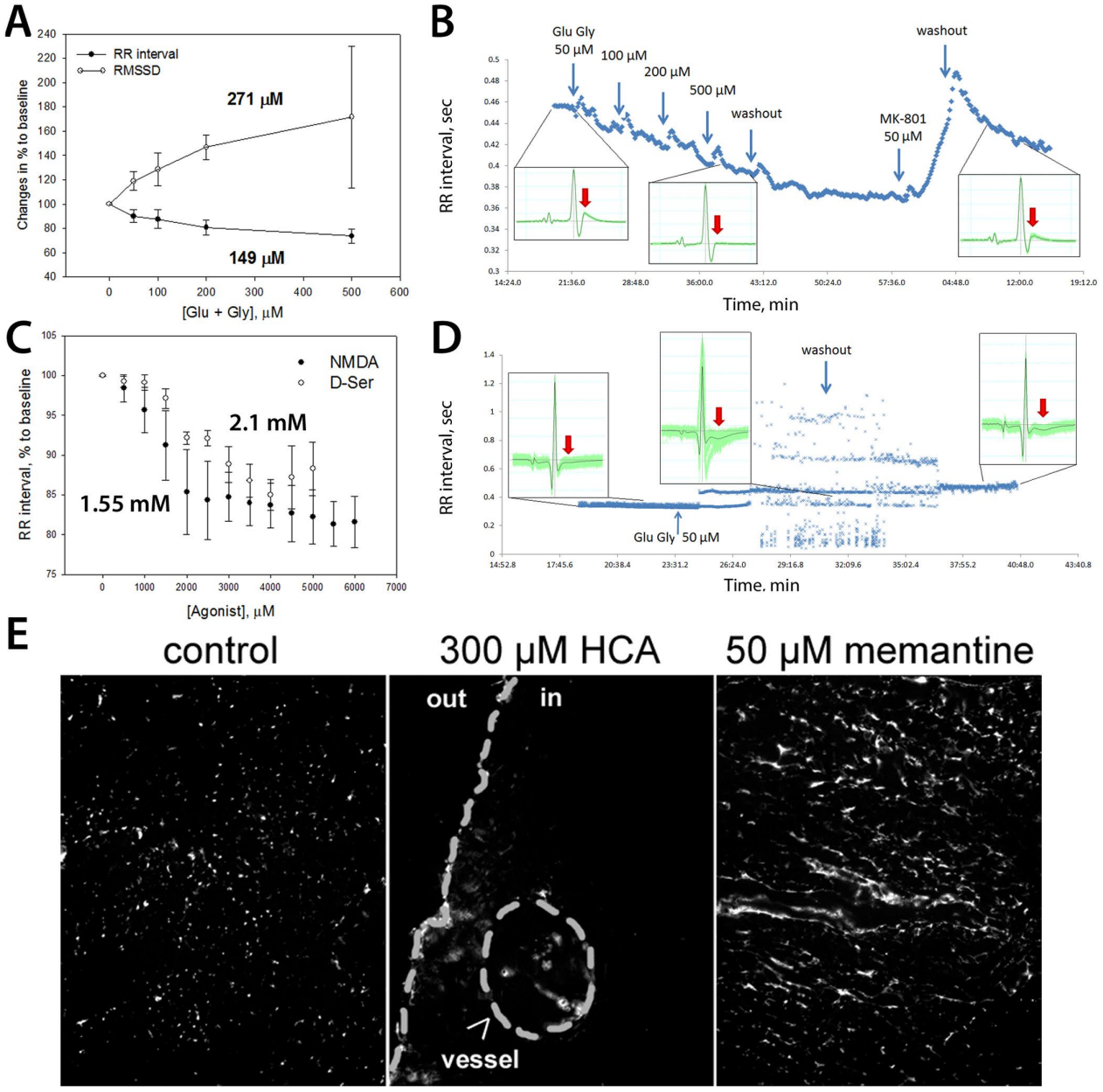
A
RR interval
RMSSD
271 μM
149 μM
Changes in % to baseline
[Glu + Gly], μM
B
Glu Gly
50 μM
100 μM
200 μM
500 μM
washout
MK-801
50 μM
washout
RR interval, sec
Time, min
C
NMDA
D-Ser
2.1 mM
1.55 mM
RR interval, % to baseline
[Agonist], μM
D
washout
Glu Gly 50 μM
RR interval, sec
Time, min
E
control
300 μM HCA
50 μM memantine
out
in
vessel

Figure 3.

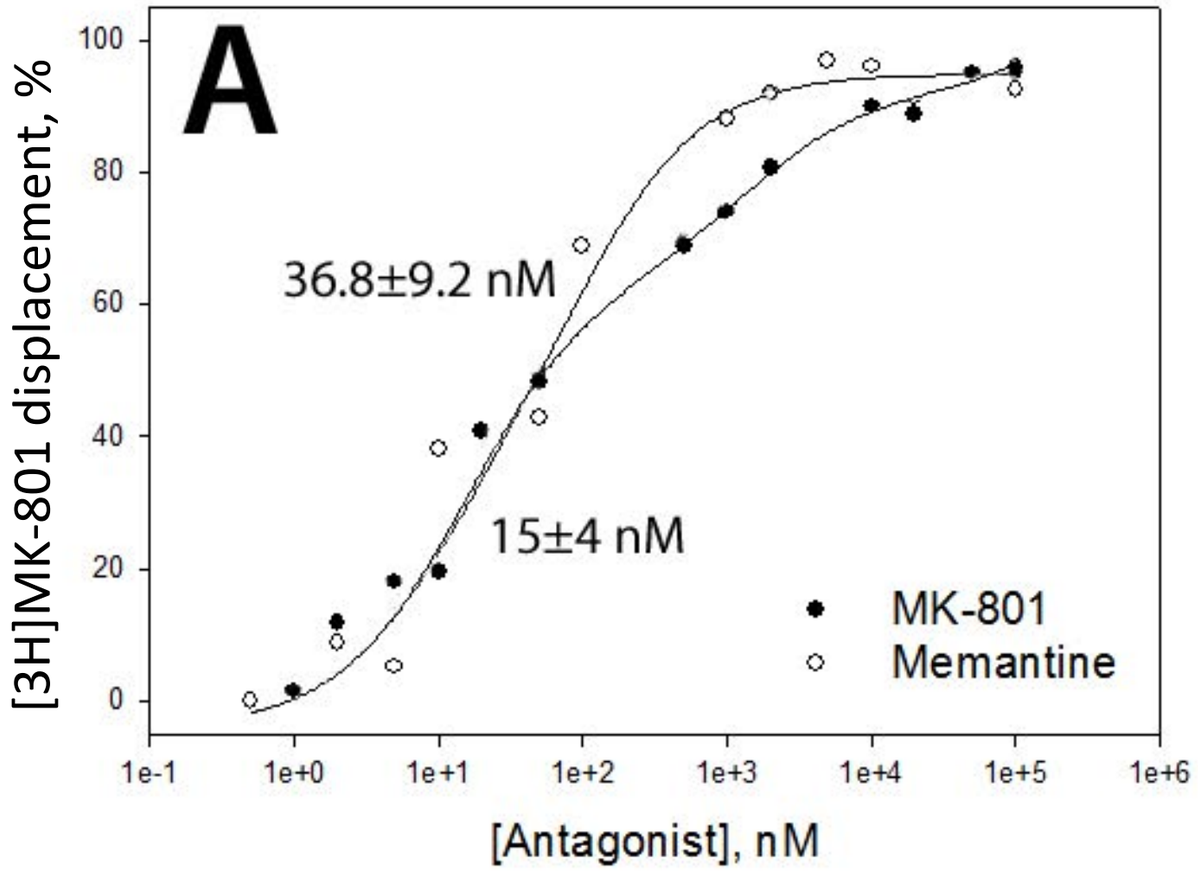
A
36.8±9.2 nM
15±4 nM
MK-801
Memantine
[3H]MK-801 displacement, %
[Antagonist], nM

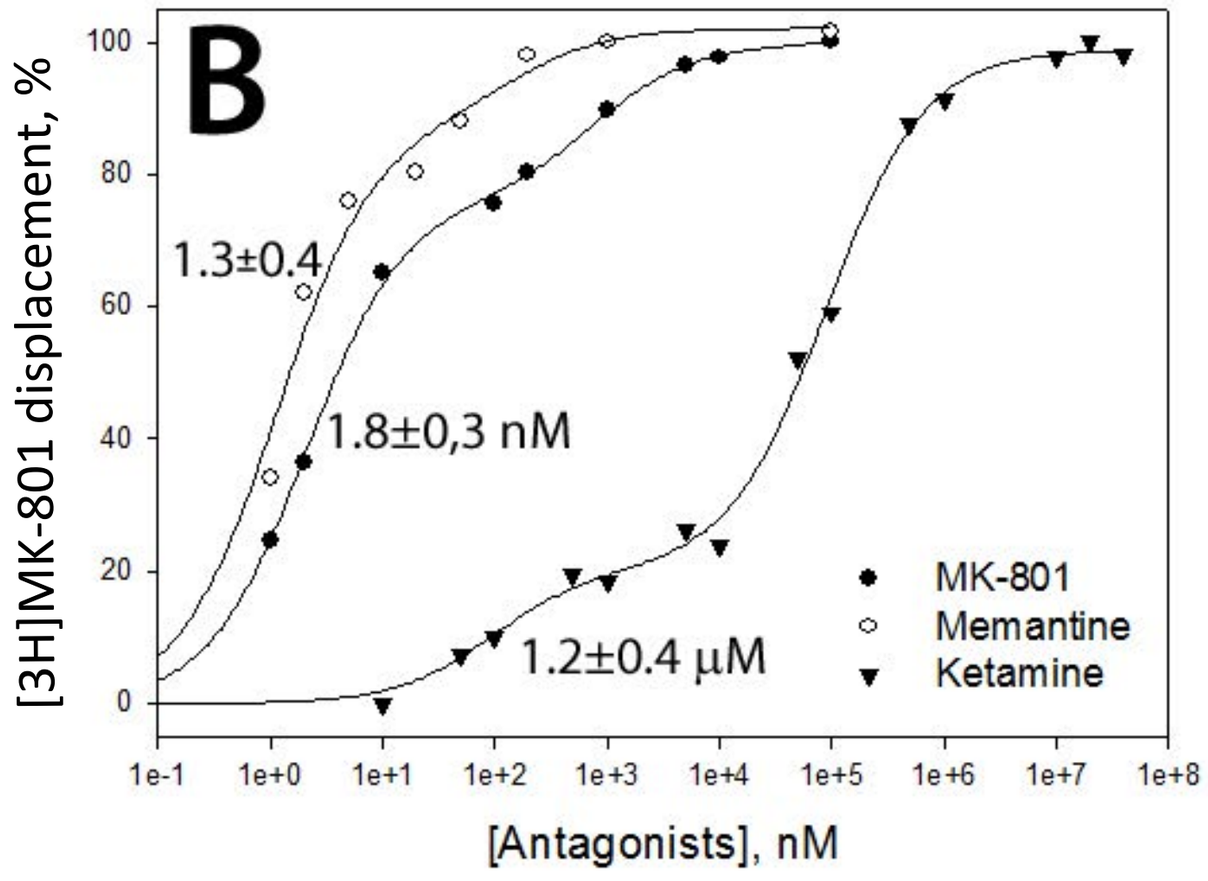
B
1.3±0.4
1.8±0,3 nM
1.2±0.4 µM
MK-801
Memantine
Ketamine
[3H]MK-801 displacement, %
[Antagonists], nM

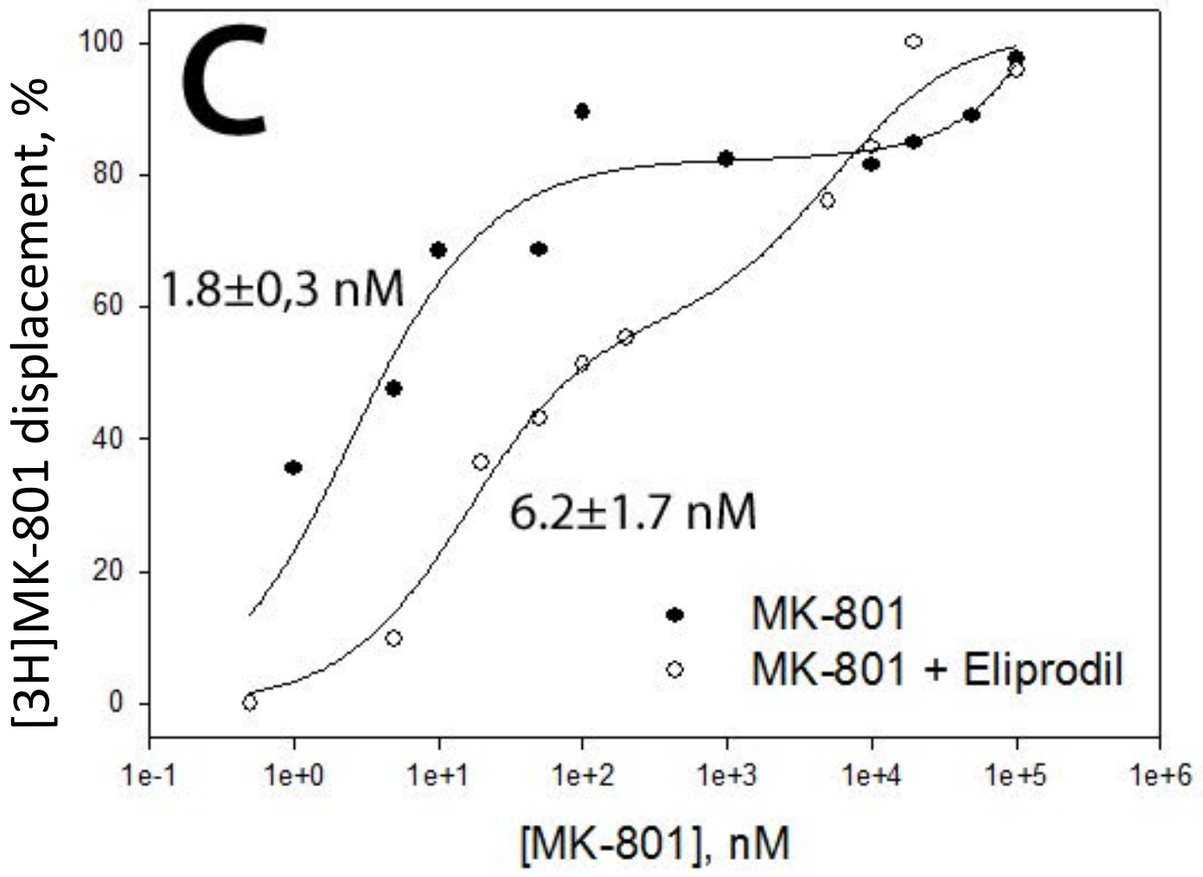
C
1.8±0,3 nM
6.2±1.7 nM
MK-801
MK-801 + Eliprodil
[3H]MK-801 displacement, %
[MK-801], nM

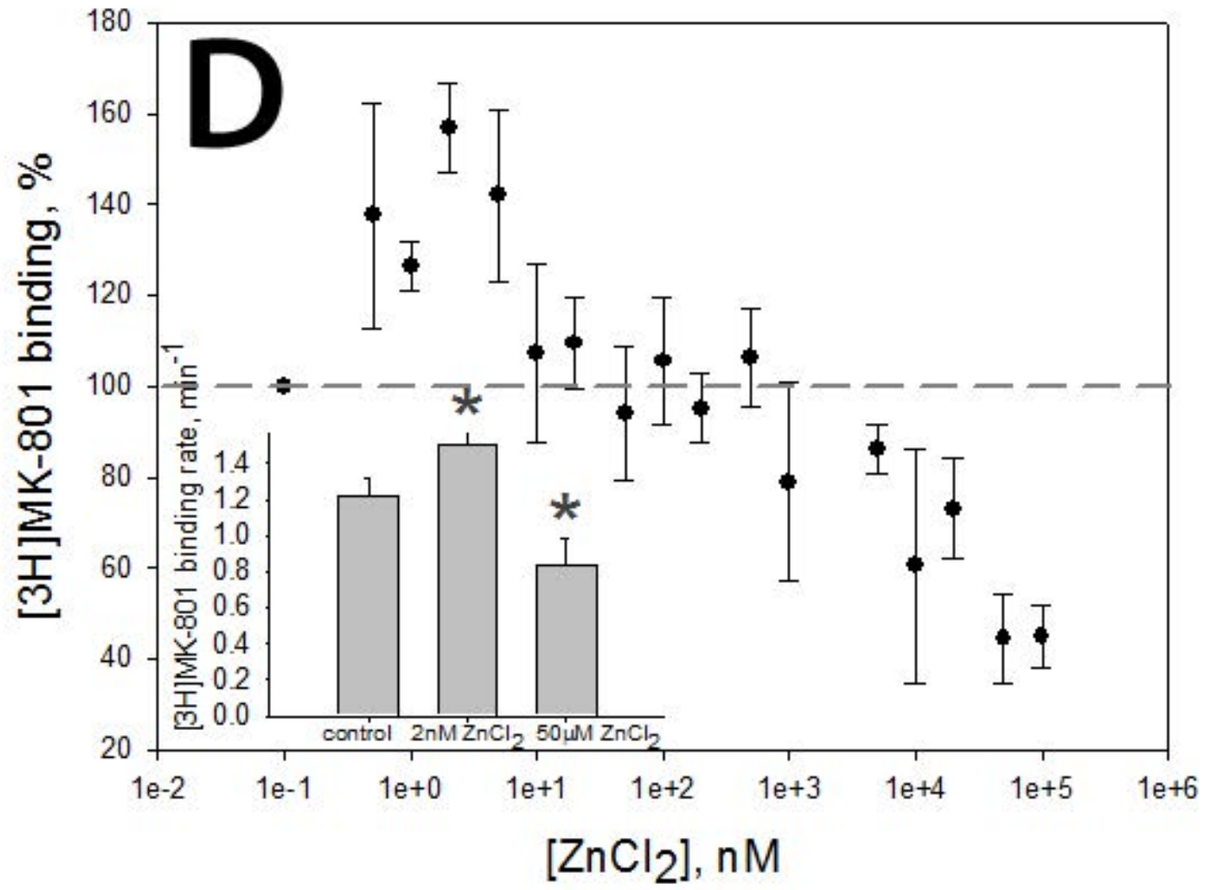
D
[3H]MK-801 binding, %
[3H]MK-801 binding rate, min-1
control
2nM ZnCl2
50µM ZnCl2
[ZnCl2], nM

Figure 4.

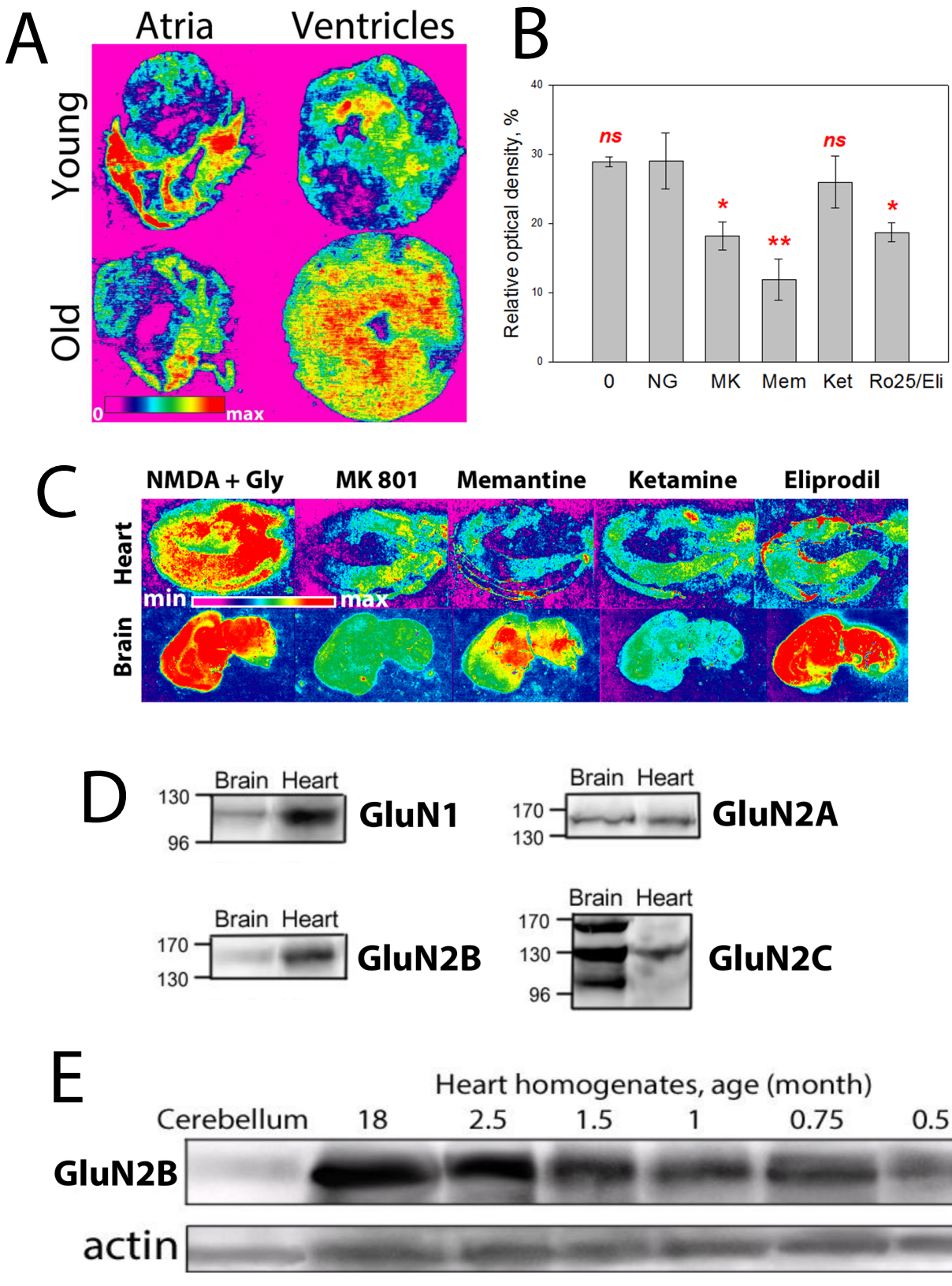
A
Atria
Ventricles
Young
Old
0
max
B
Relative optical density, %
40
30
20
10
0
ns
*
**
ns
*
0
NG
MK
Mem
Ket
Ro25/Eli
C
NMDA + Gly
MK 801
Memantine
Ketamine
Eliprodil
Heart
Brain
min
max
D
Brain Heart
130
96
GluN1
Brain Heart
170
130
GluN2A
Brain Heart
170
130
GluN2B
Brain Heart
170
130
96
GluN2C
E
Heart homogenates, age (month)
Cerebellum
18
2.5
1.5
1
0.75
0.5
GluN2B
actin

Supplementary information

Detailed materials and methods

Animals

Wistar rats of both sex, aged from 0.5 months to 2 years were used for the study. Animals were purchased from Janvier (Le Genest St Isle, France). All animal experiments were approved by the Veterinary Office of the canton Zurich and performed in accordance with Swiss animal protection laws and institutional guidelines that comply with guidelines of the American Physiological Society and the Institute of Laboratory Animal Resources.

Ex vivo blood-perfused rat-heart model

The model was described elsewhere in detail [1]. Animals were anesthetized using 3% isolfurane applied in O_2/N_2O mixture (800 ml/min), heparinized intravenously (Heparin-sodium, B.Braun, 5000 U/kg), and 8-10 ml blood were collected from the caudal vena cava. The hearts were collected immediately thereafter and chilled in the ice-cold perfusion buffer containing (mM): 120 NaCl, 25 $NaHCO_3$, 5 KCl, 10 glucose, 10 TRIS-HCl, 1 $CaCl_2$, 0.15 $MgCl_2$, pH 7.4. The blood perfusion circuit including a hollow fibre oxygenator was primed with perfusion buffer and then filled with blood which, upon mixing with the buffer, was diluted to a final hematocrit of 30-35%. The hearts were mounted on a cannula and perfused retrogradely via aorta through the coronaries with autologous diluted blood pre-warmed to 37°C. Hemoglobin oxygen saturation was maintained at 87-90% [1, 2].

To reduce amount of plasma-borne NMDAR agonists, washed human red blood cells (RBCs) were used in a separate set of experiments in which dose-response of the changes in heart rate (HR), heart rate variability (HRV), and ECG. Human blood was collected from the vein healthy donors in heparinized syringes. Blood collection was performed at the University Hospital Zurich on written consent and was approved by the cantonal ethic committee and conforms with the principles outlined in the Declaration of Helsinki. RBCs were washed 6 times by centrifugation (4000*x*g 5 min) and resuspension in the buffer containing (in mM): 120 NaCl, 5 KCl, 25 $NaHCO_3$, 2 $CaCl_2$, 0.15 $MgCl_2$, 10 TRIS-HCl, 10 glucose, 2 pyruvate, 0.1 arginine, 0.1 taurine, pH 7.4. Finally RBC were resuspended to 25% hematocirt in the same buffer, reoxygenation was assessed by humidified 95% O_2 and 5% CO_2 at 37 ^{0}C. Human RBC were chosen due to their relative stability and higher resistance to trauma mediated by passing through the peristaltic pump. Thus we could minimise gradual accumulation of glutamate and glycine leaking from RBCs in the course of lysis. Heart responses to the increasing concentrations of agonists (D-serine, and NMDA) and antagonist MK-801 were measured as a function of increasing agonists' and antagonists' concentrations. Dose dependence of heart responses to the NMDA, D-Ser and MK-801 was explored as boluses of the stock solutions of these compounds were added to the RBC suspension used for coronary perfusion every 5 min until maximal response was reached. We also performed wash-out experiments exploring reversibility of the observed effects.

Stock solutions of the agonists (N-methyl D-aspartate (NMDA), glutamate, glycine, homocysteic acid, D-serine), and antagonists (PCPBs): memantine,

MK-801, ketamine; polyamine binding site-targeting antagonists (PAAs): eliprodil, Ro25-6981; and $ZnCl_2$) of the NMDARs were used for intracoronary perfusion. L-type calcium channel blockers (CCBs) diltiazem, and verapamil were always used at concentrations, 10 μM and 5 μM respectively. The concentrations of agonists and antagonists were chosen based on their affinities to the neuronal NMDARs reported elsewhere [3, 4]. Each of the antagonists used in the study was not absolutely specific, but NMDARs were the only receptors shared by all the compounds tested, whereas the other targets were not always overlapping (Table 1 and supplementary Table 1). All compounds were administered 20 min after the onset of blood perfusion and applied for 40 min if not stated otherwise.

Classical Langendorff isolated perfused blood model

This model was used to assess the affinity of the cardiac NMDARs by monitoring HR and HRV as a function of the circulating agonists' concentration within physiolgocical concentration range. Wistar rat hearts (N=10) were perfused with Krebs-Henseleit buffer (KH) containing (in mM) 118.5 NaCl, 4.7 KCl, 1.2 $MgSO_4$, 1.25 $CaCl_2$, 1.2 KH_2PO_4, 25 $NaHCO_3$, 0.1 L-arginine, 2 pyruvate, 0.1 taurine and 11 glucose equilibrated with gas phase containing 95% O_2 and 5% CO_2 and warmed to 37ºC and supplemented with glutamate/glycine mixture (0-500 μM each) with or without 50 μM MK-801. Heart rate, heart rate variability and ECG were monitored and analyzed as described below.

ECG recordings, HR, HRV

ECG electrodes were fixed vertically on either side of the hearts so that the resulting recordings corresponded to the aVL projection. Due to high inter-individual variability, all observed effects were compared with baseline values from the same heart.

Heart rate was calculated from the RR intervals extracted from the ECG or as a peak-to-peak interval. Analysis was performed using the MLS360/7 ECG Analysis Module of the LabChart 7 Pro Software (ADInstruments Ltd). The values averaged over the last 5 minutes of the 20 min restitution period were used as controls and compared with the readouts averaged for the same heart over the period between the 10^{th} and 15^{th} minute after the onset of treatment. This approach allowed to minimise the contribution of heart-to-heart variability into the observed effects of tested compounds on HR and HRV. HR as well as ECG recorded from the isolated rat hearts perfused with autologous rat blood (Fig S2H) or washed human red cell suspension (Fig 2E) were maintained stable over the first two hours of perfusion despite certain variability in absolute values between the individual hearts.

Characterisation of the HRV included identification of intervals between normal heart beats (N), calculation of maximum, minimum and mean NN intervals (NN_max, NN_min, NN_mean) and the standard deviation of NN intervals (SDNN). The latter reflected overall variation. The square root of the mean of the sum of squares of successive NN differences (RMSSD) reflected short-term variability. Based on these indices hearts were allocated to one of two groups: those with stable rhythm (mean basal SDNN ±2xSD: 5.5 ± 1.8 msec, see Table 2) and the hearts with spontaneous sinus arrhythmia

(SDNN>7.3 msec). Graphic representation of the HRV was generated in the form of Poincaré plots (Fig 4s). The standard deviation of the NN intervals variability perpendicular (SD1) or along (SD2) the line of identity (SD1) was calculated to characterise the short-term and the long-term variability respectively [5]. The ECG time intervals measured included RR interval, PR interval, QRS duration, and QT interval. The QT interval was corrected for differences in heart rate using Bazett formula ($QTc = QT/\sqrt{RR}$).

Evans Blue as a marker of capillary perfusion

Stock solution of Evans Blue (6% in PBS) was prepared and added to blood used for coronary perfusion to a final concentration of 0.006% 60 min after 5the onset of coronary perfusion in the presence or absence of either 50 μM memantine or 300 μM homocysteic acid. Blood with Evans blue was allowed to circulate for 5 min and then perfused was stopped and the hearts were snap-frozen in isopentane and stored at -80°C. Cryosections (7 μm) of the ventricular tissue were prepared and rapidly dehydrated as described elsewhere [6]. Efficacy of capillary perfusion was then assessed as the number of Evans Blue-positive capillaries using fluorescent microscopy (Axiovert 200 M, Carl Zeiss, excitation and emission wavelength of 546 and 590 nm respectively).

Adult rat cardiomyocytes and fibroblasts isolation

Adult rat hearts (N=4) were dissected and perfused via aorta with a solution containing (mM) NaCl 137, KCl 5, HEPES 20, $MgCl_2$ 1.2, glucose 15, and

NaH_2PO_4 1, with pH 7.4 at 37°C (solution A). After 2 minutes of perfusion, the perfusion solution was switched to a solution containing (mM): NaCl 130, KCl 4.8, $NaHCO_3$ 25, $MgCl_2$ 1.2, glucose 12.5, and NaH_2PO_4 1.2 (solution B) with the type 4 Collagenase (Worthington, ~100 U/ml) and 1 mg/ml BSA for 30 minutes. Solution B without collagenase, but with 100 µM $CaCl_2$ and 1 mg/ml BSA was then used to wash the hearts free from collagenase for several minutes. The hearts were then minced and gently agitated to separate the cells. Debris was removed by filtration through a 200 µm mesh filter. Fibroblasts were separated by allowing the cells to attached to the non-coated plastic petri dishes for 2 h. Non-adgerent cells were removed by washing with solution B and restitution of fibroblasts in DMEM with 10% foetal calve serum and penicillin-streptomycin. Cardiomyocytes were permitted to settle for 10 min and then washed in solution A and then in PBS, and RNA extracted from the cells using Trizol reagent.

mRNA isolation and qPCR analysis

Male Wistar rats aged 12-14 weeks were euthanized by exposure to pure CO_2 followed decapitation. Brains and hearts were quickly collected, chilled on ice and hearts dissected to six functionally different regions: left and right ventricles, septum, left and right atria and a region containing mitral, tricuspid, aortic and pulmonary valves. Brain tissue was obtained from the same animals. Tissue pieces were than rinsed in ice cold PBS and stored in liquid nitrogen. RNA isolation procedure was used as described elsewhere [7] with some modifications. Frozen tissue was grinded in liquid nitrogen, obtained powder was mixed with TRIzol and minced further. The obtained

lysates (approx. 1 ml) were incubated at RT for 5 min and then transferred into tube contained 0.2 ml of chloroform, mixed and incubated 5 further min at RT. After centrifugation (16000xg, 5min, 4 °C), the supernatant was transferred into a mixture of 0.2 mL isopropanol and 2.5 µl glycogen, mixed and incubated 10 min at RT. The pellet was separated after the 15 min centrifugation (16 000g, 4 °C) and washed twice with 1 mL of 80% EtOH (16000xg, 5min, 4 °C). Then pellet was air dried, dissolved in nuclease free water and stored at -20 °C. cDNA was synthetized from RNA samples by "High Capacity RNA-to-cDNA Master Mix" (Applied Biosystems). "TaqMan® Gene Expression Master Mix" and commercially available primers for rat GluN1, GluN2A-D and GluN3A-B. were purchased from Applied Biosystems (see supplementary Table 1 for details). Sixty cycles at 95°C for 15 s and 60°C for 1 min were performed using 7500 Fast Real-Time PCR System, Applied Biosystems driven by the Fast System SDS software Rat GAPDH was used as a reference. Triplicate readings were taken and the average was calculated. The results were normalised to a randomly selected value obtained for the control sample, which was accepted as equal to 1.

Protein detection by Western Blotting

Rats were anesthetized and euthanized as described above. Hearts were rinsed in ice-cold PBS, cut into pieces and rinsed again. Tissue was immediately homogenized on ice in sucrose buffer containing 0.6 M sucrose, 10 mM imidazole, 1/100 inhibitors cocktail III, pH 7.0 in a ratio of 1 g of tissue in 3.5 ml of buffer. Homogenate was centrifuged (10000*x*g, 5 min, 4 °C) and supernatant then was mixed with Laemli sample buffer. Proteins

were separated on a 7.5% acrylamide gel and transferred to nitrocellulose membrane. TBST (0.1% Tween) with 5% dry milk was used for membrane blocking. Staining was performed with the following primary antibodies: mouse monolconal anti-GluN1 antibody, and rabbit polyclonal anti-GluN2C antibodies (NB300-118 and NB300-107, Novus Biologicals), and rabbit polyclonal anti-GluN2A and mouse monoclonal anti-GluN2B antibodies (ab14596 and ab28373, Abcam). After triple washing of the membranes in TBST the membranes were incubated for 1 h at room temperature with suitable horseradish peroxidase-conjugated secondary antibodies (1:1000 dilution; anti-mouse, Jackson ImmunoResearch Laboratories, West Grove, PA). The enhanced chemiluminescent detection Western blotting system (Fujifilm LAS-3000 System, FUJIFILM Life Science) was used for detection of protein.

Isolation of the sarcolemmal membranes from atria and ventricles and their utilization for ^{3}H-MK-801 displacement experiments

Hearts were harvested from the male and female Wistar rats (250-350 g) and ventricles and atria used for the isolation of the sarcolemmal membranes as described elsewhere [8]. Briefly, frozen atrial and ventricular tissue was homogenized in liquid N_2 and than mixed with a buffer containing (mM): 600 sucrose, 10 imidazol-HCl buffer adjusted to the pH 7.0 in a ratio 3.5 ml/g tissue using standard glass homogenizers. The obtained homogenates were centrifuged at 12 000*x*g for 30 min at +4 ºC. The resulting pellets was discovered and supernatants were diluted with a KCl-MOPS buffer (140 mM KCl and 10 mM MOPS-KOH buffered to the pH of 7.4) to the ratio of 5 ml per

1 g of tissue. The suspension was centrifuged at 95 000*x*g for 60 min using Sorvall Discovery 90 ultracentrifuge and the obtained pellet enriched with sarcolemmal membranes re-suspended in KCl-MOPS buffer and layered over the 30% sucrose solution containing 0.3 M KCl , 50 mM $Na_4P_2O_7$ and 0.1M Tris-HCl (pH 8.3). The membranes were collected, diluted with 3 volumes of KCl-MOPS buffer and sedimented by centrifugation at 95 000*x*g for 30 min and suspended in KCl-MOPS buffer. All procedures were performed on ice and centrifugation performed at 4ºC. So obtained sarcolemmal membranes were re-suspended in assay buffer containing (in mM): 118 NaCl, 4.7 KCl, 1.2 $MgSO_4$, 5 $NaHCO_3$, 20 HEPES, 1.2 KH_2PO_4, 2.5 $CaCl_2$, 11 glucose, pH 7.4 and used immediately after the isolation. Membranes were pre-incubated with 3 nM [^{3}H]-MK-801 for 20 min and thereafter exposed to PCPBs (MK-801, ketamine, memantine), eliprodil, or Zn^{2+} at various concentrations for 60 min. Thereafter, membranes were sedimented on a nitrocellulose filter and washed 2 times with 5 mL of assay buffer and the filters with sedimented membranes were dissolved in 10 ml of Hionic-Fluor (Packard) scintillation fluid. The amount of [^{3}H]-MK-801 bound to the membranes was assessed using TRI-CARB liquid scintillation analyser (Packard, Canada).

[^{3}H]-MK-801 binding rate was determined with SM pre-incubated with 2nM or 50 μM of $ZnCl_2$ for 60 min. [^{3}H]-MK-801 was added in concentration range from 0.3 to 3 nM and incubated for 1 min before the sedimentation and washing as described above. The linearity of [^{3}H]-MK-801 binding kinetics over the time period from 10 sec to 20 min was proven in preliminary experiments.

Autoradiography

NMDA receptor autoradiography was performed as described elsewhere [9]. Hearts and brains were harvested, briefly washed in ice-cold PBS, frozen in liquid nitrogen and stored on -80^{o}C before use. After preparation, 20 µm cryosections of heart and brain were mounted on glass coverslips and dried at RT. The sections were then rinsed in sucrose buffer (190 mM sucrose, 50 mM Tris-HCl, pH 7.4) and allowed to air-dry. Thereafter sucrose buffer solution containing 300 µM NMDA and 300 µM glycine, 30 nM [^{3}H]-MK-801 (20.5 Ci/mmol) was applied on sections. Non-specific binding and [^{3}H]-MK-801 displacement was explored as the buffer was supplemented with 200 µM of either unlabeled MK-801, or memantine, or Ro-25-6981, or 4 mM ketamine, or 200 µM eliprodil, or 200 µM Ro25-6189. Following 20 min of incubation at RT (25 ^{o}C) the sections were washed twice with 250 ml sucrose buffer at RT, dried and placed on X-ray Kodak film for 4 weeks. Developed films were scanned and converted into digital images which were then analyzed using MCID Image analysis software (InterFocus Imaging Ltd, Cambridge, UK).

Radiolabeled antagonist binding assay was also used *ex vivo* as 30 nM [^{3}H]-MK-801 was administered intracoronary and allowed to circulate for 100 min. Accumulation of the [^{3}H]MK-801 in the heart and its extraction from blood was monitored. The hearts were washed free from blood using ice-cold isotonic sucrose buffer and immediately frozen in liquid nitrogen thereafter. Series of 10 µm cross-sections through the whole organ were prepared from aorta to apex and dried out at RT on glass slides. X-ray Kodak film was

exposed to those slides during 2 months, and then film was developed and digitized by the same way as described above. Kinetics of extraction of the radiolabeled antagonist from blood is exemplified in Fig S1.

Statistical analysis

Data are presented as means ±SEM if not stated otherwise. Data analysis and statistics were performed using GraphPad Instat Software. Normality test was performed followed by either one-way two-tailed ANOVA tests followed by the Bonferroni post-test, or either Mann-Whitney or Wilcoxon tests depending on the distribution type. The level of significance was accepted at $p<0.05$. Correlation analysis performed for analysis of left ventricular pressure and heart rate variability was performed using linear (Pearson) correlation test.

Supplementary figures

Figure S1 Kinetics by the ^{3}H-MK-801 uptake from blood during the artificial perfusion into the myocardial tissue

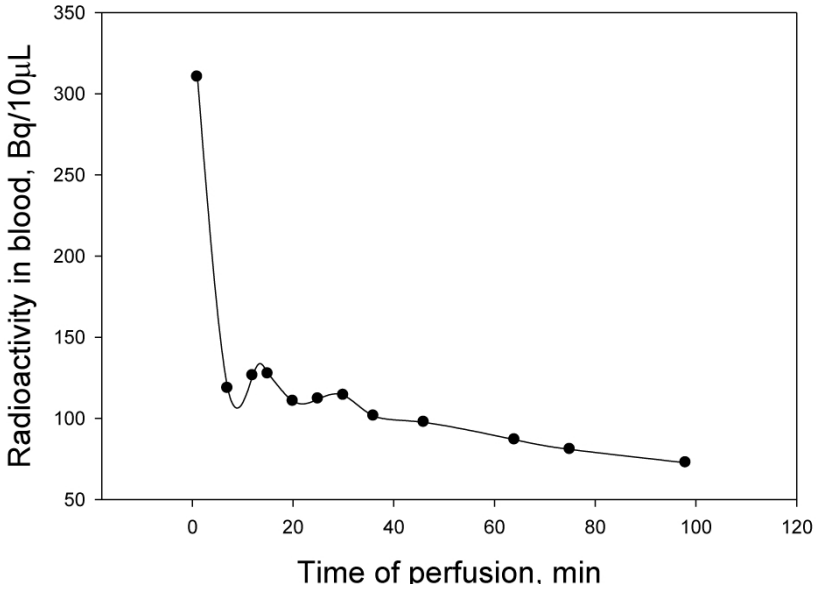

Figure S2. Isolated heart rate recording examples after the treatment with drugs of interest. **A**: positive chronotropic response to the treatment with NMDA receptor agonist NMDA (300 μM). **B:** Severe arrhythmia induced by the intracoronary supplementation of NMDA (300 μM). **C**: Intracoronary supplementation of the NMDAR channel blocker MK-801 (50 μM) induced bradycardia within 2-3 min after treatment. **D**: Polyamine site-specific NMDAR antagonist Ro25-6981 (60 μM) causing bradycardia which may be further accentuated by successive treatment with MK-801 (50 μM). **E**: Anti-arrhythmic action of MK-801 (50 μM) in the heart presented with spontaneous sinus arrhythmia (note the expanded BPM axis). **F**: Intracoronary administration of Zn^{2+} (50 μM) induces tachyarrhythmia and abolishes chronotropic effect of MK-801. **G**: Development of arrhythmia and bradycardia triggered by supplementation of the L-type channel blocker verapamil (5 μM). **H**: Untreated heart preparation with PQRST complex showed over the time.

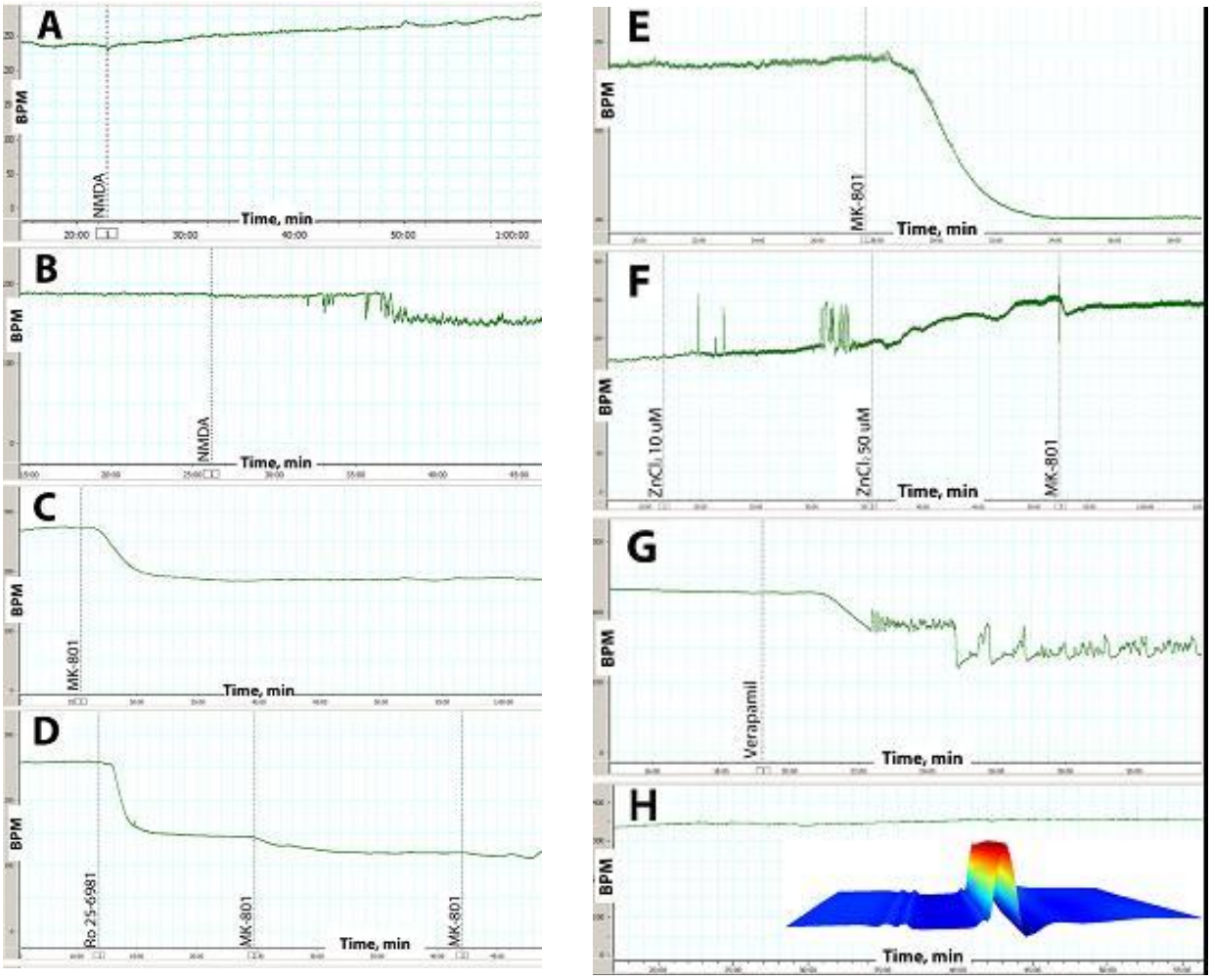

Figure S3. A: Original slips exemplifying the changes in ECG recorded in spontaneously beating blood-perfused heart in caused by the NMDAR agonist (NMDA, 300 μM, panel) application, antagonists eliprodil (60 μM) and memantine (50 μM), PVC induced by administration of 50 μM $ZnCl_2$ and L-type Ca^{2+} channel blocker verapamil (5 μM). Left sides of the panel represent ECG before the treatment and right sides show the ECG obtained from the same heart 15 min after the onset of treatment. Note the signs of sinus arrhythmia and wandering pacemaker in the heart treated with NMDA, intrinsic sinus arrhythmias in the hearts receiving eliprodil and the sinus arrest and escape rhythm pattern upon verapamil supplementation. **B**: Arrhythmia induced in buffer-perfused heat preparation subsequently treated with increased concentrations of Glu and Gly in 5 min interwals. MK-801 was applied after 5 min perfusion with 1 mM of Glu and Gly.

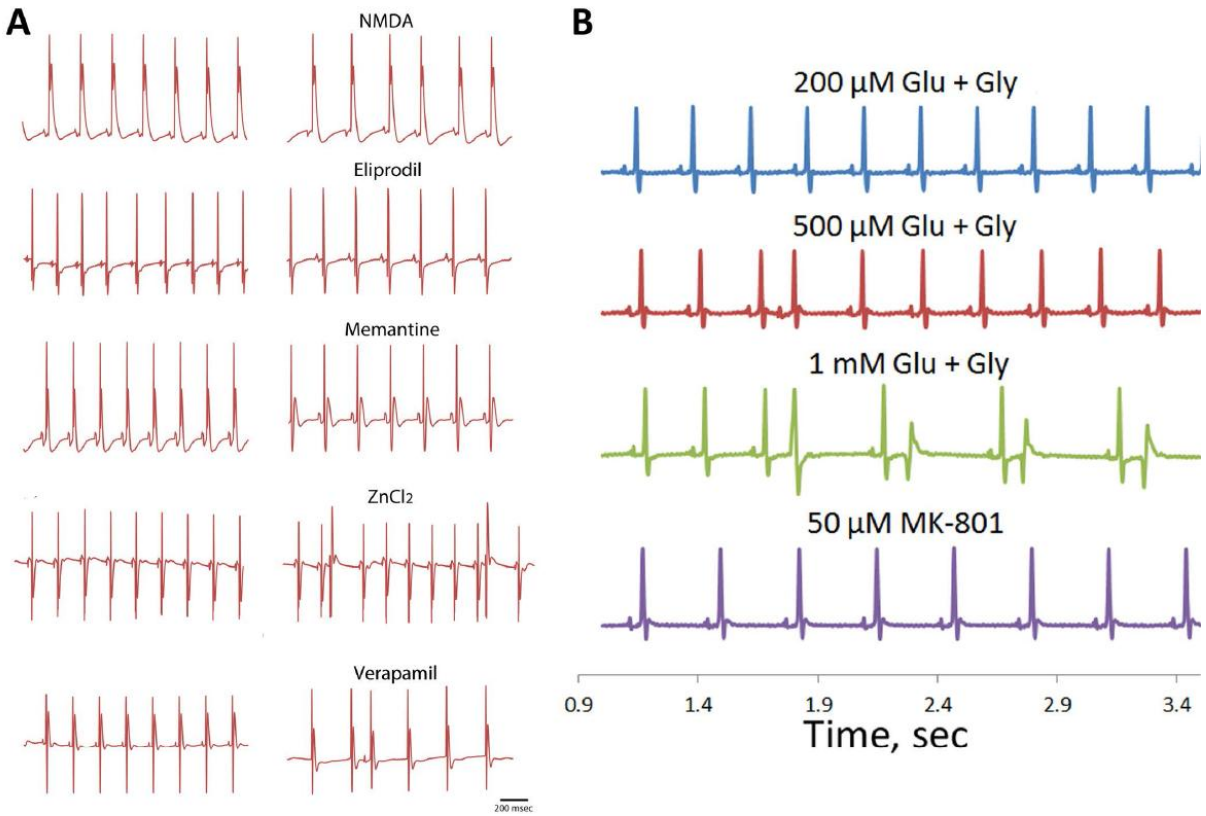

Figure S4. Representative Poincaré plots for the hearts treated with the NMDAR agonists, antagonists or L-type Ca^{2+} blockers. *X*-axis represents NN interval (RR interval between normal sinus beats at fixed time point), Y-axis shown the Next following NN interval. **A**, **B**, **C**: NMDAR agonists increased variety of distances between consecutive NN intervals and therefore increased variety of dot distribution over the Poincaré plot. **C**: Treatment with 300 μM of Glu on top of the plasma-born Glu induced arrhythmia and subsequent treatment with MK-801 reduced arrhythmia though led to increase of NN interval (bradycardia). **D**, **E**, **F**: Examples of how NMDAR channel blockers reduced pre-existing arrhythmia. **G**: Treatment with NMDAR 2B antagonist eliprodil showed the same decrease in arrhythmia. **H**, **I**: Diltiazem and verapamil provoked severe arrhythmia. Regular irregularity patterns can be seen for both drugs.

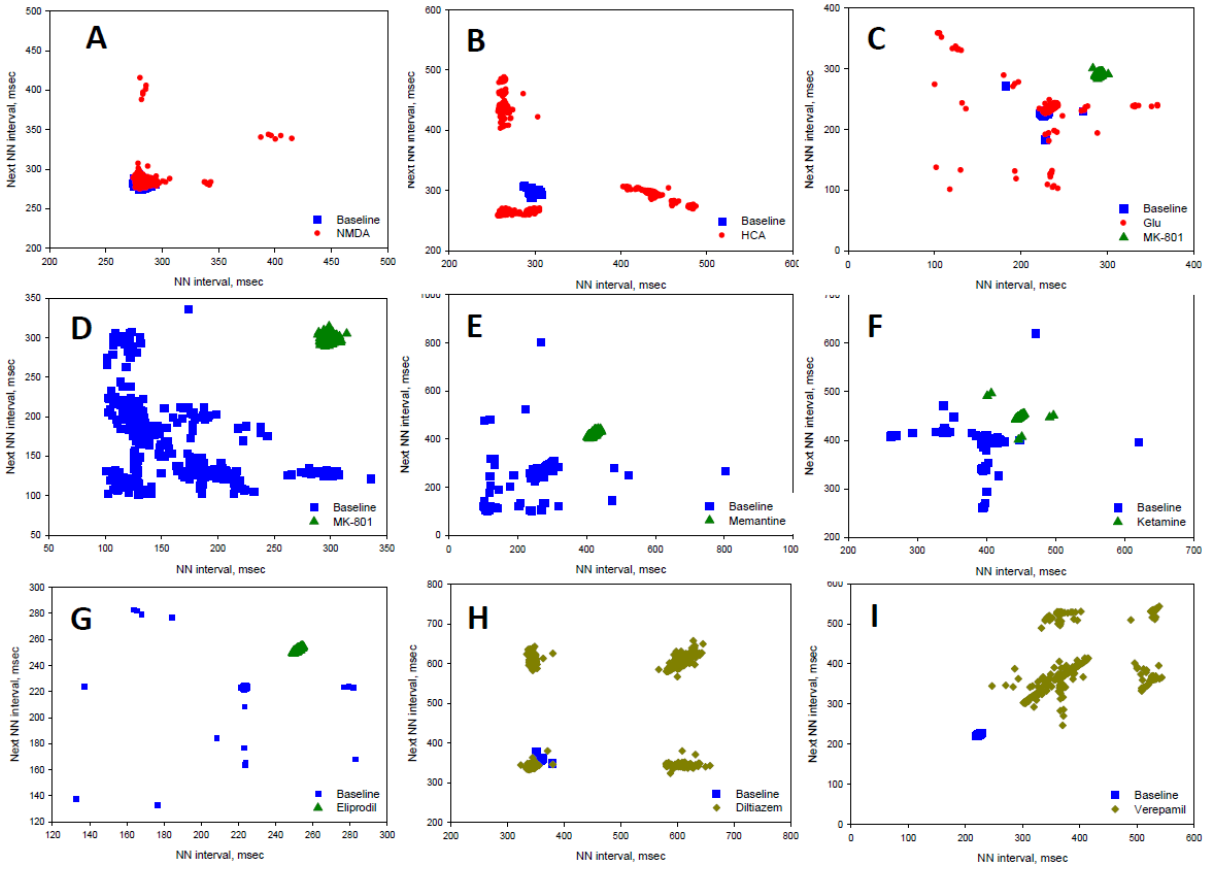

Figure S5. Analysis of ECG intervals in hearts exposed to various concentrations of MK-801 in the presence of saturating concentrations of NMDAR-specific agonists NMDA (3 mM) and D-Ser (6 mM). Changes in the **A:** RR intervals, **B:** PR, **C:** QRS and **D:** QT duration are shown as a function of MK-801 dose in RBC suspension. Panel **E** shows stability of these readouts in agonists and antagonist-free control over 120 min of perfusion. Presented are means of 4 independent experiments. * denotes $p<0.05$ and ** stands for $p<0.01$ compared to antagonist-free control.

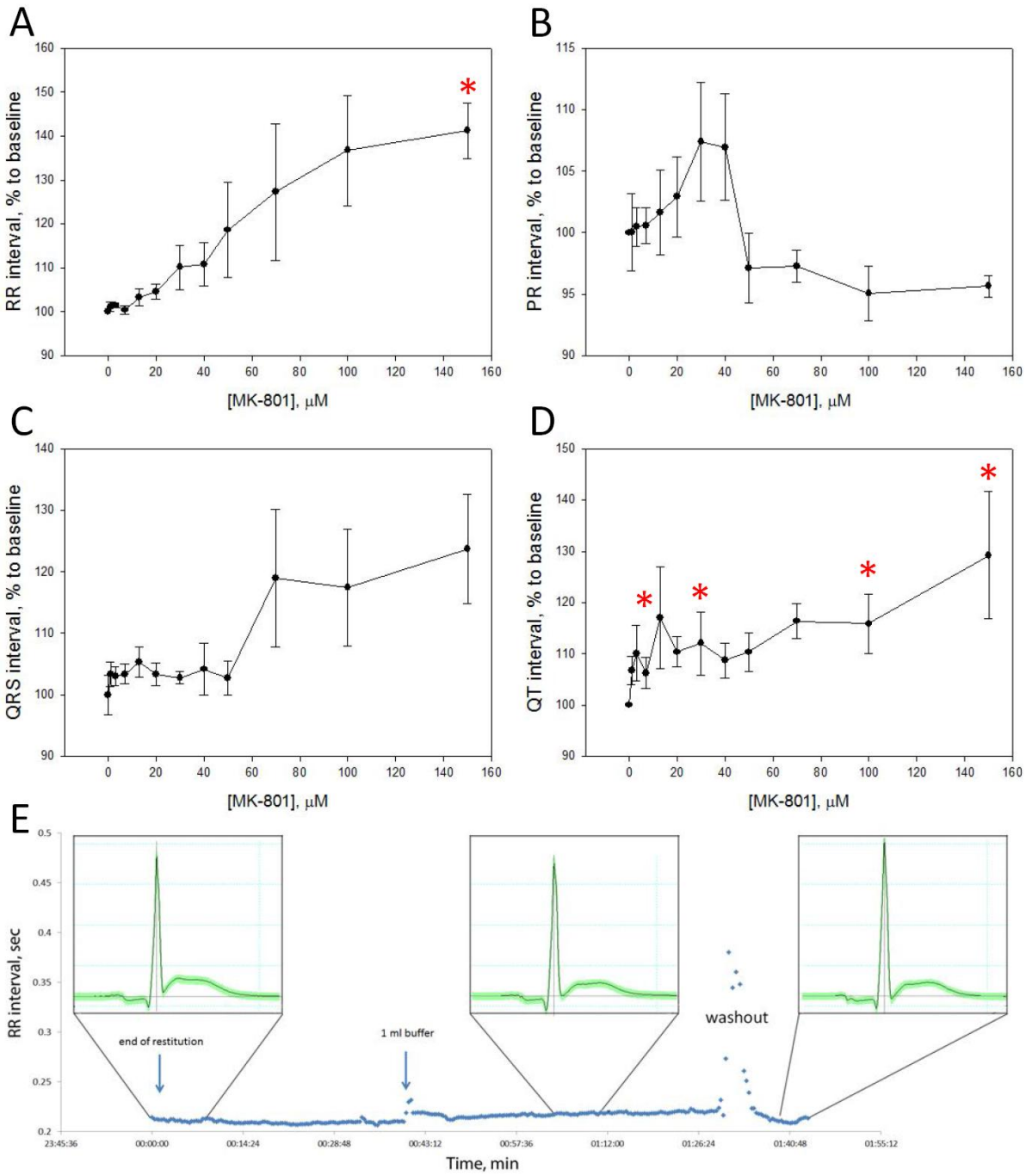

Supplementary table 1 Specificity of NMDAR antagonists

Drug	Target, IC50
Ketamine $C_{13}H_{16}ClNO$, M_r = 237.7 g/M Plasma concentration: ~1μM (274 ng/ml) Ki (vs ^{3}H-MK-801) 1-2.5 μM [10]	***ACh receptors*** nicotinic acetylcholine receptor 15 μM m1 muscarininc acetylcholine receptor 6.5 μM[11] ***NMDA receptors*** neuronal NMDA receptors, phencyclidine binding site 10-15 μM classical 40 μM[12] NR1-NR3: 100 μM - 7-9% of current blocked[13] ***GABA receptor*** – stimulation[14] ***Opioid receptors*** μ-opioid receptor[15] IC50 27 μM[15] ***Serotonin receptors*** 5-HT_3 receptor 3-30 μM[16] ***Ion channels*** Ca^{2+}-sensitive (BK) K^+ channels: 0.77 -1.66 μM[17] 20±5 μM (cell line) [18] voltage-activated K^+ channels[16] hyperpolarization-activated cyclic nucleotide-gated cation channel HCN1 channels, 4-8 μM[19] L-type Ca^{2+} channels 33 μM[16] Pentameric ligand-gated ion channels (pLGICs) in bacteria, 58 μM[20]
Memantine $C_{12}H_{21}N \cdot HCl$ M_r= 215.76 g/M	***ACh receptors*** α4β2 neuronal nicotinic receptors IC50 6.6-11.3 μM[22, 23]

Daily dose: 10-20 mg, Plasma concentrations in rat 1 µM [21] and in humans 1 µM [22]. Ki (vs ^{3}H-MK-801) 0.4-0.7 µM [10]	α7 nicotinic receptors 0.33-1.68 µM[22, 24] ***Dopamine D2 receptor*** Kd (vs ^{3}H-domperidone) ~ 1 µM[25] ***NMDA receptors*** Currents: 11.6±0.53µM[26]; Memantine in NMDARs expressed in oocytes: NR1/NR2A: 0.9 µM, NR1/NR2B 0.4µM; NR1/NR2C: 0.3 µM, NR1/NR2D: 0.3 µM (-70 mV, Mg-free) ; and 10.3, 10.9, 2.0, 1.9 µM (at -30 mV in the presence of 1 mM Mg^{2+})[27] Average IC50 ~ 1 µM at -60 mV[28] Does not inhibit NR1/NR3 receptors![29] IC50 in striatum and hippocampus 1-3 µM ***Serotonin receptors*** 5-HT3 receptors IC50 similar to those for NMDARs (around 1 µM)[30] ***GABA receptors*** **No effects**[27]
Eliprodil (SL-82.0715) $C_{20}H_{23}ClFNO$, Mr= 347.85 g/M Daily dose 2.5-10-20 mg [31] Plasma concentration in	***Opiate Sigma-Receptor*** IC50 29 nM[31, 34] ***NMDA receptors*** IC50 for Ca^{2+} uptake by rat cerebellar granule 2 µM[35] Two binding sites in spinal cord: IC50(high) 3.6 µM and IC50(low) 102 µM

humans 2.9 µM [32] Ki (vs ^{3}H-MK-801) high and low affinity sites ~7 and 100 µM [33]	single type in cortex and mid-brain 7-12 µM[36]. Eliprodil/^{3}H-ifenprodil replacement studies: IC50 0.13 µM[37] ***Ion channels*** R- and L-type Ca^{2+} channels are **<u>insensitive</u>** to eliprodil[38]
MK-801 (dizocilpine) $C_{16}H_{15}N$, Mr=221.297 g/M Daily dose - 47 nM - protective concentration in rat plasma[39] Ki (vs ^{3}H-MK-801) 2-14 nM Kd 5-26 nM[10]	***ACh receptors*** IC50 for Ca^{2+} fluxes in neurons 21 ± 2 µM IC50 for [^{3}H]-MK-801 binding 1.9 µM [40] ***Serotonin receptors*** **<u>No information</u>** available ***GABA receptors*** **<u>No effect</u>** on the GABA-R mediated currents[41] ***NMDA receptors*** IC50 13-38 nM NR1/NR3 heterotetramer : 10 µM - no effect Currents: 0.13 + 0.02 µM[26] Bi-phasic inhibition of Ca^{2+} uptake into cerebellar granule cells: IC50(1) 5 nM and IC50(2) 3 µM[35] ***Ion channels*** (+)-MK801 may be a strong I(Na) and I(to) also showing some blocking activity for I(Ca). The outward current through K(1) channels was unaffected and only slightly reduced the amplitude of L-type calcium channels [42]

References

1. Komniski MS, Yakushev S, Bogdanov N, Gassmann M, Bogdanova A. Interventricular heterogeneity in rat heart responses to hypoxia: the tuning of glucose metabolism, ion gradients, and function. *Am J Physiol Heart Circ Physiol* 2010;**300**:H1645-1652.
2. Yakushev S, Band M, Tissot van Patot M, Gassmann M, Avivi A, Bogdanova A. Cross-talk between S-nitrosylation and S-glutathionylation in control of the Na,K-ATPase regulation in hypoxic heart. *Am J Physiol Heart Circ Physiol* 2012.
3. Koller M, Urwyler S. Novel N-methyl-D-aspartate receptor antagonists: a review of compounds patented since 2006. *Expert Opin Ther Pat* 2010;**20**:1683-1702.
4. Paoletti P, Neyton J. NMDA receptor subunits: function and pharmacology. *Curr Opin Pharmacol* 2007;**7**:39-47.
5. Rajendra Acharya U, Paul Joseph K, Kannathal N, Lim CM, Suri JS. Heart rate variability: a review. *Med Biol Eng Comput* 2006;**44**:1031-1051.
6. Vogel J, Waschke KF, Kuschinsky W. Flow-independent heterogeneity of brain capillary plasma perfusion after blood exchange with a Newtonian fluid. *Am J Physiol* 1997;**272**:H1833-1837.
7. Rio DC, Ares M, Jr., Hannon GJ, Nilsen TW. Guidelines for the use of RNA purification kits. *Cold Spring Harb Protoc* 2010;**2010**:pdb ip79.
8. Povlsen JA, Lofgren B, Rasmussen LE, Nielsen JM, Norregaard R, Kristiansen SB*, et al.* Cardioprotective effect of L-glutamate in obese type 2 diabetic Zucker fatty rats. *Clin Exp Pharmacol Physiol* 2009;**36**:892-898.
9. Bowery NG, Wong EH, Hudson AL. Quantitative autoradiography of [3H]-MK-801 binding sites in mammalian brain. *Br J Pharmacol* 1988;**93**:944-954.
10. Hergovich N, Singer E, Agneter E, Eichler HG, Graselli U, Simhandl C*, et al.* Comparison of the effects of ketamine and memantine on prolactin and cortisol release in men. a randomized, double-blind, placebo-controlled trial. *Neuropsychopharmacology* 2001;**24**:590-593.
11. Hustveit O, Maurset A, Oye I. Interaction of the chiral forms of ketamine with opioid, phencyclidine, sigma and muscarinic receptors. *Pharmacol Toxicol* 1995;**77**:355-359.
12. Gonzales JM, Loeb AL, Reichard PS, Irvine S. Ketamine inhibits glutamate-, N-methyl-D-aspartate-, and quisqualate-stimulated cGMP production in cultured cerebral neurons. *Anesthesiology* 1995;**82**:205-213.
13. Smothers CT, Woodward JJ. Pharmacological characterization of glycine-activated currents in HEK 293 cells expressing N-methyl-D-aspartate NR1 and NR3 subunits. *J Pharmacol Exp Ther* 2007;**322**:739-748.
14. Irifune M, Sato T, Kamata Y, Nishikawa T, Dohi T, Kawahara M. Evidence for GABA(A) receptor agonistic properties of ketamine: convulsive and anesthetic behavioral models in mice. *Anesthesia and analgesia* 2000;**91**:230-236.
15. Smith DJ, Bouchal RL, deSanctis CA, Monroe PJ, Amedro JB, Perrotti JM*, et al.* Properties of the interaction between ketamine and opiate binding sites in vivo and in vitro. *Neuropharmacology* 1987;**26**:1253-1260.
16. Kress HG. [Mechanisms of action of ketamine]. *Anaesthesist* 1997;**46 Suppl 1**:S8-19.
17. Hayashi Y, Kawaji K, Sun L, Zhang X, Koyano K, Yokoyama T*, et al.* Microglial Ca(2+)-activated K(+) channels are possible molecular targets for the analgesic effects of S-ketamine on neuropathic pain. *J Neurosci* 2011;**31**:17370-17382.

18. Denson DD, Duchatelle P, Eaton DC. The effect of racemic ketamine on the large conductance Ca(+2)-activated potassium (BK) channels in GH3 cells. *Brain Res* 1994;**638**:61-68.
19. Zhou C, Douglas JE, Kumar NN, Shu S, Bayliss DA, Chen X. Forebrain HCN1 Channels Contribute to Hypnotic Actions of Ketamine. *Anesthesiology* 2013.
20. Pan J, Chen Q, Willenbring D, Mowrey D, Kong XP, Cohen A*, et al.* Structure of the pentameric ligand-gated ion channel GLIC bound with anesthetic ketamine. *Structure* 2012;**20**:1463-1469.
21. More L, Gravius A, Nagel J, Valastro B, Greco S, Danysz W. Therapeutically relevant plasma concentrations of memantine produce significant L-N-methyl-D-aspartate receptor occupation and do not impair learning in rats. *Behav Pharmacol* 2008;**19**:724-734.
22. Rammes G, Danysz W, Parsons CG. Pharmacodynamics of memantine: an update. *Curr Neuropharmacol* 2008;**6**:55-78.
23. Buisson B, Bertrand D. Open-channel blockers at the human alpha4beta2 neuronal nicotinic acetylcholine receptor. *Mol Pharmacol* 1998;**53**:555-563.
24. Aracava Y, Pereira EF, Maelicke A, Albuquerque EX. Memantine blocks alpha7* nicotinic acetylcholine receptors more potently than n-methyl-D-aspartate receptors in rat hippocampal neurons. *J Pharmacol Exp Ther* 2005;**312**:1195-1205.
25. Monassier L, Riehl V, Lienhard JP, Tibirica E, Feldman J, Bousquet P. Effects of ifenprodil and baclofen on exercise-induced increase of myocardial oxygen demand in normotensive rats. *J Pharmacol Exp Ther* 1999;**290**:1188-1194.
26. Frankiewicz T, Potier B, Bashir ZI, Collingridge GL, Parsons CG. Effects of memantine and MK-801 on NMDA-induced currents in cultured neurones and on synaptic transmission and LTP in area CA1 of rat hippocampal slices. *Br J Pharmacol* 1996;**117**:689-697.
27. Parsons CG, Gruner R, Rozental J, Millar J, Lodge D. Patch clamp studies on the kinetics and selectivity of N-methyl-D-aspartate receptor antagonism by memantine (1-amino-3,5-dimethyladamantan). *Neuropharmacology* 1993;**32**:1337-1350.
28. Chen HS, Lipton SA. The chemical biology of clinically tolerated NMDA receptor antagonists. *J Neurochem* 2006;**97**:1611-1626.
29. Chatterton JE, Awobuluyi M, Premkumar LS, Takahashi H, Talantova M, Shin Y*, et al.* Excitatory glycine receptors containing the NR3 family of NMDA receptor subunits. *Nature* 2002;**415**:793-798.
30. Rammes G, Rupprecht R, Ferrari U, Zieglgansberger W, Parsons CG. The N-methyl-D-aspartate receptor channel blockers memantine, MRZ 2/579 and other amino-alkyl-cyclohexanes antagonise 5-HT(3) receptor currents in cultured HEK-293 and N1E-115 cell systems in a non-competitive manner. *Neurosci Lett* 2001;**306**:81-84.
31. Modell S, Naber D, Holzbach R. Efficacy and safety of an opiate sigma-receptor antagonist (SL 82.0715) in schizophrenic patients with negative symptoms: an open dose-range study. *Pharmacopsychiatry* 1996;**29**:63-66.
32. Malavasi B, Ripamonti M, Rouchouse A, Ascalone V. Stereoselective determination of unchanged and glucuroconjugated eliprodil, a new anti-ischaemic drug, in human plasma and urine by precolumn derivatization and column-switching high-performance liquid chromatography with fluorescence detection. *J Chromatogr A* 1996;**729**:323-333.
33. Gogas KR. Glutamate-based therapeutic approaches: NR2B receptor antagonists. *Curr Opin Pharmacol* 2006;**6**:68-74.

34. Contreras PC, Bremer ME, Gray NM. Ifenprodil and SL 82.0715 potently inhibit binding of [3H](+)-3-PPP to sigma binding sites in rat brain. *Neurosci Lett* 1990;**116**:190-193.
35. Perrier ML, Benavides J. Pharmacological heterogeneity of NMDA receptors in cerebellar granule cells in immature rat slices. A microfluorimetric study with the [Ca2+]i sensitive dye Indo-1. *Neuropharmacology* 1995;**34**:35-42.
36. Nankai M, Klarica M, Fage D, Carter C. Evidence for native NMDA receptor subtype pharmacology as revealed by differential effects on the NMDA-evoked release of striatal neuromodulators: eliprodil, ifenprodil and other native NMDA receptor subtype selective compounds. *Neurochem Int* 1996;**29**:529-542.
37. Herring PL. Excitatory Amino Acids: Clinical Results with Antagonists. Academic Press, 1997.
38. Biton B, Godet D, Granger P, Avenet P. R- and L-type Ca2+ channels are insensitive to eliprodil in rat cultured cerebellar granule neurons. *Eur J Pharmacol* 1997;**323**:277-281.
39. Willis CL, Brazell C, Foster AC. Plasma and CSF levels of dizocilpine (MK-801) required for neuroprotection in the quinolinate-injected rat striatum. *Eur J Pharmacol* 1991;**196**:285-290.
40. Arias HR, McCardy EA, Blanton MP. Characterization of the dizocilpine binding site on the nicotinic acetylcholine receptor. *Mol Pharmacol* 2001;**59**:1051-1060.
41. Halliwell RF, Peters JA, Lambert JJ. The mechanism of action and pharmacological specificity of the anticonvulsant NMDA antagonist MK-801: a voltage clamp study on neuronal cells in culture. *Br J Pharmacol* 1989;**96**:480-494.
42. Huang CF, Su MJ. Positive inotropic action of NMDA receptor antagonist (+)-MK801 in rat heart. *J Biomed Sci* 1999;**6**:387-398.

Section 2: per-reviewed reviews

Review 1

Calcium in red blood cells-a perilous balance

Bogdanova A, **Makhro A**, Wang J, Lipp P, Kaestner L.

Int J Mol Sci. 2013 May 8;14(5):9848-72. Doi: 10.3390/ijms14059848.

Received: 27 February 2013; in revised form: 18 March 2013 / Accepted: 19 March 2013 / Published: 8 May 2013

Contribution:

Makhro A. participated in writing and discussions.

Int. J. Mol. Sci. **2013**, *14*, 9848-9872; doi:10.3390/ijms14059848

OPEN ACCESS
International Journal of
Molecular Sciences
ISSN 1422-0067
www.mdpi.com/journal/ijms

Review

Calcium in Red Blood Cells—A Perilous Balance

Anna Bogdanova [1], Asya Makhro [1], Jue Wang [2], Peter Lipp [2] and Lars Kaestner [2,*]

[1] Institute of Veterinary Physiology, Vetsuisse Faculty and the Zürich, Center for Integrative Human Physiology, University of Zürich, Zürich 8057, Switzerland;
E-Mails: annab@access.uzh.ch (A.B.); makhro@vetphys.uzh.ch (A.M.)

[2] Institute for Molecular Cell Biology and Research Centre for Molecular Imaging and Screening, Saarland University, Homburg/Saar 66421, Germany;
E-Mails: jue.wang@uniklinikum-saarland.de (J.W.); peter.lipp@uks.eu (P.L.)

* Author to whom correspondence should be addressed; E-Mail: lars_kaestner@me.com;
Tel.: +49-6841-16-26103; Fax: +49-6841-16-26104.

Received: 27 February 2013; in revised form: 18 March 2013 / Accepted: 19 March 2013 / Published: 8 May 2013

Abstract: Ca^{2+} is a universal signalling molecule involved in regulating cell cycle and fate, metabolism and structural integrity, motility and volume. Like other cells, red blood cells (RBCs) rely on Ca^{2+} dependent signalling during differentiation from precursor cells. Intracellular Ca^{2+} levels in the circulating human RBCs take part not only in controlling biophysical properties such as membrane composition, volume and rheological properties, but also physiological parameters such as metabolic activity, redox state and cell clearance. Extremely low basal permeability of the human RBC membrane to Ca^{2+} and a powerful Ca^{2+} pump maintains intracellular free Ca^{2+} levels between 30 and 60 nM, whereas blood plasma Ca^{2+} is approximately 1.8 mM. Thus, activation of Ca^{2+} uptake has an impressive impact on multiple processes in the cells rendering Ca^{2+} a master regulator in RBCs. Malfunction of Ca^{2+} transporters in human RBCs leads to excessive accumulation of Ca^{2+} within the cells. This is associated with a number of pathological states including sickle cell disease, thalassemia, phosphofructokinase deficiency and other forms of hereditary anaemia. Continuous progress in unravelling the molecular nature of Ca^{2+} transport pathways allows harnessing Ca^{2+} uptake, avoiding premature RBC clearance and thrombotic complications. This review summarizes our current knowledge of Ca^{2+} signalling in RBCs emphasizing the importance of this inorganic cation in RBC function and survival.

Keywords: erythrocyte; senescence; clot formation; thrombosis; cytoskeleton

1. Introduction

Ca^{2+} is a universal and ubiquitous signalling molecule [1,2], regulating cell cycle and fate, metabolism and structural integrity, motility and volume. Most of the Ca^{2+} in the cytosol is bound and buffered by numerous Ca^{2+} binding proteins, phospholipids and inorganic phosphate. When bound and buffered Ca^{2+} are included, total intracellular Ca^{2+} in red blood cells (RBCs) reaches 5.7 μM [3]. Basal free Ca^{2+} concentration in RBCs of healthy human beings under physiological conditions is estimated to be in the range of 30 to 60 nM [4]. A tremendous gradient of at least 40,000-fold between the cytosol and blood plasma where free Ca^{2+} concentration reaches up to 1.8 mM is maintained due to particularly low permeability of membranes to Ca^{2+} (~50 μmol/(l_{cells} h)) and efficient extrusion of Ca^{2+} from the cells by the plasma membrane Ca^{2+} pump (PMCA) [4]. This gradient may be used for signalling purposes as opening of a few hundreds of channels transporting 10^6 ions per second over several milliseconds may result in >10-fold changes in free Ca^{2+} levels in the sub-membrane space, causing acute changes in the activity of multiple Ca^{2+} sensitive proteins involved in structural, signalling, metabolic and transport functions. Such a huge Ca^{2+} influx seems to exceed the RBC's Ca^{2+}-buffering abilities. Long-term increases in the Ca^{2+} permeability result in serious dysregulation of multiple cellular functions. The subsequent onset of proteolysis, oxidation, irreversible shrinkage and phosphatydylserine (PS) exposure to the extracellular membrane leaflet facilitate clearance of Ca^{2+} overloaded cells in case the latter have not been haemolysed when passing through capillaries.

This review summarizes the current knowledge on the regulation of RBC Ca^{2+} levels, Ca^{2+} dependent processes and the potential role that Ca^{2+} might play in the development of RBC pathologies. For obvious reasons this review makes no claim to be complete, but wants to draw attention to open questions and mechanisms to be resolved in the field of Ca^{2+} signalling in RBCs.

2. Ca^{2+} Transport across the RBC Membrane

2.1. Ca^{2+} Extrusion Pathway: Plasma Membrane Ca^{2+} Pump

It was realised very early on that the inhibition of the energy supply in RBCs leads to a Ca^{2+} increase [5]. Although the nature of the Ca^{2+} influx remained unknown for several decades, the extrusion mechanism was realized to be mediated by a plasma membrane Ca^{2+} pump (PMCA). For human RBC membrane the presence of the B-splice isoform of the PMCA1 was shown [6]. This P-type ATPase is ubiquitously expressed. It is composed of 1220 amino acids forming ten transmembrane domains, two intracellular loops containing ATP binding and phosphorylation sites and inward-facing *N*- and *C*-terminals. The latter contains a Ca^{2+} calmodulin binding domain, phosphorylation sites and a PDZ-binding domain serving as a docking terminal for a number of proteins [7]. The maximal Ca^{2+} extrusion rate in RBCs can vary within RBC populations of a single donor between >60 mmol/(l_{cells} h) and <4 mmol/(l_{cells} h) [8]. The maximal turnover rate of the PCMA is significantly higher in RBCs from light fractions compared to that in RBCs within dehydrated RBC

fractions following density centrifugation [9]. This reduction in V_{max} in cells from the dense fraction was referred to as a hallmark of RBC senescence [10]. The maximal Ca^{2+} turnover rate of PMCA in the RBC membrane of healthy humans not loaded with Ca^{2+} is most likely never reached. The apparent V_{max} for PMCA measured in such cells is ~50 μmol/(l_{cells} h), the value equal to the passive Ca^{2+} uptake. The enzyme half-activation constant for Ca^{2+} was reported to be 4 μM, far above the actual free cytosolic Ca^{2+} levels in human RBCs [11].

Increases in the intracellular free Ca^{2+} are sensed by the PMCA and occur in response to the interaction of the Ca^{2+} calmodulin complex with the *C*-terminus of the enzyme. In Ca^{2+}-loaded RBCs the limiting factor of the PMCA transport capacity is ATP availability. The pump is fuelled preferentially by a pre-membrane ATP pool [8,12,13] and has a K_d (ATP) of 145 μM [5,14]. Under conditions of permanent Ca^{2+} leak, activation of PMCA results in rapid ATP depletion.

RBC-derived plasma membrane vesicles contain factors activating PMCA, such as arachidonic acid, ceramide and acidic phospholipids, whereas sphingosine suppresses its function [15–17]. The function of the PMCA is extremely temperature-sensitive with ~30-fold reduction in turnover rate for every 10 °C drop [18].

2.2. Ca^{2+} Influx Pathways

Ca^{2+} influx through the plasma membrane of healthy human RBCs is extremely slow but increasing up-to 5-fold in cells of patients with sickle cell disease (SCD) and several other forms of hereditary haemolytic anaemia [4]. Several cation channels mediate inward movement of Ca^{2+}. Significant progress in identification of ion channels in control of Ca^{2+} uptake has recently been reviewed [19].

Voltage-activated non-selective cation channels [20–22] were shown to be Ca^{2+} permeable [23]. These initial observations have all been performed on excised patches, but the presence of the channel was also shown in the whole cell configuration [24] and further flux-based characterisations have been performed [25–27]. However, a proof of the molecular identity remains to be provided.

Furthermore, a P-type Ca^{2+} channel was pharmacologically identified [28] and shown to be a $Ca_V2.1$ channel by Western blot analysis [29]. This channel can be inhibited by ω-agatoxin TK [29]. However, in contrast to the initial investigations, in which activation by protein kinase C (PKC) was proposed, recent findings depicted a rather indirect interaction with PKC [30].

A recent report provided evidence for the presence of a transient receptor potential (TRP) channel of subtype C6 in the RBC membrane [31]. However, most of the work done so far was performed on murine RBCs and detailed characterization of this channel in human RBCs is missing.

In addition, the expression of an NMDA receptor channel was initially reported for rat [32] and later in human RBCs using molecular biological and electrophysiological approaches [33]. NMDA receptor agonists include glutamate, *N*-methyl D-aspartate (NMDA), homocysteine, homocysteic acid, glycine and D-serine [34].

Recently, the protein PIEZO1 was reported as being mutated in RBCs in hereditary xerocytosis [35] without knowing its physiological function. However, PIEZO1 is characterized as a mechano-sensitive cation channel in heterologous expression systems [36,37].

Furthermore there is evidence for an AMPA receptor related channel activity in RBCs [38].

All the channels mentioned above were reported to be present in human RBCs from healthy donors. However, some currents were only shown to be present in cells of patients. An example is an increase in non-selective cation conductance on RBC of SCD patients mediating or contributing to P_{sickle} [39,40], an increased membrane permeability in SCD RBC. It is still not completely clear if this reflects an increased activity of one or more of the above mentioned channels or yet another conductance [40,41]. However, recent investigations provide evidence for the involvement of the NMDA receptor [42].

3. Ca^{2+}-Sensitive Proteins in RBCs

3.1. Onset of Ca^{2+}-Inducible Events and Ca^{2+} Sensors in RBCs

When in the cell, Ca^{2+} activates numerous Ca^{2+} dependent proteins. Each of them has its own activation threshold. Thus, gradual increase in Ca^{2+} levels is associated with gradual activation of various groups of Ca^{2+}-sensitive proteins involved in physiological and pathophysiological processes in RBCs. In Figure 1 we compiled current knowledge about the activation ranges of some selected proteins. This list of Ca^{2+} sensitive proteins is by far not comprehensive and can hardly be covered within one review. Despite a large number of such proteins and diversity of their functions, only few of them are "true" Ca^{2+} sensors interacting directly with calcium ions [43]. One of such ubiquitous sensors highly abundant in RBCs is calmodulin. Calmodulins 1–4 (CaM) are 17 kDa proteins comprising two globular EF hand Ca^{2+} binding domains enriched with carboxyl and carbonyl groups (Asp, Glu and Thr) interconnected with a flexible linker (for details see, e.g., [44,45]). Upon interaction with Ca^{2+}, CaM wraps around amphipathic regions of the protein compacting into a globular shape and pulling the interacting domains of the target out of lipophilic pockets or out of the membrane lipid bilayer moiety. In RBCs the proteins regulated by interaction with the Ca^{2+} calmodulin 2 complex (Ca-CaM) include, e.g., elements of the cytoskeletal network, the Na^+/H^+ exchanger NHE1, PMCA and the endothelial NO synthase (eNOS). Cytoplasmic CaM becomes active when recruited to the plasma membrane where its action is often coupled to that of phosphatidylinositol 4,5-bisphosphate (PIP_2) localised at the inner leaflet of the membrane. An example of such coupling is a competitive binding of both co-regulators to the intracellular domain of NHE1 (see Figure 2A).

Another class of "true" Ca^{2+} sensors (~650 proteins included) contain Ca^{2+} binding C2 domains interacting with 2–3 Ca^{2+} [43,46]. In RBCs proteins with C2 domains include phospholipases, PKCα, phosphoinositide 3-kinase (PI3K) and many others. Binding of Ca^{2+} to the C2 domains, triggers translocation of these proteins to the specific areas within plasma membrane containing their substrates [46].

Figure 1. Overview of concentration dependence of Ca^{2+} activated events in RBCs. The yellow column indicates the estimated range of RBCs' resting free Ca^{2+} [4]. The gray/black bars indicate the activation of the proteins with the intensity of darkness related to the activation level (details see below). The red lines depict the half activation concentration. For orientation, the green line provides the *in vivo* k_D for Fluo-4 [47], probably the most appropriate Ca^{2+} fluorophore to be used in RBCs [48]. The universal intermediate messenger calmodulin has a dissociation constant for Ca^{2+} of 920 nM [49], which can be shifted down to 100 nM (see main text), indicated by the red arrow. The Gardos channel has an open probability of EC_{50} of 4.7 μM with a Hill slope factor of approximately 1 [50]. Values were measured in excised patches at a membrane potential of 0 mV. The curve of the opening frequency is almost superimposable (EC_{50} of 4.3 μM) [50] keeping the values given in the figure valid also for whole cell and hence population based investigations. The values for half maximal activation of the scramblase were determined by different studies with varying methodologies and a slightly different result. Values varied between approximately 30 μM determined in liposomes [51] and 70 μM measured in RBC ghosts [52]. The flippase depicts almost full inhibition already at a Ca^{2+} concentration of 400 nM [53]. μ-Calpain, a protein that cleaves cytoskeleton and membrane proteins depicts half activation at 40 μM Ca^{2+} [54] but can be activated and then shifting half-maximal activation down to 200 nM [55]. Transglutaminase mediating polymerisation of RBC membrane proteins in its native form has a dissociation constant for Ca^{2+} of 190 μM [56]. Adenosine monophosphate (AMP) deaminase is an enzyme that converts AMP into inosin monophosphate and is directly stimulated by Ca^{2+} at a half maximal concentration of 50 μM free Ca^{2+} [57]. The binding of Ca^{2+} to the C2-domain of PKCα was determined *in vitro* to be 35 μM with a Hill coefficient of 0.9 [58]. Although the Ca^{2+} dependence of the membrane binding was measured to be an order of magnitude lower [58], the initial Ca^{2+} binding is the crucial step for PKCα activation and therefore the relevant number in this compilation.

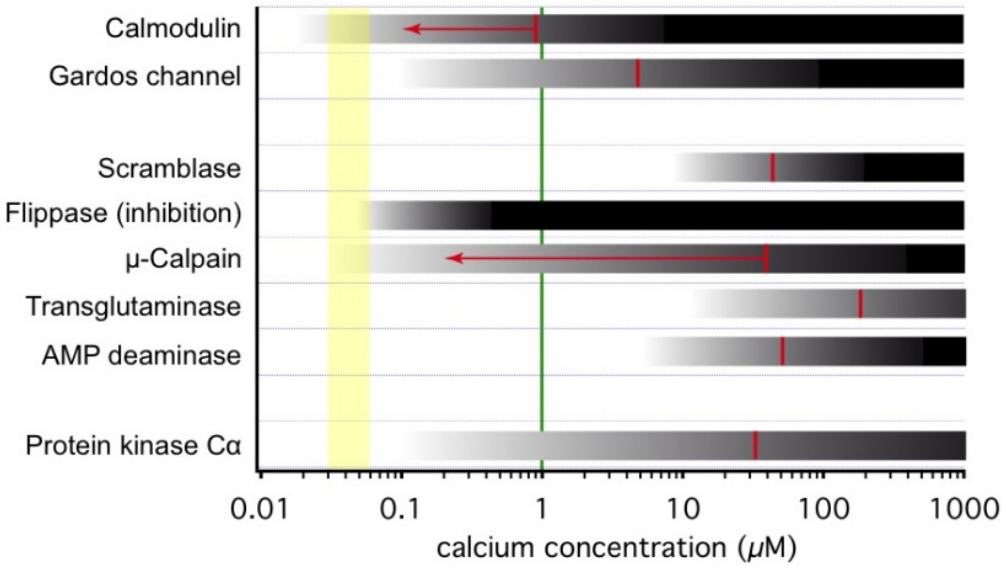

Figure 2. Ca^{2+} and RBC cytoskeleton. (**A**) Ca^{2+} sensitive elements of the cytoskeleton: band 4.1 and adducin interact with the Ca^{2+}-calmodulin (Ca-CaM) complex. Adducin binds to actin blocking elongation of the fast-growing (barbing) ends of actin filaments within junctional complexes (J). When interacting with the band 3 dimers anchoring the spectrin network to the membrane, J become a part of bigger multi-protein complexes known as 4.1R-comples (4.1RC). Interaction with Ca-CaM down-regulates capping activity of adducin regulating thereby actin filament assembly [59]. Furthermore, adducin tetramers participate in docking of carbonic anhydrase II (CAII) to band 3 tetrames. NHE1 is activated as it joins CAII and thereby becomes associated with the ankyrin complex (AC) [60,61]. Band 4.1R is an interacting partner of a number of proteins. Those include spectrin and actin which bind to the 10 kDa domain of the band 4.1R protein; band 3 protein, p55, and GPC docking to the FERM domain of it and NHE1 interacting with its *C*-terminal 24 kDa domain. Interaction of band 4.1R with Ca-CaM triggers the reduction of the affinity of this protein to all interacting partners. As a result, spectrin network interaction with the integral proteins becomes loose. Decrease in affinity of band 4.1R to the cytosolic domain of NHE1 favours its dissociation from 4.1R and interaction with phoshatidylinositol 4,5-phosphate (PIP_2), thus causing NHE activation [62]. PIP_2 also modulates interaction of band 4.1R with glycophorin C and band 3 protein [63]; (**B**) Schematic representation of the FERM (4.1/ezrin/radixin/moesin) domain of band 4.1 protein, indicating docking ports for interacting partners and Ca-CaM binding sites (for details see [64]).

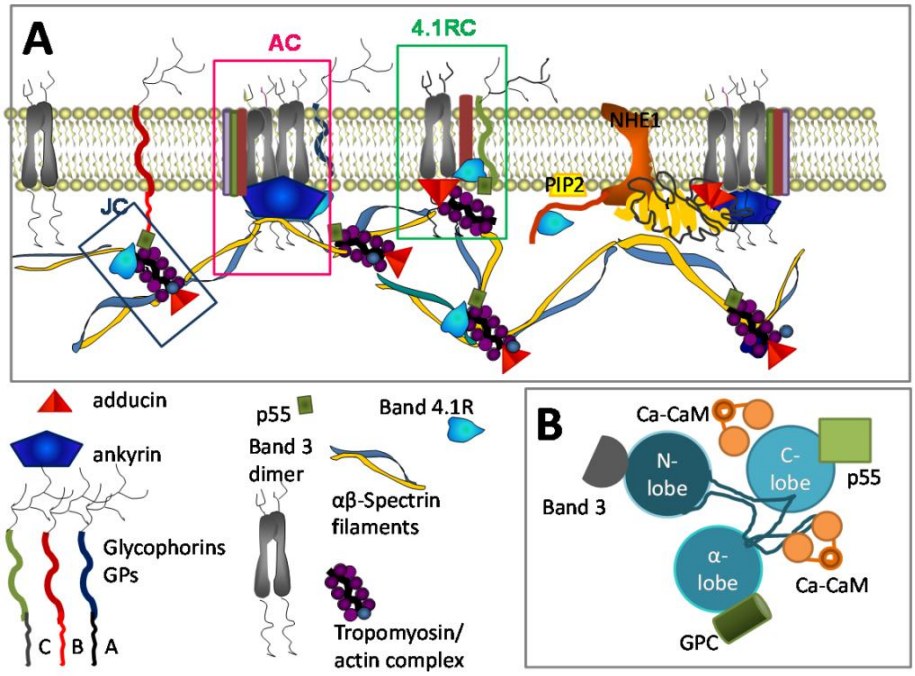

3.2. Ca^{2+}-Dependent Phosphorylation

Changes in phosphorylation are among the most important modulations of protein activity in RBCs. Among the kinases there is a group of Ca^{2+} activated protein kinases, the conventional protein kinase C (cPKC) [65]. Among cPKCs, only protein kinase Cα (PKCα) can be found in RBCs [66]. Upon Ca^{2+}

binding, PKCα translocates to the plasma membrane, where it phosphorylates its target proteins. The kinase domain of PKCs lacks specificity [67,68] and therefore numerous proteins can be phosphorylated. Reports include the PMCA [69], cytoskeletal proteins ([70,71] and see below), NADPH oxidase [72] and possibly further proteins [29,30,73] are affected.

3.3. Ca^{2+} and RBC Cytoskeleton

Opening of cation channels in response to mechanical stress and the presence of activators, such as amino acids, proinflammatory cytokines and others, result in local transient increase in Ca^{2+} levels in the vicinity of the plasma membrane. The latter, most likely serves as a signal to mediate rapid reversible changes in cytoskeletal flexibility.

The calcium-calmodulin complex (Ca-CaM) plays a key role in regulation of cytoskeletal stability. Selected elements of the cytoskeletal architecture interacting with Ca-CaM are schematically shown in Figure 2 together with their interacting partners. Those include major components of the cytoskeletal network, protein 4.1R, and adducin. These proteins function as docking stations for spectrin and actin, band 3 protein, glycophorins protein 4.2 and p55 and form a complex known as ankyrin-based complex and junctional complex (Figure 2A) [74,75]. The junctional complex is formed by the three principal components of the skeletal network junctions (spectin, actin, and 4.1R, together with tropomyosin, tropomodulin, adducin, dematin, p55). When associated with transmembrane proteins, GPC, XK, Kell, Duffy, band 3, and Rh junction complex forms a multiprotein 4.1R-based complex [76].

It is shown in Figure 2A, that the band 4.1R protein is a key constituent of all three complexes. Upon interaction with Ca-CaM, affinity of the 4.1R protein to all the interacting partners decreases and the cytoskeletal structure including spectrin-actin-tropomyosin junctions and the spectrin-actomyosin web interaction with the transmembrane protein clusters becomes loose and unstable. Such, Ca-CaM induced dissociation of NHE1 from the ankyrin complexes and band 4.1R protein. This facilitates the interaction of NHE1 with PIP_2 resulting in activation of this ion transporter and dysregulation of cell volume and cytosolic alkalosis [62,77].

The Ca^{2+} concentration required for half-activation of calmodulin is 100 nM [78]–920 nM [49], Figure 1, thus no significant dissociation of the membrane cytoskeleton is expected to occur under physiological concentration of intracellular free Ca^{2+} [79]. Phosphorylation of calmodulin at Ser-80 and -84 affects its affinity to 4.1R reducing their binding [80].

Ca^{2+} dependent phosphorylation is a second mode of action of Ca^{2+} on cytoskeletal proteins. Phosphorylation of the 4.1R protein at serine 312 and serine 331 by PKC was reported [81]. These two phosphorylation sites are localised within a domain flanked by the spectrin- and actin binding domain and a domain containing the interaction sites for transmembrane proteins (Figure 2B). When phosphorylated the 4.1R-β-spectrin interaction appears to be weakened by ~30% [81]. As Ca^{2+} uptake is known to be triggered by mechanical deformations [82], controlled reversible loosening of cytoskeletal network in cells passing through capillaries is an advantage. Uncontrolled irreversible loss of cytoskeletal stability in RBCs of patients with haemolytic anaemia, in which Ca^{2+} is permanently upregulated, on the contrary compromises mechanical stability of the RBC membrane [83]. In RBCs of healthy humans the 4.1R protein is not phosphorylated [81]. One more target of PKC is α-adducin

which, upon phosphorylation at Ser-726 decreases its affinity to F-actin, as it was observed in SCD RBCs. After the loss of F-actin capping dissociation of spectrin from actin occurs [84], which results in RBC inability to change shape.

In RBCs transaminase 2 responds to Ca^{2+} entry with a rapid release of its inhibitory GTP and activation resulting in formation of Nε (γ-glutaminyl)lysine cross-linking (Figure 1). As a result, in Ca^{2+} overloaded RBCs formation of numerous polymeric protein complexes such as Glut1-adducin-dematin adducts as well as cross-linked complexes of Band 3-ankyrin-spectrin and glycophorin *C*-band 4.1-p55 occurs [85]. This Ca^{2+} induced remodelling of the cytoskeletal structure and concomitant changes in cell shape and membrane plasticity are suggested to contribute to premature RBC clearance.

3.4. Ca^{2+} and RBC Volume Regulation

RBC volume regulation is a complex process with contributions of numerous molecular players including, e.g., band 3 protein [86]. A marked volume decrease is mediated by the so-called Gardos effect, which was among the first Ca^{2+} dependent processes recognized in RBCs [87]. The corresponding Gardos channel was the first channel measured by patch-clamp in RBCs [88,89]. This channel is a Ca^{2+} activated K^+ channel and the Gardos effect represents the Ca^{2+} induced K^+ loss of RBCs. The channel is characterized by a single channel conductance of approximately 20 pS [88], a selectivity of K^+ to Na^+ of about 15:1 [90] and an EC_{50} (Ca^{2+}) of 4.7 μM, Figure 1 with a Hill-slope of approximately 1 [50]. Later, the molecular identity of the Gardos channel was shown to be the hSK4 channel [91]. Functionally, the opening of the Gardos channel leads to a hyperpolarisation and a loss of K^+, Cl^- and water resulting in cell shrinkage. Although the physiological function of the Gardos channel is not completely elucidated, there are two complementary concepts: (i) Openings of RBC Ca^{2+} channels by platelet released substances [92,93] initialy trigger the consecutive activation of the Gardos channel. This Gardos channel mediated dehydration of the RBC fosters their contribution in clot formation as outlined below. (ii) Local membrane deformation of RBCs was shown to trigger a transient increase in Ca^{2+} permeability with secondary activation of the Gardos channels [82]. This was proposed to induce significant dehydration even during a brief deformation event in the microcirculation [82].

3.5. Ca^{2+} and Lipid Bilayer

Scramblase is a protein responsible for bidirectional transmembrane movement of phospholipids [94] leading to the break-down of the originally asymmetrical distribution of phospholipids between the inner and outer membrane leaflet [95]. It is a passive transport, but Ca^{2+} activated [51,52]. Its Ca^{2+} sensitivity is mediated by an EF hand motif [96]. The scramblase activity is complemented by the flippase (aminophospholipid translocase) inhibition [97]. This protein actively builds up phospholipid asymmetry and such can be regarded as the opponent of the scramblase. As shown in Figure 1, flippase activity is almost completely suppressed by 400 nM Ca^{2+} [53].

3.6. Ca^{2+} and Metabolism

Numerous reports emphasize the possible role of the Ca-CaM system in regulation of activity of glycolytic enzymes including pyruvate kinase [98,99]. However, even more important is its pivotal role in assembling the glycolytic enzymes at the RBC membrane. Band 3 protein and its cytosolic domain was shown to serve as a docking station for multiple glycolytic enzymes [100]. Ca^{2+} in turn was suggested to promote band 3 tyrosine phosphorylation [101]. Phosphorylation of the cytosolic domain of band 3 protein (cdb3) at Tyr9 and Tyr21 results in displacement of LDH, PK, GAPDH, PFK and aldolase from RBC membrane in intact cells [102]. A similar effect is induced by interaction of deoxyHb with band 3 protein [103].

3.7. Ca^{2+} and Redox State Preservation

In RBCs there is a direct link between the intracellular free Ca^{2+} concentration and the haemoglobin oxygen saturation. In cells of healthy individuals, passive Ca^{2+} uptake was unaffected by deoxygenation, but the V_{max} of the PMCA was reduced by 18%–32% [104]. This is not the case in RBCs of patients with SCD [4]. An increase in free Ca^{2+} levels was mainly attributed to changes in haemoglobin protonation, increases in protonation of deoxyhaemoglobin and a shift in the intracellular pH towards more alkaline values [104,105]. Along with augmentation of 2,3-diphosphoglycerate and ATP binding to haemoglobin, interaction of deoxyhaemoglobin with protons is associated with a decrease in Ca^{2+} buffering capacity of haemoglobin. In the cytosol of deoxygenated RBCs release of Ca^{2+} ions from protein binding sites and lowering of extrusion capacity of the PMCA contribute to both an increase in the ionised Ca^{2+} fraction by 34%–74% even in the absence of Ca^{2+} influx from the extracellular medium [104].

Increases in the free Ca^{2+} were recently linked to a lower oxygen affinity of haemoglobin promoting the release of oxygen [33]. Deoxygenation induced transient release of Ca^{2+} from intracellular buffers may promote further deoxygenation enhancing O_2 dissociation from haemoglobin. Molecular mechanisms of this phenomenon remain to be investigated.

Aside to the control of haemoglobin oxygenation, Ca^{2+} is also involved in the regulation of the RBC's redox state. Ca-CaM complexes are co-activators of endothelial NO synthase (eNOS) activity [106,107]. Recently eNOS was shown to be present in circulating RBCs [108,109] and is activated by Ca^{2+} uptake during shear stress [82,110]. Nitric oxide is a scavenger of superoxide anions, which interacts with them two orders of magnitude faster than superoxide dismutase (SOD) [111]. However, following shortage of tetrahydrobiopterin or L-arginine eNOS itself gets uncoupled and is capable of generating superoxide anions, which is turned into H_2O_2 in a reaction catalysed by SOD [106]. Pro-oxidative action of uncoupled eNOS was demonstrated in RBCs [112].

3.8. Calpain and Its Targets in RBCs

While the Ca^{2+} dependent cysteine protease μ-calpain (calpain-1) was mainly detected in human RBCs, m-calpain (calpain-2) was found to be virtually absent [113]. μ-Calpain is highly sensitive to Ca^{2+} with a half-activation concentration in the range of 3–50 μM [114,115]. The enzyme isolated from human RBCs displayed a value of 40 μM [54]. This is well above the free Ca^{2+} concentration

found in both human RBCs from healthy individuals (30–60 nM) and values of 100–300 nM reported in RBCs from patients with hereditary forms of anaemia [4]. However, a 40 kDa activator protein which makes μ-calpain more Ca^{2+} sensitive, shifts Ca^{2+} concentrations required for half-maximal activation from 40–50 μM down to 0.2 μM [55]. In human RBCs a fraction of membrane-associated active μ-calpain was detected [116,117]. Activation mediated recruitment of calpain to the membrane [118] was used to estimate the protease activity revealing that ~7% of the calpain pool is constitutively active in RBCs from healthy individuals [117]. Consequently, the μ-calpain activity in RBCs from patients with hereditary anaemia forms was also increased because their resting Ca^{2+} levels were raised when compared to those from healthy donors. [4].

Targets of activated calpain are mainly transmembrane or membrane-associated proteins including PMCA, and bands 1, 2, 2.1, 3, 4.1, 4.2 proteins, but also calpain itself [119]. Autolysis occurs at Ca^{2+} levels beyond physiological concentrations, namely in the range 50–150 μM [114]. Limited digestion of haemoglobin α and β chains by calpain was also reported [120].

Recently, RBCs of a μ-calpain knock-out (KO) mouse displayed an improved deformability [121]. Furthermore it was demonstrated that ankyrin, band 3, band 4.1R, adducin and dematin were degraded in the Ca^{2+} loaded normal RBCs but not in the KO RBCs [121].

Cleavage of the PMCA by μ-calpain was associated with an activation of the pump, rapid ATP depletion, inactivation of the pump and gradual loss of the transmembrane Ca^{2+} gradients [122].

Calpastatin, an endogenous inhibitor of μ-calpain, is a natural regulator of the enzyme activity in RBCs. Both major and minor components of calpastatin, calpastatin H and L were detected in human RBCs [54]. Interaction of calpastatin with calpain is also Ca^{2+} sensitive. Half-maximal activation of calpastatin occurs at 40 μM Ca^{2+} [114], in bovine skeletal muscle derived enzyme. Activity of calpain and a decrease in calpastatin levels in RBCs was shown to occur in elderly humans [123,124].

3.9. Ca^{2+} and Inter-Cellular Interactions

Due to the protein activity and lipid remodelling described above one would expect changes in rheological properties of RBC suspensions and indeed in numerous studies provoking increased cytosolic Ca^{2+} levels, an altered rheology was observed [125–127]. These changes were majorly explained by altered RBC deformability [128,129]. However, a second possibility to explain changes in rheological properties of RBC suspensions is RBC aggregation.

A participation of RBC Ca^{2+} channels in blood clot formation was proposed previously [92,93] following earlier work already suggesting an active participation of RBCs in blood clot formation [130–132]. Further support was given by investigations showing Ca^{2+} mediated aggregation of RBCs [133–136] and RBC adhesion to the endothelium [137–139]. Further investigations are necessary to specify the required and sufficient conditions for such processes, e.g., the threshold of the intracellular Ca^{2+} concentration at which aggregation occurs. Additionally the modulations of the aggregation properties under *in vivo* conditions need to be elucidated.

4. The Physiological Role of Intracellular Ca^{2+}: From RBC Birth to Clearance

4.1. Ca^{2+} in RBC Haematopoiesis

Ca^{2+} uptake is of key importance for promoting differentiation and proliferation of erythroid precursors at the stages of burst-forming units erythroid (BFU-E) colony-forming units erythroid (CFU-E) [140,141]. Increase in the intracellular Ca^{2+} is an integral part of the signalling pathway activated by binding of erythropoietin to its receptor [142,143]. In Ca^{2+}-free medium, Ca^{2+} uptake is absent and differentiation and survival of erythroid precursors is compromised [140,141]. Inhibition of Ca^{2+} uptake by erythroid precursor cells cultured from mononuclear cells by the NMDA receptor antagonist MK-801 resulted in 45.5% ± 12.8% mortality of cells at the stage of basophilic and polychromatic erythroblasts suggesting that these receptors are actively contributing to erythropoiesis [33]. Additional evidence indicating that Ca^{2+} levels in reticulocytes are higher than in mature RBCs comes from secondary Ca^{2+}-dependent processes such as phosphorylation [144]. Protein 4.1R phosphorylation by PKC appeared to be markedly elevated in reticulocytes resulting in weakened interaction between β-spectrin and actin [145].

4.2. Ca^{2+} in Relation to the Physiological Function of RBCs

For a long time, the physiological function of Ca^{2+} in mature RBCs was obscure and was believed to be limited to the involvement in RBCs aging and clearance [10,146,147]. However, a prominent part of this report reviews the physiological functions of Ca^{2+} in RBC regulating a broad range of processes including O_2 transport [33], rheology [148], clotting [135,136] and half-life of cells (see Section 4.3). Each of these functions is vital for the organism. Thus, aberrant Ca^{2+} homeostasis in RBCs results in development of severe life-threatening systemic pathologies.

Very recently, additional evidence in favour of a physiologically important Ca^{2+} associated mechanism was reported. Here, rises in the intracellular Ca^{2+} appear to promote the ability of RBCs to deliver oxygen [33].

4.3. Ca^{2+} in RBC Clearance

At present it is suggested that in senescent RBCs the intracellular Ca^{2+} levels exceed those in reticulocytes and young RBCs [149]. However, such conclusions on the relationship between cell age and steady-state Ca^{2+} levels largely depend on the age markers employed. Typical age markers include glycosylated haemoglobin HbA1c, band 4.1a/b ratio, cell density, de-sialation and changes in CD47 abundance at the membrane surface, PS exposure, and several others [149–151].

Activity of the PMCA in RBCs was shown to decrease with progressing HbA1c accumulation [152]. However, based on the pump-leak theory, this process will result in Ca^{2+} accumulation only when coupled to the unchanged or increasing activity in Ca^{2+}-transporting ion channels. However, according to recent findings, this is not necessarily the case. Young rat and human RBCs contain higher number of NMDA receptors, that upon stimulation with plasma glycine and glutamate can cause significant Ca^{2+} influx [32,33]. Young cells are preferentially removed in subjects with induced or chronic polycytemia, phenomenon known as neocytolysis [112,153–155]. Finally,

phosphatydylserine (PS) exposure does not always correlate with high Ca^{2+} levels [156]. Thus, both young and senescent RBCs appear to be prone to Ca^{2+} overload, which may well trigger RBC clearance, but the relation of this mechanism to other Ca^{2+} independent clearance mechanisms and to *in vivo* relevance is still obscure.

5. Ca^{2+} Dysbalance and Haemolytic Anaemia

Independent of its origin, hereditary haemolytic anaemia is often associated with an increase in the intracellular Ca^{2+} levels [4]. "Leakiness" of RBC plasma membrane for Ca^{2+} that could not be compensated for by the activation of PMCA was reported for patients with SCD [157–159], beta-thalassemia (although most of the Ca^{2+} seem to be sequestered in vesicles or bound to cytosolic proteins) [160–162], phosphofructokinase deficiency [163]. Most of the information on Ca^{2+} transport in diseased RBCs was so far obtained for SCD patients. In these cells relatively high rates of Ca^{2+} uptake in RBCs are partially compensated for by sequestration of Ca^{2+} into intracellular inside-out vesicles, in which Ca^{2+} is pumped actively by PMCA [164]. Apparently, this process also exists in RBCs of patients with β-thalalssemia intermedia [162,165]. Furthermore, part of Ca^{2+} taken into the cells is immobilised by the intracellular proteins. Sickle cell transformation associated with polymerisation of deoxygenated mutated *S*-haemoglobin is amplified by 20–40-fold by dehydration [166]. Deoxygenation promotes Ca^{2+} uptake and release of ionised Ca^{2+} from the intracellular proteins (reduction in buffering capacity) [104,105,167]. In deoxygenated SCD RBC, an acute increase in the intracellular free Ca^{2+} RBCs causes opening of the Ca^{2+} sensitive Gardos channel and anion channels [168–170].

Downstream events triggered by augmentation of free intracellular Ca^{2+} comprise activation of μ-calpain [171] and activation of tyrosine phosphorylation [172]. In RBCs from SCD patients, protein 4.1R and p55 appear to be phosphorylated thus contributing to the weakened interaction with beta-spectrin [84].

Cross-linked polymers have been observed in RBCs of patients with SCD suggesting hyperactivation of transglutaminase [85].

Oxidation of membrane proteins and impaired NO production by eNOS [173,174], increase in intercellular and RBC-endothelial adhesion [175] are hallmarks of SCD. Cross-linking of the nature of carrier of sickle cell conductance (P_{sickle}) mediating Ca^{2+} uptake by RBCs remains unknown (compare Section 2.2).

6. RBC Ca^{2+} Content and Medicinal Side Effects

6.1. Transfusion Medicine

Ca^{2+} overload is involved in dramatic reduction of the life span of stored RBCs used for transfusion [176]. Storage of leuco-depleted RBC concentrates is currently performed in Ca^{2+} free glucose-containing preservation citrate buffers at low temperatures. These storage conditions favour Ca^{2+} depletion of the cytosol, oxidative stress and ATP deprivation [177,178]. These processes induce deactivation of PMCA, facilitate passive Ca^{2+} transport and evoke acute Ca^{2+} overload when re-exposed to the plasma of patients receiving transfusions. The resulting processes include

dehydration, rigidity, fragmentation of cytoskeletal proteins and oxidative stress and increased adherence of RBCs to the endothelium and to each other [179,180].

6.2. Therapeutic Side Effects

Additionally, unwanted modulations of the Ca^{2+} entry into RBC may cause side effects of drugs involved in therapies unrelated to RBCs. An example is photodynamic therapy, where the oxidative stress produced by the photosensitizer leads to the activation of cation channels in the RBC membrane and the consecutive Ca^{2+} entry triggers the mechanism described above, which is the major cause of an increased formation of blood aggregates as well as haemolysis [181]. Thus, RBC remain to be model cells to develop pharmacological strategies [182] and can even be used in automated safety screens [183].

7. Conclusion and Perspective

The role of Ca^{2+} in RBCs physiology and pathophysiology cannot be overestimated. Many links between Ca^{2+} and RBC related diseases still need to be explored [184]. Methodologically single cell based methods will increase in their importance and contribution and complement cell population measurements [185]. This is due to the recent hindsight that intercellular heterogeneity and, in some cases, inhomogeneous distribution of Ca^{2+} within the cytosol are essential to predict the onset of changes related to the abnormally high Ca^{2+} levels, which are particularly important in patients with haematological disorders [42,186]. However, the properties of Ca^{2+} binding entities within the cells will need further attention and research. Following the broad variety of Ca^{2+} mediated processes mentioned here, monitoring the following parameters may be used to indirectly predict abnormally increased intracellular free Ca^{2+} levels in RBCs: (i) changes in cell volume and morphology (microcytosis, high MCHC, increase in cell density, echinocytosis or stomatocytosis); (ii) congenital haemolytic anaemia associated with stomatocytosis, reticulocytosis, and shortened RBC survival; (iii) decrease in the intracellular K^+ levels, pseudohyperkalemia; (iv) loss of RBC deformability, changes in osmotic resistance, an increase when dehydration has occurred but cytoskeletal stability is still maintained, or a decrease when cytoskeleton is partially disassembled; (v) appearance of calpain-induced band 3 cleavage fragments; (vi) oxidative stress or unusually high NO production (nitrosated Hb, met-Hb); (vii) ATP depletion due to hyperactivation of PMCA; (viii) increase in inter-RBC aggregability; and (ix) increase in PS exposure.

For many years the RBC was the cell of choice for membrane transport investigations. In the age of genomics, interest in RBC research decreased, but numerous signalling cascades—also in respect to the second messenger Ca^{2+} that occur in other cells and may involve several organelles—have been rediscovered in a modified and/or simplified form in RBCs.

Conflict of Interest

The authors declare no conflict of interest.

References

1. Berridge, M.J.; Lipp, P.; Bootman, M.D. The versatility and universality of calcium signalling. *Nat. Rev. Mol. Cell Biol.* **2000**, *1*, 11–21.
2. Bootman, M.D.; Berridge, M.J.; Lipp, P. Cooking with calcium: The recipes for composing global signals from elementary events. *Cell* **1997**, *91*, 367–373.
3. Bookchin, R.M.; Lew, V.L. Progressive inhibition of the Ca pump and Ca:Ca exchange in sickle red cells. *Nature* **1980**, *284*, 561–563.
4. Tiffert, T.; Bookchin, R.M.; Lew, V.L. Calcium Homeostasis in Normal and Abnormal Human Red Cells. In *Red Cell Membrane Transport in Health and Disease*; Bernhardt, I., Ellory, C., Eds.; Springer Verlag: Heidelberg, Germany, 2003; pp. 373–405.
5. Wilbrandt, W. A relation between the permeability of the red cell and its metabolism. *Trans. Faraday Soc.* **1937**, *33*, 956–959.
6. Pasini, E.M.; Kirkegaard, M.; Mortensen, P.; Lutz, H.U.; Thomas, A.W.; Mann, M. In-depth analysis of the membrane and cytosolic proteome of red blood cells. *Blood* **2006**, *108*, 791–801.
7. Strehler, E.E.; Caride, A.J.; Filoteo, A.G.; Xiong, Y.; Penniston, J.T.; Enyedi, A. Plasma membrane Ca^{2+} ATPases as dynamic regulators of cellular calcium handling. *Ann. N. Y. Acad. Sci.* **2007**, *1099*, 226–236.
8. Tiffert, T.; Lew, V.L. Elevated intracellular Ca^{2+} reveals a functional membrane nucleotide pool in intact human red blood cells. *J. Gen. Physiol*. **2011**, *138*, 381–391.
9. Romero, P.J.; Romero, E.A. Differences in Ca^{2+} pumping activity between sub-populations of human red cells. *Cell Calcium* **1997**, *21*, 353–358.
10. Romero, P.J.; Romero, E.A. The role of calcium metabolism in human red blood cell ageing: A proposal. *Blood Cells Mol. Dis.* **1999**, *25*, 9–19.
11. Schatzmann, H.J. Dependence on calcium concentration and stoichiometry of the calcium pump in human red cells. *J. Physiol.* **1973**, *235*, 551–569.
12. Chu, H.; Puchulu-Campanella, E.; Galan, J.A.; Taob, W.A.; Low, P.S.; Hoffman, J.F. Identification of cytoskeletal elements enclosing the ATP pools that fuel human red blood cell membrane cation pumps. *Proc. Natl. Acad. Sci. USA* **2012**, *109*, 12794–12799.
13. Hoffman, J.F.; Dodson, A.; Proverbio, F. On the functional use of the membrane compartmentalized pool of ATP by the Na^{+} and Ca^{++} pumps in human red blood cell ghosts. *J. Gen. Physiol.* **2009**, *134*, 351–361.
14. Garrahan, P.J.; Rega, A.F. Activation of partial reactions of the Ca^{2+}-ATPase from human red cells by Mg^{2+} and ATP. *Biochim. Biophys. Acta* **1978**, *513*, 59–65.
15. Bredeston, L.M.; Rega, A.F. Phosphatidylcholine makes specific activity of the purified Ca^{2+}-ATPase from plasma membranes independent of enzyme concentration. *Biochim. Biophys. Acta* **1999**, *1420*, 57–62.
16. Colina, C.; Cervino, V.; Benaim, G. Ceramide and sphingosine have an antagonistic effect on the plasma-membrane Ca^{2+}-ATPase from human erythrocytes. *Biochem. J.* **2002**, *362*, 247–251.
17. Oliveira, V.H.; Nascimento, K.S.O.; Freire, M.M.; Moreira, O.C.; Scofano, H.M.; Barrabin, H.; Mignaco, J.A. Mechanism of modulation of the plasma membrane Ca^{2+}-ATPase by arachidonic acid. *Prostaglandins Other Lipid Mediat*. **2008**, *87*, 47–53.

18. Sarkadi, B.; Szasz, I.; Gerloczy, A.; Gardos, G. Transport parameters and stoichiometry of active calcium-ion extrusion in intact human red-cells. *Biochim. Biophys. Acta* **1977**, *464*, 93–107.
19. Kaestner, L. Cation channels in erythrocytes—Historical and future perspective. *Open Biol. J.* **2011**, *4*, 27–34.
20. Christophersen, P.; Bennekou, P. Evidence for a voltage-gated, non-selective cation channel in the human red cell membrane. *Biochim. Biophys. Acta* **1991**, *1065*, 103–106.
21. Bennekou, P. The voltage-gated non-selective cation channel from human red cells is sensitive to acetylcholine. *Biochim. Biophys. Acta* **1993**, *1147*, 165–167.
22. Kaestner, L.; Bollensdorff, C.; Bernhardt, I. Non-selective voltage-activated cation channel in the human red blood cell membrane. *Biochim. Biophys. Acta* **1999**, *1417*, 9–15.
23. Kaestner, L.; Christophersen, P.; Bernhardt, I.; Bennekou, P. The non-selective voltage-activated cation channel in the human red blood cell membrane: Reconciliation between two conflicting reports and further characterisation. *Bioelectrochemistry* **2000**, *52*, 117–125.
24. Rodighiero, S.; de Simoni, A.; Formenti, A. The voltage-dependent nonselective cation current in human red blood cells studied by means of whole-cell and nystatin-perforated patch-clamp techniques. *Biochim. Biophys. Acta* **2004**, *1660*, 164–170.
25. Bennekou, P.; Kristensen, B.I.; Christophersen, P. The human red cell voltage-regulated cation channel. The interplay with the chloride conductance, the Ca^{2+}-activated K^{+} channel and the Ca^{2+} pump. *J. Membr. Biol.* **2003**, *195*, 1–8.
26. Bennekou, P.; Barksmann, T.L.; Kristensen, B.I.; Jensen, L.R.; Christophersen, P. Pharmacology of the human red cell voltage-dependent cation channel. Part II: Inactivation and blocking. *Blood Cells Mol. Dis*. **2004**, *33*, 356–361.
27. Bennekou, P.; Barksmann, T.L.; Christophersen, P.; Kristensen, B.I. The human red cell voltage-dependent cation channel. Part III: Distribution homogeneity and pH dependence. *Blood Cells Mol. Dis*. **2006**, *36*, 10–14.
28. Yang, L.; Andrews, D.A.; Low, P.S. Lysophosphatidic acid opens a Ca^{++} channel in human erythrocytes. *Blood* **2000**, *95*, 2420–2425.
29. Andrews, D.A.; Yang, L.; Low, P.S. Phorbol ester stimulates a protein kinase *C*-mediated agatoxin-TK-sensitive calcium permeability pathway in human red blood cells. *Blood* **2002**, *100*, 3392–3399.
30. Wagner-Britz, L.; Wang, J.; Kaestner, L.; Bernhardt, I. Protein Kinase Cα and P-Type Ca^{2+}-Channel CaV2.1 in Red Blood Cells cCalcium Signaling. *J. Cell. Physiol. Biochem*. **2013**, in revision.
31. Foller, M.; Kasinathan, R.S.; Koka, S.; Lang, C.; Shumilina, E.V.; Birnbaumer, L.; Lang, F.; Huber, S.M. TRPC6 contributes to the Ca^{2+} leak of human erythrocytes. *Cell Physiol. Biochem*. **2008**, *21*, 183–192.
32. Makhro, A.; Wang, J.; Vogel, J.; Boldyrev, A.A.; Gassmann, M.; Kaestner, L.; Bogdanova, A.Y. Functional NMDA receptors in rat erythrocytes. *Am. J. Physiol. Cell Physiol*. **2010**, *298*, C1315–C1325.
33. Makhro, A.; Hanggi, P.; Goede, J.; Wang, J.; Brüggemann, A.; Gassmann, M.; Kaestner, L.; Speer, O.; Bogdanova, A. *N*-Methyl D-Aspartate (NMDA) Receptors in Erythroid Precursor Cells and in Circulating Human Red Blood Cells Contributes to the Regulation of Intracellular Calcium Levels. *Am. J. Physiol*. **2013**, in revision.

34. Madry, C.; Betz, H.; Geiger, J.R.P.; Laube, B. Supralinear potentiation of NR1/NR3A excitatory glycine receptors by Zn^{2+} and NR1 antagonist. *Proc. Natl. Acad. Sci. USA* **2008**, *105*, 12563–12568.
35. Zarychanski, R.; Schulz, V.P.; Houston, B.L.; Maksimova, Y.; Houston, D.S.; Smith, B.; Rinehart, J.; Gallagher, P.G. Mutations in the mechanotransduction protein PIEZO1 are associated with hereditary xerocytosis. *Blood* **2012**, *120*, 1908–1915.
36. Gottlieb, P.A.; Sachs, F. Piezo1: Properties of a cation selective mechanical channel. *Channels (Austin)* **2012**, *6*, 214–219.
37. Gottlieb, P.A.; Bae, C.; Sachs, F. Gating the mechanical channel Piezo1: A comparison between whole-cell and patch recording. *Channels (Austin)* **2012**, *6*, 282–289.
38. Foller, M.; Mahmud, H.; Gu, S.; Kucherenko, Y.; Gehring, E.-M.; Shumilina, E.; Floride, E.; Sprengel, R.; Lang, F. Modulation of suicidal erythrocyte cation channels by an AMPA antagonist. *J. Cell. Mol. Med*. **2009**, *13*, 3680–3686.
39. Browning, J.A.; Staines, H.M.; Robinson, H.C.; Powell, T.; Ellory, J.C.; Gibson, J.S. The effect of deoxygenation on whole-cell conductance of red blood cells from healthy individuals and patients with sickle cell disease. *Blood* **2007**, *109*, 2622–2629.
40. Ma, Y.-L.; Rees, D.C.; Gibson, J.S.; Ellory, J.C. The conductance of red blood cells from sickle cell patients: Ion selectivity and inhibitors. *J. Physiol. (Lond.)* **2012**, *590*, 2095–2105.
41. Lew, V.L.; Ortiz, O.E.; Bookchin, R.M. Stochastic nature and red cell population distribution of the sickling-induced Ca^{2+} permeability. *J. Clin. Invest*. **1997**, *99*, 2727–2735.
42. Bogdanova, A.; Makhro, A.; Wang, J.; Gassmann, M.; Kaestner, L. Responses of rat erythrocytes to homocysteine and homocysteic acid treatment. *Clin. Biochem.* **2009**, *42*, 1858–1859.
43. Clapham, D.E. Calcium signaling. *Cell* **2007**, *131*, 1047–1058.
44. Meador, W.E.; Means, A.R.; Quiocho, F.A. Target enzyme recognition by calmodulin: 2.4 A structure of a calmodulin-peptide complex. *Science* **1992**, *257*, 1251–1255.
45. Meador, W.E.; Means, A.R.; Quiocho, F.A. Modulation of calmodulin plasticity in molecular recognition on the basis of X-ray structures. *Science* **1993**, *262*, 1718–1721.
46. Cho, W.; Stahelin, R.V. Membrane-protein interactions in cell signaling and membrane trafficking. *Annu. Rev. Biophys. Biomol. Struct*. **2005**, *34*, 119–151.
47. Thomas, D.; Tovey, S.C.; Collins, T.J.; Bootman, M.D.; Berridge, M.J.; Lipp, P. A comparison of fluorescent Ca^{2+} indicator properties and their use in measuring elementary and global Ca^{2+} signals. *Cell Calcium* **2000**, *28*, 213–223.
48. Kaestner, L.; Tabellion, W.; Weiss, E.; Bernhardt, I.; Lipp, P. Calcium imaging of individual erythrocytes: Problems and approaches. *Cell Calcium* **2006**, *39*, 13–19.
49. Jarrett, H.W.; Kyte, J. Human erythrocyte calmodulin. Further chemical characterization and the site of its interaction with the membrane. *J. Biol. Chem*. **1979**, *254*, 8237–8244.
50. Leinders, T.; van Kleef, R.G.; Vijverberg, H.P. Single Ca^{2+}-activated K^+ channels in human erythrocytes: Ca^{2+} dependence of opening frequency but not of open lifetimes. *Biochim. Biophys. Acta* **1992**, *1112*, 67–74.
51. Stout, J.G.; Zhou, Q.; Wiedmer, T.; Sims, P.J. Change in conformation of plasma membrane phospholipid scramblase induced by occupancy of its Ca^{2+} binding site. *Biochemistry* **1998**, *37*, 14860–14866.

52. Woon, L.A.; Holland, J.W.; Kable, E.P.; Roufogalis, B.D. Ca^{2+} sensitivity of phospholipid scrambling in human red cell ghosts. *Cell Calcium* **1999**, *25*, 313–320.
53. Bitbol, M.; Fellmann, P.; Zachowski, A.; Devaux, P.F. Ion regulation of phosphatidylserine and phosphatidylethanolamine outside-inside translocation in human erythrocytes. *Biochim. Biophys. Acta* **1987**, *904*, 268–282.
54. Murakami, T.; Hatanaka, M.; Murachi, T. The cytosol of human erythrocytes contains a highly Ca^{2+}-sensitive thiol protease (calpain I) and its specific inhibitor protein (calpastatin). *J. Biochem* **1981**, *90*, 1809–1816.
55. Salamino, F.; de Tullio, R.; Mengotti, P.; Viotti, P.L.; Melloni, E.; Pontremoli, S. Site-directed activation of calpain is promoted by a membrane-associated natural activator protein. *Biochem. J.* **1993**, *290*, 191–197.
56. Bergamini, C.M.; Signorini, M. Studies on tissue transglutaminases: Interaction of erythrocyte type-2 transglutaminase with GTP. *Biochem. J.* **1993**, *291*, 37–39.
57. Almaraz, L.; García-Sancho, J.; Lew, V.L. Calcium-induced conversion of adenine nucleotides to inosine monophosphate in human red cells. *J. Physiol. (Lond.)* **1988**, *407*, 557–567.
58. Kohout, S.C.; Corbalán-García, S.; Torrecillas, A.; Goméz-Fernandéz, J.C.; Falke, J.J. C2 domains of protein kinase C isoforms alpha, beta, and gamma: Activation parameters and calcium stoichiometries of the membrane-bound state. *Biochemistry* **2002**, *41*, 11411–11424.
59. Kuhlman, P.A.; Hughes, C.A.; Bennett, V.; Fowler, V.M. A new function for adducin. Calcium/calmodulin-regulated capping of the barbed ends of actin filaments. *J. Biol. Chem.* **1996**, *271*, 7986–7991.
60. Kifor, G.; Toon, M.R.; Janoshazi, A.; Solomon, A.K. Interaction between red cell membrane band 3 and cytosolic carbonic anhydrase. *J. Membr. Biol*. **1993**, *134*, 169–179.
61. Li, X.; Alvarez, B.; Casey, J.R.; Reithmeier, R.A.F.; Fliegel, L. Carbonic anhydrase II binds to and enhances activity of the Na^+/H^+ exchanger. *J. Biol. Chem.* **2002**, *277*, 36085–36091.
62. Nunomura, W.; Denker, S.P.; Barber, D.L.; Takakuwa, Y.; Gascard, P. Characterization of cytoskeletal protein 4.1R interaction with NHE1 (Na^+/H^+ exchanger isoform 1). *Biochem. J.* **2012**, *446*, 427–435.
63. An, X.; Zhang, X.; Debnath, G.; Baines, A.J.; Mohandas, N. Phosphatidylinositol-4,5-biphosphate (PIP2) differentially regulates the interaction of human erythrocyte protein 4.1 (4.1R) with membrane proteins. *Biochemistry* **2006**, *45*, 5725–5732.
64. Nunomura, W.; Sasakura, D.; Shiba, K.; Nakamura, S.; Kidokoro, S.-I.; Takakuwa, Y. Structural stabilization of protein 4.1R FERM domain upon binding to apo-calmodulin: Novel insights into the biological significance of the calcium-independent binding of calmodulin to protein 4.1R. *Biochem. J.* **2011**, *440*, 367–374.
65. Lipp, P.; Reither, G. Protein kinase C: The "masters" of calcium and lipid. *Cold Spring Harb. Perspect. Biol.* **2011**, *3*, doi:10.1101/cshperspect.a004556.
66. Govekar, R.B.; Zingde, S.M. Protein kinase C isoforms in human erythrocytes. *Ann. Hematol.* **2001**, *80*, 531–534.
67. Newton, A.C. Protein kinase C: Structural and spatial regulation by phosphorylation, cofactors, and macromolecular interactions. *Chem. Rev.* **2001**, *101*, 2353–2364.

68. Steinberg, S.F. Structural basis of protein kinase C isoform function. *Physiol. Rev*. **2008**, *88*, 1341–1378.
69. Wright, L.C.; Chen, S.; Roufogalis, B.D. Regulation of the activity and phosphorylation of the plasma membrane Ca^{2+}-ATPase by protein kinase C in intact human erythrocytes. *Arch. Biochem. Biophys*. **1993**, *306*, 277–284.
70. Cohen, C.M.; Gascard, P. Regulation and post-translational modification of erythrocyte membrane and membrane-skeletal proteins. *Semin. Hematol*. **1992**, *29*, 244–292.
71. De Oliveira, S.; Silva-Herdade, A.S.; Saldanha, C. Modulation of erythrocyte deformability by PKC activity. *Clin. Hemorheol. Microcirc*. **2008**, *39*, 363–373.
72. George, A.; Pushkaran, S.; Konstantinidis, D.G.; Koochaki, S.; Malik, P.; Mohandas, N.; Zheng, Y.; Joiner, C.H.; Kalfa, T.A. Erythrocyte NADPH oxidase activity modulated by Rac GTPases, PKC, and plasma cytokines contributes to oxidative stress in sickle cell disease. *Blood* **2013**, *121*, 2099–2107.
73. Ceolotto, G.; Conlin, P.; Clari, G.; Semplicini, A.; Canessa, M. Protein kinase C and insulin regulation of red blood cell Na^+/H^+ exchange. *Am. J. Physiol*. **1997**, *272*, C818–C826.
74. Mohandas, N.; Gallagher, P.G. Red cell membrane: Past, present, and future. *Blood* **2008**, *112*, 3939–3948.
75. Bruce, L.J.; Beckmann, R.; Ribeiro, M.L.; Peters, L.L.; Chasis, J.A.; Delaunay, J.; Mohandas, N.; Anstee, D.J.; Tanner, M.J.A. A band 3-based macrocomplex of integral and peripheral proteins in the RBC membrane. *Blood* **2003**, *101*, 4180–4188.
76. Salomao, M.; Zhang, X.; Yang, Y.; Lee, S.; Hartwig, J.H.; Chasis, J.A.; Mohandas, N.; An, X. Protein 4.1R-dependent multiprotein complex: New insights into the structural organization of the red blood cell membrane. *Proc. Natl. Acad. Sci. USA* **2008**, *105*, 8026–8031.
77. Rivera, A.; de Franceschi, L.; Peters, L.L.; Gascard, P.; Mohandas, N.; Brugnara, C. Effect of complete protein 4.1R deficiency on ion transport properties of murine erythrocytes. *Am. J. Physiol. Cell Physiol.* **2006**, *291*, C880–C886.
78. Hoeflich, K.P.; Ikura, M. Calmodulin in action: Diversity in target recognition and activation mechanisms. *Cell* **2002**, *108*, 739–742.
79. Chin, D.; Means, A.R. Calmodulin: A prototypical calcium sensor. *Trends Cell Biol*. **2000**, *10*, 322–328.
80. Vetter, S.W.; Leclerc, E. Phosphorylation of serine residues affects the conformation of the calmodulin binding domain of human protein 4.1. *Eur. J. Biochem. FEBS* **2001**, *268*, 4292–4299.
81. Gauthier, E.; Guo, X.; Mohandas, N.; An, X. Phosphorylation-dependent perturbations of the 4.1R-associated multiprotein complex of the erythrocyte membrane. *Biochemistry* **2011**, *50*, 4561–4567.
82. Dyrda, A.; Cytlak, U.; Ciuraszkiewicz, A.; Lipinska, A.; Cueff, A.; Bouyer, G.; Egée, S.; Bennekou, P.; Lew, V.L.; Thomas, S.L.Y. Local membrane deformations activate Ca^{2+}-dependent K+ and anionic currents in intact human red blood cells. *PLoS One* **2010**, *5*, e9447.
83. Manno, S.; Takakuwa, Y.; Mohandas, N. Modulation of erythrocyte membrane mechanical function by protein 4.1 phosphorylation. *J. Biol. Chem*. **2005**, *280*, 7581–7587.

84. George, A.; Pushkaran, S.; Li, L.; An, X.; Zheng, Y.; Mohandas, N.; Joiner, C.H.; Kalfa, T.A. Altered phosphorylation of cytoskeleton proteins in sickle red blood cells: The role of protein kinase C, Rac GTPases, and reactive oxygen species. *Blood Cells Mol. Dis*. **2010**, *45*, 41–45.
85. Lorand, L.; Murthy, S.N.P.; Khan, A.A.; Xue, W.; Lockridge, O.; Chishti, A.H. Transglutaminase-mediated remodeling of the human erythrocyte membrane skeleton: Relevance for erythrocyte diseases with shortened cell lifespan. *Adv. Enzymol. Relat. Areas Mol. Biol.* **2011**, *78*, 385–414.
86. Guizouarn, H.; Gabillat, N.; Motais, R.; Borgese, F. Multiple transport functions of a red blood cell anion exchanger, tAE1: Its role in cell volume regulation. *J. Physiol. (Lond.)* **2001**, *535*, 497–506.
87. Gardos, G. The function of calcium in the potassium permeability of human erythrocytes. *Biochim. Biophys. Acta* **1958**, *30*, 653–654.
88. Hamill, O.P. Potassium channel currents in human red blood cells. *J. Physiol. (Lond.)* **1981**, *319*, 97P–98P.
89. Hamill, O.P. Potassium and Chloride Channels in Red Blood Cells. In *Single Channel Recording*; Sakmann, B., Neher, E., Eds.; Plenum Press: New York, NY, USA and London, UK, 1983; pp. 451–471.
90. Grygorczyk, R.; Schwarz, W. Properties of the Ca^{2+}-activated K^+ conductance of human red cells as revealed by the patch-clamp technique. *Cell Calcium* **1983**, *4*, 499–510.
91. Hoffman, J.F.; Joiner, W.; Nehrke, K.; Potapova, O.; Foye, K.; Wickrema, A. The hSK4 (KCNN4) isoform is the Ca^{2+}-activated K^+ channel (Gardos channel) in human red blood cells. *Proc. Natl. Acad. Sci. USA* **2003**, *100*, 7366–7371.
92. Kaestner, L.; Bernhardt, I. Ion channels in the human red blood cell membrane: Their further investigation and physiological relevance. *Bioelectrochemistry* **2002**, *55*, 71–74.
93. Kaestner, L.; Tabellion, W.; Lipp, P.; Bernhardt, I. Prostaglandin E2 activates channel-mediated calcium entry in human erythrocytes: An indication for a blood clot formation supporting process. *Thromb. Haemostasis* **2004**, *92*, 1269–1272.
94. Bassé, F.; Stout, J.G.; Sims, P.J.; Wiedmer, T. Isolation of an erythrocyte membrane protein that mediates Ca^{2+}-dependent transbilayer movement of phospholipid. *J. Biol. Chem.* **1996**, *271*, 17205–17210.
95. Verkleij, A.J.; Zwaal, R.F.; Roelofsen, B.; Comfurius, P.; Kastelijn, D.; van Deenen, L.L. The asymmetric distribution of phospholipids in the human red cell membrane. A combined study using phospholipases and freeze-etch electron microscopy. *Biochim. Biophys. Acta* **1973**, *323*, 178–193.
96. Zhou, Q.; Zhao, J.; Stout, J.G.; Luhm, R.A.; Wiedmer, T.; Sims, P.J. Molecular cloning of human plasma membrane phospholipid scramblase. A protein mediating transbilayer movement of plasma membrane phospholipids. *J. Biol. Chem*. **1997**, *272*, 18240–18244.
97. Morrot, G.; Hervé, P.; Zachowski, A.; Fellmann, P.; Devaux, P.F. Aminophospholipid translocase of human erythrocytes: Phospholipid substrate specificity and effect of cholesterol. *Biochemistry* **1989**, *28*, 3456–3462.

98. Beitner, R. Control of glycolytic enzymes through binding to cell structures and by glucose-1,6-bisphosphate under different conditions. The role of Ca^{2+} and calmodulin. *Int. J. Biochem*. **1993**, *25*, 297–305.
99. Nakashima, K.; Fujii, S.; Kaku, K.; Kaneko, T. Calcium-calmodulin dependent phosphorylation of erythrocyte pyruvate kinase. *Biochem. Biophys. Res. Commun*. **1982**, *104*, 285–289.
100. Campanella, M.E.; Chu, H.; Low, P.S. Assembly and regulation of a glycolytic enzyme complex on the human erythrocyte membrane. *Proc. Natl. Acad. Sci. USA* **2005**, *102*, 2402–2407.
101. Zipser, Y.; Piade, A.; Barbul, A.; Korenstein, R.; Kosower, N.S. Ca^{2+} promotes erythrocyte band 3 tyrosine phosphorylation via dissociation of phosphotyrosine phosphatase from band 3. *Biochem. J.* **2002**, *368*, 137–144.
102. Chu, H.; Low, P.S. Mapping of glycolytic enzyme-binding sites on human erythrocyte band 3. *Biochem. J.* **2006**, *400*, 143–151.
103. Chu, H.; Breite, A.; Ciraolo, P.; Franco, R.S.; Low, P.S. Characterization of the deoxyhemoglobin binding site on human erythrocyte band 3: Implications for O_2 regulation of erythrocyte properties. *Blood* **2008**, *111*, 932–938.
104. Tiffert, T.; Etzion, Z.; Bookchin, R.M.; Lew, V.L. Effects of deoxygenation on active and passive Ca^{2+} transport and cytoplasmic Ca^{2+} buffering in normal human red cells. *J. Physiol. (Lond.)* **1993**, *464*, 529–544.
105. Tiffert, T.; Lew, V.L. Cytoplasmic calcium buffers in intact humanred cells. *J. Physiol. (Lond.)* **1997**, *500*, 139–154.
106. Alderton, W.K.; Cooper, C.E.; Knowles, R.G. Nitric oxide synthases: Structure, function and inhibition. *Biochem. J.* **2001**, *357*, 593–615.
107. Spratt, D.E.; Newman, E.; Mosher, J.; Ghosh, D.K.; Salerno, J.C.; Guillemette, J.G. Binding and activation of nitric oxide synthase isozymes by calmodulin EF hand pairs. *FEBS J.* **2006**, *273*, 1759–1771.
108. Kleinbongard, P.; Schulz, R.; Rassaf, T.; Lauer, T.; Dejam, A.; Jax, T.; Kumara, I.; Gharini, P.; Kabanova, S.; Ozüyaman, B.; *et al.* Red blood cells express a functional endothelial nitric oxide synthase. *Blood* **2006**, *107*, 2943–2951.
109. Ozüyaman, B.; Grau, M.; Kelm, M.; Merx, M.W.; Kleinbongard, P. RBC NOS: Regulatory mechanisms and therapeutic aspects. *Trends Mol. Med.* **2008**, *14*, 314–322.
110. Ulker, P.; Yaras, N.; Yalcin, O.; Celik-Ozenci, C.; Johnson, P.C.; Meiselman, H.J.; Baskurt, O.K. Shear stress activation of nitric oxide synthase and increased nitric oxide levels in human red blood cells. *Nitric Oxide* **2011**, *24*, 184–191.
111. Cave, A.C.; Brewer, A.C.; Narayanapanicker, A.; Ray, R.; Grieve, D.J.; Walker, S.; Shah, A.M. NADPH oxidases in cardiovascular health and disease. *Antioxid. Redox Signal*. **2006**, *8*, 691–728.
112. Mihov, D.; Vogel, J.; Gassmann, M.; Bogdanova, A.Y. Erythropoietin activates nitric oxide synthase in murine erythrocytes. *Am. J. Physiol. Cell Physiol.* **2009**, *297*, C378–C388.
113. Inomata, M.; Nakamura, M., Imajoh-Ohmi, S.; Kawashima, S. A variety of calpain/calpastatin systems in mammalian erythrocytes. *Biochim. Biophys. Acta* **1993**, *1178*, 207–214.
114. Goll, D.E.; Thompson, V.F.; Li, H.; Wei, W.; Cong, J. The calpain system. *Physiol. Rev.* **2003**, *83*, 731–801.

115. Campbell, R.L.; Davies, P.L. Structure–function relationships in calpains. *Biochem. J.* **2012**, *447*, 335–351.
116. Hatanaka, M.; Yoshimura, N.; Murakami, T.; Kannagi, R.; Murachi, T. Evidence for membrane-associated calpain I in human erythrocytes. Detection by an immunoelectrophoretic blotting method using monospecific antibody. *Biochemistry* **1984**, *23*, 3272–3276.
117. Samis, J.A.; Elce, J.S. Immunogold electron-microscopic localization of calpain I in human erythrocytes. *Thromb. Haemost*. **1989**, *61*, 250–253.
118. Molinari, M.; Anagli, J.; Carafoli, E. Ca^{2+}-activated neutral protease is active in the erythrocyte membrane in its nonautolyzed 80-kDa form. *J. Biol. Chem*. **1994**, *269*, 27992–27995.
119. Mortensen, A.M.; Novak, R.F. Dynamic changes in the distribution of the calcium-activated neutral protease in human red blood cells following cellular insult and altered Ca^{2+} homeostasis. *Toxicol. Appl. Pharmacol*. **1992**, *117*, 180–188.
120. Melloni, E.; Salamino, F.; Sparatore, B.; Michetti, M.; Pontremoli, S. Ca2+-dependent neutral proteinase from human erythrocytes: Activation by Ca^{2+} ions and substrate and regulation by the endogenous inhibitor. *Biochem. Int.* **1984**, *8*, 477–489.
121. Wieschhaus, A.; Khan, A.; Zaidi, A.; Rogalin, H.; Hanada, T.; Liu, F.; de Franceschi, L.; Brugnara, C.; Rivera, A.; Chishti, A.H. Calpain-1 knockout reveals broad effects on erythrocyte deformability and physiology. *Biochem. J.* **2012**, *448*, 141–152.
122. Molinari, M.; Maki, M.; Carafoli, E. Purification of mu-calpain by a novel affinity chromatography approach. New insights into the mechanism of the interaction of the protease with targets. *J. Biol. Chem*. **1995**, *270*, 14576–14581.
123. Schwarz-Benmeir, N.; Glaser, T.; Barnoy, S.; Kosower, N.S. Calpastatin in erythrocytes of young and old individuals. *Biochem. J.* **1994**, *304*, 365–370.
124. Glaser, T.; Schwarz-Benmeir, N.; Barnoy, S.; Barak, S.; Eshhar, Z.; Kosower, N.S. Calpain (Ca^{2+}-dependent thiol protease) in erythrocytes of young and old individuals. *Proc. Natl. Acad. Sci. USA* **1994**, *91*, 7879–7883.
125. Rademaker, M.; Thomas, R.H.; Kirby, J.D.; Kovacs, I.B. Calcium influx into red blood cells: The effect of sera from patients with systemic sclerosis. *Clin. Exp. Rheumatol*. **1991**, *9*, 247–251.
126. Hung, T.C.; Pham, S.; Steed, D.L.; Webster, M.W.; Butter, D.B. Alterations in erythrocyte rheology in patients with severe peripheral vascular disease: 1. Cell volume dependence of erythrocyte rigidity. *Angiology* **1991**, *42*, 210–217.
127. Jendryczko, A.; Pardela, M. Abnormal effect of sera from patients with atherosclerosis on calcium influx into normal erythrocytes. *Cor. Vasa* **1992**, *34*, 428–433.
128. Piagnerelli, M.; Boudjeltia, K.Z.; Vanhaeverbeek, M.; Vincent, J.-L. Red blood cell rheology in sepsis. *Intensive Care Med*. **2003**, *29*, 1052–1061.
129. Baskurt, O.; Neu, B.; Meiselman, H.J. *Red Blood Cell Aggregation*; CRC Press: Boca Raton, FL, USA, 2012.
130. Duke, W.W. The relation of blood platelets to hemorrhagic disease. Description of a method for determining the bleeding time and coagulation time and report of three cases of hemorrhagic disease relieved by transfusion. *J. Am. Med. Assoc*. **1910**, *55*, 1185–1192.
131. Hellem, A.J.; Borchgrevink, C.F.; Ames, S.B. The role of red cells in haemostasis: The relation between haematocrit, bleeding time and platelet adhesiveness. *Br. J. Haematol*. **1961**, *7*, 42–50.

132. Andrews, D.A.; Low, P.S. Role of red blood cells in thrombosis. *Curr. Opin. Hematol*. **1999**, *6*, 76–82.
133. Chung, S.M.; Bae, O.N.; Lim, K.M.; Noh, J.Y.; Lee, M.Y.; Jung, Y.S.; Chung, J.H. Lysophosphatidic acid induces thrombogenic activity through phosphatidylserine exposure and procoagulant microvesicle generation in human erythrocytes. *Arterioscl. Thromb. Vasc. Biol.* **2007**, *27*, 414–421.
134. Noh, J.-Y.; Lim, K.-M.; Bae, O.-N.; Chung, S.-M.; Lee, S.-W.; Joo, K.-M.; Lee, S.-D.; Chung, J.-H. Procoagulant and prothrombotic activation of human erythrocytes by phosphatidic acid. *AJP Heart Circ. Physiol*. **2010**, *299*, H347–H355.
135. Steffen, P.; Jung, A.; Nguyen, D.B.; Müller, T.; Bernhardt, I.; Kaestner, L.; Wagner, C. Stimulation of human red blood cells leads to Ca^{2+}-mediated intercellular adhesion. *Cell Calcium* **2011**, *50*, 54–61.
136. Kaestner, L.; Steffen, P.; Nguyen, D.B.; Wang, J.; Wagner-Britz, L.; Jung, A.; Wagner, C.; Bernhardt, I. Lysophosphatidic acid induced red blood cell aggregation *in vitro*. *Bioelectrochemistry* **2012**, *87*, 89–95.
137. Wautier, M.-P.; Nemer, El, W.; Gane, P.; Rain, J.-D.; Cartron, J.-P.; Colin, Y.; le van Kim, C.; Wautier, J.-L. Increased adhesion to endothelial cells of erythrocytes from patients with polycythemia vera is mediated by laminin alpha5 chain and Lu/BCAM. *Blood* **2007**, *110*, 894–901.
138. Yedgar, S.; Kaul, D.K.; Barshtein, G. RBC adhesion to vascular endothelial cells: More potent than RBC aggregation in inducing circulatory disorders. *Microcirculation* **2008**, *15*, 581–583.
139. Wautier, M.-P.; Héron, E.; Picot, J.; Colin, Y.; Hermine, O.; Wautier, J.-L. Red blood cell phosphatidylserine exposure is responsible for increased erythrocyte adhesion to endothelium in central retinal vein occlusion. *J. Thromb. Haemost*. **2011**, *9*, 1049–1055.
140. Miller, B.A.; Cheung, J.Y. Mechanisms of erythropoietin signal transduction: Involvement of calcium channels. *Proc. Soc. Exp. Biol. Med*. **1994**, *206*, 263–267.
141. Schaefer, A.; Magócsi, M.; Marquardt, H. Signalling mechanisms in erythropoiesis: The enigmatic role of calcium. *Cell. Signal*. **1997**, *9*, 483–495.
142. Cheung, J.Y.; Zhang, X.Q.; Bokvist, K.; Tillotson, D.L.; Miller, B.A. Modulation of calcium channels in human erythroblasts by erythropoietin. *Blood* **1997**, *89*, 92–100.
143. Miller, B.A.; Cheung, J.Y.; Tillotson, D.L.; Hope, S.M.; Scaduto, R.C. Erythropoietin stimulates a rise in intracellular-free calcium concentration in single BFU-E derived erythroblasts at specific stages of differentiation. *Blood* **1989**, *73*, 1188–1194.
144. De Haro, C.; de Herreros, A.G.; Ochoa, S. Protein phosphorylation and translational control in reticulocytes: Activation of the heme-controlled translational inhibitor by calcium ions and phospholipid. *Curr. Top. Cell. Regul*. **1985**, *27*, 63–81.
145. Liu, J.; Guo, X.; Mohandas, N.; Chasis, J.A.; An, X. Membrane remodeling during reticulocyte maturation. *Blood* **2010**, *115*, 2021–2027.
146. Bookchin, R.M.; Lew, V.L.; Roth, E.F. Elevated Red Cell Calcium: Innocent Bystander or Kiss of Death? In *Cellular and Molecular Aspects of Aging: The Red Cell as a Model*; Eaton, J.W., Ed.; John Wiley & Sons: New York, NY, USA, 1985; pp. 369–375.

147. Clark, M.R. Senescence of red blood cells: Progress and problems. *Physiol. Rev*. **1988**, *68*, 503–554.
148. Friederichs, E.; Meiselman, H.J. Effects of calcium permeabilization on RBC rheologic behavior. *Biorheology* **1994**, *31*, 207–215.
149. Bosman, G.J.; Willekens, F.L.; Werre, J.M. Erythrocyte aging: A more than superficial resemblance to apoptosis? *Cell Physiol. Biochem*. **2005**, *16*, 1–8.
150. Mohandas, N.; Groner, W. Cell membrane and volume changes during red cell development and aging. *Ann. N. Y. Acad. Sci*. **1989**, *554*, 217–224.
151. Lutz, H.U. Innate immune and non-immune mediators of erythrocyte clearance. *Cell. Mol. Biol. (Noisy-le-grand)* **2004**, *50*, 107–116.
152. Lew, V.L.; Daw, N.; Etzion, Z.; Tiffert, T.; Muoma, A.; Vanagas, L.; Bookchin, R.M. Effects of age-dependent membrane transport changes on the homeostasis of senescent human red blood cells. *Blood* **2007**, *110*, 1334–1342.
153. Rice, L.; Alfrey, C.P. The negative regulation of red cell mass by neocytolysis: Physiologic and pathophysiologic manifestations. *Cell Physiol. Biochem*. **2005**, *15*, 245–250.
154. Risso, A.; Turello, M.; Biffoni, F.; Antonutto, G. Red blood cell senescence and neocytolysis in humans after high altitude acclimatization. *Blood Cells Mol. Dis*. **2007**, *38*, 83–92.
155. Chang, C.-C.; Chen, Y.; Modi, K.; Awar, O.; Alfrey, C.; Rice, L. Changes of red blood cell surface markers in a blood doping model of neocytolysis. *J. Investig. Med*. **2009**, *57*, 650–654.
156. Nguyen, D.B.; Wagner-Britz, L.; Maia, S.; Steffen, P.; Wagner, C.; Kaestner, L.; Bernhardt, I. Regulation of phosphatidylserine exposure in red blood cells. *Cell Physiol. Biochem*. **2011**, *28*, 847–856.
157. Eaton, J.W.; Skelton, T.D.; Swofford, H.S.; Kolpin, C.E.; Jacob, H.S. Elevated erythrocyte calcium in sickle cell disease. *Nature* **1973**, *246*, 105–106.
158. Etzion, Z.; Tiffert, T.; Bookchin, R.M.; Lew, V.L. Effects of deoxygenation on active and passive Ca^{2+} transport and on the cytoplasmic Ca^{2+} levels of sickle cell anemia red cells. *J. Clin. Invest*. **1993**, *92*, 2489–2498.
159. Joiner, C.H.; Jiang, M.; Franco, R.S. Deoxygenation-induced cation fluxes in sickle cells. IV. Modulation by external calcium. *Am. J. Physiol*. **1995**, *269*, C403–C409.
160. Wiley, J.S. Increased erythrocyte cation permeability in thalassemia and conditions of marrow stress. *J. Clin. Invest*. **1981**, *67*, 917–922.
161. Shalev, O.; Mogilner, S.; Shinar, E.; Rachmilewitz, E.A.; Schrier, S.L. Impaired erythrocyte calcium homeostasis in beta-thalassemia. *Blood* **1984**, *64*, 564–566.
162. Bookchin, R.M.; Ortiz, O.E.; Shalev, O.; Tsurel, S.; Rachmilewitz, E.A.; Hockaday, A.; Lew, V.L. Calcium transport and ultrastructure of red cells in beta-thalassemia intermedia. *Blood* **1988**, *72*, 1602–1607.
163. Sabina, R.L.; Waldenström, A.; Ronquist, G. The contribution of Ca+ calmodulin activation of human erythrocyte AMP deaminase (isoform E) to the erythrocyte metabolic dysregulation of familial phosphofructokinase deficiency. *Haematologica* **2006**, *91*, 652–655.
164. Bookchin, R.M.; Ortiz, O.E.; Somlyo, A.V.; Somlyo, A.P.; Sepulveda, M.I.; Hockaday, A.; Lew, V.L. Calcium-accumulating inside-out vesicles in sickle cell anemia red cells. *Trans. Assoc. Am. Phys*. **1985**, *98*, 10–20.

165. Lew, V.L.; Hockaday, A.; Sepulveda, M.I.; Somlyo, A.P.; Somlyo, A.V.; Ortiz, O.E.; Bookchin, R.M. Compartmentalization of sickle-cell calcium in endocytic inside-out vesicles. *Nature* **1985**, *315*, 586–589.
166. Eaton, W.A.; Hofrichter, J. Sickle cell hemoglobin polymerization. *Adv. Protein Chem*. **1990**, *40*, 263–279.
167. Vandorpe, D.H.; Xu, C.; Shmukler, B.E.; Otterbein, L.E.; Trudel, M.; Sachs, F.; Gottlieb, P.A.; Brugnara, C.; Alper, S.L. Hypoxia activates a Ca^{2+}-permeable cation conductance sensitive to carbon monoxide and to GsMTx-4 in human and mouse sickle erythrocytes. *PLoS One* **2010**, *5*, e8732.
168. Ortiz, O.E.; Lew, V.L.; Bookchin, R.M. Calcium accumulated by sickle cell anemia red cells does not affect their potassium (86Rb+) flux components. *Blood* **1986**, *67*, 710–715.
169. Rhoda, M.D.; Apovo, M.; Beuzard, Y.; Giraud, F. Ca^{2+} permeability in deoxygenated sickle cells. *Blood* **1990**, *75*, 2453–2458.
170. Clark, M.R.; Rossi, M.E. Permeability characteristics of deoxygenated sickle cells. *Blood* **1990**, *76*, 2139–2145.
171. De Franceschi, L.; Franco, R.S.; Bertoldi, M.; Brugnara, C.; Matte, A.; Siciliano, A.; Wieschhaus, A.J.; Chishti, A.H.; Joiner, C.H. Pharmacological inhibition of calpain-1 prevents red cell dehydration and reduces Gardos channel activity in a mouse model of sickle cell disease. *FASEB J.* **2013**, *27*, 750–759.
172. Siciliano, A.; Turrini, F.; Bertoldi, M.; Matte, A.; Pantaleo, A.; Olivieri, O.; de Franceschi, L. Deoxygenation affects tyrosine phosphoproteome of red cell membrane from patients with sickle cell disease. *Blood Cells Mol. Dis.* **2010**, *44*, 233–242.
173. Rank, B.H.; Hebbel, R.P.; Carlsson, J. Oxidation of membrane thiols in sickle erythrocytes. *Prog. Clin. Biol. Res*. **1984**, *165*, 473–477.
174. Wood, K.C.; Hebbel, R.P.; Lefer, D.J.; Granger, D.N. Critical role of endothelial cell-derived nitric oxide synthase in sickle cell disease-induced microvascular dysfunction. *Free Radic. Biol. Med*. **2006**, *40*, 1443–1453.
175. Hebbel, R.P. Perspectives series: Cell adhesion in vascular biology. Adhesive interactions of sickle erythrocytes with endothelium. *J. Clin. Invest*. **1997**, *99*, 2561–2564.
176. Antonelou, M.H.; Tzounakas, V.L.; Velentzas, A.D.; Stamoulis, K.E.; Kriebardis, A.G.; Papassideri, I.S. Effects of pre-storage leukoreduction on stored red blood cells signaling: A time-course evaluation from shape to proteome. *J. Proteomics* **2012**, *76*, 220–238.
177. Schrier, S.L.; Sohmer, P.R.; Moore, G.L.; Ma, L.; Junga, I. Red blood cell membrane abnormalities during storage: Correlation with *in vivo* survival. *Transfusion* **1982**, *22*, 261–265.
178. Wolfe, L. The red cell membrane and the storage lesion. *Clin. Haematol*. **1985**, *14*, 259–276.
179. Chin-Yee, I.H.; Gray-Statchuk, L.; Milkovich, S.; Ellis, C.G. Transfusion of stored red blood cells adhere in the rat microvasculature. *Transfusion* **2009**, *49*, 2304–2310.
180. Chaudhary, R.; Katharia, R. Oxidative injury as contributory factor for red cells storage lesion during twenty eight days of storage. *Blood Transfus*. **2012**, *10*, 59–62.
181. Kaestner, L.; Juzeniene, A.; Moan, J. Erythrocytes-the "house elves" of photodynamic therapy. *Photochem. Photobiol. Sci.* **2004**, *3*, 981–989.

182. Kaestner, L. Evaluation of human erythrocytes as model cells in photodynamic therapy. *Gen. Physiol. Biophys*. **2003**, *22*, 455–465.
183. Muller, O.; Tian, Q.; Zantl, R.; Kahl, V.; Lipp, P.; Kaestner, L. A system for optical high resolution screening of electrical excitable cells. *Cell Calcium* **2010**, *47*, 224–233.
184. Kaestner, L. *Calcium Signalling. Approaches and Findings in the Heart and Blood*; Springer: Heidelberg, Germany, 2013.
185. Minetti, G.; Egée, S.; Mörsdorf, D.; Steffen, P.; Makhro, A.; Achilli, C.; Ciana, A.; Wang, J.; Bouyer, G.; Bernhardt, I.; *et al.* Red cell investigations: Art and artefacts. *Blood Rev*. **2013**, *27*, 91–101.
186. Wang, J.; Wagner-Britz, L.; Bogdanova, A.; Ruppenthal, S.; Wiesen, K.; Kaiser, E.; Tian, Q.; Krause, E.; Bernhardt, I.; Lipp, P.; *et al.* Morphologically homogeneous red blood cells present a heterogeneous response to hormonal stimulation. *PLoS One* **2013**, submitted for publication.

Review 2

Red cell investigations: art and artefacts

Minetti G, Egée S, Mörsdorf D, Steffen P, **Makhro A**, Achilli C, Ciana A, Wang J, Bouyer G, Bernhardt I, Wagner C, Thomas S, Bogdanova A, Kaestner L.

Blood Rev. 2013 Mar;27(2):91-101. Doi: 10.1016/j.blre.2013.02.002. Epub 2013 Feb 18.

Contribution:

Makhro A. participated in writing and produced results on Figure 2.

Blood Reviews 27 (2013) 91–101

Contents lists available at SciVerse ScienceDirect

Blood Reviews

journal homepage: www.elsevier.com/locate/blre

REVIEW

Red cell investigations: Art and artefacts

Giampaolo Minetti [a,b,1,2], Stephane Egée [a,c,1,3], Daniel Mörsdorf [a,d,1,4], Patrick Steffen [a,e,1,5], Asya Makhro [a,f,1,6], Cesare Achilli [a,b,1,2], Annarita Ciana [a,b,1,2], Jue Wang [a,g,1,7], Guillaume Bouyer [a,c,1,3], Ingolf Bernhardt [a,d,1,8], Christian Wagner [a,e,1,9], Serge Thomas [a,c,1,3], Anna Bogdanova [a,f,1,6], Lars Kaestner [a,g,*,1,10]

[a] European Red Cell Society, Europe
[b] Department of Biology and Biotechnology "L. Spallanzani", Laboratories of Biochemistry, University of Pavia, 27100 Pavia, Italy
[c] Station Biologique de Roscoff, UMR7150 Mer & Santé, 29680 Roscoff, France
[d] Biophysics Laboratory, Saarland University, Building A2 4, 66123 Saarbrücken, Germany
[e] Experimental Physics Department, Building E2 6, Saarland University, 66123 Saarbrücken, Germany
[f] Institute of Veterinary Physiology and the Zurich Center for Integrative Human Physiology (ZIHP), University of Zurich, Zurich, Switzerland
[g] Institute for Molecular Cell Biology and Research Centre for Molecular Imaging and Screening, School of Medicine, Saarland University, Building 61, 66421 Homburg/Saar, Germany

ARTICLE INFO

Keywords:
Erythrocytes
Biochemical analysis
Flux measurements
Flow cytometry
Patch-clamp
Fluorescence imaging
Optical tweezers
Atomic force microscopy

ABSTRACT

Red blood cell research is important for both, the clinical haematology, such as transfusion medicine or anaemia investigations, and the basic research fields like exploring general membrane physiology or rheology.
Investigations of red blood cells include a wide spectrum of methodologies ranging from population measurements with a billion cells evaluated simultaneously to single-cell approaches. All methods have a potential for pitfalls, and the comparison of data achieved by different technical approaches requires a consistent set of standards.
Here, we give an overview of common mistakes using the most popular methodologies in red blood cell research and how to avoid them. Additionally, we propose a number of standards that we believe will allow for data comparison between the different techniques and different labs. We consider biochemical analysis, flux measurements, flow cytometry, patch-clamp measurements and dynamic fluorescence imaging as well as emerging single-cell techniques, such as the use of optical tweezers and atomic force microscopy.

1. Introduction

Contrary to a common belief, the red blood cell (RBC) is a cell type that is neither simple, nor easily obtainable in a pure form. Yet, it is probably the most studied cell type in the history of the life sciences starting with the microscopic observations of Jan Swammerdam in approximately 1660.[1] Nevertheless, as in most other fields of science, contradictory data are common. Sometimes it is possible to unify initially opposing results, e.g., reconciling reports on the electrogenic permeabilities in malaria-infected RBCs[2,3] or on the isolation of lipid rafts from RBCs.[4–6] In other cases, specific issues have not been completely resolved, for example, the number of Gardos channels per RBC[7,8] or contradictory data regarding prostaglandin E_2-induced cation fluxes.[9–11] However, discrepancies often originate from different experimental protocols, inducing different or even opposing degrees of artefacts. Sometimes, artefacts may lead to completely wrong conclusions. This is a serious problem, as revealed in a recent publication[12] in Nature. Here, a standard method intended for the isolation of mononuclear cells (MNCs), based on the density-gradient centrifugation of blood, was mistakenly used to isolate RBCs in an allegedly pure form. This artefact affects the entire paper, but it obviously passed the review process in one of the most prestigious journals.

To avoid this and other common artefacts, as well as to establish a basis for good laboratory practices in RBC research, a subgroup of the European Red Cell Society (ERCS) was formed to initiate standards for a better inter-methodological as well as inter-laboratory comparison

* Corresponding author at: Institute for Molecular Cell Biology and Research Centre for Molecular Imaging and Screening, School of Medicine, Saarland University, Building 61, 66421 Homburg/Saar, Germany. Tel./fax: +49 6841 1626 149/104.
E-mail addresses: minetti@unipv.it (G. Minetti), egee@sb-roscoff.fr (S. Egée), d.moersdorf@mx.uni-saarland.de (D. Mörsdorf), p.steffen@mx.uni-saarland.de (P. Steffen), makhro@vetphys.uzh.ch (A. Makhro), cesare.achilli@unipv.it (C. Achilli), annarita.ciana@unipv.it (A. Ciana), anjwan@uniklinikum-saarland.de (J. Wang), bouyer@sb-roscoff.fr (G. Bouyer), i.bernhardt@mx.uni-saarland.de (I. Bernhardt), c.wagner@mx.uni-saarland.de (C. Wagner), thomas@sb-roscoff.fr (S. Thomas), annab@access.uzh.ch (A. Bogdanova), lars_kaestner@me.com (L. Kaestner).
[1] www.EARCR.nl.
[2] Tel./fax: +39 0382 987 891/240.
[3] Tel./fax: +33 298 2923 82/24.
[4] Tel./fax: +49 681 302 64163/6690.
[5] Tel./fax: +49 681 302 2977/4676.
[6] Tel./fax: +41 44 6358 811/932.
[7] Tel./fax: +49 6841 1626 103/104.
[8] Tel./fax: +49 681 302 6689/6690.
[9] Tel./fax: +49 681 302 3003/4676.
[10] Tel./fax: +49 6841 1626 149/104.

0268-960X
http://dx.doi.org/10.1016/j.blre.2013.02.002

of RBC-derived data. As an initial attempt, here, we present the first "guidelines" for avoiding artefacts in RBC research: In the first part, we discuss the general challenges, such as obtaining pure RBC preparations, experimental conditions in general and the comparison of studies between different species. In the second part, we review a selection of methods in RBC research, discussing possible pitfalls, how to avoid them and the conditions for comparing/combining different methodologies. Obviously, this cannot be a comprehensive selection, but covers a bunch of the most popular methods and emerging technologies.

Our hope is that this report will be useful to all scientists approaching the study of RBCs or considering RBC research, to avoid stumbling into major artefactual conditions and obtaining or concluding the best from the experiments.

2. Ethics

The data presented in this paper has been acquired after approval by the local ethical committees related to the authors institutions.

3. General considerations

3.1. Obtaining pure cell preparations

The vast majority of biochemical studies, but also all other types of cell population measurements, have been carried out, and still are, using bulk suspensions of supposedly pure RBCs. The RBCs are obtained by sedimenting the cells by centrifugation from a sample of whole blood that has been "washed" with variants of a physiologic solution, followed by removal of the supernatant and the thin superficial layer of cells. The latter, the so-called "buffy-coat", is indeed enriched in white blood cells (WBCs), or leukocytes, but these cells belong chiefly to the MNC type, i.e., lymphocytes and monocytes. The most abundant WBCs, however, the polymorphonuclear neutrophil granulocytes (PMNs), tend to remain mixed with the RBCs owing to the similar density of the two cell types, contaminating the RBC sample.[6] The only way of removing most of the WBCs is by filtering the blood with leukodepletion filters. Roughly speaking, if the total content of PMNs per million RBCs is 1000 in whole blood, it will decrease, at best, to 100 in washed blood and to <10 in filtered blood.[6]

3.1.1. Purification of RBCs

A simple and reliable procedure for RBC purification that is suitable for samples of small volumes and easy to implement in every lab is filtration through cellulose, as was originally proposed by Beutler et al.[13] and described in detail in the supplementary material of Achilli et al.[14]

We propose this simple concept as a standard method and good laboratory practice in RBC research. It should be emphasised, however, that filtration might not be applicable in all instances, e.g., for pathological RBCs, because its functioning principle appears to be based largely on the difference in deformability between RBCs and WBCs.[15] The latter are much less deformable than normal RBCs and are therefore retained in the filter for a longer time than RBCs. However, in certain RBC pathologies, RBC deformability is abnormally reduced, and this may result in reduced filterability (hereditary spherocytosis, hereditary elliptocytosis, ovalocytosis, sickle cell anaemia).

3.1.2. Quantifying RBC purity

The task of quantifying low WBC levels is by no means a simple one, and special techniques have been devised for this purpose. As a general remark, microscope counting using conventional haemocytometer chambers is impractical and not sensitive enough. The flow cytometry (FCM) approach is meaningful only if the number of total events counted in each analysis is sufficiently high to reveal 1 WBC per 10^6 RBCs, which implies long analysis times.[16] An extremely sensitive and inexpensive method for the quantification of PMNs in blood samples that can be easily implemented in all labs is the technique of gelatin zymography, as recently adapted.[14]

3.1.3. Consequences of contaminated RBC suspensions

The consequences of having a PMN-contaminated RBC suspension can be deleterious. Two main types of artefacts can result from such a situation: (i) attribution to the RBCs of a component/function that in fact belongs to the PMNs; (ii) damage to RBCs resulting from hydrolases and oxidases released by activated or broken PMNs.

The first issue has already been exemplified in the Introduction. The wrong method used in a recent Nature article[12] for the purification of RBCs results, instead, in the isolation of a fraction of RBCs together with all the PMNs that were originally present in the blood sample, without even reducing the number of PMNs, as would occur if a conventional centrifugation-based wash of the blood and removal of the "buffy-coat" were performed. Fig. 1A indicates the amount of PMNs left by different separation methods.

The artefactual results that originate from PMN hydrolases damaging RBC components are exemplified by the controversy on the isolation and characterisation of lipid rafts from RBCs.[6] The most powerful and constitutively active hydrolases in the PMNs are the serine proteases elastase and cathepsin G. These hydrolases are normally confined at high concentrations in cytoplasmic vesicles (granules) and only released upon cell activation. Detergents can easily free the proteases from the granules. It was shown that even the presence of one PMN per million RBCs is able to release enough proteolytic power to damage, if not fully inhibited, highly sensitive RBC proteins such as ankyrin and protein 4.1.[6]

Another common situation that could give rise to artefactual results is the preparation of "ghosts" from RBCs by hypotonic haemolysis.[17] If the RBCs are contaminated by PMNs and the buffers used are not effectively supplemented with anti-proteases, the RBC membrane proteins will almost certainly be damaged (Fig. 1B, C). The workaround to this problem is the filtration of the blood and the use of freshly prepared lysing buffers containing a working concentration of anti-proteases.

3.2. Experimental conditions

Other factors that must be standardised to be able to compare the obtained data between different laboratories are the temperature, shear stress, medium content, especially traces of serum, and the condition of cells used in the experiments. Furthermore, recent studies emphasise the importance of co-factors and substrates of several receptors, which may contribute to the experimental outcome.

3.2.1. Possible artefacts and their causes

3.2.1.1. The influence of temperature. Temperature-related artefacts include ion misbalance and the ensuing changes in cell volume and Ca^{2+}-dependent processes. Temperature sensitivity depends on the particular approach, but it can be severe, differing, e.g., between different types of ion transporters. The decrease in the activity of ion transporters with a decrease in temperature by 10° (Q10) is approximately 30-fold for the Ca^{2+} pump,[18] approximately 3-fold for the Na^+/K^+ pump[19] and approximately 1.5–3-fold for most of the ion transporter systems.[20,21] Thus, temperature changes may have a pronounced effect on the intracellular Ca^{2+} levels and the Na^+/K^+ distribution. The temperature may not necessarily be fixed at 37 °C in particular experimental settings (e.g., controlling the temperature can be complicate for patch-clamp investigations). However, temperature as a factor has to be taken into account, and the potential side effects must be controlled.

3.2.1.2. Impact of medium supplements. Serum and the multiple biologically active factors it contains, including albumin and factors bound to it, such as interleukins, prostaglandins, insulin and amino acids,

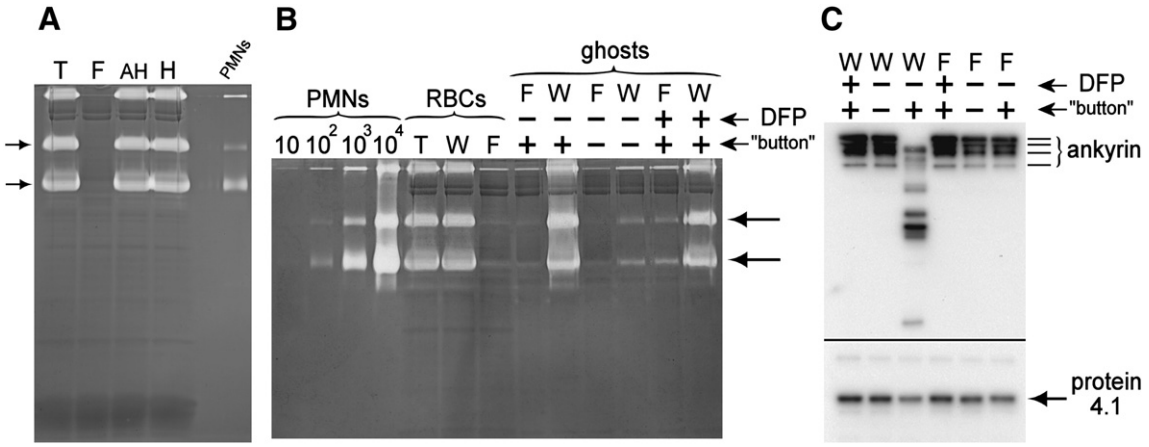

Fig. 1. (A) Gelatin zymography of the pelleted cell fraction obtained by the "Accuspin™ System-Histopaque®-1077" method (Sigma-Aldrich, Inc., St. Louis, MO, USA) used in a recent work for isolating RBCs in supposedly pure form.[12] As per the manufacturer's instructions, a blood sample was freshly drawn in 0.1 volumes of 3.8% (w/v) tri-sodium citrate as the anticoagulant and immediately layered in the Accuspin™ tube. After centrifugation, the RBC pellet was collected (after removal of the septum from the Accuspin™ tube), washed two times in ten volumes of PBS and processed for gelatin zymography, as previously described.[14] The arrows indicate the bands corresponding to the typical pattern of in-gel digestion of gelatin by the granulocytic pro-metalloproteinase 9 and its higher molecular weight aggregate with lipocalin and are indicative of the presence of PMNs in the RBC fractions. The lane marked "T" corresponds to unseparated blood cells. The lane marked "F" contains a sample of RBCs that was passed through a cellulose filter to remove leukocytes and platelets and is indeed free of PMNs. The pellet of supposedly pure RBCs resulting from the Accuspin™ separation contains almost all of the PMNs that were present in the unseparated blood ("AH"). The lane marked "H" is a sample of RBCs obtained by density centrifugation in the Histopaque®-1077 solution but in a standard tube (not Accuspin™). In each lane, the equivalent of 10^7 cells was loaded. In the lane "PMNs", 2×10^2 pure PMNs were loaded. (B) Contaminating PMNs are carried all along during the preparation of ghost membranes, and they ended up in the final sample of supposedly pure ghosts. PMNs were detected using gelatin zymography[14] in ghosts prepared from washed ("W") or filtered ("F") RBCs with the method of Dodge[17] as previously detailed,[5] but with the omission of phenyl-methyl-sulphonyl-fluoride to show the consequences of proteolysis. Where proteolysis was inhibited, diisopropylfluorophosphate (DFP) was used at a final concentration of 1 mM in PBS, to pre-treat RBCs for 5 min at 25 °C before hypotonic haemolysis to prepare the ghosts. During ghost preparation, at the end of the third sedimentation, the **"**button**"** of dark, thick material that forms at the bottom of the ghosts and that is especially visible in samples where contamination by PMNs is high was either removed or left in place ("button" − or +). After preparation, the ghost suspension was brought to the volume of the original packed RBCs and processed for gelatin zymography as described.[14] In each lane, the equivalent of 10^7 RBCs was loaded. Pure PMNs were loaded as a standard in the adjacent lanes, in the numbers given. (C) The ghosts prepared in the various modes described above were processed for SDS-PAGE and Western blotting. Analysis of ankyrin and protein 4.1 revealed that both proteins were quantitatively decreased when the ghosts were prepared from filtered or washed RBCs in the absence of DFP. When the "button" of debris was not removed, both proteins were heavily damaged.

can introduce artefacts. Depending on the experimental settings, investigations are conducted in serum-containing or serum-free media. Proteins introduced with serum have been shown to play an active role in regulating the activity of ion transporters in RBCs obtained from healthy and diseased subjects. Little is known about the serum components mediating the effects. It has been shown that lysophosphatidic acid (LPA) activates Ca^{2+} uptake by RBCs.[22] Insulin interacts with its receptors, inducing activation of endothelial nitric oxide synthase (eNOS) in RBCs.[23] From studies on malaria-infected cells, it is now well recognised that traces of serum change the membrane conductance upon infection.[2,24] Nevertheless, such a phenomenon may also be observed when performing experiments on uninfected cells.[25] This leads to the conclusion that serum-proteins play a role in modulating the activity of transport proteins.[26] This is a potential source of discrepancy between single cell and bulk measurements. In most of the latter, at least serum albumin is present (usually 5%) as a supplement in the suspending medium. The presence of several amino acids in the incubation medium makes a substantial difference in the response of cells to oxygen, insulin and erythropoietin stimulation. Among these amino acids are L-arginine, which is a substrate for eNOS,[27] and the N-methyl D-aspartate receptor agonists glutamate and glycine, as well as homocysteine, which stimulates Ca^{2+} uptake by human and rat RBCs.[28] Treatment of RBCs with relatively high concentrations of orthovanadate, the most popular Ca^{2+} pump inhibitor, in the presence of 1–2 mM extracellular Ca^{2+} results in irreversible pathological alterations of cell morphology, followed by blebbing and finally the loss of membrane integrity, particularly at room temperature when the Ca^{2+} pump function is reduced (Fig. 2A). This often remains unnoticed when working with RBC suspensions.

3.2.1.3. Pre-treatment of RBCs. Intercellular differences originating from storage (fresh cells vs. stored cells and storage conditions), inter-individual and inter-cellular variability are sources of artefacts. Often, stored/conserved RBCs are used for measurements. RBC preservation media are Ca^{2+}-free, low in Na^+ and enriched with K^+ and glucose. RBC preservation results in gradual adenosine triphosphate (ATP) and 2,3-bisphosphoglycerate deprivation and oxidation of glutathione, which begin after one day of storage. Replacement of the storage medium with Ca^{2+}-containing plasma-like medium (1.8 mM $CaCl_2$, 150 mM NaCl, 4 mM KCl, 5 mM glucose) results in acute morphological alterations illustrated in Fig. 2B. The cells will shrink due to acute Ca^{2+} overload, and further ATP deprivation occurs due to acute activation of the Na^+/K^+ pump and Ca^{2+} pump caused by acute Na^+ and Ca^{2+} overload. The results obtained using such cells may hardly be compared with those obtained from fresh RBCs. Restitution of stored cells may be useful for avoiding storage-induced artefacts. Preconditioning of stored blood (rejuvenation) has been proposed,[29] and the corresponding "Rejuvenation Solution" (Rejuvesol; enCyte Systems, Inc., Braintree, Mass) containing phosphate, inosine, pyruvate, and adenine, or 15 mM D-ribose was shown to be beneficial when applied before the transfusion.[30] Because the components of rejuvenation solutions actively interfere with intracellular metabolism and the redox state, we propose to use a "minimally invasive" preconditioning protocol. The stored cells are re-suspended in the incubation medium of interest in the presence 0.5 mM Ca^{2+}, 10 mM glucose and 0.1% BSA at room temperature one hour prior to the experiment. This time is required to restore the activity of the Ca^{2+} pump at a sub-physiological temperature and to provide substrates for glycolytic enzymes.

3.2.1.4. Consequences of different conditions. Most artefacts arise from the lack of attention to these factors. The composition of incubation media varies markedly between experiments. The impact of oxidation, methaemoglobinemia, phosphatidyl serine (PS) exposure and other membrane-related events, as well as that of the addition of ion transport inhibitors (e.g., vanadate often present during Ca^{2+} uptake measurements, see Fig. 2A), on the cell morphology, ion content,

redox state and metabolic status may be dramatic, but it has rarely been taken into account.

The redox status of the cells is an important parameter to control. Oxidation has a profound effect on metabolism, regulation of cell volume, and cytoskeletal structure. Reducing cell deformability induces Ca^{2+} entry, leading to PS exposure, membrane blebbing and eventually premature cell death.[31] Nevertheless, it was also shown that oxidation may activate anion channels, mimicking pathways that are activated upon malaria infection.[32,33] Even if the threshold seems to be rather high, the oxidation level might be high enough in some cells to trigger artificial responses in some protocols. Most importantly, throughout their lifetime, RBCs are continuously exposed to high oxidative stress. Oxidative defence capacities may decrease with RBC aging,[34] and senescent RBCs show alterations (e.g., increased denaturation of haemoglobin, membrane binding of hemichromes and free iron, aggregation of band 3 protein, deposition of antibodies and complement fragments, PS exposure) similar to those of oxidised cells.[35,36]

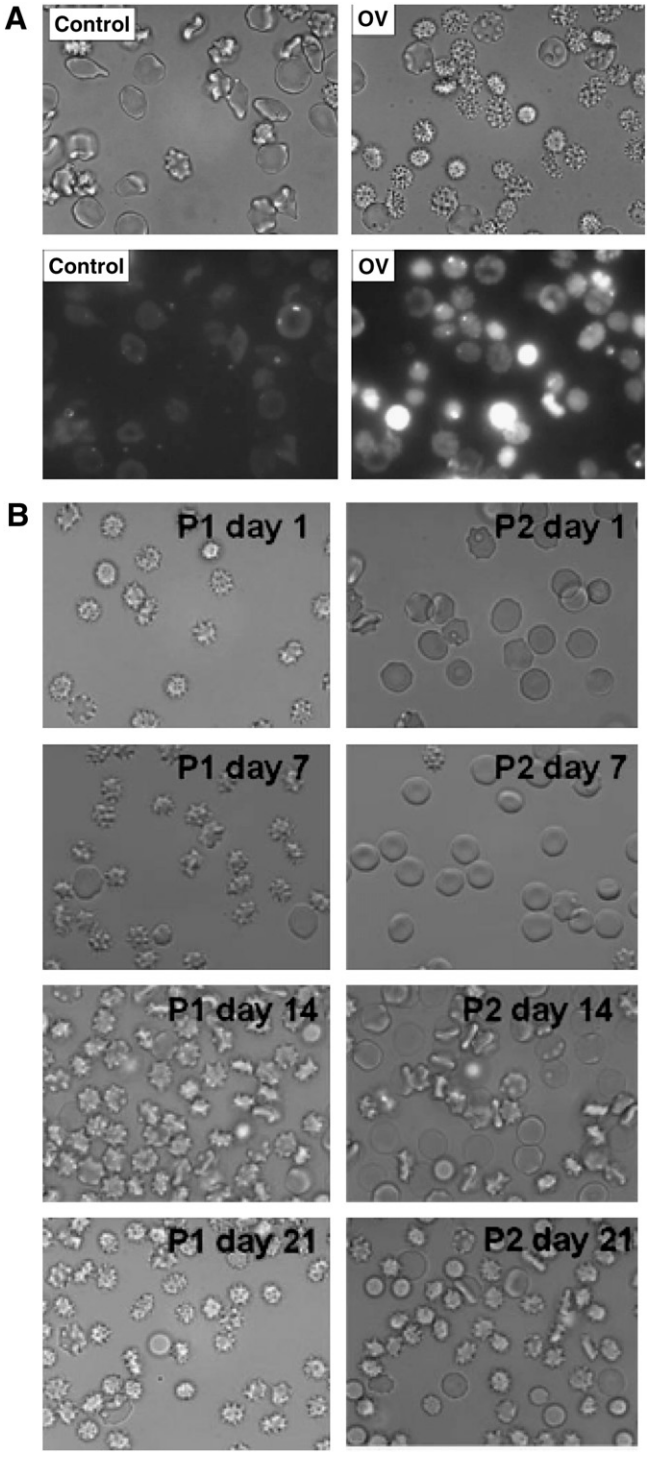

Facilitated ageing occurring under conditions of shear stress (e.g., in patients with polycythaemia) is also associated with oxidative stress.[37] Furthermore, storage of RBCs results in progressive oxidative stress and loss of reduced glutathione along with ATP deprivation. For that reason experimental observations obtained using RBCs from a blood bank may differ significantly from those generated using freshly withdrawn blood. Further support comes from whole-cell patch-clamp experiments reporting oxidation induced anion selective currents.[32,38,39]

Sufficient levels of glucose, a lack of Ca^{2+} overload and shear stress are essential for maintenance of the glutathione pool. Recent studies revealed that some plasma components are required for eNOS to function. L-arginine (100–300 μM) and nitrite (~150 nM in human plasma) are essential for maintenance of NO production by RBCs under normoxic and hypoxic conditions, respectively,[23,40] and their absence in the incubation medium, as well as manipulation of the intracellular Ca^{2+} levels, will result in uncoupling of NO production and progressive oxidative stress, especially when the treatment includes manipulation of oxygen levels or activation of eNOS.[27,28,41]

Another example of the importance of the ionic composition of the incubation media arises from patch-clamp measurements of malaria-infected RBCs: Whereas at physiological saline concentrations, at least two different types of anion channel activity can be described, when supraphysiological concentrations of Cl^- are used,[42,43] one of the channels has (i) a saturated single conductance and (ii) an open probability close to zero above the threshold chloride concentration.[3] This last phenomenon explains the majority of the discrepancies reported in the field, and it is tempting to think that the same limitation may apply to uninfected RBCs.

3.3. Interspecies studies

The challenge of how to compare studies performed in different species is widespread in biomedical science. The power of genetic manipulation in combination with the short generation cycle makes mice an increasingly popular animal model. Obvious advantages often overwhelm concerns about the reliability of results derived from animal models of human diseases. This problem also applies to RBC research and originates from the fact that the basic characterisation of mouse RBCs is rather limited. Before the advent of transgenic animals, mice were not a particularly widespread model for studying RBCs.

3.3.1. Potentials of comparative studies

Comparative RBC research continues to build on species-specific studies involving, e.g., domestic animals. In this field, a substantial number of publications and even textbooks are available.[44,45] Sometimes,

Fig. 2. (A) Changes in morphology and in the intracellular Ca^{2+} levels in RBCs from a sickle cell patient caused by inhibition of the Ca^{2+} pump. RBCs from a sickle cell disease patient suspended in isotonic medium containing 1.8 mM $CaCl_2$, 10 mM glucose and 0.1% bovine serum albumin. The cells were loaded with 10 μM Fluo-4AM for 40 min in the presence or absence of 5 mM Na-orthovanadate (OV). The upper panels show bright field images of control and orthovanadate-treated cells, and the lower panels represent the corresponding readouts of Fluo-4 fluorescence. Extensive vesiculation, cell disintegration and echinocytosis followed uncontrolled Ca^{2+} loading. (B) RBCs from two healthy subjects (P1 and P2) were collected, filtered and stored for 1–21 days in Ca^{2+}-free citrate-containing glutathione (GSH) conservation solution, and they were then re-suspended in the incubation medium containing 145 mM NaCl, 4 mM KCl, 1.8 mM Ca^{2+}, 10 mM glucose and 0.1% bovine serum albumin. The cells of both donors retained normal discocyte morphology over at least one week in the citrate phosphate dextrose solution, and P1 was considered "a better quality donor" during conventional quality control tests. Of importance are the inter-individual differences in the responses and acute changes in morphology in the presence of extracellular Ca^{2+} and the progressive deterioration of cellular quality associated with ATP and GSH depletion and changes in the ion and water content.

the switch to animal RBCs may provide invaluable advantages over human RBCs. These advantages might be such simple properties as the cell size. For instance the amphiuma RBCs have an elliptical size of ~62 μm in length and ~36 μm in width and are used to perform the initial potential measurements in RBCs.[46] The RBCs of fish (6.5–44.6 μm diameter), amphibians (16–70 μm) and birds (9.7–15.4 μm) contain organelles such as a nucleus, mitochondria and ribosomes. These qualitative differences compared to human RBCs might be advantageous or disadvantageous and can be used as experimental tools.

The great variations in RBCs between species on the one hand and a broad conservation on the other hand allows the use of animal RBCs as particular models for certain protein manipulations, even in the organelle-free mammalian RBCs, that would otherwise require the breeding of transgenic animals. Examples include the RBCs of carnivora that lack the Na^+/K^+ pump[47] (instead, they have a Na^+/Ca^{2+} exchanger, which is absent in the RBCs of other species) or sheep RBCs that do not seem to contain scramblase.[48] There is list of differences[49] that cannot be covered in this paper — furthermore, the protein and lipid distributions of RBCs between species can differ considerably.[50,51]

Thus, vast amounts of information on the alternative models that may be used to study the pathological alterations in human RBCs are not used. Making the results of comparative studies on RBCs more "visible" will help to acknowledge the advantages that these cells provide.

3.3.2. Guideline for "switching" species within a study

Knowing all these differences, it should be a habit of good laboratory praxis (as well as reviewing praxis) to either perform studies (publications) just within a defined species or, when mixing species (except for comparative studies), to show — whenever possible — explicitly the transferability of the "previous step", at least in the supplemental material. This rule of course needs to be adapted if the animal model is used as a "modified source" of RBCs.

4. Methodological considerations

4.1. Proteomics

Proteomics is likely the method that is most affected by contamination of cell preparations. This holds true because proteomic studies are still carried out on cell suspensions, although single-cell approaches have been introduced.[52] The importance of the pure cell preparations is efficiently and impressively illustrated by some of the most recent proteomic studies, where care was taken to reduce WBC contamination of the RBCs, resulting in a list of less than 300 recognised RBC membrane proteins,[53,54] compared to the much larger number of supposedly erythrocytic proteins presented in earlier catalogues.

Presently, the proteomic studies of RBCs are still somewhat separated from functional studies, resulting in protein catalogues that do not (yet) fit with functional identified proteins from, e.g., patch-clamp recordings. Bridging this gap will be one of the challenges of future RBC research.

4.2. Ion fluxes

Measurements of ion fluxes through the RBC membrane are performed using various approaches. Radioactive tracers have been used for unidirectional flux measurements for many decades.[55,56] This technique allows quantification of unidirectional movements of ions by electroneutral and electrogenic ion transporters as well as residual ion fluxes. Other methods to assess ion movements through the membrane are based on monitoring of net ion uptake/loss by means of ion-selective electrodes, flame photometry, atomic absorption spectrophotometry, etc.

Accumulation or loss of radioactive tracers may be estimated with high sensitivity (up to single disintegration events) using beta- and gamma-counters. For most ions, the corresponding radionuclides, which may play a role as isotopic carriers, have relatively long half-lives (weeks to months). Rubidium-86 ($T_{1/2} = 18.6$ d) is often used as a tracer because the most suitable $^{42}K^+$ radionuclide has a rather short half-life ($T_{1/2} = 12.5$ h) and requires a supply for fresh radioisotopes, e.g., the proximity of a cyclotron to the lab where the ion fluxes are assessed. With some rare exceptions,[57] discrimination between K^+ and Rb^+ by ion transport systems in RBCs does not exceed 20%.[58]

4.2.1. Pitfalls and limitations

For monitoring the kinetics of the radioactive tracer distribution, one may assess the unidirectional inward and outward fluxes as well as a steady-state distribution of selected ion species between the cell and the medium, considering that the cell lacks compartmentalisation. If this is not the case, as for intracellular Ca^{2+} in RBCs of patients with sickle cell disease,[59] cytosolic free Ca^{2+} cannot be estimated from the $^{45}Ca^{2+}$ distribution between the cells and the medium. Most of the Ca^{2+} in that case is accumulated in the intracellular inside-out vesicles that are most likely enriched with Ca^{2+} pumps,[60] and an increase in the intracellular$^{45}Ca^{2+}$ levels is not always followed by the activation of Ca^{2+}-sensitive K^+ (Gardos) channels.

Measurements of ion fluxes bear a common limitation: flux measurements are performed in suspension, and the considerations discussed above in "Obtaining pure cell preparations" (Section 3.1) apply. So far, studies to assess the role of WBC and platelet contamination in possible artefact generation when measuring ion fluxes using radioactive tracers are lacking.

Another point that is seldom taken into account is the effect of the electro-neutrality of compartments on ion movements. Cation movements, such as those mediated by Gardos channel activity, that lead to cell dehydration are known to be rate limited by anion movements. In many cell suspension experiments, thiocyanate (SCN^-) is used to bypass this limitation of anion movements. Ten millimolar is usually sufficient to saturate this effect,[61] avoiding important changes in the isoelectric point of impermeant anions and RBC hydration that are observed at higher SCN^- concentrations.[62] Apart from ion flux experiments, this could also apply to patch-clamp experiments aiming to investigate cation channel activity. Even if this consideration does not apply in the whole-cell configuration because the anion supply is provided by the pipette content, it can impair the movement of cations in the cell-attached configuration. In this case, run-down of channel activity might be observed and conclusions can be drawn erroneously.

4.3. Patch-clamp

During the past three decades, electrophysiological studies have revealed that the human RBC membrane is endowed with a large variety of ion channels.[63–67] However, their physiological role remains widely unclear; they barely participate in the RBC homeostasis, which is based on an almost total absence of cationic permeability and minute anionic conductance.[68] Nevertheless, due to the pioneering work of Hamill on human and frog RBCs,[61,69] the patch-clamp technique applied to RBCs has proven to be a powerful method to decipher the involvement of ionic conductances mainly in pathophysiological scenarios.[32,42,62,65,70–72]

4.3.1. Challenges to patch-clamp RBCs

The main problem when attempting to perform patch-clamp on RBCs lies in the small size of the cells, which especially holds true for mammalian RBCs (2.1–9.4 μm) (cp. Section (3.3) "Interspecies studies"). This small size imposes major challenges.

4.3.1.1. Optomechanical requirements. The opto-mechanical properties of the hardware require high-quality microscopes and at least 20× objectives. A 40× objective with phase or Nomarski contrast is usually necessary for recordings on malaria-infected cells to recognise the infected RBCs. When approaching the pipette to form a seal, very precise micromanipulators are required.

4.3.1.2. Patch pipettes and seal formation. RBCs are "designed" for passing through small capillaries. When passing through the spleen, RBCs have to go through tiny slits whose mean size has been recently measured at 1.89 μm in length and 0.65 μm in width.[43] Therefore, patch-pipette tips must be rather thin, with an opening smaller than 1 μm (corresponds to roughly 10–15 MΩ in physiological saline solutions) to avoid the entry of the cell into the pipette. Besides the pipette size, its shape has to be adapted such that a piece of membrane enters the pipette for seal formation without totally entering into the pipette when depression (typically 20 mbar) is applied. The pipette tip must be thin enough, but at the same time tapered enough, to preserve a low electrical access resistance. Another issue arises from RBC's high deformability. The portion of the RBC membrane that enters into the pipettes during seal formation varies. Furthermore, it has been recognised that membrane deformation induces transient Ca^{2+} entry in RBCs.[73] Such transient activity may generate secondary transient anionic channel activity.[74] This phenomenon leads to a change in the intracellular K^+ concentration that has to be taken into account for data interpretation. Therefore, the time of seal formation and calibrated depression must be mentioned in publications.

4.3.1.3. Transition between configurations. The small RBC size results in a small membrane capacitance of approximately 1–1.3 pF.[75,76] This becomes relevant during the transition from the cell-attached to whole-cell configuration. The rupture of the membrane fragment inside the pipette tip is typically achieved by a brief electrical pulse (200 ms, 500 mV). A successful whole-cell configuration can be checked via the sudden appearance of membrane capacitance transient currents, which can be easily compensated on the amplifier. Nevertheless, the situation is different in plate-based "pipettes" as they are used by automated patch-robots (Fig. 3). There, the basal capacitance of the plate is much higher and an increase of 1 pF is almost invisible. Therefore, the major indication for reaching the whole-cell state is the increase in current, which is a challenge because differentiation between the loss of seal resistance and the whole cell current needs to be probed in the experimental protocol. However, if the seal resistance is approximately 10 GΩ, the current leakage at +100 mV can be calculated to be 10 pA, presenting a relation to Ohm's law. Typical whole-cell recordings show current values between 200 and 1000 pA or even higher, which often are rectifying, i.e., they do not follow Ohm's law; then, the leak remains below 1–5% of the total current.

4.3.2. Automated patch-clamp

Automated patch-clamp recordings allow probing an increased cell number under exactly the same conditions and were therefore used to test for the heterogeneity of naive RBC conductance among the RBCs of a donor as well as investigating the variability between different donors. Fig. 3 depicts this comparison for two healthy donors.

The simultaneous measurements of 4 to 96 RBCs (depending on the model of the automated patch systems) allow for measurement of a population of RBCs with exactly the same experimental procedure, and there is no experimental bias towards choosing a (particular) cell. In contrast, classical patch-clamp allows for more (visual) control over the particular experiment/cell and at least an order of magnitude lower noise level, typically approximately 1 pA.

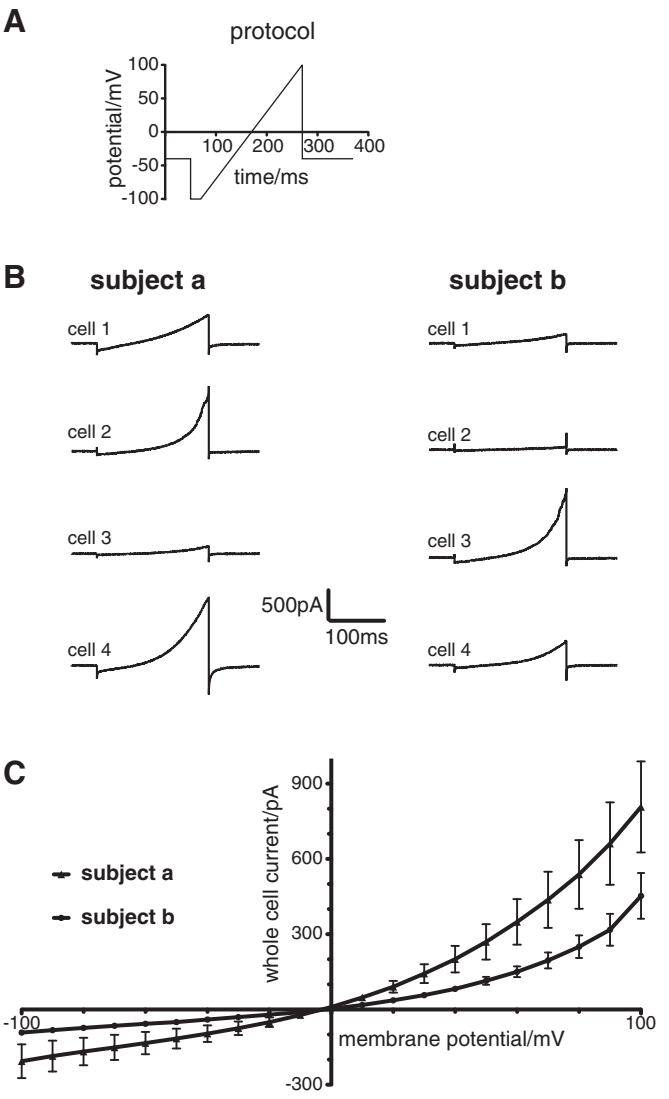

Fig. 3. Heterogeneity of RBCs — measurements derived from automated patch-clamp whole cell recordings (NPC-16 Patchliner, Nanion, Munich, Germany). (A) depicts the voltage protocol. The bath solution contained 80 mM NaCl, 3 mM KCl, 10 mM $MgCl_2$, 35 mM $CaCl_2$, and 10 mM HEPES/NaOH, pH 7.4, while the pipette solution contained 50 mM CsCl, 10 mM NaCl, 60 mM CsF, 20 mM EGTA, 10 mM HEPES/CsOH, pH 7.2. The seal resistance was in the range of 1–5 GΩ at a holding potential of −40 mV. (B) exemplifies the recordings from single RBCs of 2 healthy subjects, (a) and (b). The current traces are superpositions of leak currents and channel-mediated currents. The non-Ohmic appearance of the currents indicates to differences in the cellular properties rather than in the patch resistance. Panel (C) shows the I/V plots for the whole cell currents (mean ± SD, n = 24 cells per subject). Please note that both samples were from freshly drawn RBCs (experiments within 2 h) and are not attributed to different cell treatments as outlined in Fig. 2.

4.3.3. Comparison of patch-clamp data with other entities

Comparing data from cell suspension experiments (cp. Section (4.2) "Ion fluxes") and those issued from patch-clamp studies is a common but difficult task, which can be exemplified by the entry of Ca^{2+} observed in sickle cells upon deoxygenation. This entry, designated P_{sickle}, is best characterised as a poorly selective permeability pathway for small, inorganic monovalent and divalent cations.[77] Experiments in which the fraction of activated cells was studied as a function of the external Ca^{2+} concentration showed that sickling is a stochastic event of random intensity among HbSS RBCs, capable of generating maximal Gardos channel activation in a small fraction of cells during each deoxygenation-sickling pulse. Consistent with the stochastic nature of

P_{sickle}, repeated pulses led to the progressive accumulation of dense cells, whereas a single long pulse caused only an early production of a single small fraction of dense RBCs.[78] Lew et al. eventually depicted this nature clearly by writing: "When electrophysiologists finally approach the study of P_{sickle} under patch-clamp, they ought to bear in mind the probabilistic nature of P_{sickle} in each deoxygenation pulse before consulting their psychiatrist for the lack of reproducibility!".[77]

One has to keep in mind that electrophysiology conclusions are drawn from results where the membrane potential is changed at will by the experimenter, meaning that they are rarely obtained at the resting membrane potential, rendering comparison with cell suspensions difficult. This is exemplified in a recent study, where it was shown that increased membrane permeability for sorbitol in malaria-infected RBCs could not easily be reconciled with data from whole-cell experiments.[79] Indeed, in isosmotic sorbitol haemolysis, the membrane potential reaches values above +50 mV due to the absence of charges at the extracellular side of the membrane. Subsequent comparison of these data to that obtained with patch-clamp (at this membrane potential, inwardly rectified currents induced by infection are almost totally abolished[62,65]) seems impossible.

4.4. Flow cytometry

FCM is a technique that uses optical detection methods for counting and analysing particles in the size range of micrometres. In comparison to microscopic investigations of single RBCs (see below), the application of FCM and cell sorting present some advantages as well as disadvantages.

4.4.1. Advantages of flow cytometry

A major advantage of FCM compared to single-cell imaging is the inherent analysis of a larger amount of cells within a shorter time (a minimum of several 10,000 cells vs. a few hundred cells). This reduces the statistical noise. The gating for cell populations is easy and reduces the analysed cells to a dedicated population out of a heterogeneous sample.

The forward scatter mode shows the size distribution of the cells. Although it is by no means an exact measure of the absolute cell volume, it can be used as an indicator of the relative size changes of the RBC samples.

The side scatter mode shows the "granularity" of the cell, which is related to the complexity of structures in the cell interior. It can provide information on the presence of different cell types in a single suspension of cells (e.g., in blood). A useful feature of flow cytometry is connected with the possibility of measuring the fluorescence emitted by suitable fluorochromes that are used as probes for a given particular cell property. Fluorescently labelled antibodies and fluorescent probes sensitive for a particular chemico-physical parameter of the cell (e.g., pH, Ca^{2+}, PS exposure, mesomorphic state of the lipids) are the most commonly used fluorescent molecules.

4.4.2. Limitations of flow cytometry

Due to the measurement technique, cells have to pass the cuvette in a high-speed fluid stream. This limits measurements to cells in a suspension and excludes larger aggregates. However, doublets of RBCs can be easily recognised by the fluorescence signal forward or side scatter. Although the side scatter is an indicator for the granularity and surface shape, it is not possible to measure and reliably distinguish the different shapes (echinocytes, discocytes, stomatocytes) of RBCs. In the forward and the side scatter, RBCs present shapes that are nearly similar and overlapping signals.

The fluorescence intensities observed by FCM are integrated values of the entire cell and do not resolve a subcellular distribution of the fluorescence as in imaging (see below).

In some experiments, the formation of microvesicles can be observed. Due to the small size of the microvesicles, they will be shown in the forward and side scatter below the threshold together with the cell debris and dead cells and will normally be discarded. However, the fluorescence might be used to discriminate the vesicles from the debris, and this could allow a quantitative analysis.

In contrast to single-cell imaging approaches, it is not possible to follow the kinetics of any signal in a single cell. After measurement of the optical parameters, the cell is either discarded or collected in a tube with RBCs depicting the same properties.

In all fluorescence measurements of RBCs, haemoglobin shows a strong absorption of UV and visible light (for more details and discussion, see Section (4.5) "Cellular imaging"). This requires dyes with emission wavelengths above 600 nm or brighter fluorophores (compared to thresholds that are known for haemoglobin-free cells).

4.4.3. Potential artefacts

Before measuring the different parameters, the cells are sucked under pressure in a fluid stream through a small capillary into the measurement chamber. While the cell suspension is passing through a capillary in the FCM to the measurement chamber, the cells can be exposed to shear stress because of the different speeds of the sample and the sheath fluid. An applied shear stress can induce different mechanisms such as the activation or inactivation of physiological processes in the cells (e.g., Ca^{2+} increase in RBCs exposed to mechanical stress[80]) or even damage the membrane. Values for the applied pressure can reach 500 kPa and higher (manufacturer information), which exceed the normal systolic arterial blood pressure value of approximately 15 kPa by a factor of more than 30. It is well known from other cell types that cell damage can occur because of the applied pressure,[81] and our own observations showed that a population of fragile RBCs (observed in imaging) can disappear in FCM (unpublished observations).

4.5. Cellular imaging

Live cell imaging is a popular method to explore cellular signalling.[82] However, for the investigation of RBCs, it is rather sparsely applied. This might be due to three major drawbacks:

(i) The absorption spectrum of the haemoglobin heavily interferes with the absorption of many commonly used dyes and additionally quenches their emission, as exemplified by the most popular Ca^{2+} fluorophores.[83]
(ii) Due to the lack of a protein translation mechanism, the application of fluorescent proteins and genetically encoded biosensors as an emerging tool in biomedical research is limited to the generation of transgenic animals (cp. also[84]).
(iii) In live cell imaging (time lapse), each experiment follows a substantial number of cells (not just one as, e.g., in patch-clamp recordings), and each cell is followed over an arbitrary time course (not just one time point as, e.g., in FCM). This leads to a large amount of data. In light of the increasing awareness that RBCs can form a highly heterogeneous population (Fig. 3), there is a requirement for analysis guidelines that are not yet filed and that would exceed the size of this section.

Although these 3 points are serious and have to be taken into account, cellular imaging is a powerful tool in RBC research.

4.5.1. Potential artefacts and how to avoid them

A number of points have to be considered to avoid artefacts. In imaging approaches, dye molecules and photons are used to probe the cells. Photons can interact with the cellular constituents and may induce what is commonly referred to as phototoxicity. For RBCs, this is known for near infrared light[85] and for the interaction of UV light

with haemoglobin, resulting in the generation of a highly fluorescent photoproduct, most likely bilirubin.[86]

The interaction of the photons with the dye can lead to photobleaching and induce a "loss of signal". This decreased fluorescence leads to underestimation of the signal of interest. Furthermore, there is another almost opposite effect that is often neglected but may occur with some dyes, e.g., with Fluo-4, the so-called "antibleaching".[87] This is, in this example, the light-mediated induction of Ca^{2+} insensitive but highly fluorescent dye molecules that can occur if illumination of high intensity is used. Consequently, the signal of interest is prone to be overestimated.

Additionally, triple interactions between endogenous proteins, fluorescent dyes and photons may alter the properties of the fluorescent read-out. If there is a binding affinity between the endogenous proteins and the fluorescent dye under certain conditions,[88] Förster Resonance Energy Transfer (FRET) occurs and consequently alters the fluorescence intensity, spectral properties and fluorescence lifetime. In RBCs, FRET can occur, e.g., between the dye Fura-red and haemoglobin (unpublished results).

It must be noted that FRET can also be used in a beneficial way, as nicely shown by Esposito et al.[89] for imaging the haemoglobin concentrations in malaria-infected RBCs.

Yet another factor that influences the fluorescence intensity is RBC volume changes because a change in volume results in a change in the dye concentration and hence an altered fluorescence signal.

Fortunately, most of the above mentioned sources of artefacts are rather small and might be neglected when the observed signals are robust. However, if minute signals are expected or observed, the artefacts are likely to become relevant.

An almost unavoidable artificial situation in live cell imaging is the fact that the RBCs are attached to a (coated or uncoated) coverslip. The only way to exclude artificial conclusions is the comparison/combination with complementary methods.

Last but not least, live cell imaging is often used to detect hormonal or pharmacological stimulation of RBCs. To have a proper control of the solution surrounding the cell, a local perfusion (a micromanipulator-associated cannula placed close to the RBCs to apply a laminar flow) is preferred over an exchange of the bulk solution of the entire dish that almost certainly would lead to slow gradients of the exchanged solutions and a loss of control concerning the timing of the drug or hormonal stimulation. Because RBCs contain a number of mechanically sensitive proteins,[38] one has to make sure that the flow does not change with the application, and therefore, the flow must be kept constant (also under control conditions) and just the solution composition needs to be switched from the battery of solutions.

4.6. Adhesion force measurements

Adhesion is traditionally measured by either microscopic investigation, quantifying a microscopic aggregation index[90] or by indirect methods based on the properties of RBC suspensions. Such techniques include sedimentation-associated procedures, transmission light or ultrasound scattering, impedance measurements, determination of viscosity or other rheometric methods.[91] The classical methods to measure RBC aggregation have been recently reviewed.[92] However, with regard to adhesion force measurements, a focus was set to rheometric techniques.[93,94] These methods are all indirect and suffer from a limited amount of information on the number of cells involved or the impact of RBC morphological and deformability changes.

4.6.1. Quantitative force measurements

Recently, two quantitative RBC intercellular adhesion measurements were introduced at the single-cell level and compared to each other.[95,96] The two techniques are holographic optical tweezers (HOT) and atomic force microscope-based single cell force spectroscopy (SCFS). To exert forces on cells with optical tweezers, a limited force regime is available due to cell damage with increasing laser power, i.e., there exists an upper limit of force at which the adhesion forces between cells can be measured. In addition to that, a lower limit of measurable adhesion forces exists for the SCFS, which is due to both the limited force resolution of the system and the squeezing of the cells during the measurements that can possibly induce adhesion force artefacts (see below). Both limits could be illustrated by measuring the small adhesion forces between single RBCs under physiological conditions (Fig. 4).

The only way to explain the difference in both techniques is the slightly invasive nature of the SCFS. An inevitable part of the SCFS measurements is the requirement for a preset force set point that is used as a marker if both cells have come into close contact (i.e., squeezing the two cells together with a certain set point force). This invasive squeezing of the cells is artificial, and it most likely induces a small adhesion by itself.

The above mentioned problems should not arise when probing RBCs for specific molecules, e.g., for testing receptor binding.[97] In this case, the cantilever is functionalised with the specific molecules (e.g., fibrinogen), the binding between receptor and agonist is specific and thus allows measuring the adhesion between a molecule-coated cantilever and the RBC.

4.6.2. Selection criteria for force measurements

When measuring forces between RBCs, it would be desirable to combine the complementary methods of SCFS and HOT. Unfortunately, both methods are complex and laborious, and this advice might not always be feasible. Therefore, the tool can be chosen according to the dimension of the expected force. The SCFS is advised for adhesion forces larger than 30 pN and the HOT for adhesion forces smaller than 30 pN. While the squeezing of the cells in the SCFS measurements is the critical parameter, the laser power is the critical parameter in the HOT measurements.

5. Conclusions

We are left with the impression that a significant portion of the past literature on RBCs should be re-read to verify whether it could have been affected by the problem of cell contamination. Of course, one will not incur such problems when studying RBCs at a single-cell level.

Recent studies provided first indications that RBC populations are rather heterogeneous,[10] Fig. 3, which may result in additional problems when working with bulk suspensions as well as with single RBCs. A major reason for the inhomogeneities of circulating RBCs are differences in the cell age.[98] There are indications that the plasma membrane Ca^{2+} pump activity decreases with RBC age in a monotonic fashion,[99] which may lead, at least for some cells, to changes in the sodium and potassium content. However, when performing single-cell experiments, the cells are chosen randomly, i.e., cells can be from one or the other end of the age scale. Moreover, variable amounts of circulating reticulocytes also contribute to the variability of measurements performed on bulk RBC suspensions, even after WBCs and platelets have been carefully removed. Therefore, a flow chart of an optimised protocol for studying a property/component of mature RBCs should involve the following: leukodepletion by any suitable method/filter; gelatin zymography to ascertain the level of residual PMNs; the efficient use of anti-proteases; reticulocyte quantification (count and/or Western Blotting of, for instance, CD71, the transferrin receptor); separation of RBCs into subpopulations of different density/age and isolation of a population of "mature" RBCs.[98] However, the availability of a reliable and artefact-free separation technique is still debated.

Alternatively, to elucidate the inter-cellular variability of responses, measurements in cell suspensions should be combined with single-cell techniques such as fluorescent live cell imaging, FCM and/or patch-clamp approaches. However, even between single-cell techniques,

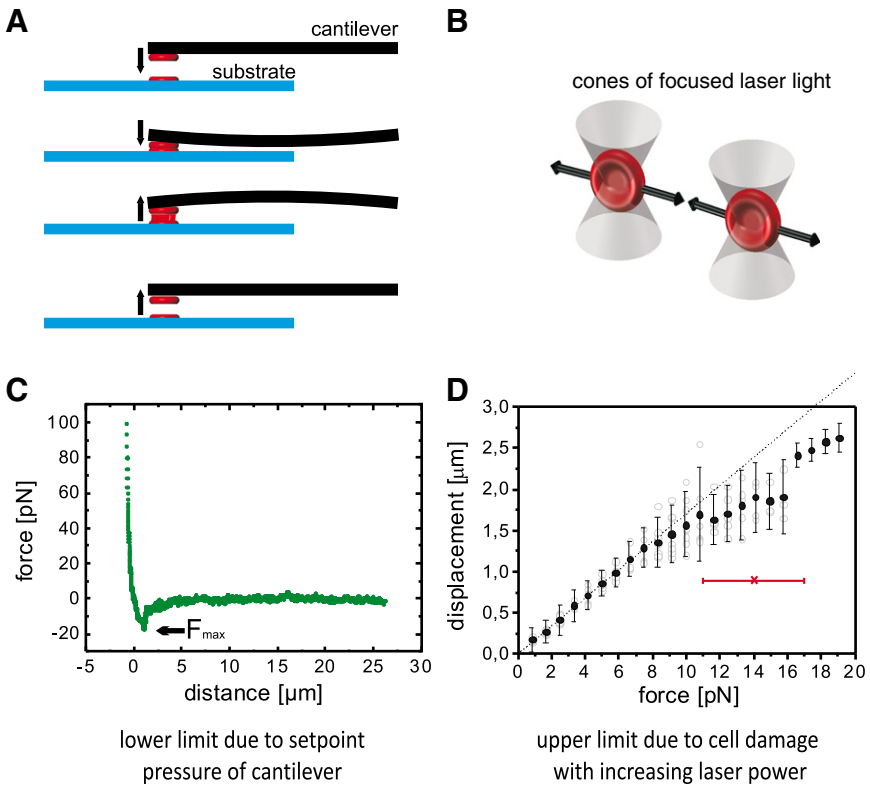

Fig. 4. Panel (A) shows a sketch of the working principle of single-cell force spectroscopy (SCFS). A cell is bound to a cantilever and is brought into contact with another cell at the surface. During the approach and withdrawal of the cell, the deflection is monitored and gives direct information about the adhesion force between the cells. Panel (B) shows a sketch of the working principle of the optical tweezers measurements. Two RBCs are trapped in the foci of two laser beams and are brought into contact. By measuring the deflection of the cells out of the centre of the laser foci, one can determine the adhesion force between the cells. Panel (C) shows a force vs. distance curve derived from the SSFS measurements. A weak interaction of approximately 20 pN can be observed that is only due to an artefact of the measurement (see text). This 20 pN is the lower limit that one can measure using this type of cell with this technique. Panel (D) shows a force calibration of one RBC in an optical trap. It can be observed that with the given laser power, the trap is only linear up to forces of 15 pN, i.e., this is the upper limit that can be measured with this technique on these types of cells. Panels (A), (B) and (D) are reproductions with kind permission from Elsevier. (A) is a reprint of the original publication by Steffen et al. 2011,[95] and panels (B) and (D) are reprints from the original publication by Kaestner et al. 2012.[96]

there are regularly discrepancies and confusing interpretations because cell behaviour is highly sensitive, and often the devil is in the experimental details. Therefore, considerations that will lead to better harmonisation of experimental conditions are timely and relevant, especially regarding the accumulation of large amounts of data in the literature.

6. Research agenda

- Matching RBC protein libraries with functional observations.
- RBC storage conditions for transfusion bear a high potential for improvements.
- Potential of comparative studies should be better utilised.
- Single cell investigations should become more prominent.

Conflict of interest statement

None on the authors reports a conflict of interest.

Acknowledgements

We wish to thank Prof. Walter Reinhart and Dr. Thomas Schulzki (Cantonal Hospital Graubünden, Switzerland) for collaboration in data generation for Fig. 2B, as well as Dr. Andrea Brüggemann and Dr. Claudia Haarmann (Nanion Technologies GmbH, Munich, Germany) for their assistance with data acquisition for Fig. 3. The work was partially funded by the Ministero dell'Università e della Ricerca, Italy, with PRIN2008 funds to G.M.

References

1. Swammerdam J. Bybel der Natuur. Hill J, editor. London: Bookseller C. G. Seyffert; 1737.
2. Staines HM, Alkhalil A, Allen RJ, De Jonge HR, Derbyshire E, Egée S, et al. Electrophysiological studies of malaria parasite-infected erythrocytes: current status. *Int J Parasitol* 2007;**37**:475–482.
3. Bouyer G, Egée S, Thomas SLY. Toward a unifying model of malaria-induced channel activity. *Proc Natl Acad Sci U S A* 2007;**104**:11044–11049.
4. Salzer U, Prohaska R. Stomatin, flotillin-1, and flotillin-2 are major integral proteins of erythrocyte lipid rafts. *Blood* 2001;**97**:1141–1143.
5. Ciana A, Balduini C, Minetti G. Detergent-resistant membranes in human erythrocytes and their connection to the membrane-skeleton. *J Biosci* 2005;**30**:317–328.
6. Ciana A, Achilli C, Balduini C, Minetti G. On the association of lipid rafts to the spectrin skeleton in human erythrocytes. *Biochim Biophys Acta* 2011;**1808**:183–190.
7. Grygorczyk R, Schwarz W, Passow H. Ca^{2+}-activated K^+ channels in human red cells. Comparison of single-channel currents with ion fluxes. *Biophys J* 1984;**45**:693–698.
8. Brugnara C, de Franceschi L, Alper SL. Ca(2+)-activated K+ transport in erythrocytes. Comparison of binding and transport inhibition by scorpion toxins. *J Biol Chem* 1993;**268**:8760–8768.
9. Li Q, Jungmann V, Kiyatkin A, Low PS. Prostaglandin E2 stimulates a Ca2+-dependent K+ channel in human erythrocytes and alters cell volume and filterability. *J Biol Chem* 1996;**271**:18651–18656.
10. Kaestner L, Tabellion W, Lipp P, Bernhardt I. Prostaglandin E2 activates channel-mediated calcium entry in human erythrocytes: an indication for a blood clot formation supporting process. *Thromb Haemost* 2004;**92**:1269–1272.
11. Kucherenko YV, Weiss E, Bernhardt I. Effect of the ionic strength and prostaglandin E2 on the free Ca^{2+} concentration and the Ca^{2+} influx in human red blood cells. *Bioelectrochemistry* 2004;**62**:127–133.
12. O'Neill JS, Reddy AB. Circadian clocks in human red blood cells. *Nature* 2011;**469**:498–503.

13. Beutler E, West C, Blume KG. Removal of leukocytes and platelets from whole-blood. *J Lab Clin Med* 1976;**88**:328–333.
14. Achilli C, Ciana A, Balduini C, Risso A, Minetti G. Application of gelatin zymography for evaluating low levels of contaminating neutrophils in red blood cell samples. *Anal Biochem* 2011;**409**:296–297.
15. Beutler E, Gelbart T. The mechanism of removal of leukocytes by cellulose columns. *Blood Cells* 1986;**12**:57–64.
16. Rebulla P, Porretti L, Bertolini F, Marangoni F, Prati D, Smacchia C, et al. White cell-reduced red cells prepared by filtration: a critical evaluation of current filters and methods for counting residual white cells. *Transfusion* 1993;**33**:128–133.
17. Dodge JT, Mitchell C, Hanahan DJ. The preparation and chemical characteristics of hemoglobin-free ghosts of human erythrocytes. *Arch Biochem Biophys* 1963;**100**: 119–130.
18. Sarkadi B, Szasz I, Gerloczy A, Gardos G. Transport parameters and stoichiometry of active calcium-ion extrusion in intact human red-cells. *Biochim Biophys Acta* 1977;**464**:93–107.
19. Canestrari F, Galli F, Boschi S, Albertini MC, Gheller G, De Crescentini S, et al. Erythrocyte Na+, K(+)-ATPase properties and adenylate energy charge in normotensives and in essential hypertensives. *Clin Chim Acta* 1994;**224**:167–179.
20. Ellory JC, Hall AC. Temperature effects on red cell membrane transport processes. *Symp Soc Exp Biol* 1987;**41**:53–66.
21. Grygorczyk R. Temperature dependence of Ca2+-activated K+ currents in the membrane of human erythrocytes. *Biochim Biophys Acta* 1987;**902**:159–168.
22. Yang L, Andrews DA, Low PS. Lysophosphatidic acid opens a Ca(++) channel in human erythrocytes. *Blood* 2000;**95**:2420–2425.
23. Kleinbongard P, Schulz R, Rassaf T, Lauer T, Dejam A, Jax T, et al. Red blood cells express a functional endothelial nitric oxide synthase. *Blood* 2006;**107**: 2943–2951.
24. Staines HM, Powell T, Ellory JC, Egée S, Lapaix F, Decherf G, et al. Modulation of whole-cell currents in *Plasmodium falciparum*-infected human red blood cells by holding potential and serum. *J Physiol (Lond)* 2003;**552**:177–183.
25. Glogowska E, Dyrda A, Cueff A, Bouyer G, Egée S, Bennekou P, et al. Anion conductance of the human red cell is carried by a maxi-anion channel. *Blood Cells Mol Dis* 2010;**44**:243–251.
26. Duranton C, Tanneur V, Lang C, Brand VB, Koka S, Kasinathan RS, et al. A high specificity and affinity interaction with serum albumin stimulates an anion conductance in malaria-infected erythrocytes. *Cell Physiol Biochem* 2008;**22**:395–404.
27. Mihov D, Vogel J, Gassmann M, Bogdanova AY. Erythropoietin activates nitric oxide synthase in murine erythrocytes. *Am J Physiol Cell Physiol* 2009;**297**:C378–C388.
28. Makhro A, Wang J, Vogel J, Boldyrev AA, Gassmann M, Kaestner L, et al. Functional NMDA receptors in rat erythrocytes. *Am J Physiol Cell Physiol* 2010;**298**:C1315–C1325.
29. Valeri CR, Zaroulis CG. Rejuvenation and freezing of outdated stored human red-cells. *New Engl J Med* 1972;**287**:1307–1313.
30. Barshtein G, Manny N, Yedgar S. Circulatory risk in the transfusion of red blood cells with impaired flow properties induced by storage. *Transfus Med Rev* 2011;**25**:24–35.
31. Lang KS, Lang PA, Bauer C, Duranton C, Wieder T, Huber S, et al. Mechanisms of suicidal erythrocyte death. *Cell Physiol Biochem* 2005;**15**:195–202.
32. Huber SM, Uhlemann AC, Gamper NL, Duranton C, Kremsner PG, Lang F. *Plasmodium falciparum* activates endogenous Cl(−) channels of human erythrocytes by membrane oxidation. *EMBO J* 2002;**21**:22–30.
33. Huber S, Uhlemann A, Gamper N, Duranton C, Lang F, Kremsner PG. Oxidative permeabilization? *Trends Parasitol* 2002;**18**:346.
34. Dumaswala UJ, Zhuo L, Jacobsen DW, Jain SK, Sukalski KA. Protein and lipid oxidation of banked human erythrocytes: role of glutathione. *Free Radic Biol Med* 1999;**27**: 1041–1049.
35. Lutz H, Bussolino F, Flepp R, Fasler S. Naturally occurring anti-band-3 antibodies and complement activation together mediate phagocytosis of oxidatively stressed human erythrocytes. *Proc Natl Acad Sci U S A* 1987;**84**:7368–87372.
36. Lang KS, Duranton C, Poehlmann H, Myssina S, Bauer C, Lang F, et al. Cation channels trigger apoptotic death of erythrocytes. *Cell Death Differ* 2003;**10**:249–256.
37. Bogdanova A, Mihov D, Lutz H, Saam B, Gassmann M, Vogel J. Enhanced erythro-phagocytosis in polycythemic mice overexpressing erythropoietin. *Blood* 2007;**110**:762–769.
38. Huber SM, Gamper N, Lang F. Chloride conductance and volume-regulatory nonselective cation conductance in human red blood cell ghosts. *Pflugers Arch Eur J Physiol* 2001;**441**:551–558.
39. Huber SM, Duranton C, Henke G, van de Sand C, Heussler V, Shumilina EV, et al. Plasmodium induces swelling-activated ClC-2 anion channels in the host erythrocyte. *J Biol Chem* 2004;**279**:41444–41452.
40. van Faassen EE, Babrami S, Feelisch M, Hogg N, Kelm M, Kim-Shapiro DB, et al. Nitrite as regulator of hypoxic signaling in mammalian physiology. *Med Res Rev* 2009;**29**: 683–741.
41. Bogdanova A, Berenbrink M, Nikinmaa M. Oxygen-dependent ion transport in erythrocytes. *Acta Physiol* 2009;**195**:305–319.
42. Decherf G, Bouyer G, Egée S, Thomas SLY. Chloride channels in normal and cystic fibrosis human erythrocyte membrane. *Blood Cells Mol Dis* 2007;**39**:24–34.
43. Deplaine G, Safeukui I, Jeddi F, Lacoste F, Brousse V, Perrot S, et al. The sensing of poorly deformable red blood cells by the human spleen can be mimicked *in vitro*. *Blood* 2011;**117**:e88–e95.
44. Agar NS, Board PG, editors. Red blood cells of domestic mammals. Amsterdam, New York: Elsevier Science Ltd.; 1983. p. 1–438.
45. Glomski CA, Pica A. The avian erythrocyte: its phylogenetic odyssey. Science Publishers, CRC Press; 2011. p. 1–650.
46. Lassen UV, Pape L, Vestergaard-Bogind B, Bengtson O. Calcium-related hyperpolarization of the Amphiuma red cell membrane following micropuncture. *J Membr Biol* 1974;**18**:125–144.
47. Ellory JC, Tucker EM. Cation transport in red blood cells. In: Agar NS, Board PG, editors. Red blood cells of domestic mammals. Amsterdam: Elsevier; 1983. p. 291–314.
48. Nguyen DB, Wagner-Britz L, Maia S, Steffen P, Wagner C, Kaestner L, et al. Regulation of phosphatidylserine exposure in red blood cells. *Cell Physiol Biochem* 2011;**28**:847–856.
49. Bernhardt I, Hall AC, Ellory JC. Transport pathways for monovalent cations through erythrocyte membranes. *Stud Biophys* 1988;**126**:5–21.
50. Van Dijck PW, De Kruijff B, Van Deenen LL, De Gier J, Demel RA. The preference of cholesterol for phosphatidylcholine in mixed phosphatidylcholine–phosphatidylethanolamine bilayers. *Biochim Biophys Acta* 1976;**455**:576–587.
51. Saito M, Tanaka Y, Ando S. Thin-layer chromatography-densitometry of minor acidic phospholipids: application to lipids from erythrocytes, liver, and kidney. *Anal Biochem* 1983;**132**:376–383.
52. Dovichi NJ, Hu S, Michels D, Mao D, Dambrowitz A. Single Cell Proteomics. In: Anselmetti D, editor. Single cell analysis: technologies and applications. Wiley-Blackwell; 2009. p. 69–90.
53. Pasini EM, Kirkegaard M, Mortensen P, Lutz HU, Thomas AW, Mann M. In-depth analysis of the membrane and cytosolic proteome of red blood cells. *Blood* 2006;**108**:791–801.
54. De Palma A, Roveri A, Zaccarin M, Benazzi L, Daminelli S, Pantano G, et al. Extraction methods of red blood cell membrane proteins for Multidimensional Protein Identification Technology (MudPIT) analysis. *J Chromatogr A* 2010;**1217**:5328–5336.
55. Cohn WE, Cohn ET. Permeability of red corpuscles of the dog to sodium ion. *Proc Soc Exp Biol Med* 1939;**41**:445–449.
56. Hoffman JF. The active transport of sodium by ghosts of human red blood cells. *J Gen Physiol* 1962;**45**:837–859.
57. Gusev GP, Fleishman DG, Nikiforov VA, Sherstobitov AO. Potassium channels of the lamprey erythrocyte membrane exhibit a high selectivity to K+ over Rb+: a comparative study of 86Rb and 41K transport. *Gen Physiol Biophys* 1997;**16**: 273–284.
58. Cavieres JD, Ellory JC. The interaction of monovalent cations with the sodium pump of low-potassium goat erythrocytes. *J Physiol (Lond)* 1977;**271**:289–318.
59. Lew VL, Hockaday A, Sepulveda MI, Somlyo AP, Somlyo AV, Ortiz OE, et al. Compartmentalization of sickle-cell calcium in endocytic inside-out vesicles. *Nature* 1985;**315**:586–589.
60. Rhoda MD, Giraud F, Craescu CT, Beuzard Y. Compartmentalization of Ca^{2+} in sickle cells. *Cell Calcium* 1985;**6**:397–411.
61. Hamill OP. Potassium and chloride channels in red blood cells. In: Sakmann B, Neher E, editors. Single Channel Recording. New York, London: Plenum Press; 1983. p. 451–471.
62. Desai S, Bezrukov S, Zimmerberg J. A voltage-dependent channel involved in nutrient uptake by red blood cells infected with the malaria parasite. *Nature* 2000;**406**: 1001–1005.
63. Christophersen P, Bennekou P. Evidence for a voltage-gated, non-selective cation channel in the human red cell membrane. *Biochim Biophys Acta* 1991;**1065**: 103–106.
64. Kaestner L, Bollensdorff C, Bernhardt I. Non-selective voltage-activated cation channel in the human red blood cell membrane. *Biochim Biophys Acta* 1999;**1417**:9–15.
65. Egée S, Lapaix F, Decherf G, Staines HM, Ellory JC, Doerig C, et al. A stretch-activated anion channel is up-regulated by the malaria parasite *Plasmodium falciparum*. *J Physiol (Lond)* 2002;**542**:795–801.
66. Duranton C, Huber SM, Lang F. Oxidation induces a Cl(−)-dependent cation conductance in human red blood cells. *J Physiol (Lond)* 2002;**539**:847–855.
67. Bouyer G, Cueff A, Egée S, Kmiecik J, Maksimova Y, Glogowska E, et al. Erythrocyte peripheral type benzodiazepine receptor/voltage-dependent anion channels are upregulated by *Plasmodium falciparum*. *Blood* 2011;**118**:2305–2312.
68. Thomas SLY, Bouyer G, Cueff A, Egée S, Glogowska E, Ollivaux C. Ion channels in human red blood cell membrane: actors or relics? *Blood Cells Mol Dis* 2011;**46**: 261–265.
69. Hamill OP. Potassium channel currents in human red blood cells. *J Physiol (Lond)* 1981;**319**:97P–98P.
70. Kaestner L, Bernhardt I. Ion channels in the human red blood cell membrane: their further investigation and physiological relevance. *Bioelectrochemistry* 2002;**55**: 71–74.
71. Huber SM, Duranton C, Lang F. Patch-clamp analysis of the "new permeability pathways" in malaria-infected erythrocytes. *Int Rev Cytol* 2005;**246**:59–134.
72. Browning JA, Staines HM, Robinson HC, Powell T, Ellory JC, Gibson JS. The effect of deoxygenation on whole-cell conductance of red blood cells from healthy individuals and patients with sickle cell disease. *Blood* 2007;**109**:2622–2629.
73. Johnson RM. Membrane stress increases cation permeability in red cells. *Biophys J* 1994;**67**:1876–1881.
74. Dyrda A, Cytlak U, Ciuraszkiewicz A, Lipinska A, Cueff A, Bouyer G, et al. Local membrane deformations activate Ca^{2+}-dependent K+ and anionic currents in intact human red blood cells. *PLoS One* 2010;**5**:e9447.
75. Fettiplace R, Andrews D. The thickness, composition and structure of some lipid bilayers and natural membranes. *J Membr Biol* 1971;**5**:277–296.
76. Rodighiero S, De Simoni A, Formenti A. The voltage-dependent nonselective cation current in human red blood cells studied by means of whole-cell and nystatin-perforated patch-clamp techniques. *Biochim Biophys Acta* 2004;**1660**: 164–170.
77. Lew VL, Bookchin RM. Ion transport pathology in the mechanism of sickle cell dehydration. *Physiol Rev* 2005;**85**:179–200.
78. Lew VL, Etzion Z, Bookchin RM. Dehydration response of sickle cells to sickling-induced Ca(++) permeabilization. *Blood* 2002;**99**:2578–2585.
79. Staines HM, Ashmore S, Felgate H, Moore J, Powell T, Ellory JC. Solute transport via the new permeability pathways in *Plasmodium falciparum*-infected human red

blood cells is not consistent with a simple single-channel model. *Blood* 2006;**108**: 3187–3194.
80. Larsen FL, Katz S, Roufogalis BD, Brooks DE. Physiological shear stresses enhance the Ca^{2+} permeability of human erythrocytes. *Nature* 1981;**294**:667–668.
81. Suh TK, Schenk JL, Seidel GE. High pressure flow cytometric sorting damages sperm. *Theriogenology* 2005;**64**:1035–1048.
82. Kaestner L, Lipp P. Towards imaging the dynamics of protein signalling. In: Shorte SL, Frischknecht F, editors. Imaging cellular and molecular biological functions. Berlin, Heidelberg: Springer; 2007. p. 289–312.
83. Kaestner L, Tabellion W, Weiss E, Bernhardt I, Lipp P. Calcium imaging of individual erythrocytes: problems and approaches. *Cell Calcium* 2006;**39**:13–19.
84. Kaestner L. Cation channels in erythrocytes — historical and future perspective. *Open Biol J* 2011;**4**:27–34.
85. Komorowska M, Cuissot A, Czarnołeski A, Białas W. Erythrocyte response to near-infrared radiation. *J Photochem Photobiol B* 2002;**68**:93–100.
86. Kaestner L, Juzeniene A, Moan J. Erythrocytes—the "house elves" of photodynamic therapy. *Photochem Photobiol Sci* 2004;**3**:981–989.
87. Kaestner L. Calcium signalling: approaches and findings in the heart and blood. Heidelberg: Springer Verlag; 2013.
88. Förster T. Intermolecular energy migration and fluorescence. *Ann Phys* 1948;**6**.
89. Esposito A, Tiffert T, Mauritz JMA, Schlachter S, Bannister LH, Kaminski CF, et al. FRET imaging of hemoglobin concentration in *Plasmodium falciparum*-infected red cells. *PLoS One* 2008;**3**:e3780.
90. Chien S, Jan K-M. Ultrastructural basis of the mechanism of rouleaux formation. *Microvasc Res* 1973;**5**:155–166.
91. Rampling MW, Whittingstall P. A comparison of five methods for estimating red cell aggregation. *Klin Wochenschr* 1986;**64**:1084–1088.
92. Baskurt O, Neu B, Meiselman HJ. Red blood cell aggregation. Boca Raton: CRC Press; 2012.
93. Picart C, Piau JM, Galliard H, Carpentier P. Human blood shear yield stress and its hematocrit dependence. *J Rheol* 1998;**42**:1–12.
94. Shin S, Park M, Jang J, Ku Y, Suh J. Measurement of red blood cell aggregation by analysis of light transmission in a pressure-driven slit flow system. *Korea-Aust Rheol J* 2004;**16**:129–134.
95. Steffen P, Jung A, Nguyen DB, Müller T, Bernhardt I, Kaestner L, et al. Stimulation of human red blood cells leads to Ca^{2+}-mediated intercellular adhesion. *Cell Calcium* 2011;**50**:54–61.
96. Kaestner L, Steffen P, Nguyen DB, Wang J, Wagner-Britz L, Jung A, et al. Lysophosphatidic acid induced red blood cell aggregation *in vitro*. *Bioelectrochemistry* 2012;**87**:89–95.
97. Carvalho FA, de Oliveira S, Freitas T, Gonçalves S, Santos NC. Variations on fibrinogen-erythrocyte interactions during cell aging. *PLoS One* 2011;**6**:e18167.
98. Minetti G, Ciana A, Profumo A, Zappa M, Vercellati C, Zanella A, et al. Cell age-related monovalent cations content and density changes in stored human erythrocytes. *Biochim Biophys Acta* 2001;**1527**:149–155.
99. Lew VL, Daw N, Perdomo D, Etzion Z, Bookchin RM, Tiffert T. Distribution of plasma membrane Ca^{2+} pump activity in normal human red blood cells. *Blood* 2003;**102**: 4206–4213.

6. Discussion

NMDA receptor in red blood cells as a novel calcium influx pathway

NMDA receptors in bone marrow and erythroid precursor cells (EPCs)

We were the first to show the presence of NMDA receptors in the EPCs and in the circulating RBCs of rats and humans. In line with our observations systemic exposure to glutamate was shown to induce a massive accumulation of adipose tissue and reduction of hematopoietic tissue within the bone marrow in mice [291]. These processes were earlier on largely attributed to the action of glutamate on NMDA receptors in megakaryocytes. In these cells expression of the NR1 and NR2D mRNA and NR1 protein was reported by Genever and colleagues [292]. Staining for the presence of NR1 subunit (immunohistochemistry) and the receptor activity ([^{3}H]MK 801 binding) revealed high levels of the NMDARs in megakaryocytes [292]. However, staining specific for the NR1 subunit in bone marrow sections was not entirely restricted to the megakaryocytes alone (See Fig 1). No attempts were done to identify the localization of the NR2D and NR3 subunits in this study.

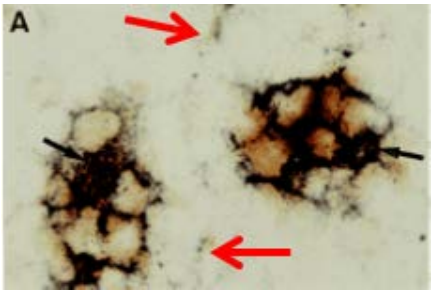

Figure 1. Binding of [^{3}H]MK-801 (black dots, silver staining) and staining with the NR1 antibody (brown staining) in rat bone marrow (from the Genever *et al* [292]). The highest intensity of staining was attributed to megakaryocytes, however, some staining is seen in the plasma membranes of surrounding cells (red arrows).

We showed that the NMDA receptors are present in the cells populating bone marrow, in particular those forming erythroid progeny in rats and humans. In rat bone marrow NR1 subunit was co-expressed with early erythropoetic marker CD36 (**Paper 1**, Figure 1). The presence of NR1 was later on tracked in CD71+ rat reticulocytes (**Paper 1**, Figure 1). Using ex vivo erythropoiesis system we have observed expression of the receptor subunits NR1, NR2A, 2C, 2D, 3A and 3B in human CD34+ monocytes-derived proerythroblasts, polychromatic and orthochromatic erythroblasts and reticulocytes (**Paper 2**, Figure 1, 2). In human erythroid precursor cells NR2D and 3B appeared to be the dominating subunits (**Paper 2**).

High abundance of the NR3 subunits in EPCs defines specific features of the receptor channel. Channels formed by the NR1 and NR3 subunits expressed in *Xenopus* oocytes were resistant to Mg^{2+} block and therefore may be activated at the transmembrane potentials as low as -70 mV [293]. The ligand sensitivity of NR3-containing receptors differs from that of NR1/NR2 heterotetramers. Receptors formed by the NR1 and NR3 subunits and expressed in *Xenopus* oocytes reaches their maximal activation at glycine concentration of 10 μM, higher concentrations have an inhibitory action (plasma glycine concentration is around 200-300 μM). D-serine known as an agonist of the conventional NMDA receptors inhibits the ones formed by NR1 and 3 [293]. Such "glycine receptors" are activated in response to local *decrease* of the glycine or D-serine concentrations and do not require glutamate or NMDA for their activation [293]. They have low cation selectivity and low affinity to the channel pore blockers MK-801 and memantine. Furthermore, of NR3-containing receptors, unlike NR1/NR2 receptors, are able to respond only by the partial activation (see Chapter 1) [294]. Moreover, unlike "neuronal" NR1/NR2 receptors NR1/NR3, are insensitive to MK-801 and memantine ([295], see also Table 1 in Chapter 1).

Some of these properties are lacking in the receptors expressed in the EPCs and present in RBCs. Activation of erythroid receptors with NMDA/glutamate (100-300 μM) and glycine (100 μM) in the precursor cells is clearly associated with Ca^{2+} uptake that can be blocked by memantine or MK-801 (**Paper 2** Figure 3A). In human EPCs glycine administration induces tiny currents whereas co-administration of NMDA causes their pronounced amplification (P. Haenggi

unpublished data). The NMDA receptors in early EPCs (proerythroblasts and basophilic erythroblasts) respond to the stimulation with agonists with high amplitude currents with fast deactivation kinetics whereas cells at the later differentiation stages the EPCs switch from expression of the NR2A (fast-inactivating currents with high amplitude) to NR2C (slow-inactivating currents with small amplitude) resulting in receptor-mediated currents with smaller amplitude and longer decay time (P. Haenggi unpulished data).

To our knowledge, receptors formed by the NR2D and 3B as well as NR2A (early stages)/2C (late stages) similar to those expressed in the EPCs have never been studied in model systems. Their properties remain largely unknown and await further investigation.

Possible physiological role of the erythroid NMDA receptors is one more thrilling and poorly explored area. The nature of signals sensed by these receptors in the EPCs remains unknown. The presence of glutamate/aspartate transporters (GLAST) and GLT-1 and the proteins required for controlled vesicle release in megakaryocytic membranes suggests that these cells may actively release glutamate into the intercellular space in bone marrow [296], [292]. These changes in glutamate levels, when occurring, will be sensed by the NMDA receptors in erythroid progenitor cells. EPCs will also respond to the "systemic" changes in glutamate, NMDA and D-serine levels occurring in blood plasma. Furthermore, the receptors are known to respond to the changes in pH, voltage, and the changes in redox state and NO. They are mechanosensitive and thus sensing shear stress in particular when passing through the cellulose column of during separation on Percoll gradient (**Paper 3**).

Calcium-driven signaling was reported to be a very essential part of differentiation program of the EPCs [297], [298]. Calcium was required for the Epo to Epo receptor signaling cascade to function [298], and to support viability of cells at the earlier (CFU and BFU-e) stages of erythropoietic development [299]. Among the Ca^{2+} uptake pathways expressed in the EPCs are transient receptor potential channels (TRPCs 2,3 and 6), Cav2.1 channels, and NMDA receptors (**Paper 2**, Fig 3A). Importance of the erythroid NMDA receptors for the EPCs is reflected by high sensitivity of the cells in culture to high doses of MK-801 or memantine, channel-pore targeting antagonists of the receptor. Exposure to antagonists

resulted in an increase in mortality which was most prominent at the proerythroblastic stage (**Paper 2**, Figure 3B**, Paper 3**, Figure 7). For the unknown reasons sensitivity to antagonists is markedly blunted in proerythroblasts of patients with sickle cell disease (**Paper 3** Figure 7B) which are significantly less sensitive to the antagonsits, than those of healthy humans (**Paper 3**, Figure 7A). Polychromatic and ortochromatic erythroblasts appeared to be less sensitive to the antagonists. Hyperactivation of the NMDA receptors in EPCs by supplementing incubation medium with NMDA showed no adverse effects. Our preliminary data (Pascal Haenggi, unpublished) indicate that inhibition of the NMDA receptor is associated with activation of caspases, externalisation of phosphatidylserineand induction of apoptosis (**Paper 3**, Figure 7C, vacuolization).

We observed substantial inter-cellular and inter-individual heterogeneity between the NMDA receptor subunits expression and the receptor abundance in healthy EPCs within one differentiation stage (**Paper 2**, Figure 1, 2). These findings most probably indicate the existence of several sub-populations of cells with different sets of properties that provide more flexibility in regulation of erythropoiesis. Heterogeneity of precursor cells is followed by heterogeneity of the functional NMDA receptor levels in mature RBC (**Paper 2**, Figure 6) and in NMDA-mediated responses (**Paper 2**, Figure 4C, 7D). These findings supports current paradigm about RBC heterogeneity [300].

Further characterization of the physiological and pathophysiological role of the NMDA receptor in EPCs and other hematopoietic progenitor cells including megakaryocytes and lymphocytic progenitors is crucial for understanding of pathologies associated with progression of congenital anemias. Pharmacological regulation of NMDA receptor activity in the EPCs can be beneficial for upregulation of RBC production in cases of congenital anemia, platelet production in patients with thrombocytopenia and downregulation of leukocyte production in patients with leukemia Differences in NMDA receptor subunit composition we have observed between the EPCs (lack of NR2B subunit) and white blood cells (**Paper 2**, Table 1) and other lineage-specific properties allow development of specific compounds targeting distinct of bone marrow-driven blood disorders.

Mammalian bone marrow pluripotent cells are capable to differentiate into neurons and express neuronal proteins including NMDA receptors [301]. Bone marrow was developed very early in the vertebrate evolution, it already exist cartilaginous fishes (e.g. sharks) [302]. Studies of embryogenesis of vertebrates and anatomy of a primitive chordate *B. lanceolatum* indicate that hematopoiesis generally takes place concomitantly with cardiovascular development. Within the embryo, hematopoietic regions form within the aorta-gonads-mesonephros region. Later in development part of hematopoetic cells forming this region migrates into the cardiogenic domain. Furthermore, evolutionary hematopoietic cells appear to be precursors of endothelial cells in vertebrates [303]. In humans with severe congenital anemia erythropoietic pool can be expanded from the normal location in the bone marrow of axial bones (e.g. vertebra, skull and rib cage) to other bones, spleen, liver and soft tissues adjacent to bone ([304], p 293). Thus, it seems that NMDA receptors could be an attribute of pluripotent non-differentiated cells (stem and cancer cells [305]). In some cell types (podocytes [306], osteoclasts, thrombocytes etc) NMDA receptor protein is preserved up to the terminal stage of development.

NMDA receptor function in rat and human erythrocytes

During the last steps of the maturation human and rat RBCs are losing the majority of their NMDA receptors (Fig 2). From several thousands per cell NMDA receptor copies is reduced to several dozen in young red blood cell population and further to few receptor copies per cell on average in mature and senescent population (**Paper 1**: $3.5*10^5$ NMDAR per cell in human erytroid progenitor cell line, **Paper 2**: 18,300 –540,000 copies of NR2D subunit per cell at day 12 of differentiation). In healthy circulating human and rat RBCs these receptors are involved in regulation of RBC volume and density (**Paper 2,** Figure 7D) as they regulate activity of the Ca^{2+}-sensitive K^+ (Gardos) channels (**Paper 1,** Figures 4 and 5, **Paper 2,** Table 2). NMDA receptors are active players in control of intracellular Ca^{2+} levels (**Paper 1,** Figure 3, **Paper 2** Figure 4 and 7) contributing thereby to the regulation of activity of eNOS and NOX in RBCs (**Paper 1,** Figure 7A and B) by that regulating intracellular redox state (**Paper 1**, Figure 7C), rheology and vascular tone [307]. Very essential, but yet poorly understood finding

of ours study is the involvement of the intracellular Ca^{2+} in regulation of hemoglobin oxygen affinity (**Paper 2** Figure 8). This striking feature seems to be closely related with the adaptive optimization of oxygen supply in athletes as exhaustive exercise is associated with a transient increase in plasma glutamate levels (Makhro unpublished data, [308]). Calpain activity and gradual oxidation are the two Ca^{2+}-dependent factors defining RBC life span that is reduced in endurance athletes [309].

Our most fundamental findings on the composition and possible physiological/pathophysiological function of the NMDA receptors in human and rat RBC are summarized in the Table 1:

Table 1. NMDA receptor properties and function in rat and human erythrocytes.

	Human (Papers 2 and 3)	Rat (Paper 1)
Abundance in EPCs and RBC	GRIN1, 2A, 2C, 2D, 3A, 3B transcripts were found in erythroid progenitors (from day 6 to day 18 in culture). Protein detection: NR1 (in circulating RBCs) and NR2C, NR2D, NR3A and NR3B subunits (EPCs) were identified ~350 000 of NMDAR copies in UT-7/Epo cells (erythroid progenitor cell line)	NR1 subunit protein co-localized with CD36 (early erythroid precursors) in bone marrow;
Function in EPCs	Agonists-driven Ca^{2+} influx; a complete NMDA receptor block at the early stages of erythropoiesis induced apoptotic cell death	Not accessed
Abundance in	All detected NR subunits	NR1 subunit colocalized

reticulocytes (transferrin receptor CD71 as a marker)	were co-expressed with CD71	with CD71. NR1 subunit abundance correlated with high intracellular Ca^{2+} content in circulating red blood cells
Number of NMDA receptor copies in circulating red blood cells	Young RBC: 34.9±7.5, mature RBC: 4.1 ± 0.7, senescent RBC: 4.3± 0.6	General RBC population: 8 per cell
Ca^{2+} entrance	Produced by NMDA, HCA. Glu and Gly, high intracellular and intraindividual heterogeneity of response; blocked by NMDA receptor antagonists	Produced by NMDA, HCA. Glu and Gly, high intracellular heterogeneity of response; blocked by NMDA receptor antagonists
K^+ fluxes	NMDA/Gly produced NMDAR antagonist-sensitive flux	NMDA, HCA and Glu produced concentration-dependent NMDAR-antagonists sensitive fluxes; NMDA-induced flux was completely abolished by clotrimazole or Ca^{2+} chelators
RBC volume	Transient volume reduction in response to NMDA treatment; High inter-individual and inter-cellular variability	NMDA and HCA treatment produced reversible volume reduction and echinocyte formation; Reversibility was abolished by Ca^{2+}pump inhibitor
Oxidative stress	Not accessed in healthy	NO-synthase – mediated

	humans	oxidative damage
Intracellular pH and oxygen saturation	NMDA treatment produced pH-mediated transient changes in hemoglobin-oxygen binding	Not accessed
Hemolysis	Never observed	NMDA and HCA treatment induced severe hemolysis; NMDA receptor antagonists had protective effect

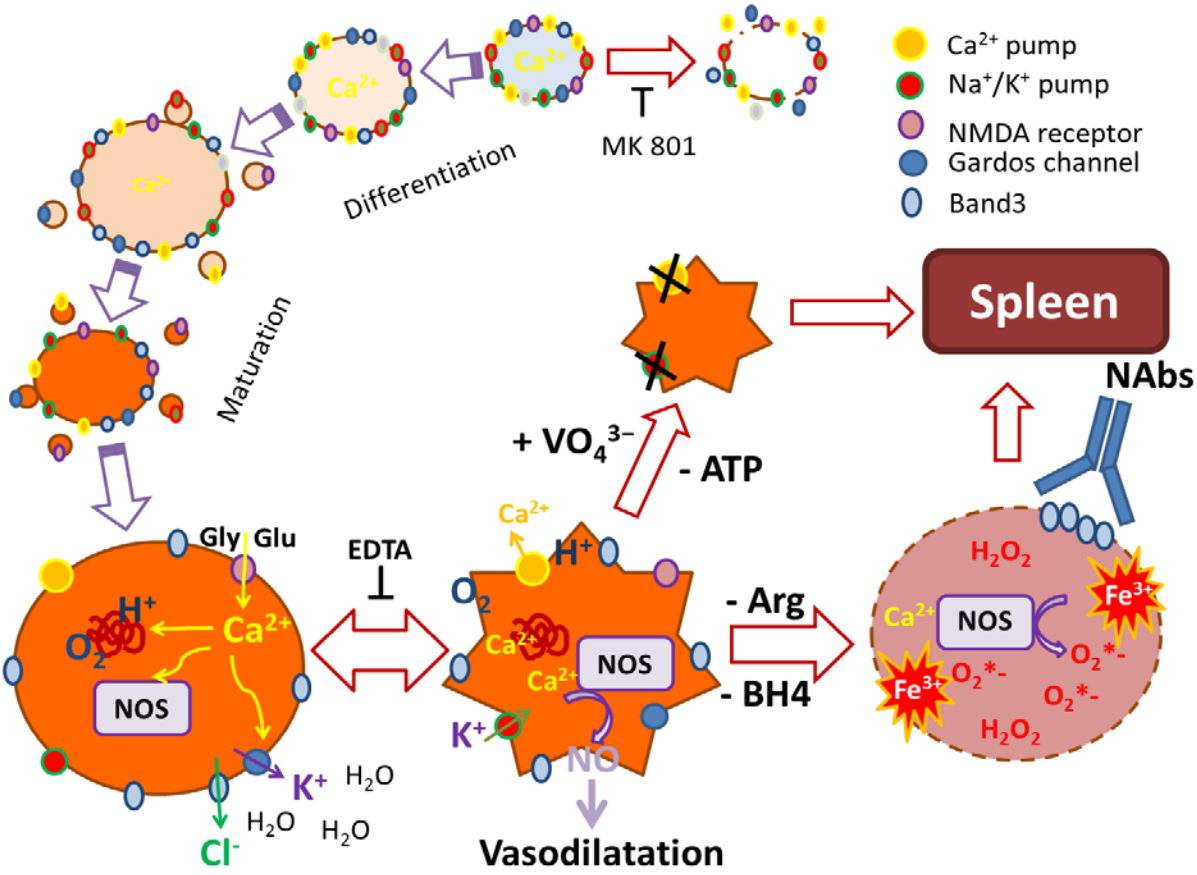

Figure 2. NMDA receptors in human and rat red blood cells. A schematic representation of the data published in papers 1 and 2. NMDA receptors (as well as other membrane proteins) are highly abundant in hematopoietic stem cells. They are required for the Ca^{2+} signaling and essential for the cell survival. Orthochromatic erythroblasts and reticulocytes lose most of their NMDA receptors during the maturation. Clearance of the receptors continues in

reticulocytes and young RBCs (neocytes) after they are released into the circulation. Enriched with receptors, these young cells are more susceptible to Ca^{2+} overload and subsequent elimination than mature cells in a process known as neocytolysis [310]. In mature erythrocytes only few copies of the NMDA receptor are present. NMDA receptor is activated by plasma amino acids Glu and Gly followed by the Ca^{2+} entrance into the erythrocyte. We followed two targets modified by NMDA receptor-mediated Ca^{2+} influx: Gardos channel and endothelial NO synthase (eNOS). Ca^{2+} activates Gardos channels and therefore K^+ loss leading to the cellular dehydration and volume reduction. The cell shape and volume will recover as soon as Ca^{2+} and Na^+/K^+ pumps will re-establish ion gradients. Plasma membrane Ca^{2+} ATPase inhibition by orthovanadate (VO_4^{3-}) prevents shape and volume recovery and eventually leads to the cell destruction in the spleen. Ca^{2+} interacts with hemoglobin molecules and induces oxygen and proton release. Activation of eNOS in the presence of a substrate arginine leads to the NO production and vasodialatation. In the Arg- or tetrahydrobiopterin (BH4) – deprived environment active eNOS produces superoxide anion which is converted to H_2O_2 by superoxide dismutase. Oxidative stress causes methemoglobin production (Fe^{2+} oxidation), glutathione depletion, Band3 clustering [311] (Band3 clusters bind to naturally occurring antibodies, Nabs, which facilitates RBC removal [312]) and result in premature clearance.

In membranes of erythrocytes of patients with sickle cell disease (SCD) NMDA receptors are more abundant than in healthy controls (**Paper 3,** Figure 1B,C) although the receptor expression (mRNA and protein, **Paper 3,** Figures 5, 6) during the hematopoiesis was not altered. For the "mature" red cell population this reflects the fact that the lifespan sickle cell erythrocytes is substantially reduced (RBC lifespan being on average 15 days instead of 70 – 140 days in healthy subjects [313], [314]) and the circulating cells are about 10 times younger than healthy erythrocytes having more of NMDA receptors retained. However, this does not explain a two to 10-fold increase in the number of active receptors in the young population of SCD-RBCs compared to the young population of healthy human donors which is most susceptible to premature clearance [315]. It suggests that the excessive NMDA receptor abundance in SCD RBC results from the incomplete clearance in the course of disturbed maturation process. During the final stage of erythropoiesis RBC precursor cells are losing the nucleus, most of the intracellular organelles including mitochondria, and many of the proteins located within the plasma membrane. The mutated hemoglobin S is known to have higher affinity to the membrane cytoskeleton [316] disturbing thereby

cytoskeletal remodeling occurring during the RBC maturation and resulting in delayed clearance of integral and cytoskeletal proteins and increasing membrane rigidity. Indeed, proteomic studies showed that two main cytoskeletal proteins 4.1 and ankyrin are upregulated in SCD RBC [317].

Similar to that in the EPCs activation of the NMDA receptor by various agonists induces calcium influx into human and rat RBCs (**Paper 1,** Figure 3, **Paper 2,** Figures 4 and 7, **Paper 3,** Figure 3 and 4).

Calcium uptake is followed by the activation of Ca^{2+}-sensitive K^+ (Gardos)-channels . Net loss of K^+ and Cl^- and water results in transient shrinkage. The reduction in cell volume was associated with the formation of "91otential91 cells" (echinocytes) and "cup cells" (stomatocytes) (**Paper 1,** Figure 6A, **Paper 3,** Figure 4D). Such shape changes are known to affect red cell deformability, mechanical stability and rheology [318]. In line with that hemolysis was induced by stimulation of the NMDA receptors in RBC from the anemia patients (SCD and some cases of hereditary spherocytosis, unpublished observations) with abnormally high NMDA receptor abundance. Long-term up-regulation of intraerythrocytic Ca^{2+} levels occurring *in vivo* in the circulation further contributes to the loss of mechanical stability by induction of proteolysis of cytoskeletal proteins by Ca^{2+}-sensitive protease μ-calpain and stimulation of superoxide anion production by NADPH oxidases [201] making cells of patients even more fragile and prone to shear-stress-induced hemolysis.

In SCD patients more factors add to the the *in vivo* the mechanism of the NMDA receptor-mediated hemolysis which are related to the specific properties of HbS. Deoxygenation, low pH values and increase in shear stress normally occurring in the capillaries of tissues as well as pro-inflammatory cytokines present in blood of this group of patients during the crises activate P_{sickle} conductive pathway (for details see Chapter 3) along with the onset of polymerization of HbS. P_{sickle} is caring both inward Ca^{2+} and Na^+ current and outward K^+ flux. Uptake of Ca^{2+} triggers further K^+ loss via the activated Ca^{2+} activated K^+-channels (Gardos), causing severe dehydration. The hemoglobin S concentration in the sickled cells is increasing favoring irreversible polymerization of deoxyhaemoglobin. Based on our experimental data and striking similarities between known P_{sickle} and NMDA receptor properties, we assume that P_{sickle} is at least partially carried by

NMDA receptors. The cells undergo sickle cell transformation getting mechanically fragile. Excess of calcium triggers extensive oxidative damage due to the abnormally high abundance and activity of NOXes [319]. Gardos channel is further activated upon cleavage by μ-calpain [320] and band 3 protein cleavage by this protease is prominent [321]. As a result premature clearance and hemolysis occur. Patients with SCD are asymptomatic most of the time, but decrease in oxygen availability (hypobaric hypoxia, diving, lung disease), hyperthermia, inflammatory process or dehydration result in development of pain crises associated with an increase in number of terminally dehydrated RBCs with polymerized HbS. The number of NMDA receptors in RBCs during pain crises increases above that in asymptomatic period as does sensitivity to agonist stimulation (**Paper 3**, Figures 1 and 2).

Ex vivo we showed that SCD RBC pretreated by NMDA receptor channel blocker memantine exhibit almost no sickling even in 0.5% O_2 atmosphere during 15 min (Paper 3 Figure 4B). Furthermore, decrease in the intracellular calcium was followed by rehydration of SCD-RBCs. Long-term effects could not be monitored in our ex vivo experimental settings. The expected ones include lower adherability [322] and decrease in incidence of vaso-occlusive crises are often associated with hemolytic and pain crises in patients with SCD. Calcium was shown to be ultimately required to promote adherence of SCD-RBCs to the endothelial cells [323, 324, 325]). Increased rigidity, poor membrane stability and high adherence give rise to facilitated thrombus formation, stroke, myocardial infarction or multi-organ failure in patients with SCD [326].

According to the World Health Organisation (2011), about 5% of the humanity carries abnormal hemoglobin genes, mostly hemoglobin S (HbS). Why these mutations in beta chain of hemoglobin gene, although leading to such devastating diseases, were not eliminated but actually preserved by the natural selection? Reversible polymerization/crystallization of hemogolobin as an adaptive hemoparasite defense strategy is relatively wide-spread in vertebrates. It was described in fishes [327, 328], reptiles and mammals (cervidae deer, [329]). In humans the appearance of hemoglobin S in Africa (2000-3000 years ago) and Asia (4000 years ago) followed the development of iron tools and advanced agricultural system that promoted increased human habitation density ([304], p

565). Bigger settlements provided better breeding environments for the mosquitos caring the malaria plasmodium parasite. Hemoglobin S allele (as well as thalassemia and other abnormal hemoglobin alleles) geographically coexist with current or historical malaria regions. While HbS homozygotes (who carry two alleles of abnormal hemoglobin) have very short life expectancy, heterozygotes do not suffer from anemia and pain crisis and exhibit high resistance to malaria. One of the proposed mechanisms of such resistance is the increased RBC fragility due to spontaneous irreversible (in contrast to other vertebrats) polymerization of deoxyHbS. The attempt of the plasmodium parasite to invade such red cells results in their facilitated hemolysis and prevention of progression of the disease [330]. In addition, excessive amounts of intracellular Ca^{2+} in hemoglobin S containing RBC can also does not favor the parasite invasion [331]. Thus, expression of hemoglobin S is an adaptive tool to confront the malaria via increased NMDA receptor abundance in mature red blood cells. The point mutation GAG → GTG creates substitution Glu → Val in position 6 on the β chain which attaches to the plasma membrane proteins and affects red blood cell maturation. That substitution was strongly supported by natural selection in at least five geographically separated regions of Africa, India and Arabia ([304], p 566) leading to 10-20% prevalence of hemoglobin S genotype.

A role of myocardial NMDA receptor in rhythm formation and ventricular signal transduction

(Table and figure references to the manuscript "Cardiac N-methyl D-aspartate receptors as a pharmacological target" are in **bold**.)

Earlier on expression of the NMDA receptor subunits was reported in mouse, rat, sea lion and human myocardium [332, 333, 334, 335, 336]. We were the first to perform extensive screening for the GRIN gene expression patterns and the receptor activity in various areas in the heart. Furthermore we characterized responses of denervated rat heart to agonists and antagonists of NMDA receptors and obtained cardiac receptor pharmacological profile for the rat (see the attached manuscript), as well as for human and horse ventricular and atrial tissue (Makhro, Mitchell and Kosenkov unpublished data).

Our knowledge of molecular and pharmacological characterization of cardiac NMDA receptors may be implicated in the pathobiology of some cardiac disease. Epidemiological studies revealed that high plasma concentrations of NMDA receptor agonist homocysteine predict one-year survival in patients with severe systolic heart failure [337], post-infarctional development of the heart failure [338], high plasma homocysteine concentration correlates with the severity of heart failure in patients with chronic myocardial infarction [339]. Moreover, plasma homocysteine predicts the risk of recurrence of nonvalvular atrial fibrillation [340], [341]. Plasma homocysteine is associated with an alteration in the electrical atrial conduction, possibly contributing, at least in part, to the increased risk of cardiac arrhythmias in the denervated hearts of orthotopic heart transplantation patients [342]. Based on our data, we may propose cardiac NMDA receptor as a novel target for pharmacological interventions in patients suffering from arrhythmias and heart failure. Moreover, NMDA receptor antagonists could be beneficial during the surgical interventions or for the post-operational treatment to prevent cardiological complications in patients undergoing heart surgery.

Site-specific subunit composition of the receptor and its pharmacological properties

One of the unexpected findings of our work is a marked diversity of the subunit composition and the receptor density in various regions of rat heart. As shown in **Table 3**, in most parts of the rat myocardium NMDA receptors are formed by the NR2D/NR3A subunits similarly to that in human erythroid precursor cells where NR2D and NR3 subunits were dominant. Receptors containing that types of subunits are known to have very slow deactivation kinetics (several seconds [59], [60]). But in contrast to erythroid lineage, NR2B subunit is also present in heart chambers and its amount is increasing with the age of animal (**Figure 4E**). NR2B forms relatively high amplitude fast inactivating receptors and represents a well–known pharmacological target for ifenprodil-like compounds [343]. In atria more of the subunits commonly found in the rat brain are expressed. Those including NR2A subunit forming together with NR1 fast receptors with high current amplitude [59]. NR3B subunit transcripts in rat atria

were below the direction limits. What is the actual NMDA receptor composition (NR1/NR2A or NR1/NR3A/NR2B/NR2D etc.) in the myocardial cells remains unknown. However, since the inhibitory effect of the NMDA receptor channel pore targeting antagonist MK-801 on the heart rate had no synergetic effect with NR2B specific antagonists, we assume that NMDA receptors of pacemaker cells have an obligatory NR2B subunit in their composition (**Figure S2**). High abundance of NR2B subunit in rat myocardium was confirmed by autoradiography (**Figure 4 C**). In presence of eliprodil [^{3}H]MK-801 binding was suppressed in all regions of heart. NR1, NR2A, NR2B and NR2C subunits were detected in the whole heart homogenates by western blot using specific antibodies. However, other groups could not detect some of these subunits, for example, the group of Seeber could detect NR2B subunit only in neonates. This group failed to detect any other NMDA receptor subunits in rat heart. They showed that NR2B subunit in rat cardiomyocytes underwent cardiac-specific post-translational modifications [134]. Group of Leung [131] could not detect any of the NR2 subunits by immunoblotting. The possible reason for these contradictory findings obtained in several groups including the present study most likely are cardiac-specific posttranslational modifications of NMDA receptor subunits making them invisible for many of the brain-specific antibodies.

Expression of the NMDA receptor transcripts is restricted to the cardiomyocytes. Isolated adult ventricular cardiomyocytes expressed the same subunits (NR3A/NR2D/NR2B) as ventricular tissue (**Table 3**. None of them could be detected in isolated fibroblasts.

A striking feature of the myocardial NMDA receptors making them different from the well-studied neuronal receptors is the lack of NR1 glycine binding subunit in ventricles. Very low expression of this subunit was detected in atria. At present it is believed that NR1 subunit is obligatory for the NMDA receptor trafficking from the endoplasmic reticulum to the surface of sarcolemmal membrane (see Chapter 1). Moreover, each NR1 subunit is associated with NR2 subunit in functional dimer within the NMDA receptor complex (see Fig 3B in Chapter 1).

Thus what we observed in the heart could be:

1) a novel type of NMDA receptor composed of NR3A-NR2 subunits with low affinity to NMDA and D-Ser, but high affinity of glutamate and glycine (**Figure 2A-D**);
2) a chimeric type of glutamate receptor with unusual properties (AMPA-NMDA receptor or kainate-NMDA receptor or in combination with other channels like ryanodine receptors [134]);
3) it remains unclear if AMPA or kainate receptors are required to prime the NMDA receptor activation in the heart. Membrane depolarization in prior to the NMDA receptor activation may be triggered by other cardiac channels. Also, cardiac NMDA receptors may not possess voltage-dependent channel block (NR1/NR3 receptors are resistant to Mg block, see Table 1.1 in Chapter 1) and consequently may not require membrane depolarization for the channel activation.

Pharmacological properties of the rat cardiac NMDA receptors were assessed in isolated myocardial sarcollemal membranes and in tissue sections by using displacement of [^{3}H]MK-801, NMDA receptor channel pore targeting ligand. In both atrial and ventricular sarcolemmal membrane MK-801 affinity was similar to that in the brain [66] (see also Chapter 1 Table 1), Figure 3. However, affinity of the cardiac NMDA receptors to memantine was 3 orders of magnitude higher in the ventricular tissue than in the brain (IC_{50} 1 nM vs ~1μM). Receptors in the atrial tissue had lower affinity to memantine than ventricular tissue (IC_{50} ~40 nM) but still much higher than that in the brain tissue. Sensitivity of the cardiac NMDA receptoir to ketamine (racemate) was similar in the myocardium and brain membranes. Pretreatment of the sarcolemmal membranes or tissue sections with NR2B subunit targeting drug eliprodil decreased [^{3}H]MK-801 binding (**Figures 3C and 4C**). Electrophysiological studies in neurons revealed that eliprodil analog ifenprodil reduces the frequency of channel opening [344]. Therefore, the probability for the radiolabeled channel pore blocker to bind to the receptor was reduced in the presence of ifenprodil-like compounds.

Thus, specific pharmacological properties of rat cardiac NMDA receptors resulted from their unusual subunit composition. That feature of cardiac NMDA receptors makes them an attractive target for cardiac-specific drug development.

Similar to that in EPCs and circulating RBCs, hyperactivation of the NMDA receptors was not deleterious for the neonatal cardiomyocytes, whereas exposure of them to the channel pore-targeting inhibitor memantine was toxic and caused massive cell death (Figure 3). Adult rat heart on the contrary responded to the intracoronary administration of the NMDA receptor agonists with induction of arrhythmia and impairment of miscroperfusion of ventricular capillaries (**Figure 2E**).

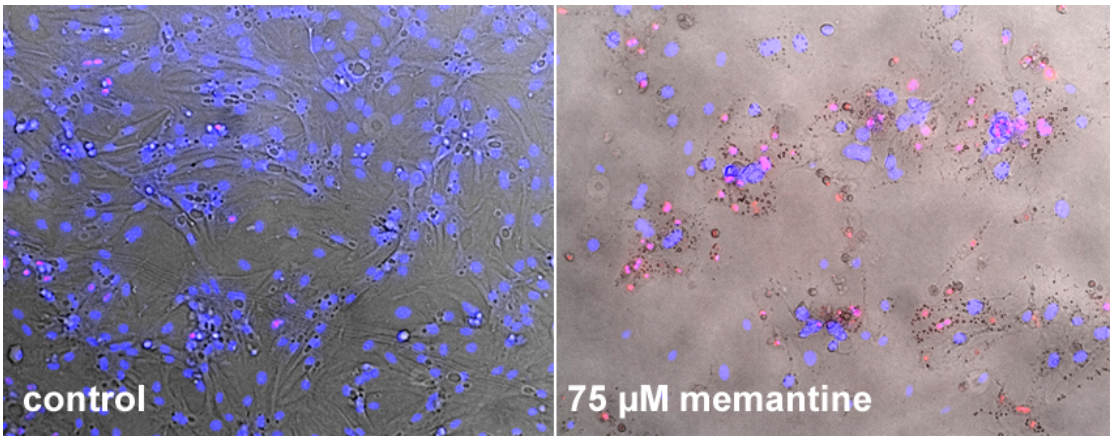

Figure 3. Cultured neonatal cardiomyocytes with or without memantine. Blue color designates nuclei of intact cells (Hoechst staining), red color (propidium iodide, PI) indicates PI-positive nuclei of dead cells. Memantine treatment for 24 h resulted in massive death of neonatal cardiomyocytes.

We have observed the corresponding changes in heart rhythmicity following the changes in activity of NMDA receptors in isolated rat heat.

Rhythm and ECG

To study the role of cardiac NMDA receptors in rat heart we have chosen isolated rat heart model. The main advantage of our setup is that heart is free from the all kinds of neuronal or neurohormonal regulation. Hearts were perfused either with buffer, or with the blood obtained from the same animal.

Hearts perfused with Krebs-Henseleit (KH) buffer instead of blood had about two times lower spontaneous contractility rate. However, in that experimental setup we controlled amino acid concentration acting on myocardial NMDA receptors. Treatment with Glu-Gly mixture showed reversible increase of the heart rate and heart rate variability within the physiological range (EC_{50} for

tachycardia 149 μM, for heart rate variability 271 μM). Surprisingly, specific NMDA receptor agonist NMDA and co-agonist D-serine affected the heart rate only within the millimolar range. As we know from electrophysiological studies on NMDA receptors expressed in neurons (cultured cells or tissue slices), in model cell cultures (human embryonic kidney cells), Xenopus oocytes, affinity and efficiency of NMDA and D-Ser were similar to Glu and Gly (see Chapter 1). There are two possible reasons explaining the difference between Glu and NMDA-driven effects: specific cardiac NMDA receptor properties (see below) or coupling with other glutamate receptors (similar to the AMPAR-NMDAR coupling in the brain).

Unlike neuronal NMDA receptors, myocardial receptors are constantly exposed to the plasma-borne high concentrations of their main agonist glutamate and co-agonist glycine because these amino acids are very abundant components of the blood plasma (~150 μM of Glu [345], 300-500 μM of Gly [346]). Hyperactivation of the cardiac NMDA receptors by addition of high doses of agonists to the perfusate (blood or KH buffer – (Glu, NMDA or homocysteic acid) provoked either tachycardic or arrhythmic responses (**Figure S2**). Administration of pore-targeting antagonists was causing negative chronotropic effect in blood-perfused hearts even in the absence of additional stimulation with agonists. These findings obtained using isolated blood-perfused rat hearts suggested that the cardiac NMDA receptors are most likely permanently active in the pacemaker cells. Ifenprodil-like compounds eliprodil and Ro25-6981, targets NMDA receptor regulatory site, both induced bradycardia. Glutamate-binding site competitive antagonists APV and PEAQX (or NVP-AAM077) had no effect on the heart rate probably due to the presence of excessive glutamate in the blood plasma (~200 μM of Glu). Glycine binding site competitive antagonist L-701,324 failed to produce any changes in the heart rate as well (plasma Gly concentration is >300 μM).

As a ligand-gated non-selective cation channel NMDA receptor contributes to the electric activity of the heart including autonomous rhythm formation in pacemaker cells and in excitation propagation thought the ventricular walls in cardiomyocytes. Slow depolarization of the pacemaker cells is mediated by the activation of several channels and ion transporters are involved in that process

forming K^+-Na^+-Ca^{2+} "funny" current including hyperpolarization-activated, cyclic-nucleotide-gated channels (HCN). These channels share certain structural-functional similarities with NMDA receptors including their chimeric origin (see Figure 1 in Chapter 2).

Both HCN and NMDA receptor channels respond to the same channel blocker ZD7288, used as heart rate-reducing agent ([151], p 109) which inhibits hippocampal NMDA receptors *in vivo* [347]. The inhibitory potential of the pore-targeting NMDA receptor antagonists towards the HCN channels has never been tested. We have shown that the NMDA receptor pore-targeting inhibitors were acting as anti-arrhythmic drugs (**Table 2**). This anti-arrhythmic effect of the channel pore-targeting drugs MK-801, memantine or ketamine may be hence attributed to their non-specific action on HCN channels. However, similar bradycardic and anti-arrhythmic action has been demonstrated for the antagonists targeting alternative binding sites (such as Ro25-6981 and eliprodil which bind to the ifenprodil binding site localized within the NR2B subunit (Chapter 1 Figure 1.3A). In line with these observations bradycardia has been reported in human clinical trials of ifenprodil and eliprodil and anti-arrhythmic action (reduction in dysrhythmia) noted for aptiganel, a competitive NMDA receptor blocker [150].

In experiments on isolated blood-perfused rat hearts we observed that NMDA receptors remain permanently active in the heart pacemaker cells. We can always reduce the pacemaker activity (or hyperactivity in case of tachyarrhythmia) using NMDA receptor antagonists. Unlike neuronal NMDA receptors, myocardial receptors are constantly exposed to high concentrations of their main agonist glutamate and co-agonist glycine because these amino acids are very abundant components of the blood plasma.

NMDA receptor-related effects in the myocardial tissue could be seen on ECG recordings (**Figure 1**). Channel pore-targeting NMDA receptor antagonists were prolonging QTc interval (QT interval corrected for the heart rhythm), i.e. prolonging ventricular repolarization. Both channel pore- and ifenprodil-like drugs also prolonged QRS interval, meaning that NMDA receptors somehow contribute to the rapid ventricular depolarization. NMDA receptor agonists had no effect on the ECG intervals.

In blood-perfused rat heart the presence of NMDA receptor agonists and antagonists affected capillary perfusion of the ventricular tissue (**Figure 2E**). Receptor activation caused tissue edema (swelled cardiomyocytes and restricted capillary perfusion), while treatment with antagonist facilitated capillary perfusion (reduced cardiomyocyte's volume).

We used L-type calcium channels blockers (CCB) verapamil and diltiatazem to compare their action on heart rhythmicity with that of NMDA receptor antagonists. In our model CCB induced second degree AV block and irregular bradycardia. Moreover, similar effects of CCB on atrio-ventricular conductance were observed in human patients [348]. In contrast to that, NMDA receptor antagonists produced regular bradycardia (**Table 2**). Thus, CCB had pro-arrithmogenic effects while NMDA receptor antagonists were increasing rhythm regularity in all experiments. Therefore it's highly unlikely that both classes of compounds hit the same target.

Initially Zn^{2+} was used in our study as a potential NMDA receptor antagonist (NR2A specific, see Chapter 1). However, treatment with Zn^{2+} caused tachycardia and premature ventricular contractions (i.e. hyperactivation of ventricular cardiomyocytes), (**Figure 1D**, **Figure S2F**). Moreover, those effects were insensitive to MK 801 treatment. In isolated sarcolemmal membranes Zn^{2+} ions were reducing [^{3}H]MK 801 binding within the channel pore at high concentrations (>1 μM) (**Figure 3D**). Low concentrations of Zn^{2+} ions (1 – 10 nM) facilitated [^{3}H]MK 801 binding kinetics as well as a steady state binding (after 1 hour of incubation). In NMDA receptors composed only from NR1 and NR3 subunits Zn^{2+} ions are known to be a potent activators [349]. Zn^{2+} most likely binds to regulatory site on the receptor and facilitates channel opening probability. At the same time Zn^{2+} at high concentrations (10 – 100 μM) was shown to block NMDA receptor channel pore in the voltage-depended manner, in that way Zn^{2+} acts as inhibitor [350]. In our experiments Zn^{2+} probably interacted with both channel pore and with the regulatory binding site. Acting as an activator by binging to the NTD Zn^{2+} was interfering with MK 801 binding within the receptor pore. Since Zn^{2+} ions precipitate in the protein-rich environment such as blood plasma, it is hard to say what was the concentration of free Zn^{2+} ions in our experiments, and what the amount of Zn^{2+} ions was reaching for

cardiomyocytes and pacemaker cells. Further studies on Zn^{2+} binding to cardiac NMDA receptors are needed to clarify the mechanism of Zn^{2+} -driven effects in the heart.

Comparison with clinical data

The data we have obtained were on the rodent heart. Can we use this model to predict the *in vivo* effects of NMDA receptor antagonists and CCB in humans? There are two examples of acute drug poisoning by verapamil (suicidal ingestion) and ketamine (drug addiction) suggesting that our findings can be translated, at some extent, to human.

Example 1

In healthy young man (18 years old) verapamil overdose caused depression of the sinus node function and atrioventricular dissociation (Fig 4A) [351]. In 24 h ECG completely recovered and expressed no abnormalities. Similar results we obtained on isolated hearts from the young healthy rats treated with verapamil or diltiatazem. The resulting atrioventricular block is shown on Fig 4B, P wave inversion also occurred in some experiments. Thus, the effect of high acute doses of L-type calcium blockers in humans can be recreated in isolated rat heart model.

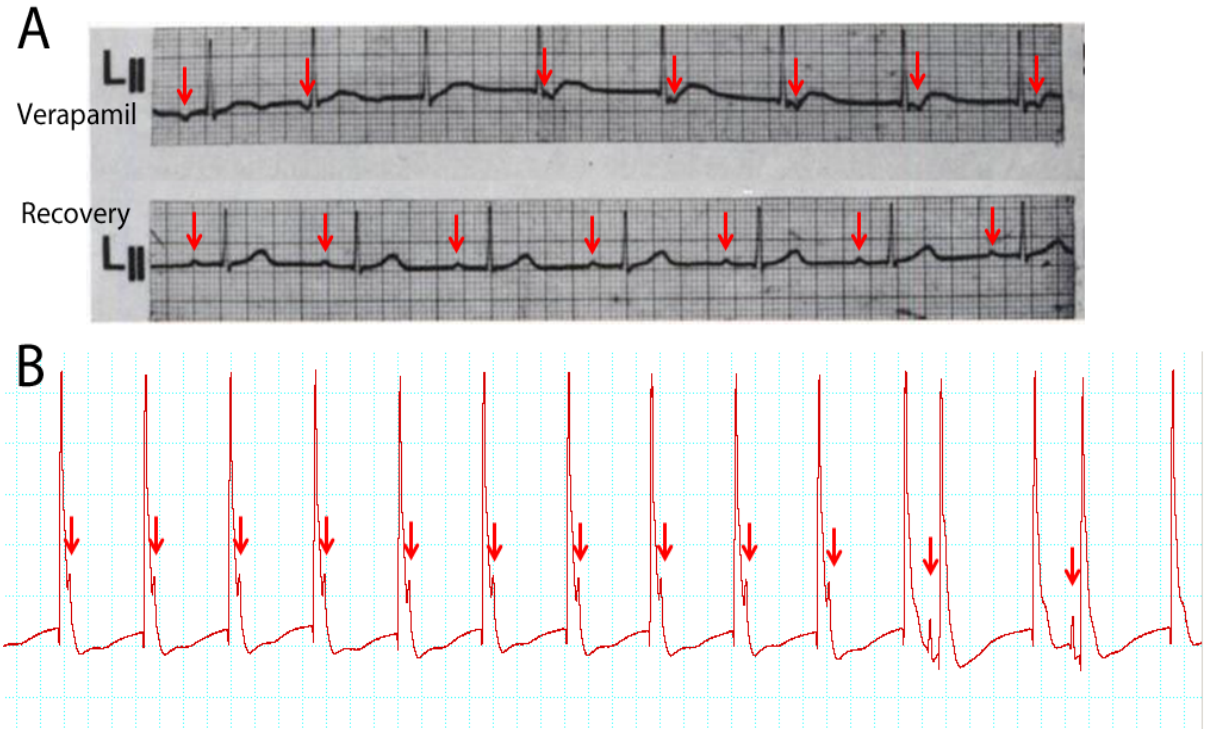

Figure 4. A. Verapamil intoxication in human subject [351]. Upper part is

representing ECG of patient on admission to the hospital in two hours after ingestion of 2 g of verapamil. P wave is inverted, activity of sino-atrial node is suppressed (atrio-ventricular node is maintaining the rhythm of ventricular contraction while atria contracting independently). Red arrows show P wave positions. After 11 hours of recovery sinus rhythm was reappeared. **B.** The acute treatment of isolated rat heart with diltiatazem. Similarly to A, heart rhythm is maintained by atrio-ventricular node activity. Excitation of atria is seen first as a "shoulder" of QRS complex and then as independent peak.

Example 2

31-years-old man without significant past medical history and family history of syncope or sudden cardiac death used high dose of ketamine for recreational purpose (391 μg/L in blood plasma at the moment of hospital admission) [352]. No rhythm abnormalities were observed, however, ST segment prolongation and elevation (on V2 lead) were present (Fig 5A). In 12 hours ST segment normalized and no more pathological changes on the ECG record were seen. On the ECG obtained from the isolated rat heart ST segment prolongation was detected for ketamine as well for other NMDA receptor channel blockers (Fig 5B). We were using only one ECG lead in our experiments (similar to the lead II), thus, we could not detect ST segment shape abnormalities as present on V2 lead (Fig 5A).

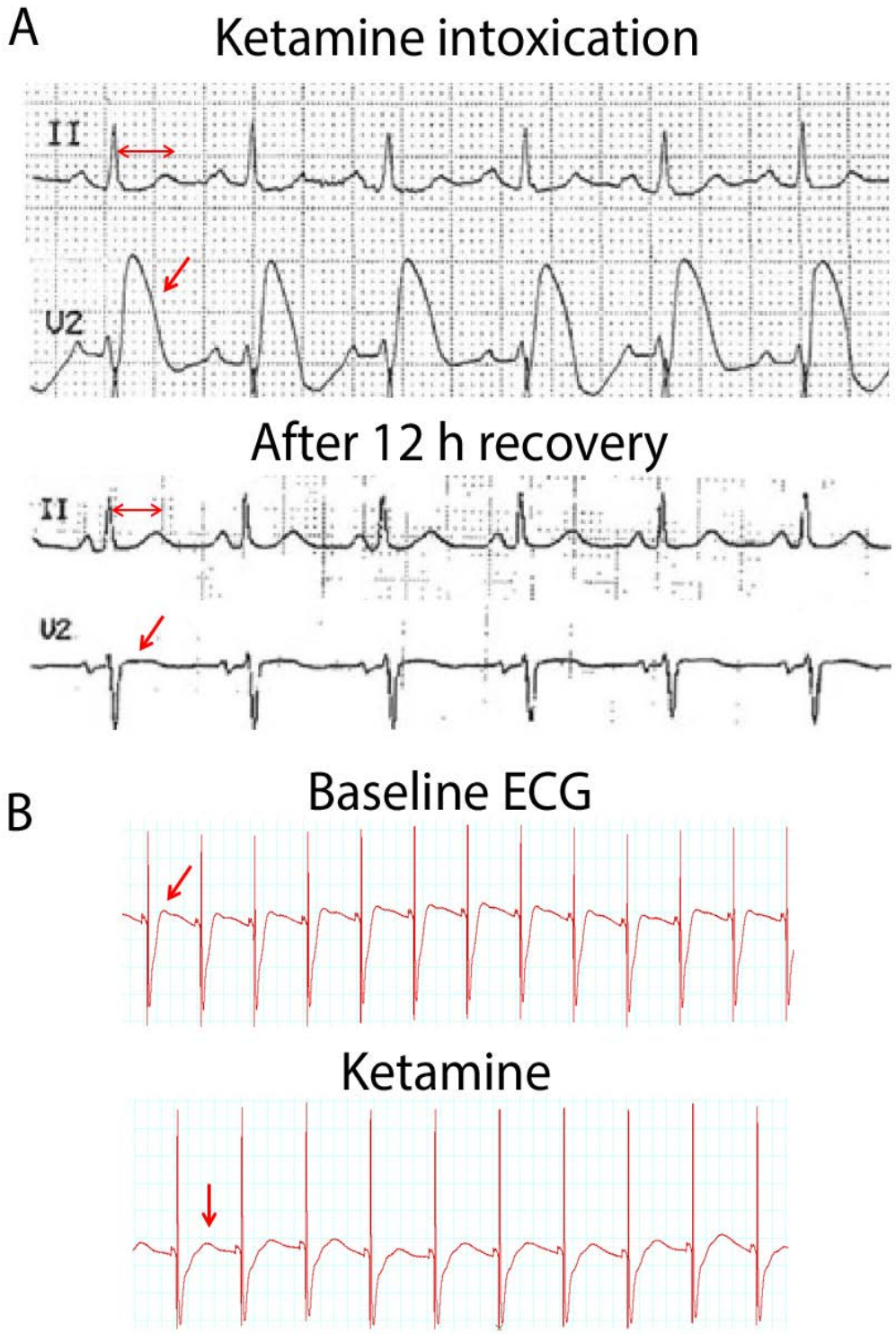

Figure 5. A. Ketamine overdose in healthy human subject [352]. ST segment prolongation in all leads and ST segment elevation in lead V2 were detected. After the recovery period ECG record was normal. **B.** Ketamine provoking ST segment prolongation in isolated rat heart.

Poisoning by NMDA receptor agonists such as glutamate and domoic acid (sea food) was associated with chest pain (a major symptom of Chinese restaurant

syndrome) and arrhythmias [353], [354], [355]. However, neurological symptoms of NMDA receptor agonist poisoning are much more pronounced and taken under consideration by physicians, so no ECG records from intoxicated patients are available.

According to these examples, blood perfused isolated rat heart may be a fair model of acute drug effects in the human heart. Although effective drug concentrations could differ between human and rat, the character of ECG changes seems to be the same at least for acute high doses of NMDA receptor agonists and antagonists.

7. Conclusion

NMDA receptors have been traditionally viewed as an integral part of neurotransmission process endemic to the central and peripheral nervous systems. Recent findings including those in the present study clearly indicate that this is not entirely true. Impressive diversity of properties of currents mediated by the tetrameric receptors formed by four out of seven subunits, most of which are presented with several splice isoforms makes these receptors into a multisensory modality responding to the changes in availability of external amino acids, mechanic stress, voltage, pH, redox state. These responses can be further modulated by the intracellular regulators and signals from other receptors. This type of the receptors appeared early in evolution and was successfully used thereafter by the organisms some of which lacked or possessed very primitive nervous system. It is therefore not unexpected that various subsets of NMDA receptor appear to be in multiple organs perform a variety of tissue-specific tasks. We have unraveled a small number of those focusing on the erythroid and cardiac NMDA receptors. In both tissues these channels appear to be responding to the changes in agonists levels, and mechanical stimuli (shear stress and mechanical overload). NMDA receptors contribute to the changes in volume as their activation results in RBC shrinkage and swelling of adult rat cardiomyocytes. Activation or inhibition of the NMDA receptors impacts transmembrane potential in the EPCs and in cardiomyocytes modulating activity of pacemaker cells. Changes in plasma glutamate or homocysteine levels and the following activation of the NMDA receptors result in transient reduction in oxygen affinity of hemoglobin and in development of tachycardia and increased incidence of arrhythmia. All these processes have to be taken into account when designing and applying drugs antagonizing the NMDA receptors. Further investigations are needed to gain more insights into the structure and function of non-neuronal NMDA receptors in health and disease.

8. Outlook

Functionally active erythroid and cardiac NMDA receptors represent a novel target for pharmacological intervention in a disease.

At present in collaboration with our colleagues from the Divisions of Haematology of the University Hospital and Children's Hospital Zurich we prepare a proof-of-principle trial in which the efficiency of memantine will be tested in a small cohort of patient sickle cell disease. The start of the trial is planned for the coming fall 2014. Our further goals regarding the erythroid NMDA receptors include: (i) a detailed study on a role of NMDA receptors in control of oxygen delivery and RBC properties in subjects practicing physical exercises (now in progress) and in regulation of red cell mass upon ascent and descent from the high altitude; (ii) screening of the other hereditary forms of hemolytic anemia associated with an increased cytoplasmic Ca^{2+} concentration (e. g. thalassemia, PFK deficiency, spherocytosis etc.) for the abundance and activity of the NMDA receptors in circulating RBCs.

Together with the Division of Cardiac Surgery of the University Hospital of Verona, Italy, and Prof Colin Schwarzwald and his group from the Equine Clinic, Animal Hospital Zurich, as well as with the Division of Health and Medical Care of the Russian Railways company we follow up on the characterization of the cardiac NMDA receptors. (i) We are currently exploring NMDA receptor subunit composition and pharmacology of human and equine cardiac NMDA receptors and their relation to the pathology. Our preliminary data reveal the presence of NMDA receptors in human and horse heart. However, remarkable differences were observed between human and rodent cardiac NMDA receptor subunit composition and pharmacology. This finding questions the possibility of direct transfer the findings obtained using rat model to human or equine settings directly. In fact, NMDA receptors in horse heart appear to share similarities in subunit composition and pharmacology with those in human heart making horses into an expensive, but fair model for studying NMDA receptors in human heart. (ii) We have demonstrated pro-arrhythmogenic potential of hyperactivation of the NMDA receptors in isolated spontaneously beating rat heart. We now elaborate on characterization of the possible relationship

between the activation state of cardiac NMDA receptors and the incidence of arrhythmia in horses and humans. In contrast to rats, horses and humans are known to develop spontaneous arrhythmia and atrial fibrillation which is commonly triggered by physical exercises (races, exhaustive training). Non-trained humans and endurance athletes are also known to produce premature ventricular contraction, AV block, atrial fibrillation, and sudden cardiac death in response to exhaustive exercises. We are currently following the links between exercise and open-heart surgical intervention, arrhythmia, and the levels of NMDA receptor agonists/activation state of the receptors. A long-standing goal we pursue involves characterization of the cause-consequence relations between arrhythmia development and NMDA receptors and testing of the anti-arrhythmic potential of specific antagonists of the cardiac NMDA receptors in vivo.

9. Literature

1. Traynelis, S. F. *et al.* Glutamate receptor ion channels: structure, regulation, and function. *Pharmacol. Rev.* **62,** 405–496 (2010).
2. MacLean, D. M. The delta2 glutamate-like receptor undergoes similar conformational changes as other ionotropic glutamate receptors. *J. Neurosci.* **29,** 6767–6768 (2009).
3. Dingledine, R., Borges, K., Bowie, D. & Traynelis, S. F. The glutamate receptor ion channels. *Pharmacol. Rev.* **51,** 7–61 (1999).
4. Traynelis, S. F. *et al.* Glutamate receptor ion channels: structure, regulation, and function. *Pharmacol. Rev.* **62,** 405–496 (2010).
5. Madry, C., Betz, H., Geiger, J. R. P. & Laube, B. Potentiation of Glycine-Gated NR1/NR3A NMDA Receptors Relieves Ca-Dependent Outward Rectification. *Front Mol Neurosci* **3,** 6 (2010).
6. Nakamichi, N. *et al.* Blockade by ferrous iron of Ca2+ influx through N-methyl-D-aspartate receptor channels in immature cultured rat cortical neurons. *J. Neurochem.* **83,** 1–11 (2002).
7. Reynolds, I. J. & Miller, R. J. [3H]MK801 binding to the NMDA receptor/ionophore complex is regulated by divalent cations: evidence for multiple regulatory sites. *Eur. J. Pharmacol.* **151,** 103–112 (1988).
8. Davies, J., Evans, R. H., Francis, A. A. & Watkins, J. C. Excitatory amino acid receptors and synaptic excitation in the mammalian central nervous system. *J. Physiol. (Paris)* **75,** 641–654 (1979).
9. Johnson, J. W. & Ascher, P. Glycine potentiates the NMDA response in cultured mouse brain neurons. *Nature* **325,** 529–531 (1987).
10. Mayer, M. L., Westbrook, G. L. & Guthrie, P. B. Voltage-dependent block by Mg2+ of NMDA responses in spinal cord neurones. *Nature* **309,** 261–263 (1984).
11. Johnson, J. W. & Ascher, P. Voltage-dependent block by intracellular Mg2+ of N-methyl-D-aspartate-activated channels. *Biophys. J.* **57,** 1085–1090 (1990).
12. Jahr, C. E. & Stevens, C. F. Glutamate activates multiple single channel conductances in hippocampal neurons. *Nature* **325,** 522–525 (1987).
13. Nahum-Levy, R., Lipinski, D., Shavit, S. & Benveniste, M. Desensitization of NMDA receptor channels is modulated by glutamate agonists. *Biophys. J.* **80,** 2152–2166 (2001).
14. *Molecular biology of the cell*. (Garland Science, 2002).
15. Abdrachmanova, G., Teisinger, J. & Vyklický, L. Axotomy-induced changes in the properties of NMDA receptor channels in rat spinal cord motoneurons. *J. Physiol. (Lond.)* **538,** 53–63 (2002).
16. Seeburg, P. H. *et al.* The NMDA receptor channel: molecular design of a coincidence detector. *Recent Prog. Horm. Res.* **50,** 19–34 (1995).

17. Blanke, M. L. & VanDongen, A. M. J. in *Biology of the NMDA Receptor* (ed. Van Dongen, A. M.) (CRC Press, 2009). at <http://www.ncbi.nlm.nih.gov/books/NBK5274/>
18. Pachernegg, S., Strutz-Seebohm, N. & Hollmann, M. GluN3 subunit-containing NMDA receptors: not just one-trick ponies. *Trends Neurosci.* **35,** 240–249 (2012).
19. Furukawa, H., Singh, S. K., Mancusso, R. & Gouaux, E. Subunit arrangement and function in NMDA receptors. *Nature* **438,** 185–192 (2005).
20. Jones, K. S., VanDongen, H. M. A. & VanDongen, A. M. J. The NMDA receptor M3 segment is a conserved transduction element coupling ligand binding to channel opening. *J. Neurosci.* **22,** 2044–2053 (2002).
21. Williams, K. in *Biology of the NMDA Receptor* (ed. Van Dongen, A. M.) (CRC Press, 2009). at <http://www.ncbi.nlm.nih.gov/books/NBK5272/>
22. Awobuluyi, M. *et al.* Subunit-specific roles of glycine-binding domains in activation of NR1/NR3 N-methyl-D-aspartate receptors. *Mol. Pharmacol.* **71,** 112–122 (2007).
23. Kashiwagi, K. *et al.* Channel blockers acting at N-methyl-D-aspartate receptors: differential effects of mutations in the vestibule and ion channel pore. *Mol. Pharmacol.* **61,** 533–545 (2002).
24. Siegler Retchless, B., Gao, W. & Johnson, J. W. A single GluN2 subunit residue controls NMDA receptor channel properties via intersubunit interaction. *Nat. Neurosci.* **15,** 406–413, S1–2 (2012).
25. Sasaki, Y. F. *et al.* Characterization and comparison of the NR3A subunit of the NMDA receptor in recombinant systems and primary cortical neurons. *J. Neurophysiol.* **87,** 2052–2063 (2002).
26. Cavara, N. A., Orth, A., Hicking, G., Seebohm, G. & Hollmann, M. Residues at the tip of the pore loop of NR3B-containing NMDA receptors determine Ca2+ permeability and Mg2+ block. *BMC Neurosci* **11,** 133 (2010).
27. Andersson, O., Stenqvist, A., Attersand, A. & von Euler, G. Nucleotide sequence, genomic organization, and chromosomal localization of genes encoding the human NMDA receptor subunits NR3A and NR3B. *Genomics* **78,** 178–184 (2001).
28. Smothers, C. T. & Woodward, J. J. Pharmacological characterization of glycine-activated currents in HEK 293 cells expressing N-methyl-D-aspartate NR1 and NR3 subunits. *J. Pharmacol. Exp. Ther.* **322,** 739–748 (2007).
29. Perez-Otano, I. *et al.* Assembly with the NR1 subunit is required for surface expression of NR3A-containing NMDA receptors. *J. Neurosci.* **21,** 1228–1237 (2001).
30. Cavara, N. A., Orth, A. & Hollmann, M. Effects of NR1 splicing on NR1/NR3B-type excitatory glycine receptors. *BMC Neurosci* **10,** 32 (2009).
31. Matsuda, K., Kamiya, Y., Matsuda, S. & Yuzaki, M. Cloning and characterization of a novel NMDA receptor subunit NR3B: a dominant

subunit that reduces calcium permeability. *Brain Res. Mol. Brain Res.* **100,** 43–52 (2002).
32. Wollmuth, L. P., Kuner, T., Seeburg, P. H. & Sakmann, B. Differential contribution of the NR1- and NR2A-subunits to the selectivity filter of recombinant NMDA receptor channels. *J. Physiol. (Lond.)* **491 (Pt 3),** 779–797 (1996).
33. Yamakura, T. *et al.* The NR3B subunit does not alter the anesthetic sensitivities of recombinant N-methyl-D-aspartate receptors. *Anesth. Analg.* **100,** 1687–1692 (2005).
34. Chatterton, J. E. *et al.* Excitatory glycine receptors containing the NR3 family of NMDA receptor subunits. *Nature* **415,** 793–798 (2002).
35. Burnashev, N. *et al.* Control by asparagine residues of calcium permeability and magnesium blockade in the NMDA receptor. *Science* **257,** 1415–1419 (1992).
36. Chen, P. E., Johnston, A. R., Mok, M. H. S., Schoepfer, R. & Wyllie, D. J. A. Influence of a threonine residue in the S2 ligand binding domain in determining agonist potency and deactivation rate of recombinant NR1a/NR2D NMDA receptors. *J. Physiol. (Lond.)* **558,** 45–58 (2004).
37. Rumbaugh, G., Prybylowski, K., Wang, J. F. & Vicini, S. Exon 5 and spermine regulate deactivation of NMDA receptor subtypes. *J. Neurophysiol.* **83,** 1300–1306 (2000).
38. Husi, H., Ward, M. A., Choudhary, J. S., Blackstock, W. P. & Grant, S. G. Proteomic analysis of NMDA receptor-adhesion protein signaling complexes. *Nat. Neurosci.* **3,** 661–669 (2000).
39. Jahr, C. E. & Stevens, C. F. Calcium permeability of the N-methyl-D-aspartate receptor channel in hippocampal neurons in culture. *Proc. Natl. Acad. Sci. U.S.A.* **90,** 11573–11577 (1993).
40. Church, P. J. & Stanley, E. F. Single L-type calcium channel conductance with physiological levels of calcium in chick ciliary ganglion neurons. *J. Physiol. (Lond.)* **496 (Pt 1),** 59–68 (1996).
41. Popescu, G., Robert, A., Howe, J. R. & Auerbach, A. Reaction mechanism determines NMDA receptor response to repetitive stimulation. *Nature* **430,** 790–793 (2004).
42. Clements, J. D., Lester, R. A., Tong, G., Jahr, C. E. & Westbrook, G. L. The time course of glutamate in the synaptic cleft. *Science* **258,** 1498–1501 (1992).
43. Nilsson, A., Duan, J., Mo-Boquist, L.-L., Benedikz, E. & Sundström, E. Characterisation of the human NMDA receptor subunit NR3A glycine binding site. *Neuropharmacology* **52,** 1151–1159 (2007).
44. Blanke, M. L. & VanDongen, A. M. J. in *Biology of the NMDA Receptor* (ed. Van Dongen, A. M.) (CRC Press, 2009). at <http://www.ncbi.nlm.nih.gov/books/NBK5274/>

45. Shleper, M., Kartvelishvily, E. & Wolosker, H. D-serine is the dominant endogenous coagonist for NMDA receptor neurotoxicity in organotypic hippocampal slices. *J. Neurosci.* **25,** 9413–9417 (2005).
46. Grimwood, S., Foster, A. C. & Kemp, J. A. The pharmacological specificity of N-methyl-D-aspartate receptors in rat cerebral cortex: correspondence between radioligand binding and electrophysiological measurements. *Br. J. Pharmacol.* **103,** 1385–1392 (1991).
47. Low, C.-M. *et al.* Molecular determinants of proton-sensitive N-methyl-D-aspartate receptor gating. *Mol. Pharmacol.* **63,** 1212–1222 (2003).
48. Doppenberg, E. M. *et al.* Correlations between brain tissue oxygen tension, carbon dioxide tension, pH, and cerebral blood flow--a better way of monitoring the severely injured brain? *Surg Neurol* **49,** 650–654 (1998).
49. Gielen, M., Siegler Retchless, B., Mony, L., Johnson, J. W. & Paoletti, P. Mechanism of differential control of NMDA receptor activity by NR2 subunits. *Nature* **459,** 703–707 (2009).
50. Traynelis, S. F., Hartley, M. & Heinemann, S. F. Control of proton sensitivity of the NMDA receptor by RNA splicing and polyamines. *Science* **268,** 873–876 (1995).
51. Smart, T. G., Hosie, A. M. & Miller, P. S. Zn2+ ions: modulators of excitatory and inhibitory synaptic activity. *Neuroscientist* **10,** 432–442 (2004).
52. Christine, C. W. & Choi, D. W. Effect of zinc on NMDA receptor-mediated channel currents in cortical neurons. *J. Neurosci.* **10,** 108–116 (1990).
53. Frederickson, C. J., Koh, J.-Y. & Bush, A. I. The neurobiology of zinc in health and disease. *Nat. Rev. Neurosci.* **6,** 449–462 (2005).
54. Kotermanski, S. E. & Johnson, J. W. Mg2+ imparts NMDA receptor subtype selectivity to the Alzheimer's drug memantine. *J. Neurosci.* **29,** 2774–2779 (2009).
55. Chen, H.-S. V. & Lipton, S. A. Pharmacological implications of two distinct mechanisms of interaction of memantine with N-methyl-D-aspartate-gated channels. *J. Pharmacol. Exp. Ther.* **314,** 961–971 (2005).
56. Green, T., Rogers, C. A., Contractor, A. & Heinemann, S. F. NMDA receptors formed by NR1 in Xenopus laevis oocytes do not contain the endogenous subunit XenU1. *Mol. Pharmacol.* **61,** 326–333 (2002).
57. Yamakura, T. & Shimoji, K. Subunit- and site-specific pharmacology of the NMDA receptor channel. *Prog. Neurobiol.* **59,** 279–298 (1999).
58. Yao, Y. & Mayer, M. L. Characterization of a soluble ligand binding domain of the NMDA receptor regulatory subunit NR3A. *J. Neurosci.* **26,** 4559–4566 (2006).
59. Vicini, S. *et al.* Functional and pharmacological differences between recombinant N-methyl-D-aspartate receptors. *J. Neurophysiol.* **79,** 555–566 (1998).
60. Smothers, C. T. & Woodward, J. J. Expression of glycine-activated diheteromeric NR1/NR3 receptors in human embryonic kidney 293 cells Is

NR1 splice variant-dependent. *J. Pharmacol. Exp. Ther.* **331,** 975–984 (2009).
61. Monyer, H., Burnashev, N., Laurie, D. J., Sakmann, B. & Seeburg, P. H. Developmental and regional expression in the rat brain and functional properties of four NMDA receptors. *Neuron* **12,** 529–540 (1994).
62. Wrighton, D. C., Baker, E. J., Chen, P. E. & Wyllie, D. J. A. Mg2+ and memantine block of rat recombinant NMDA receptors containing chimeric NR2A/2D subunits expressed in Xenopus laevis oocytes. *J. Physiol. (Lond.)* **586,** 211–225 (2008).
63. Zheng, X., Zhang, L., Durand, G. M., Bennett, M. V. & Zukin, R. S. Mutagenesis rescues spermine and Zn2+ potentiation of recombinant NMDA receptors. *Neuron* **12,** 811–818 (1994).
64. Fayyazuddin, A., Villarroel, A., Le Goff, A., Lerma, J. & Neyton, J. Four residues of the extracellular N-terminal domain of the NR2A subunit control high-affinity Zn2+ binding to NMDA receptors. *Neuron* **25,** 683–694 (2000).
65. Ferrer-Montiel, A. V., Sun, W. & Montal, M. Molecular design of the N-methyl-D-aspartate receptor binding site for phencyclidine and dizolcipine. *Proc. Natl. Acad. Sci. U.S.A.* **92,** 8021–8025 (1995).
66. Monaghan, D. T. & Larsen, H. NR1 and NR2 subunit contributions to N-methyl-D-aspartate receptor channel blocker pharmacology. *J. Pharmacol. Exp. Ther.* **280,** 614–620 (1997).
67. Mieler, W. F. & Aaberg, T. M. Vitreous surgery in the management of peripheral uveitis. *Dev Ophthalmol* **23,** 239–250 (1992).
68. Williams, K. Ifenprodil discriminates subtypes of the N-methyl-D-aspartate receptor: selectivity and mechanisms at recombinant heteromeric receptors. *Mol. Pharmacol.* **44,** 851–859 (1993).
69. Williams, K. Pharmacological properties of recombinant N-methyl-D-aspartate (NMDA) receptors containing the epsilon 4 (NR2D) subunit. *Neurosci. Lett.* **184,** 181–184 (1995).
70. Bhagavan, H. N., Coursin, D. B. & Stewart, C. N. Monosodium glutamate induces convulsive disorders in rats. *Nature* **232,** 275–276 (1971).
71. Lam, H. M. *et al.* Glutamate-receptor genes in plants. *Nature* **396,** 125–126 (1998).
72. Bowman, J. L., Floyd, S. K. & Sakakibara, K. Green genes-comparative genomics of the green branch of life. *Cell* **129,** 229–234 (2007).
73. Chiu, J., DeSalle, R., Lam, H. M., Meisel, L. & Coruzzi, G. Molecular evolution of glutamate receptors: a primitive signaling mechanism that existed before plants and animals diverged. *Mol. Biol. Evol.* **16,** 826–838 (1999).
74. Wo, Z. G. & Oswald, R. E. Unraveling the modular design of glutamate-gated ion channels. *Trends Neurosci.* **18,** 161–168 (1995).
75. Tikhonov, D. B. & Magazanik, L. G. Origin and molecular evolution of ionotropic glutamate receptors. *Neurosci. Behav. Physiol.* **39,** 763–773 (2009).

76. Nagy, A. & Patthy, L. Reassessing domain architecture evolution of metazoan proteins: the contribution of different evolutionary mechanisms. *Genes (Basel)* **2,** 578–598 (2011).
77. Chen, G. Q., Cui, C., Mayer, M. L. & Gouaux, E. Functional characterization of a potassium-selective prokaryotic glutamate receptor. *Nature* **402,** 817–821 (1999).
78. Bot, C. T. & Prodan, C. Quantifying the membrane potential during E. coli growth stages. *Biophys. Chem.* **146,** 133–137 (2010).
79. Turano, F. J., Panta, G. R., Allard, M. W. & van Berkum, P. The putative glutamate receptors from plants are related to two superfamilies of animal neurotransmitter receptors via distinct evolutionary mechanisms. *Mol. Biol. Evol.* **18,** 1417–1420 (2001).
80. Vincill, E. D., Bieck, A. M. & Spalding, E. P. Ca(2+) conduction by an amino acid-gated ion channel related to glutamate receptors. *Plant Physiol.* **159,** 40–46 (2012).
81. Dubos, C., Huggins, D., Grant, G. H., Knight, M. R. & Campbell, M. M. A role for glycine in the gating of plant NMDA-like receptors. *Plant J.* **35,** 800–810 (2003).
82. Roy, S. J. *et al.* Investigating glutamate receptor-like gene co-expression in Arabidopsis thaliana. *Plant Cell Environ.* **31,** 861–871 (2008).
83. Kang, J. & Turano, F. J. The putative glutamate receptor 1.1 (AtGLR1.1) functions as a regulator of carbon and nitrogen metabolism in Arabidopsis thaliana. *Proc. Natl. Acad. Sci. U.S.A.* **100,** 6872–6877 (2003).
84. Kang, J., Mehta, S. & Turano, F. J. The putative glutamate receptor 1.1 (AtGLR1.1) in Arabidopsis thaliana regulates abscisic acid biosynthesis and signaling to control development and water loss. *Plant Cell Physiol.* **45,** 1380–1389 (2004).
85. Naur, P. *et al.* Ionotropic glutamate-like receptor delta2 binds D-serine and glycine. *Proc. Natl. Acad. Sci. U.S.A.* **104,** 14116–14121 (2007).
86. Schmid, S. M., Kott, S., Sager, C., Huelsken, T. & Hollmann, M. The glutamate receptor subunit delta2 is capable of gating its intrinsic ion channel as revealed by ligand binding domain transplantation. *Proc. Natl. Acad. Sci. U.S.A.* **106,** 10320–10325 (2009).
87. Kakegawa, W., Kohda, K. & Yuzaki, M. The delta2 'ionotropic' glutamate receptor functions as a non-ionotropic receptor to control cerebellar synaptic plasticity. *J. Physiol. (Lond.)* **584,** 89–96 (2007).
88. Ramoino, P. *et al.* Pharmacological characterization of NMDA-like receptors in the single-celled organism Paramecium primaurelia. *J. Exp. Biol.* **217,** 463–471 (2014).
89. Fillingham, J. S. *et al.* Analysis of expressed sequence tags (ESTs) in the ciliated protozoan Tetrahymena thermophila. *J. Eukaryot. Microbiol.* **49,** 99–107 (2002).

90. Xiao, S. & Laflamme, M. On the eve of animal radiation: phylogeny, ecology and evolution of the Ediacara biota. *Trends Ecol. Evol. (Amst.)* **24,** 31–40 (2009).
91. Bellis, S. L., Grosvenor, W., Kass-Simon, G. & Rhoads, D. E. Chemoreception in Hydra vulgaris (attenuata): initial characterization of two distinct binding sites for L-glutamic acid. *Biochim. Biophys. Acta* **1061,** 89–94 (1991).
92. Kass-Simon, G., Zompa, M. A., Scappaticci, A. A., Zackroff, R. V. & Hufnagel, L. A. Nucleolar binding of an anti-NMDA receptor antibody in hydra: a non-canonical role for an NMDA receptor protein? *J Exp Zool A Ecol Genet Physiol* **311,** 763–775 (2009).
93. Ruggieri, R. D., Pierobon, P. & Kass-Simon, G. Pacemaker activity in hydra is modulated by glycine receptor ligands. *Comp. Biochem. Physiol., Part A Mol. Integr. Physiol.* **138,** 193–202 (2004).
94. Pierobon, P. *et al.* Putative NMDA receptors in Hydra: a biochemical and functional study. *Eur. J. Neurosci.* **20,** 2598–2604 (2004).
95. Kay, J. C. & Kass-Simon, G. Glutamatergic transmission in hydra: NMDA/D-serine affects the electrical activity of the body and tentacles of Hydra vulgaris (Cnidaria, Hydrozoa). *Biol. Bull.* **216,** 113–125 (2009).
96. Kenny, N. J. & Dearden, P. K. NMDA receptor expression and C terminus structure in the rotifer Brachionus plicatilis and long-term potentiation across the Metazoa. *Invert. Neurosci.* **13,** 125–134 (2013).
97. Anctil, M. Chemical transmission in the sea anemone Nematostella vectensis: A genomic perspective. *Comp. Biochem. Physiol. Part D Genomics Proteomics* **4,** 268–289 (2009).
98. Miller, D. J., Ball, E. E. & Technau, U. Cnidarians and ancestral genetic complexity in the animal kingdom. *Trends Genet.* **21,** 536–539 (2005).
99. Xia, S. & Chiang, A.-S. in *Biology of the NMDA Receptor* (ed. Van Dongen, A. M.) (CRC Press, 2009). at <http://www.ncbi.nlm.nih.gov/books/NBK5286/>
100. Brockie, P. J., Madsen, D. M., Zheng, Y., Mellem, J. & Maricq, A. V. Differential expression of glutamate receptor subunits in the nervous system of Caenorhabditis elegans and their regulation by the homeodomain protein UNC-42. *J. Neurosci.* **21,** 1510–1522 (2001).
101. Technau, U. *et al.* Maintenance of ancestral complexity and non-metazoan genes in two basal cnidarians. *Trends Genet.* **21,** 633–639 (2005).
102. Ikuta, T. & Saiga, H. Organization of Hox genes in ascidians: present, past, and future. *Dev. Dyn.* **233,** 382–389 (2005).
103. Dehal, P. *et al.* The draft genome of Ciona intestinalis: insights into chordate and vertebrate origins. *Science* **298,** 2157–2167 (2002).
104. Buznikov, G. A. *et al.* Amyloid precursor protein 96-110 and beta-amyloid 1-42 elicit developmental anomalies in sea urchin embryos and larvae that are alleviated by neurotransmitter analogs for acetylcholine, serotonin and cannabinoids. *Neurotoxicol Teratol* **30,** 503–509 (2008).

105. Teng, H. *et al.* Evolutionary mode and functional divergence of vertebrate NMDA receptor subunit 2 genes. *PLoS ONE* **5,** e13342 (2010).
106. Ito, H., Ishikawa, Y., Yoshimoto, M. & Yamamoto, N. Diversity of brain morphology in teleosts: brain and ecological niche. *Brain Behav. Evol.* **69,** 76–86 (2007).
107. Cox, J. A., Kucenas, S. & Voigt, M. M. Molecular characterization and embryonic expression of the family of N-methyl-D-aspartate receptor subunit genes in the zebrafish. *Dev. Dyn.* **234,** 756–766 (2005).
108. Niemann, S. *et al.* Motoneuron-specific NR3B gene: no association with ALS and evidence for a common null allele. *Neurology* **70,** 666–676 (2008).
109. Ali, F. & Meier, R. Primate home range and GRIN2A, a receptor gene involved in neuronal plasticity: implications for the evolution of spatial memory. *Genes Brain Behav.* **8,** 435–441 (2009).
110. De Quervain, D. J.-F. & Papassotiropoulos, A. Identification of a genetic cluster influencing memory performance and hippocampal activity in humans. *Proc. Natl. Acad. Sci. U.S.A.* **103,** 4270–4274 (2006).
111. Schell, M. J. The N-methyl D-aspartate receptor glycine site and D-serine metabolism: an evolutionary perspective. *Philos. Trans. R. Soc. Lond., B, Biol. Sci.* **359,** 943–964 (2004).
112. D'Aniello, S. *et al.* N-methyl-D-aspartic acid (NMDA) in the nervous system of the amphioxus Branchiostoma lanceolatum. *BMC Neurosci* **8,** 109 (2007).
113. D'Aniello, A. *et al.* A specific enzymatic high-performance liquid chromatography method to determine N-methyl-D-aspartic acid in biological tissues. *Anal. Biochem.* **308,** 42–51 (2002).
114. Monge-Acuña, A. A. & Fornaguera-Trías, J. A high performance liquid chromatography method with electrochemical detection of gamma-aminobutyric acid, glutamate and glutamine in rat brain homogenates. *J. Neurosci. Methods* **183,** 176–181 (2009).
115. D'Aniello, A. *et al.* Occurrence and neuroendocrine role of D-aspartic acid and N-methyl-D-aspartic acid in Ciona intestinalis. *FEBS Lett.* **552,** 193–198 (2003).
116. Shibata, K. *et al.* Determination of D-aspartate N-methyltransferase activity in the starfish by direct analysis of N-methyl-D-aspartate with high-performance liquid chromatography. *J. Chromatogr. B Analyt. Technol. Biomed. Life Sci.* **879,** 3229–3234 (2011).
117. Hashimoto, A. & Oka, T. Free D-aspartate and D-serine in the mammalian brain and periphery. *Prog. Neurobiol.* **52,** 325–353 (1997).
118. Anderson, M., Suh, J. M., Kim, E. Y. & Dryer, S. E. Functional NMDA receptors with atypical properties are expressed in podocytes. *Am. J. Physiol., Cell Physiol.* **300,** C22–32 (2011).
119. Spencer, G. J., McGrath, C. J. & Genever, P. G. Current perspectives on NMDA-type glutamate signalling in bone. *Int. J. Biochem. Cell Biol.* **39,** 1089–1104 (2007).

120. Boldyrev, A. A., Bryushkova, E. A. & Vladychenskaya, E. A. NMDA receptors in immune competent cells. *Biochemistry Mosc.* **77,** 128–134 (2012).
121. Lau, A. & Tymianski, M. Glutamate receptors, neurotoxicity and neurodegeneration. *Pflugers Arch.* **460,** 525–542 (2010).
122. Poddar, R. & Paul, S. Homocysteine-NMDA receptor-mediated activation of extracellular signal-regulated kinase leads to neuronal cell death. *J. Neurochem.* **110,** 1095–1106 (2009).
123. Yamin, G. NMDA receptor-dependent signaling pathways that underlie amyloid beta-protein disruption of LTP in the hippocampus. *J. Neurosci. Res.* **87,** 1729–1736 (2009).
124. Hoeffer, C. A. & Klann, E. in *Biology of the NMDA Receptor* (ed. Van Dongen, A. M.) (CRC Press, 2009). at <http://www.ncbi.nlm.nih.gov/books/NBK5278/>
125. Oliet, S. H. R. & Mothet, J.-P. Regulation of N-methyl-D-aspartate receptors by astrocytic D-serine. *Neuroscience* **158,** 275–283 (2009).
126. Le Meur, K., Galante, M., Angulo, M. C. & Audinat, E. Tonic activation of NMDA receptors by ambient glutamate of non-synaptic origin in the rat hippocampus. *J. Physiol. (Lond.)* **580,** 373–383 (2007).
127. Lee, M.-C. *et al.* Characterisation of the expression of NMDA receptors in human astrocytes. *PLoS ONE* **5,** e14123 (2010).
128. Hawkins, R. A. The blood-brain barrier and glutamate. *Am. J. Clin. Nutr.* **90,** 867S–874S (2009).
129. Strapkova, A. & Antosova, M. Glutamate receptors and the airways hyperreactivity. *Gen. Physiol. Biophys.* **31,** 93–100 (2012).
130. Hitchcock, I. S., Skerry, T. M., Howard, M. R. & Genever, P. G. NMDA receptor-mediated regulation of human megakaryocytopoiesis. *Blood* **102,** 1254–1259 (2003).
131. Leung, J. C. *et al.* Expression and developmental regulation of the NMDA receptor subunits in the kidney and cardiovascular system. *Am. J. Physiol. Regul. Integr. Comp. Physiol.* **283,** R964–971 (2002).
132. Hinoi, E., Takarada, T., Ueshima, T., Tsuchihashi, Y. & Yoneda, Y. Glutamate signaling in peripheral tissues. *Eur. J. Biochem.* **271,** 1–13 (2004).
133. Seeber, S. *et al.* Transient expression of NMDA receptor subunit NR2B in the developing rat heart. *J. Neurochem.* **75,** 2472–2477 (2000).
134. Seeber, S. *et al.* Formation of molecular complexes by N-methyl-D-aspartate receptor subunit NR2B and ryanodine receptor 2 in neonatal rat myocard. *J. Biol. Chem.* **279,** 21062–21068 (2004).
135. Hu, D., Cao, K., Peterson-Wakeman, R. & Wang, R. Altered profile of gene expression in rat hearts induced by chronic nicotine consumption. *Biochem. Biophys. Res. Commun.* **297,** 729–736 (2002).
136. Gill, S. *et al.* Cloning and characterization of glutamate receptors in Californian sea lions (Zalophus californianus). *Mar Drugs* **8,** 1637–1649 (2010).

137. Gill, S., Veinot, J., Kavanagh, M. & Pulido, O. Human heart glutamate receptors - implications for toxicology, food safety, and drug discovery. *Toxicol Pathol* **35,** 411–417 (2007).
138. Mueller, R. W., Gill, S. S. & Pulido, O. M. The monkey (Macaca fascicularis) heart neural structures and conducting system: an immunochemical study of selected neural biomarkers and glutamate receptors. *Toxicol Pathol* **31,** 227–234 (2003).
139. Moshal, K. S. *et al.* Restoration of contractility in hyperhomocysteinemia by cardiac-specific deletion of NMDA-R1. *Am. J. Physiol. Heart Circ. Physiol.* **296,** H887–892 (2009).
140. Moshal, K. S. *et al.* Mitochondrial matrix metalloproteinase activation decreases myocyte contractility in hyperhomocysteinemia. *Am. J. Physiol. Heart Circ. Physiol.* **295,** H890–897 (2008).
141. Winter, C. R. & Baker, R. C. L-glutamate-induced changes in intracellular calcium oscillation frequency through non-classical glutamate receptor binding in cultured rat myocardial cells. *Life Sci.* **57,** 1925–1934 (1995).
142. Gao, X. *et al.* NMDA receptor activation induces mitochondrial dysfunction, oxidative stress and apoptosis in cultured neonatal rat cardiomyocytes. *Physiol Res* **56,** 559–569 (2007).
143. Kabon, B. *et al.* Thoracic epidural anesthesia increases tissue oxygenation during major abdominal surgery. *Anesth. Analg.* **97,** 1812–1817 (2003).
144. Rumsey, W. L., Pawlowski, M., Lejavardi, N. & Wilson, D. F. Oxygen pressure distribution in the heart in vivo and evaluation of the ischemic "border zone" *Am. J. Physiol.* **266,** H1676–1680 (1994).
145. Huang, C. F. & Su, M. J. Positive inotropic action of NMDA receptor antagonist (+)-MK801 in rat heart. *J. Biomed. Sci.* **6,** 387–398 (1999).
146. Baum, V. C. & Tecson, M. E. Ketamine inhibits transsarcolemmal calcium entry in guinea pig myocardium: direct evidence by single cell voltage clamp. *Anesth. Analg.* **73,** 804–807 (1991).
147. Sekino, N., Endou, M., Hajiri, E. & Okumura, F. Nonstereospecific actions of ketamine isomers on the force of contraction, spontaneous beating rate, and Ca2+ current in the guinea pig heart. *Anesth. Analg.* **83,** 75–80 (1996).
148. Stowe, D. F., Bosnjak, Z. J. & Kampine, J. P. Comparison of etomidate, ketamine, midazolam, propofol, and thiopental on function and metabolism of isolated hearts. *Anesth. Analg.* **74,** 547–558 (1992).
149. Aya, A. G. *et al.* Effects of ketamine on ventricular conduction, refractoriness, and wavelength: potential antiarrhythmic effects: a high-resolution epicardial mapping in rabbit hearts. *Anesthesiology* **87,** 1417–1427 (1997).
150. Herrling, P. L. *Excitatory amino acids clinical results with antagonists*. (Academic Press, 1997). at <http://site.ebrary.com/id/10206411>
151. Zipes, D. P. & Jalife, J. *Cardiac electrophysiology: from cell to bedside*. (Saunders/Elsevier, 2009).

152. Rollin, A., Maury, P., Guilbeau-Frugier, C. & Brugada, J. Transient ST elevation after ketamine intoxication: a new cause of acquired brugada ECG pattern. *J. Cardiovasc. Electrophysiol.* **22,** 91–94 (2011).
153. Chan, W. M., Liang, Y., Wai, M. S. M., Hung, A. S. M. & Yew, D. T. Cardiotoxicity induced in mice by long term ketamine and ketamine plus alcohol treatment. *Toxicol. Lett.* **207,** 191–196 (2011).
154. Chaves, A. A. *et al.* Age and anesthetic effects on murine electrocardiography. *Life Sci.* **72,** 2401–2412 (2003).
155. Hergovich, N. *et al.* Comparison of the effects of ketamine and memantine on prolactin and cortisol release in men. a randomized, double-blind, placebo-controlled trial. *Neuropsychopharmacology* **24,** 590–593 (2001).
156. Lewis, S. J., Barres, C., Jacob, H. J., Ohta, H. & Brody, M. J. Cardiovascular effects of the N-methyl-D-aspartate receptor antagonist MK-801 in conscious rats. *Hypertension* **13,** 759–765 (1989).
157. Monassier, L. *et al.* Effects of ifenprodil and baclofen on exercise-induced increase of myocardial oxygen demand in normotensive rats. *J. Pharmacol. Exp. Ther.* **290,** 1188–1194 (1999).
158. Penney, D. G. & Chen, K. NMDA receptor-blocker ketamine protects during acute carbon monoxide poisoning, while calcium channel-blocker verapamil does not. *J Appl Toxicol* **16,** 297–304 (1996).
159. Monassier, L., Tibiriça, E., Roegel, J. C., Feldman, J. & Bousquet, P. MK-801 and memantine inhibit a centrally induced increase in myocardial oxygen demand in rabbits. *Eur. J. Pharmacol.* **305,** 109–113 (1996).
160. Baczkó, I., Leprán, I. & Papp, J. G. Influence of anesthetics on the incidence of reperfusion-induced arrhythmias and sudden death in rats. *J. Cardiovasc. Pharmacol.* **29,** 196–201 (1997).
161. Hageman, G. R. & Simor, T. Attenuation of the cardiac effects of cocaine by dizocilpine. *Am. J. Physiol.* **264,** H1890–1895 (1993).
162. D'Amico, M., Di Filippo, C., Rossi, F. & Rossi, F. Arrhythmias induced by myocardial ischaemia-reperfusion are sensitive to ionotropic excitatory amino acid receptor antagonists. *Eur. J. Pharmacol.* **366,** 167–174 (1999).
163. Bennett, A. J. & DePetrillo, P. B. Differential effects of MK801 and lorazepam on heart rate variability in adolescent rhesus monkeys (macaca mulatta). *J. Cardiovasc. Pharmacol.* **45,** 383–388 (2005).
164. Mozayani, A., Schrode, P., Carter, J. & Danielson, T. J. A multiple drug fatality involving MK-801 (dizocilpine), a mimic of phencyclidine. *Forensic Sci. Int.* **133,** 113–117 (2003).
165. Moe, S. T. *et al.* Design, synthesis, and biological evaluation of spider toxin (argiotoxin-636) analogs as NMDA receptor antagonists. *Pharm. Res.* **15,** 31–38 (1998).
166. Tian, B. & Hartle, D. K. Cardiovascular effects of NMDA and MK-801 infusion at area postrema and mNTS in rat. *Pharmacol. Biochem. Behav.* **49,** 489–495 (1994).

167. Canesin, R. O., Bonagamba, L. G. & Machado, B. H. Bradycardic and hypotensive responses to microinjection of L-glutamate into the lateral aspect of the commissural NTS are blocked by an NMDA receptor antagonist. *Brain Res.* **852,** 68–75 (2000).
168. Corbett, E. K. A., Saha, S., Deuchars, J., McWilliam, P. N. & Batten, T. F. C. Ionotropic glutamate receptor subunit immunoreactivity of vagal preganglionic neurones projecting to the rat heart. *Auton Neurosci* **105,** 105–117 (2003).
169. Wang, L.-G., Zeng, J., Yuan, W.-J., Su, D.-F. & Wang, W.-Z. Comparative study of NMDA and AMPA/kainate receptors involved in cardiovascular inhibition produced by imidazoline-like drugs in anaesthetized rats. *Exp. Physiol.* **92,** 849–858 (2007).
170. Paoletti, P. & Ascher, P. Mechanosensitivity of NMDA receptors in cultured mouse central neurons. *Neuron* **13,** 645–655 (1994).
171. Kohl, P. & Ravens, U. Cardiac mechano-electric feedback: past, present, and prospect. *Prog. Biophys. Mol. Biol.* **82,** 3–9 (2003).
172. Takahashi, K., Kakimoto, Y., Toda, K. & Naruse, K. Mechanobiology in cardiac physiology and diseases. *J. Cell. Mol. Med.* **17,** 225–232 (2013).
173. Martinac, B. Mechanosensitive ion channels: molecules of mechanotransduction. *J. Cell. Sci.* **117,** 2449–2460 (2004).
174. Szczesniak, A. M., Gilbert, R. W., Mukhida, M. & Anderson, G. I. Mechanical loading modulates glutamate receptor subunit expression in bone. *Bone* **37,** 63–73 (2005).
175. Mashkina, A. P., Cizkova, D., Vanicky, I. & Boldyrev, A. A. NMDA receptors are expressed in lymphocytes activated both in vitro and in vivo. *Cell. Mol. Neurobiol.* **30,** 901–907 (2010).
176. Mashkina, A. P. *et al.* The excitotoxic effect of NMDA on human lymphocyte immune function. *Neurochem. Int.* **51,** 356–360 (2007).
177. Bryushkova, E. A., Vladychenskaya, E. A., Stepanova, M. S. & Boldyrev, A. A. Effect of homocysteine on properties of neutrophils activated in vivo. *Biochemistry Mosc.* **76,** 467–472 (2011).
178. Dickman, K. G., Youssef, J. G., Mathew, S. M. & Said, S. I. Ionotropic glutamate receptors in lungs and airways: molecular basis for glutamate toxicity. *Am. J. Respir. Cell Mol. Biol.* **30,** 139–144 (2004).
179. Genever, P. G. *et al.* Expression of a functional N-methyl-D-aspartate-type glutamate receptor by bone marrow megakaryocytes. *Blood* **93,** 2876–2883 (1999).
180. Bar-Shavit, Z. The osteoclast: a multinucleated, hematopoietic-origin, bone-resorbing osteoimmune cell. *J. Cell. Biochem.* **102,** 1130–1139 (2007).
181. Merle, B., Itzstein, C., Delmas, P. D. & Chenu, C. NMDA glutamate receptors are expressed by osteoclast precursors and involved in the regulation of osteoclastogenesis. *J. Cell. Biochem.* **90,** 424–436 (2003).

182. Mentaverri, R. *et al.* Regulation of bone resorption and osteoclast survival by nitric oxide: possible involvement of NMDA-receptor. *J. Cell. Biochem.* **88,** 1145–1156 (2003).
183. Lindblad, S. S., Mydel, P., Hellvard, A., Jonsson, I.-M. & Bokarewa, M. I. The N-methyl-d-aspartic acid receptor antagonist memantine ameliorates and delays the development of arthritis by enhancing regulatory T cells. *Neurosignals* **20,** 61–71 (2012).
184. Gao, M. *et al.* Effect of N-methyl-D-aspartate receptor antagonist on T helper cell differentiation induced by phorbol-myristate-acetate and ionomycin. *Cytokine* **56,** 458–465 (2011).
185. Miglio, G., Varsaldi, F. & Lombardi, G. Human T lymphocytes express N-methyl-D-aspartate receptors functionally active in controlling T cell activation. *Biochem. Biophys. Res. Commun.* **338,** 1875–1883 (2005).
186. Boldyrev, A. A. *et al.* Rodent lymphocytes express functionally active glutamate receptors. *Biochem. Biophys. Res. Commun.* **324,** 133–139 (2004).
187. Miglio, G., Dianzani, C., Fallarini, S., Fantozzi, R. & Lombardi, G. Stimulation of N-methyl-D-aspartate receptors modulates Jurkat T cell growth and adhesion to fibronectin. *Biochem. Biophys. Res. Commun.* **361,** 404–409 (2007).
188. Franconi, F. *et al.* Further insights into the anti-aggregating activity of NMDA in human platelets. *Br. J. Pharmacol.* **124,** 35–40 (1998).
189. Franconi, F. *et al.* NMDA receptors play an anti-aggregating role in human platelets. *Thromb. Haemost.* **76,** 84–87 (1996).
190. Tremolizzo, L. *et al.* Human platelets express the synaptic markers VGLUT1 and 2 and release glutamate following aggregation. *Neurosci. Lett.* **404,** 262–265 (2006).
191. Nakamura, T. & Lipton, S. A. Preventing Ca2+-mediated nitrosative stress in neurodegenerative diseases: possible pharmacological strategies. *Cell Calcium* **47,** 190–197 (2010).
192. Lee, Y. S. *et al.* Homocysteine induces COX-2 expression in macrophages through ROS generated by NMDA receptor-calcium signaling pathways. *Free Radic. Res.* **47,** 422–431 (2013).
193. Kishida, K. T., Pao, M., Holland, S. M. & Klann, E. NADPH oxidase is required for NMDA receptor-dependent activation of ERK in hippocampal area CA1. *J. Neurochem.* **94,** 299–306 (2005).
194. Nakamura, T. & Lipton, S. A. Cell death: protein misfolding and neurodegenerative diseases. *Apoptosis* **14,** 455–468 (2009).
195. Fialkow, L., Wang, Y. & Downey, G. P. Reactive oxygen and nitrogen species as signaling molecules regulating neutrophil function. *Free Radic. Biol. Med.* **42,** 153–164 (2007).
196. Sardina, J. L. *et al.* p22phox-dependent NADPH oxidase activity is required for megakaryocytic differentiation. *Cell Death Differ.* **17,** 1842–1854 (2010).

197. Kawahara, T., Quinn, M. T. & Lambeth, J. D. Molecular evolution of the reactive oxygen-generating NADPH oxidase (Nox/Duox) family of enzymes. *BMC Evol. Biol.* **7,** 109 (2007).
198. Piñón, R. Effects of N-methyl-D-aspartate receptor ligands on yeast sporulation. *Mol. Microbiol.* **4,** 1765–1769 (1990).
199. Kaye, S. L., Sansom, M. S. P. & Biggin, P. C. In silico mutation of cysteine residues in the ligand-binding domain of an N-methyl-D-aspartate receptor. *Biochemistry* **46,** 2136–2145 (2007).
200. Kumar, A. & Foster, T. C. Linking redox regulation of NMDAR synaptic function to cognitive decline during aging. *J. Neurosci.* **33,** 15710–15715 (2013).
201. Bogdanova, A., Makhro, A., Wang, J., Lipp, P. & Kaestner, L. Calcium in red blood cells-a perilous balance. *Int J Mol Sci* **14,** 9848–9872 (2013).
202. Schaefer, A., Magócsi, M. & Marquardt, H. Signalling mechanisms in erythropoiesis: the enigmatic role of calcium. *Cell. Signal.* **9,** 483–495 (1997).
203. Miller, B. A., Cheung, J. Y., Tillotson, D. L., Hope, S. M. & Scaduto, R. C. Erythropoietin stimulates a rise in intracellular-free calcium concentration in single BFU-E derived erythroblasts at specific stages of differentiation. *Blood* **73,** 1188–1194 (1989).
204. Misiti, J. & Spivak, J. L. Erythropoiesis in vitro. Role of calcium. *J. Clin. Invest.* **64,** 1573–1579 (1979).
205. Tong, Q. *et al.* Erythropoietin-modulated calcium influx through TRPC2 is mediated by phospholipase Cgamma and IP3R. *Am. J. Physiol., Cell Physiol.* **287,** C1667–1678 (2004).
206. Kim, H. D., Koury, M. J., Lee, S. J., Im, J. H. & Sawyer, S. T. Metabolic adaptation during erythropoietin-mediated terminal differentiation of mouse erythroid cells. *Blood* **77,** 387–392 (1991).
207. Thomas, S. L. Y. *et al.* Ion channels in human red blood cell membrane: actors or relics? *Blood Cells Mol. Dis.* **46,** 261–265 (2011).
208. Yang, L., Andrews, D. A. & Low, P. S. Lysophosphatidic acid opens a Ca(++) channel in human erythrocytes. *Blood* **95,** 2420–2425 (2000).
209. Wagner-Britz, L., Wang, J., Kaestner, L. & Bernhardt, I. Protein kinase Cα and P-type Ca channel CaV2.1 in red blood cell calcium signalling. *Cell. Physiol. Biochem.* **31,** 883–891 (2013).
210. Huber, S. M., Gamper, N. & Lang, F. Chloride conductance and volume-regulatory nonselective cation conductance in human red blood cell ghosts. *Pflugers Arch.* **441,** 551–558 (2001).
211. Foller, M. *et al.* TRPC6 contributes to the Ca(2+) leak of human erythrocytes. *Cell. Physiol. Biochem.* **21,** 183–192 (2008).
212. Ramsey, I. S., Delling, M. & Clapham, D. E. An introduction to TRP channels. *Annu. Rev. Physiol.* **68,** 619–647 (2006).

213. Gottlieb, P. *et al.* Revisiting TRPC1 and TRPC6 mechanosensitivity. *Pflugers Arch.* **455,** 1097–1103 (2008).
214. Chu, X. *et al.* Interaction of TRPC2 and TRPC6 in erythropoietin modulation of calcium influx. *J. Biol. Chem.* **279,** 10514–10522 (2004).
215. Moritz, A. T., Newkirk, G., Powers, R. K. & Binder, M. D. Facilitation of somatic calcium channels can evoke prolonged tail currents in rat hypoglossal motoneurons. *J. Neurophysiol.* **98,** 1042–1047 (2007).
216. Nowak, L. M. & Wright, J. M. Slow voltage-dependent changes in channel open-state probability underlie hysteresis of NMDA responses in Mg(2+)-free solutions. *Neuron* **8,** 181–187 (1992).
217. Kaestner, L., Christophersen, P., Bernhardt, I. & Bennekou, P. The non-selective voltage-activated cation channel in the human red blood cell membrane: reconciliation between two conflicting reports and further characterisation. *Bioelectrochemistry* **52,** 117–125 (2000).
218. Bennekou, P. The voltage-gated non-selective cation channel from human red cells is sensitive to acetylcholine. *Biochim. Biophys. Acta* **1147,** 165–167 (1993).
219. Bennekou, P., Barksmann, T. L., Kristensen, B. I., Jensen, L. R. & Christophersen, P. Pharmacology of the human red cell voltage-dependent cation channel. Part II: inactivation and blocking. *Blood Cells Mol. Dis.* **33,** 356–361 (2004).
220. Cull-Candy, S. G. & Usowicz, M. M. Multiple-conductance channels activated by excitatory amino acids in cerebellar neurons. *Nature* **325,** 525–528 (1987).
221. Christophersen, P. & Bennekou, P. Evidence for a voltage-gated, non-selective cation channel in the human red cell membrane. *Biochim. Biophys. Acta* **1065,** 103–106 (1991).
222. Faucherre, A., Kissa, K., Nargeot, J., Mangoni, M. E. & Jopling, C. Piezo1 plays a role in erythrocyte volume homeostasis. *Haematologica* **99,** 70–75 (2014).
223. Zarychanski, R. *et al.* Mutations in the mechanotransduction protein PIEZO1 are associated with hereditary xerocytosis. *Blood* **120,** 1908–1915 (2012).
224. Andolfo, I. *et al.* Multiple clinical forms of dehydrated hereditary stomatocytosis arise from mutations in PIEZO1. *Blood* **121,** 3925–3935, S1–12 (2013).
225. Bernhardt, I. & Ellory, J. C. *Red Cell Membrane Transport in Health and Disease*. (Springer Berlin Heidelberg, 2003). at <http://dx.doi.org/10.1007/978-3-662-05181-8>
226. Wright, J. M., Kline, P. A. & Nowak, L. M. Multiple effects of tetraethylammonium on N-methyl-D-aspartate receptor-channels in mouse brain neurons in cell culture. *J. Physiol. (Lond.)* **439,** 579–604 (1991).
227. Lew, V. L. & Bookchin, R. M. Ion transport pathology in the mechanism of sickle cell dehydration. *Physiol. Rev.* **85,** 179–200 (2005).

228. Browning, J. A. *et al.* The effect of deoxygenation on whole-cell conductance of red blood cells from healthy individuals and patients with sickle cell disease. *Blood* **109,** 2622–2629 (2007).
229. Sensi, S. L. *et al.* Measurement of intracellular free zinc in living cortical neurons: routes of entry. *J. Neurosci.* **17,** 9554–9564 (1997).
230. Joiner, C. H., Morris, C. L. & Cooper, E. S. Deoxygenation-induced cation fluxes in sickle cells. III. Cation selectivity and response to pH and membrane potential. *Am. J. Physiol.* **264,** C734–744 (1993).
231. Labotka, R. J. Measurement of intracellular pH and deoxyhemoglobin concentration in deoxygenated erythrocytes by phosphorus-31 nuclear magnetic resonance. *Biochemistry* **23,** 5549–5555 (1984).
232. Lew, V. L., Tsien, R. Y., Miner, C. & Bookchin, R. M. Physiological [Ca2+]i level and pump-leak turnover in intact red cells measured using an incorporated Ca chelator. *Nature* **298,** 478–481 (1982).
233. Ronquist, G., Rudolphi, O., Engström, I. & Waldenström, A. Familial phosphofructokinase deficiency is associated with a disturbed calcium homeostasis in erythrocytes. *J. Intern. Med.* **249,** 85–95 (2001).
234. Johnsson, R., Santaholma, S. & Saris, N. E. Calcium transport and adenosine triphosphatase activities of erythrocyte membranes in congenital spherocytosis. *Scand. J. Clin. Lab. Invest.* **38,** 121–125 (1978).
235. Wiley, J. S. Increased erythrocyte cation permeability in thalassemia and conditions of marrow stress. *J. Clin. Invest.* **67,** 917–922 (1981).
236. Berenbrink, M. Evolution of vertebrate haemoglobins: Histidine side chains, specific buffer value and Bohr effect. *Respir Physiol Neurobiol* **154,** 165–184 (2006).
237. Poillon, W. N. & Kim, B. C. 2,3-Diphosphoglycerate and intracellular pH as interdependent determinants of the physiologic solubility of deoxyhemoglobin S. *Blood* **76,** 1028–1036 (1990).
238. Rotter, M. A., Chu, H., Low, P. S. & Ferrone, F. A. Band 3 catalyzes sickle hemoglobin polymerization. *Biophys. Chem.* **146,** 55–59 (2010).
239. Liu, S. C. *et al.* Red cell membrane remodeling in sickle cell anemia. Sequestration of membrane lipids and proteins in Heinz bodies. *J. Clin. Invest.* **97,** 29–36 (1996).
240. MARILYNN J. JOHNSTON., A. M. B. Stimulation of lactate production by Ca+ionophore A23187 in inosine-fed human red cells. *he Journal of Physiology* **341,** 63 (1983).
241. Mayr, G. W. & Heilmeyer, L. M. Phosphofructokinase is a calmodulin binding protein. *FEBS Lett.* **159,** 51–57 (1983).
242. M. L. Harrison, P. S. L. Control of erythrocyte metabolism by redox-regulated tyrosine phosphatases and kinases. *Protoplasma* **184,** 196–202 (1995).
243. Zancan, P. & Sola-Penna, M. Calcium influx: a possible role for insulin modulation of intracellular distribution and activity of 6-phosphofructo-1-kinase in human erythrocytes. *Mol. Genet. Metab.* **86,** 392–400 (2005).

244. Simons, T. J. Calcium-dependent potassium exchange in human red cell ghosts. *J. Physiol. (Lond.)* **256,** 227–244 (1976).
245. Dyrda, A. *et al.* Local membrane deformations activate Ca2+-dependent K+ and anionic currents in intact human red blood cells. *PLoS ONE* **5,** e9447 (2010).
246. Tu, Y. P., Xiao, L., Su, X. F. & Yang, F. Y. Cytoplasmic Ca2+ inhibits the glucose transporter of human erythrocytes. *Biochem. Mol. Biol. Int.* **36,** 383–391 (1995).
247. Almaraz, L., García-Sancho, J. & Lew, V. L. Calcium-induced conversion of adenine nucleotides to inosine monophosphate in human red cells. *J. Physiol. (Lond.)* **407,** 557–567 (1988).
248. Sabina, R. L., Waldenström, A. & Ronquist, G. The contribution of Ca+ calmodulin activation of human erythrocyte AMP deaminase (isoform E) to the erythrocyte metabolic dysregulation of familial phosphofructokinase deficiency. *Haematologica* **91,** 652–655 (2006).
249. Heard, K. S., Fidyk, N. & Carruthers, A. ATP-dependent substrate occlusion by the human erythrocyte sugar transporter. *Biochemistry* **39,** 3005–3014 (2000).
250. Palek, J., Stewart, G. & Lionetti, F. J. The dependence of shape of human erythrocyte ghosts on calcium, magnesium, and adenosine triphosphate. *Blood* **44,** 583–597 (1974).
251. Nunomura, W. & Takakuwa, Y. Regulation of protein 4.1R interactions with membrane proteins by Ca2+ and calmodulin. *Front. Biosci.* **11,** 1522–1539 (2006).
252. Govekar, R. B. & Zingde, S. M. Protein kinase C isoforms in human erythrocytes. *Ann. Hematol.* **80,** 531–534 (2001).
253. De Oliveira, S., Silva-Herdade, A. S. & Saldanha, C. Modulation of erythrocyte deformability by PKC activity. *Clin. Hemorheol. Microcirc.* **39,** 363–373 (2008).
254. Raval, P. J. & Allan, D. The effects of phorbol ester, diacylglycerol, phospholipase C and Ca2+ ionophore on protein phosphorylation in human and sheep erythrocytes. *Biochem. J.* **232,** 43–47 (1985).
255. Kohout, S. C., Corbalán-García, S., Torrecillas, A., Goméz-Fernandéz, J. C. & Falke, J. J. C2 domains of protein kinase C isoforms alpha, beta, and gamma: activation parameters and calcium stoichiometries of the membrane-bound state. *Biochemistry* **41,** 11411–11424 (2002).
256. Allan, D. & Michell, R. H. Production of 1,2-diacylglycerol in human erythrocyte membranes exposed to low concentrations of calcium ions. *Biochim. Biophys. Acta* **455,** 824–830 (1976).
257. Wright, L. C., Chen, S. & Roufogalis, B. D. Regulation of the activity and phosphorylation of the plasma membrane Ca(2+)-ATPase by protein kinase C in intact human erythrocytes. *Arch. Biochem. Biophys.* **306,** 277–284 (1993).

258. Del Carlo, B., Pellegrini, M. & Pellegrino, M. Modulation of Ca2+-activated K+ channels of human erythrocytes by endogenous protein kinase C. *Biochim. Biophys. Acta* **1612,** 107–116 (2003).
259. Vincenzi, F. F., Hinds, T. R. & Raess, B. U. Calmodulin and the plasma membrane calcium pump. *Ann. N. Y. Acad. Sci.* **356,** 232–244 (1980).
260. Wang, K. K., Roufogalis, B. D. & Villalobo, A. Calpain I activates Ca2+ transport by the reconstituted erythrocyte Ca2+ pump. *J. Membr. Biol.* **112,** 233–245 (1989).
261. Matsumura, Y. *et al.* Intracellular calcium level required for calpain activation in a single myocardial cell. *J. Mol. Cell. Cardiol.* **33,** 1133–1142 (2001).
262. Salamino, F. *et al.* The plasma membrane calcium pump is the preferred calpain substrate within the erythrocyte. *Cell Calcium* **15,** 28–35 (1994).
263. Molitoris, B. A., Dahl, R. & Hosford, M. Cellular ATP depletion induces disruption of the spectrin cytoskeletal network. *Am. J. Physiol.* **271,** F790–798 (1996).
264. Kurata, M. & Suzuki, M. Glutathione regeneration in calcium-loaded erythrocytes: a possible relationship among calcium accumulation, ATP decrement and oxidative damage. *Comp. Biochem. Physiol. B, Biochem. Mol. Biol.* **109,** 305–312 (1994).
265. Alderton, W. K., Cooper, C. E. & Knowles, R. G. Nitric oxide synthases: structure, function and inhibition. *Biochem. J.* **357,** 593–615 (2001).
266. Kleinbongard, P. *et al.* Red blood cells express a functional endothelial nitric oxide synthase. *Blood* **107,** 2943–2951 (2006).
267. Daff, S. NO synthase: structures and mechanisms. *Nitric Oxide* **23,** 1–11 (2010).
268. Beppu, M., Mizukami, A., Nagoya, M. & Kikugawa, K. Binding of anti-band 3 autoantibody to oxidatively damaged erythrocytes. Formation of senescent antigen on erythrocyte surface by an oxidative mechanism. *J. Biol. Chem.* **265,** 3226–3233 (1990).
269. Lutz, H. U. Homeostatic roles of naturally occurring antibodies: an overview. *J. Autoimmun.* **29,** 287–294 (2007).
270. Nagel, R. L. *et al.* The erythrocyte effects of haemoglobin O(ARAB). *Br. J. Haematol.* **107,** 516–521 (1999).
271. Filippini, A., Villa, G., Corrocher, R. & De Franceschi, L. Acute hemolytic anemia with acanthocytosis associated with high-dose misoprostol for medical abortion. *Ann Emerg Med* **50,** 289–291 (2007).
272. De Franceschi, L. *et al.* Evidence for a protective role of the Gardos channel against hemolysis in murine spherocytosis. *Blood* **106,** 1454–1459 (2005).
273. Peters, L. L. *et al.* Mild spherocytosis and altered red cell ion transport in protein 4. 2-null mice. *J. Clin. Invest.* **103,** 1527–1537 (1999).

274. Gallagher, P. G. & Smith, B. D. Dehydrated hereditary stomatocytosis is not linked to the hlK1 locus, a Gardos channel candidate, on chromosome 19q13.2. *Blood* **93,** 2134–2135 (1999).
275. Ohashi, I., Pohoreki, R., Morita, K. & Stemmer, P. M. Alcohols increase calmodulin affinity for Ca2+ and decrease target affinity for calmodulin. *Biochim. Biophys. Acta* **1691,** 161–167 (2004).
276. Sabina, R. L., Wandersee, N. J. & Hillery, C. A. Ca2+-CaM activation of AMP deaminase contributes to adenine nucleotide dysregulation and phosphatidylserine externalization in human sickle erythrocytes. *Br. J. Haematol.* **144,** 434–445 (2009).
277. Dixon, E. & Winslow, R. M. The interaction between (Ca2+ + Mg2+)-ATPase and the soluble activator (calmodulin) in erythrocytes containing haemoglobin S. *Br. J. Haematol.* **47,** 391–397 (1981).
278. Liu, F., Mizukami, H., Sarnaik, S. & Ostafin, A. Calcium-dependent human erythrocyte cytoskeleton stability analysis through atomic force microscopy. *J. Struct. Biol.* **150,** 200–210 (2005).
279. King, M.-J. & Zanella, A. Hereditary red cell membrane disorders and laboratory diagnostic testing. *Int J Lab Hematol* **35,** 237–243 (2013).
280. Rivera, A. *et al.* Effect of complete protein 4.1R deficiency on ion transport properties of murine erythrocytes. *Am. J. Physiol., Cell Physiol.* **291,** C880–886 (2006).
281. George, A. *et al.* Erythrocyte NADPH oxidase activity modulated by Rac GTPases, PKC, and plasma cytokines contributes to oxidative stress in sickle cell disease. *Blood* **121,** 2099–2107 (2013).
282. George, A. *et al.* Altered phosphorylation of cytoskeleton proteins in sickle red blood cells: the role of protein kinase C, Rac GTPases, and reactive oxygen species. *Blood Cells Mol. Dis.* **45,** 41–45 (2010).
283. Adragna, N. C., Di Fulvio, M. & Lauf, P. K. Regulation of K-Cl cotransport: from function to genes. *J. Membr. Biol.* **201,** 109–137 (2004).
284. Zipser, Y., Piade, A., Barbul, A., Korenstein, R. & Kosower, N. S. Ca2+ promotes erythrocyte band 3 tyrosine phosphorylation via dissociation of phosphotyrosine phosphatase from band 3. *Biochem. J.* **368,** 137–144 (2002).
285. Chu, H. & Low, P. S. Mapping of glycolytic enzyme-binding sites on human erythrocyte band 3. *Biochem. J.* **400,** 143–151 (2006).
286. Salamino, F. *et al.* Site-directed activation of calpain is promoted by a membrane-associated natural activator protein. *Biochem. J.* **290 (Pt 1),** 191–197 (1993).
287. Sukati, S. *et al.* Clinical severity of β-thalassaemia/Hb E disease is associated with differential activities of the calpain-calpastatin proteolytic system. *PLoS ONE* **7,** e37133 (2012).
288. Damonte, G. *et al.* Mechanisms of perturbation of erythrocyte calcium homeostasis in favism. *Cell Calcium* **13,** 649–658 (1992).

289. Biggerstaff, R. H. & Phillips, J. R. A quantitative comparison of paralleling long-cone and bisection-of-angle periapical radiography. *Oral Surg. Oral Med. Oral Pathol.* **62,** 673–677 (1976).
290. Do, K. Q., Herrling, P. L., Streit, P. & Cuénod, M. Release of neuroactive substances: homocysteic acid as an endogenous agonist of the NMDA receptor. *J. Neural Transm.* **72,** 185–190 (1988).
291. Dhindsa, K. S., Omran, R. G. & Bhup, R. Effect of monosodium glutamate on the histogenesis of bone marrow in mice. *Acta Anat (Basel)* **101,** 212–217 (1978).
292. Genever, P. G. *et al.* Expression of a functional N-methyl-D-aspartate-type glutamate receptor by bone marrow megakaryocytes. *Blood* **93,** 2876–2883 (1999).
293. Chatterton, J. E. *et al.* Excitatory glycine receptors containing the NR3 family of NMDA receptor subunits. *Nature* **415,** 793–798 (2002).
294. Awobuluyi, M. *et al.* Subunit-specific roles of glycine-binding domains in activation of NR1/NR3 N-methyl-D-aspartate receptors. *Mol. Pharmacol.* **71,** 112–122 (2007).
295. Smothers, C. T. & Woodward, J. J. Pharmacological characterization of glycine-activated currents in HEK 293 cells expressing N-methyl-D-aspartate NR1 and NR3 subunits. *J. Pharmacol. Exp. Ther.* **322,** 739–748 (2007).
296. Mason, D. J. *et al.* Mechanically regulated expression of a neural glutamate transporter in bone: a role for excitatory amino acids as osteotropic agents? *Bone* **20,** 199–205 (1997).
297. Schaefer, A., Magócsi, M. & Marquardt, H. Signalling mechanisms in erythropoiesis: the enigmatic role of calcium. *Cell. Signal.* **9,** 483–495 (1997).
298. Miller, B. A., Cheung, J. Y., Tillotson, D. L., Hope, S. M. & Scaduto, R. C. Erythropoietin stimulates a rise in intracellular-free calcium concentration in single BFU-E derived erythroblasts at specific stages of differentiation. *Blood* **73,** 1188–1194 (1989).
299. Misiti, J. & Spivak, J. L. Erythropoiesis in vitro. Role of calcium. *J. Clin. Invest.* **64,** 1573–1579 (1979).
300. Minetti, G. *et al.* Red cell investigations: art and artefacts. *Blood Rev.* **27,** 91–101 (2013).
301. Woodbury, D., Reynolds, K. & Black, I. B. Adult bone marrow stromal stem cells express germline, ectodermal, endodermal, and mesodermal genes prior to neurogenesis. *J. Neurosci. Res.* **69,** 908–917 (2002).
302. Tavassoli, M. Bone marrow in boneless fish: lessons of evolution. *Med. Hypotheses* **20,** 9–15 (1986).
303. Pascual-Anaya, J. *et al.* The evolutionary origins of chordate hematopoiesis and vertebrate endothelia. *Dev. Biol.* **375,** 182–192 (2013).

304. *Hematology: basic principles and practice*. (Churchill Livingstone/Elsevier, 2009).
305. Deutsch, S. I., Tang, A. H., Burket, J. A. & Benson, A. D. NMDA receptors on the surface of cancer cells: target for chemotherapy? *Biomed. Pharmacother.* **68,** 493–496 (2014).
306. Anderson, M., Suh, J. M., Kim, E. Y. & Dryer, S. E. Functional NMDA receptors with atypical properties are expressed in podocytes. *Am. J. Physiol., Cell Physiol.* **300,** C22–32 (2011).
307. Simmonds, M. J., Detterich, J. A. & Connes, P. Nitric oxide, vasodilation and the red blood cell. *Biorheology* **51,** 121–134 (2014).
308. Resende, N. M. *et al.* Metabolic changes during a field experiment in a world-class windsurfing athlete: a trial with multivariate analyses. *OMICS* **15,** 695–704 (2011).
309. Mairbäurl, H. Red blood cells in sports: effects of exercise and training on oxygen supply by red blood cells. *Front Physiol* **4,** 332 (2013).
310. Risso, A., Ciana, A., Achilli, C., Antonutto, G. & Minetti, G. Neocytolysis: none, one or many? A reappraisal and future perspectives. *Front Physiol* **5,** 54 (2014).
311. Arashiki, N., Kimata, N., Manno, S., Mohandas, N. & Takakuwa, Y. Membrane peroxidation and methemoglobin formation are both necessary for band 3 clustering: mechanistic insights into human erythrocyte senescence. *Biochemistry* **52,** 5760–5769 (2013).
312. Lutz, H. U. Naturally occurring autoantibodies in mediating clearance of senescent red blood cells. *Adv. Exp. Med. Biol.* **750,** 76–90 (2012).
313. Milner, P. F. & Charache, S. Life span of carbamylated red cells in sickle cell anemia. *J. Clin. Invest.* **52,** 3161–3171 (1973).
314. Franco, R. S. Measurement of red cell lifespan and aging. *Transfus Med Hemother* **39,** 302–307 (2012).
315. Barabino, G. A., McIntire, L. V., Eskin, S. G., Sears, D. A. & Udden, M. Rheological studies of erythrocyte-endothelial cell interactions in sickle cell disease. *Prog. Clin. Biol. Res.* **240,** 113–127 (1987).
316. Hebbel, R. P. Beyond hemoglobin polymerization: the red blood cell membrane and sickle disease pathophysiology. *Blood* **77,** 214–237 (1991).
317. Yuditskaya, S., Suffredini, A. F. & Kato, G. J. The proteome of sickle cell disease: insights from exploratory proteomic profiling. *Expert Rev Proteomics* **7,** 833–848 (2010).
318. Reinhart, W. H. & Chien, S. Red cell rheology in stomatocyte-echinocyte transformation: roles of cell geometry and cell shape. *Blood* **67,** 1110–1118 (1986).
319. George, A. *et al.* Erythrocyte NADPH oxidase activity modulated by Rac GTPases, PKC, and plasma cytokines contributes to oxidative stress in sickle cell disease. *Blood* **121,** 2099–2107 (2013).

320. De Franceschi, L. *et al.* Pharmacological inhibition of calpain-1 prevents red cell dehydration and reduces Gardos channel activity in a mouse model of sickle cell disease. *FASEB J.* **27,** 750–759 (2013).
321. Salamino, F. *et al.* The plasma membrane calcium pump is the preferred calpain substrate within the erythrocyte. *Cell Calcium* **15,** 28–35 (1994).
322. Steffen, P. *et al.* Stimulation of human red blood cells leads to Ca2+-mediated intercellular adhesion. *Cell Calcium* **50,** 54–61 (2011).
323. Mohandas, N. & Evans, E. Sickle erythrocyte adherence to vascular endothelium. Morphologic correlates and the requirement for divalent cations and collagen-binding plasma proteins. *J. Clin. Invest.* **76,** 1605–1612 (1985).
324. Hebbel, R. P. *et al.* Abnormal adherence of sickle erythrocytes to cultured vascular endothelium: possible mechanism for microvascular occlusion in sickle cell disease. *J. Clin. Invest.* **65,** 154–160 (1980).
325. Hebbel, R. P., Steinberg, M. H. & Eaton, J. W. Erythrocyte calcium abnormalities in sickle cell disease. *Prog. Clin. Biol. Res.* **51,** 321–332 (1981).
326. Bender, M. A. & Hobbs, W. in *GeneReviews(®)* (eds. Pagon, R. A. et al.) (University of Washington, Seattle, 1993). at <http://www.ncbi.nlm.nih.gov/books/NBK1377/>
327. Koldkjaer, P., McDonald, M. D., Prior, I. & Berenbrink, M. Pronounced in vivo hemoglobin polymerization in red blood cells of Gulf toadfish: a general role for hemoglobin aggregation in vertebrate hemoparasite defense? *Am. J. Physiol. Regul. Integr. Comp. Physiol.* **305,** R1190–1199 (2013).
328. Koldkjaer, P. & Berenbrink, M. In vivo red blood cell sickling and mechanism of recovery in whiting, Merlangius merlangus. *J. Exp. Biol.* **210,** 3451–3460 (2007).
329. Butcher, P. D. Kinetics of the in vitro gelation of a sickling haemoglobin from Hog deer (Axis porcinus). *Biochim. Biophys. Acta* **579,** 432–441 (1979).
330. Nagel, R. L. Innate resistance to malaria: the intraerythrocytic cycle. *Blood Cells* **16,** 321–339; discussion 340–349 (1990).
331. Wasserman, M. & Chaparro, J. Intraerythrocytic calcium chelators inhibit the invasion of Plasmodium falciparum. *Parasitol. Res.* **82,** 102–107 (1996).
332. Moshal, K. S. *et al.* Restoration of contractility in hyperhomocysteinemia by cardiac-specific deletion of NMDA-R1. *Am. J. Physiol. Heart Circ. Physiol.* **296,** H887–892 (2009).
333. Gill, S. S., Pulido, O. M., Mueller, R. W. & McGuire, P. F. Molecular and immunochemical characterization of the ionotropic glutamate receptors in the rat heart. *Brain Res. Bull.* **46,** 429–434 (1998).
334. Seeber, S. *et al.* Transient expression of NMDA receptor subunit NR2B in the developing rat heart. *J. Neurochem.* **75,** 2472–2477 (2000).
335. Gill, S. *et al.* Cloning and characterization of glutamate receptors in Californian sea lions (Zalophus californianus). *Mar Drugs* **8,** 1637–1649 (2010).

336. Gill, S., Veinot, J., Kavanagh, M. & Pulido, O. Human heart glutamate receptors - implications for toxicology, food safety, and drug discovery. *Toxicol Pathol* **35,** 411–417 (2007).
337. Tekin, A. S., Sengül, C., Kılıçaslan, B., Ozveren, O. & Kozdağ, G. [The value of serum homocysteine in predicting one-year survival in patients with severe systolic heart failure]. *Turk Kardiyol Dern Ars* **40,** 699–705 (2012).
338. Washio, T. *et al.* Relationship between plasma homocysteine levels and congestive heart failure in patients with acute myocardial infarction. Homocysteine and congestive heart failure. *Int Heart J* **52,** 224–228 (2011).
339. Agoston-Coldea, L., Mocan, T., Gatfosse, M., Lupu, S. & Dumitrascu, D. L. Plasma homocysteine and the severity of heart failure in patients with previous myocardial infarction. *Cardiol J* **18,** 55–62 (2011).
340. Nasso, G. *et al.* Increased plasma homocysteine predicts arrhythmia recurrence after minimally invasive epicardial ablation for nonvalvular atrial fibrillation. *J. Thorac. Cardiovasc. Surg.* **146,** 848–853 (2013).
341. Dunn, M. J. *et al.* Demonstration by western blotting of antiheart antibodies before and after cardiac transplantation. *Transplantation* **51,** 806–812 (1991).
342. Acampa, M. *et al.* Homocysteine and P wave dispersion in patients with heart transplantation. *Clin Transplant* **25,** 119–125 (2011).
343. Paoletti, P., Bellone, C. & Zhou, Q. NMDA receptor subunit diversity: impact on receptor properties, synaptic plasticity and disease. *Nat. Rev. Neurosci.* **14,** 383–400 (2013).
344. Legendre, P. & Westbrook, G. L. Ifenprodil blocks N-methyl-D-aspartate receptors by a two-component mechanism. *Mol. Pharmacol.* **40,** 289–298 (1991).
345. Watford, M. Net interorgan transport of L-glutamate in rats occurs via the plasma, not via erythrocytes. *J. Nutr.* **132,** 952–956 (2002).
346. Kihlberg, R., Sterner, G., Wennberg, A. & Denneberg, T. Plasma free amino acid levels in uremic rats given high and low protein diets or intravenous infusions of amino acid solutions. *J. Nutr.* **112,** 2058–2070 (1982).
347. He, W. *et al.* ZD7288-induced suppression of long-term potentiation was attenuated by exogenous NMDA at the Schaffer collateral-CA1 synapse in the rat in vivo. *Eur. J. Pharmacol.* **631,** 10–16 (2010).
348. Cohen, A. S., Matharu, M. S. & Goadsby, P. J. Electrocardiographic abnormalities in patients with cluster headache on verapamil therapy. *Neurology* **69,** 668–675 (2007).
349. Madry, C., Betz, H., Geiger, J. R. P. & Laube, B. Potentiation of Glycine-Gated NR1/NR3A NMDA Receptors Relieves Ca-Dependent Outward Rectification. *Front Mol Neurosci* **3,** 6 (2010).
350. Christine, C. W. & Choi, D. W. Effect of zinc on NMDA receptor-mediated channel currents in cortical neurons. *J. Neurosci.* **10,** 108–116 (1990).

351. Candell, J., Valle, V., Soler, M. & Rius, J. Acute intoxication with verapamil. *Chest* **75,** 200–201 (1979).
352. Rollin, A., Maury, P., Guilbeau-Frugier, C. & Brugada, J. Transient ST elevation after ketamine intoxication: a new cause of acquired brugada ECG pattern. *J. Cardiovasc. Electrophysiol.* **22,** 91–94 (2011).
353. Gann, D. Ventricular tachycardia in a patient with the "Chinese restaurant syndrome" *South. Med. J.* **70,** 879–881 (1977).
354. Perl, T. M. *et al.* An outbreak of toxic encephalopathy caused by eating mussels contaminated with domoic acid. *N. Engl. J. Med.* **322,** 1775–1780 (1990).
355. Schaumburg, H. H., Byck, R., Gerstl, R. & Mashman, J. H. Monosodium L-glutamate: its pharmacology and role in the Chinese restaurant syndrome. *Science* **163,** 826–828 (1969).

7) **Makhro A**, Wang J, Vogel J, Boldyrev AA, Gassmann M, Kaestner L, Bogdanova A, (2010) *Evidence for the presence of functional NMDA receptors in mammalian erythrocytes*, Am J Physiol (Cell Physiol), **298(6)**: 1315-25.
8) Sergeeva I, **Makhro A**, Pegova A, Bulygina E, (2012) *The effects of homocysteine and homocysteic acid on the metabotropic glutamate receptors of cerebellar neurons.* Neurochem J, **4(2):116-121.**
9) **Makhro A,** Mashkina A, Solenaya O, Trunova O, Kozina L, Arutyunian A, Bulygina E, *Prenatal hyperhomocysteinemia as a model of oxidative stress of the brain* (2008) Bulletin of Experimental Biology and Medicine, **146(1)**:33-5.
10) **Makhro A,** Mashkina A, Solenaya O, Trunova O, Tyulina O, Bulygina E, Boldyrev AA, (2008) *Carnosine Protects Cells from Oxidative Stress Induced by Hyperhomocysteinemia*, Neurochem J, **2(3)**:202-208.
11) **Makhro A**, Bulygina E, Boldyrev AA, *Effects of homocysteine and homocysteinic acid on cerebellar granule cells* (2007) Neurochem J, **1(2)**:127-132.
12) Boldyrev AA, Bulygina E, **Makhro A,** (2004) *Glutamate receptors modulate oxidative stress in neuronal cells*, Neurotox Res, **6**:581-587.
13) Boldyrev AA, Bulygina E, **Makhro A**, (2004) *Na/K-ATPase involves in signal transduction pathway in neurons via regulation of reactive oxygen species (ROS)*. Neurochem J, **90**:102.

11. Acknowledgments

Many people were involved in my work during the years of my PhD studies, and there was a lot of *studying* itself; I learned how to work independently and how to follow my own ideas. My scientific "father" was my former professor from the Moscow State University Alexander Boldyrev (1940–2012). He taught me to think beyond the current scientific paradigms. Based only on his intuition, he suggested that glutamate receptors may exist outside the brain.

I'm thanking my PhD supervisor Dr. Anna Bogdanova for her enthusiasm and faith in this new and unexpected field of research. Her exceptional productivity at work was always inspiring me. She taught me new techniques and new approaches during our collaboration. Many experiments described in this manuscript we did together in the operation room and on the lab bench.

I'm very grateful to the director of the Institute of Veterinary Physiology professor Max Gassmann, who was always welcoming and supporting our crazy ideas. He organized free and friendly environment at the institute, where people can easily share their ideas and offer their help.

I thank Dr. med. Jeroen Goede for his help in studies of the red blood cells from sickle cell anemia patients. He believed in my idea based on theoretical assumption about NMDA receptor prevalence in the erythrocytes of sickle cell patients and provided me with all materials for the study. He is a very kind and thoughtful person, it was always a very big pleasure to collaborate with him and I'm very happy to continue our collaboration during the clinical trial.

I was (and still is) very much enjoying our collaboration with Dr. Lars Kaestner during the RBC and heart studies. I'm grateful for his help in my PhD studies and even more for the organization of the red blood cell research project (http://rare-anaemia.eu/) where I have an opportunity to continue my work.

I'm grateful to Prof. Dr. med. Johannes Vogel who developed blood-perfused circuit for the studies of isolated rat heart. He was also helping me many times with all kinds of technical problems in the operation room and beyond.

Special thanks to my colleague and collaborator Pascal Haenggi for his willingness to participate in the study of NMDA receptors in red blood cell precursors. The data he obtained were supporting our initial hypothesis and my confidence in the project. Being a great scientific worker, he brought our knowledge to the level which I would not be able to reach by myself.

Many thanks to our technicians Beat Grenacher and Nikolai Bogdanov. Beat's professionalism and cheerful personality provided an excellent support for our studies. Nikolai was participating in many experiments and helping with the lab problems as well.

I'm thankful to my colleagues in the field of cardiovascular research Dr. med. vet. Katharine Mitchell, Prof. Dr. med. vet. Colin Schwarzwald, Dr. med. Dmitry Kosenkov and Prof. Dr. med. Giuseppe Faggian. With their help we are going to bring our findings in use of human and veterinary medicine.

I'm grateful to Dr. Florian Steiner for financial support of my research and for his efforts in bringing our research findings to the industry.

Finally, I want to thank my husband Dr. Maxim Makhinya for his help in my work (he wrote a program for analyzing RBC images) and for his tremendous support outside of the lab. I also want to mention our two year old son Viktor who always inspires my curiosity in science.